

**MAGNETIC NANO-ADSORBENTS APPLICATIONS AND  
MODELLING FOR GREEN ENVIRONMENTAL  
REMIATIONS**

**MUHAMMAD ABDUR REHMAN**

**FACULTY OF SCIENCE  
UNIVERSITY OF MALAYA  
KUALA LUMPUR**

**2017**

**MAGNETIC NANO-ADSORBENTS APPLICATIONS  
AND MODELLING FOR GREEN ENVIRONMENTAL  
REMEDICATIONS**

**MUHAMMAD ABDUR REHMAN**

**THESIS SUBMITTED IN FULFILMENT OF THE  
REQUIREMENTS FOR THE DEGREE OF DOCTOR  
OF PHILOSOPY**

**DEPARTMENT OF GEOLOGY  
UNIVERSITY OF MALAYA  
KUALA LUMPUR**

**2017**

**UNIVERSITY OF MALAYA**

**ORIGINAL LITERARY WORK DECLARATION**

Name of Candidate: MUHAMMAD ABDUR REHMAN

Registration/Matric No: SHC10031

Name of Degree: Doctor of Philosophy

Title of Project Paper/Research Report/Dissertation/Thesis ("this Work"):  
**MAGNETIC NANO-ADSORBENTS APPLICATIONS AND MODELLING FOR GREEN ENVIRONMENTAL REMEDIATIONS**

Field of Study: GEOLOGY EARTH SCIENCE

I do solemnly and sincerely declare that:

- (1) I am the sole author/writer of this work;
- (2) This work is original;
- (3) Any use of any work in which copyright exists was done by way of fair dealing and for permitted purposes and any excerpt or extract from, or reference to or reproduction of any copyright work has been disclosed expressly and sufficiently and the title of the Work and its authorship have been acknowledged in this Work;
- (4) I do not have any actual knowledge nor do I ought reasonably to know that the making of this work constitutes an infringement of any copyright work;
- (5) I hereby assign all and every rights in the copyright to this work to the University of Malaya ("UM"), who henceforth shall be owner of the copyright in this Work and that any reproduction or use in any form or by any means whatsoever is prohibited without the written consent of UM having been first had and obtained;
- (6) I am fully aware that if in the course of making this Work I have infringed any copyright whether intentionally or otherwise, I may be subject to legal action or any other action as may be determined by UM.

Candidate's Signature

Date:

Subscribed and solemnly declared before,

Witness's Signature

Date:

Name:

Designation:

## ABSTRACT

This work describes some general procedures for the preparation, characterization of adsorbents,  $\text{CuFe}_2\text{O}_4$ ,  $\text{CuCe}_{0.1}\text{Fe}_2\text{O}_4$ ,  $\text{CuCe}_{0.2}\text{Fe}_2\text{O}_4$ ,  $\text{CuCe}_{0.3}\text{Fe}_2\text{O}_4$ ,  $\text{CuCe}_{0.4}\text{Fe}_2\text{O}_4$ ,  $\text{CuCe}_{0.5}\text{Fe}_2\text{O}_4$ ,  $\text{CuCe}_{0.2}\text{Fe}_2\text{O}_4\text{-rGO}$ , POCS (X=4.75), POCS (X=2.36), POCS (X=1.18), POCS (X=0.6), POCS (X=0.3), POCS (X=0.15) and their application for the decontamination of hydrological samples in an environment of high competitions for available active sites on the surface of adsorbents. A detailed characterization and analysis were carried out by the Fourier Transform Infrared spectroscopy (FTIR), Raman spectroscopy, X-ray Diffraction (XRD), BET surface area, particle size analyzer, Zeta Potential (ZP), Thermal gravimetric analysis (TGA & DTA), Field emission scanning electron microscopy (FESEM), Transmission Electron microscopy (TEM), Nuclear magnetic resonance (NMR), High performance liquid chromatography (HPLC), ion chromatography (IC), Inductively coupled mass spectroscopy (ICPMS), Electrochemical impedance spectroscopy (EIS), Linear scan cyclic voltammetry (LSCV) and UV-Visible spectroscopy that revealed the formation of impurity free magnetic adsorbents. The adsorbents were applied for the green environment remediation of heavy metals, anionic species and organophosphorus acephate. The properties of these synthetic adsorbents were fine-tuned by the facile process of doping rare earths, monitored by Autolab PGSTAT 302N and NOVA 1.10 software. Response surface methodology (RSM) for optimum adsorption and central composite design (CCD) was selected to study the main effects and interaction effects of various controlling parameter such as Adsorbent dose ( $\text{g L}^{-1}$ ), mixing speed ( $\text{r/min}$ ), temperature ( $^{\circ}\text{C}$ ) and initial concentration ( $\text{mgL}^{-1}$ ). The nature of all the interaction was explained by a number of isotherms and kinetic models. Kinetic models include, pseudo first order, pseudo second order, Banghams, intra-particle diffusion, while the equilibrium models such as Langmuir, Freundlich, Temkin, Dubenin Redushkvich (DR), and Flory Huggins

(FH). The equilibrium and kinetic models were tested for goodness of fit between the observed and model predicted adsorption capacities ( $Q_e$ ) to explain the interaction removal mechanisms. The results were further used to prepare adsorbents, characterize, apply and check for the best fit model that explains the adsorption process. The series of  $\text{CuCe}_x\text{Fe}_{2-x}\text{O}_4$  ( $x=0.0$  to  $0.5$ ) retained magnetic properties for fluoride adsorption with coefficient values of  $X1(74.29)$ ,  $X2(25.31)$ ,  $X3(36.99)$  and  $X4(8.31)$  respectively. The natural POCS displayed Arsenic adsorption coefficient  $X1(1.62)$ ,  $X2(1.81)$ ,  $X3(0.80)$  and  $X4(3.10)$ . The isotherms results of Acephate show the value of  $Q_e$  (Langmuir),  $11.23 \text{ mgg}^{-1}$  or  $10.67 \text{ mgg}^{-1}$  at  $293\text{K}$  and  $313\text{K}$  respectively. The pseudo second order kinetic model give best fit to the results ( $R^2 = 0.998$ ), and the value of  $Q_e$  (pseudo second order) were  $12.427 \text{ mgg}^{-1}$  and  $12.280 \text{ mgg}^{-1}$  at  $293\text{K}$  and  $313 \text{ K}$  respectively. The magnetic separations, dopant facilitated dispersions and graphene layers provided some novel series of energy efficient adsorbent. The design of experiments strategy with various statistical standards designs helps optimize the adsorption conduction with minimal number of experiments, reducing the cost and time of research and development in green environmental remediation.

## ABSTRAK

Kerja ini menerangkan beberapa prosedur am bagi penyediaan, pencirian penjerap,  $\text{CuFe}_2\text{O}_4$ ,  $\text{CuCe}_{0.1}\text{Fe}_2\text{O}_4$ ,  $\text{CuCe}_{0.2}\text{Fe}_2\text{O}_4$ ,  $\text{CuCe}_{0.3}\text{Fe}_2\text{O}_4$ ,  $\text{CuCe}_{0.4}\text{Fe}_2\text{O}_4$ ,  $\text{CuCe}_{0.5}\text{Fe}_2\text{O}_4$ ,  $\text{CuCe}_{0.2}\text{Fe}_2\text{O}_4\text{-rGO}$ , POCS ( $X=4.75$ ), POCS ( $X=2.36$ ), POCS ( $X=1.18$ ), POCS ( $X=0.6$ ), POCS ( $X=0.3$ ), POCS ( $X=0.15$ ) dan aplikasi mereka untuk penyahkontaminasi sampel hidrologi dalam suasana pertandingan yang tinggi bagi laman aktif yang tersedia pada permukaan penjerap. Pencirian dan analisis terperinci telah dijalankan oleh Fourier Transform spektroskopi inframerah (FTIR), spektroskopi Raman, Difraksi X-ray (XRD), kawasan permukaan BET, analisa saiz zarah, Zeta Berpotensi (ZP), analisis gravimetrik terma (TGA & DTA), Field imbasan pancaran elektron mikroskop (FESEM), Bahagian penghantaran mikroskopi elektron (TEM), Nuklear magnet resonans (NMR), prestasi tinggi kromatografi cecair (HPLC), ion kromatografi (IC), Induktif ditambah spektroskopi jisim (ICPMS), Elektrokimia impedans spektroskopi (EIS), Linear mengimbas siklik voltametri (LSCV) dan spektroskopi UV-nyata yang mendedahkan pembentukan berhadap percuma penjerap magnet. Penjerap yang digunakan untuk pemulihan alam sekitar hijau logam berat seperti, spesies anionik seperti, pewarna organik, dan organofosforus acefat. Sifat-sifat penjerap sintetik ini telah diperhalusi oleh proses mudah daripada pendopan nadir bumi, dipantau oleh Autolab PGSTAT 302N dan NOVA perisian 1.10. Kaedah gerak balas permukaan (RSM) untuk penjerapan optimum dan reka bentuk komposit pusat (CCD) telah dipilih untuk mengkaji kesan utama dan kesan interaksi pelbagai parameter kawalan seperti dos penjerap ( $\text{g L}^{-1}$ ), pencampuran kelajuan ( $\text{r / min}$ ), suhu ( $^{\circ}\text{C}$ ) dan kepekatan awal ( $\text{mgL}^{-1}$ ). Sifat semua interaksi telah dijelaskan oleh beberapa isoterma dan model kinetik. Model kinetik termasuk, pseudo tertib pertama, pseudo tertib kedua, Banghams, intra-zarah penyebaran, manakala model keseimbangan seperti Langmuir, Freundlich, Temkin, Dubenin Redushkovich (DR), dan Flory Huggins (FH). Keseimbangan dan model kinetik

telah diuji untuk padankan di antara yang model yang diperhati dan ramalan kapasiti penjerapan ( $Q_e$ ) untuk menerangkan mekanisma interaksi penyingkiran. Hasil kajian diagnostik ini seterusnya digunakan untuk menyediakan penjerap, pencirian, aplikasi dan memeriksa model padanan terbaik yang menerangkan proses penjerapan. Siri  $\text{CuCe}_x\text{Fe}_{2-x}\text{O}_4$  ( $x = 0.0$  hingga  $0.5$ ) mengekalkan sifat-sifat magnet untuk penjerapan fluorida dengan nilai-nilai pekali X1 (74,29), X2 (25.31), X3 (36.99) dan X4 (8.31) masing-masing. The POCS semulajadi dipaparkan Arsenic X1 pekali penjerapan (1.62), X2 (1.81), X3 (0.80) dan X4 (3.10). Keputusan isoterma Acefat menunjukkan nilai  $Q_e$  (Langmuir),  $11.23 \text{ mgg}^{-1}$  atau  $10.67 \text{ mgg}^{-1}$  masing-masing pada 293K dan 313K. Pseudo tertib kedua model kinetik memberi padanan terbaik untuk keputusan ( $R^2 = 0.998$ ), dan nilai  $Q_e$  (tertib pseudo kedua) masing-masing adalah  $12.427 \text{ mgg}^{-1}$  dan  $12.280 \text{ mgg}^{-1}$  pada 293K dan 313 K. Pemisahan magnetik, pendopan memudahkan penyebaran dan lapisan graphene menyediakan beberapa siri novel bahan penjerap yang cekap tenaga. Strategi reka bentuk eksperimen dengan pelbagai reka bentuk standard statistikal membantu mengoptimumkan pengaliran penjerapan dengan bilangan minimum eksperimen, mengurangkan kos dan masa penyelidikan dan pembangunan dalam pemulihan alam sekitar hijau.

## ACKNOWLEDGEMENTS

Bismillah hir rahman nir Raheem, In the name of Allah (subhanaho watala), the most beneficent and the most merciful for countless favors, guidance and his beloved prophet Muhammad (Sallaho Elahe Wasalam). “Obedience to him is a cause of approach and gratitude in increase of benefits. Every inhalation of the breath prolong life and every expiration of it gladdens our nature, wherefore every breath confers two benefits and for every benefit gratitude is due. Whose hand and tongue is capable, to fulfil the obligations of thanks to Him (The Gulistan of Saadi)”. It is an honor to acknowledge the supervision and treasurable supports provided by Prof. Dr. Ismail Yusoff, Associate Prof. Dr. Ng Tham Fatt and Prof. Dr. Yatimah Alias. The meetings and discussions were the basic contrivance to keep this project on track and to meet the desired research aims and objectives. The best thing to mention and acknowledge is that I benefited a very caring and patron relation with my supervisor. The conversion of all the research designs into a reality was only possible by the useful and productive collaborations. The University of Malaya, Kuala Lumpur, Malaysia, provided the excellent laboratory facilities to complete the laboratory preparations, characterization, optimization and applications of the novel materials. A look back in the past, there are friends, colleagues, researchers and their help and support that will be remembered throughout my life. The moral support and courage from my parents, sisters, brother, wife and my children Ahmad and Fatima is also greatly acknowledged. Thanks to the Ministry of Education (MOE) Malaysia and University of Malaya (UM), Bright Spark Program (BSP). The UM IPPP research grants No PG215-2014 and MOE grant UM .C/625/1/HIR/MOE/SC/04 is gratefully acknowledged. I also convey cardiac felicitation to the UM department of Geology, Chemistry, Physics, Civil Engineering, Center for ionic liquids (UMCiI), NANOCAT, and HITEC labs for the analysis and research facilities.

## TABLE OF CONTENTS

<b>Abstract.....</b>	<b>iii</b>
<b>Abstrak.....</b>	<b>v</b>
<b>Acknowledgements.....</b>	<b>vii</b>
<b>Table of Contents .....</b>	<b>viii</b>
<b>List of Figures.....</b>	<b>xiv</b>
<b>List of Tables .....</b>	<b>xvii</b>
<b>List of equations .....</b>	<b>xix</b>
<b>List of Symbols and Abbreviations.....</b>	<b>xxii</b>
<b>List of Appendices.....</b>	<b>xxiv</b>
<b>CHAPTER 1: INTRODUCTION.....</b>	<b>1</b>
1.1 Adsorbents .....	1
1.2 Characterizations methods.....	2
1.3 Applications or modelling .....	3
1.4 Problem statement .....	3
1.5 Aims and objectives.....	4
1.6 Thesis outline.....	5
<b>CHAPTER 2: LITERATURE REVIEW.....</b>	<b>7</b>
2.1 Green environmental remediation .....	8
2.2 Preparation of Nano-adsorbents .....	9
2.2.1 Top-down approach.....	13
2.2.2 Bottom-up approach .....	13
2.2.3 Auto-combustion method .....	14
2.2.4 Sol-gel process .....	14

2.2.5	Micro emulsions .....	15
2.2.6	Hydrothermal fabrication .....	15
2.2.7	Sono-chemical technique .....	17
2.2.8	Agro-industrial waste for environmental remediation .....	19
2.2.9	Palm oil clinker sand (POCS) .....	19
2.2.10	Properties of adsorbents .....	20
2.2.11	Fine-tuned Nano-adsorbents.....	23
2.2.12	Magnetic separation .....	24
2.2.13	Graphene and carbon nanotubes.....	25
2.2.14	Metal oxides and magnetic ferrites.....	32
2.2.15	Comparing adsorbents performance.....	36
2.3	Modelling adsorption.....	40
2.3.1	Design of experiments.....	40
2.3.2	Response surface methodology .....	41
2.3.3	Adsorption Kinetics.....	42
2.4	Challenges and role of adsorbents in remediation.....	43
2.5	Research advancement in adsorbents protections.....	45
2.5.1	Socio-economic development and public health.....	48
2.5.2	Resources scarcity .....	50
2.6	Comparative hydrological remediation .....	51
2.7	The competitive adsorption technique.....	54
2.8	Summary of the literature review .....	58
<b>CHAPTER 3: RESEARCH METHODOLOGY .....</b>		<b>59</b>
3.1	Materials .....	60
3.2	Preparation of magnetic adsorbents.....	60
3.2.1	Co-precipitation method for the preparation of $\text{CuCe}_{0.2}\text{Fe}_{1.8}\text{O}_4$ .....	62

3.2.2	Micro-emulsion method for $\text{CuCe}_x\text{Fe}_{2-x}\text{O}_4$ ( $x=0$ to $0.5$ ). .....	62
3.2.3	Hydrothermal reductive fabrication of $\text{CuCe}_{0.2}\text{Fe}_{1.8}\text{O}_4$ -rGO.....	63
3.2.4	Mechanical milling to form grades of POCS .....	64
3.3	Characterization of fabricated Nano-adsorbents .....	66
3.3.1	Powder X-ray diffraction (XRD) .....	66
3.3.2	Thermogravimetric analysis .....	68
3.3.3	Electron microscopic analysis .....	69
3.3.3.1	Scanning electron microscopy (SEM).....	69
3.3.3.2	High resolution transmission electron microscopy .....	70
3.3.3.3	Surface analysis of Magnetic Nano-adsorbents .....	71
3.3.4	Fourier Transform Infrared Spectroscopy (FTIR).....	72
3.3.4.1	Sample preparation & analysis.....	72
3.3.5	Ion Chromatography.....	73
3.3.5.1	IC Measurement conditions .....	74
3.3.6	Electrochemical methods .....	74
3.3.6.1	Cyclic voltammetry .....	74
3.3.6.2	Electrochemical Impedance Spectroscopy (EIS) .....	77
3.4	Nano-ferrites applications.....	78
3.4.1	Nano-ferrites.....	78
3.4.2	Analysis techniques .....	78
3.5	Modelling adsorption.....	79
3.5.1	Response Surface Model .....	79
3.5.2	Isotherms .....	80
3.5.2.1	Langmuir Isotherm for monolayer adsorption .....	81
3.5.2.2	Freundlich isotherm for heterogeneous adsorption.....	82
3.5.2.3	Temkin Isotherm for energetics of adsorption .....	82

3.5.2.4	Flory Huggin (FH) model for degree of surface coverage .....	83
3.5.2.5	Dubinin-Radushkevich (D-R) isotherm .....	83
3.5.3	Adsorption Kinetics .....	84
3.5.3.1	Rate law .....	84
3.5.3.2	Zero order .....	85
3.5.3.3	First order .....	86
3.5.3.4	Second order .....	86
3.5.3.5	Pseudo order reactions .....	87
3.5.3.6	Pseudo-First Order Kinetic Model .....	88
3.5.3.7	Pseudo second order model .....	88
3.5.3.8	Intraparticle Diffusion Model .....	88
3.5.3.9	Banghams's Model .....	89
3.5.4	Thermodynamics .....	89
 <b>CHAPTER 4: RESULTS AND DISCUSSIONS .....</b>		<b>90</b>
4.1	Characterization results of $\text{CuCe}_{0.2}\text{Fe}_{1.8}\text{O}_4\text{-rGO}$ .....	90
4.1.1	XRD analysis .....	91
4.1.2	FTIR functional groups .....	93
4.1.3	Thermogravimetric analysis (TGA) .....	94
4.1.4	Morphology and microstructural analysis .....	95
4.1.5	EDS and elements maps .....	97
4.1.6	Raman Spectroscopy .....	98
4.1.7	Magnetic hysteresis loops .....	99
4.2	Characterization results of Palm oil waste clinker sand. ....	103
4.2.1	POCS mechanical and physical treatments .....	104
4.2.2	Application of POCS for As adsorption .....	104
4.2.3	Batch adsorption .....	106

4.2.4	POCS Particle size distribution .....	106
4.2.5	Functional groups analysis .....	107
4.2.6	FESEM and EDX analysis .....	109
4.2.7	A quantitative comparison of efficiencies .....	110
4.3	Modelling adsorption.....	110
4.3.1.1	The variables influence on model response .....	111
4.3.1.2	RSM 3D plots.....	113
4.3.1.3	2D adsorption contour plots (CPs).....	115
4.4	Modelling Acephate adsorption.....	117
4.4.1	HPLC for acephate .....	119
4.4.2	Sonication time optimization.....	120
4.4.3	Isotherm models for acephate.....	121
4.4.4	Kinetics models for Acephate .....	124
4.4.5	Thermodynamics of Acephate adsorption.....	126
4.5	Fluoride remediation using doped and un-doped magnetic ferrites. ....	126
4.6	Characterization of doped and undoped magnetic ferrites .....	129
4.6.1	XRD analysis.....	129
4.6.2	Electro-analytical results .....	131
4.6.3	FTIR of spinel ferrites .....	132
4.6.4	FESEM results.....	133
4.6.5	Magnetic properties .....	136
4.6.6	Ion chromatography separation results.....	138
4.6.7	Effect of competing anions.....	139
4.7	Fluoride adsorption Model. ....	141
<b>CHAPTER 5: CONCLUSIONS.....</b>		<b>144</b>
5.1	Conclusions .....	144

5.2 Recommendation .....	145
<b>References .....</b>	<b>148</b>
<b>List of Publications and Papers Presented .....</b>	<b>172</b>
<b>List of Presentations.....</b>	<b>173</b>

University of Malaya

## LIST OF FIGURES

Figure 1.1	WoS key words analysis.	1
Figure 1.2	Country wise estimate of increase in the research activity in the area of adsorbents for hydrological remediation.	2
Figure 2.1	The principles of green environment remediation.	9
Figure 2.2	The top-down and bottom-up approach.	14
Figure 2.3	Reverse and normal micelle structure.	15
Figure 2.4	Sonochemical primary and secondary reactions for the formation of nanomaterial.	18
Figure 2.5	Burning of old Palm oil trees for Land clearance.	20
Figure 2.6	Adsorbents large surface area supports (A) Single wall carbon nanotubes (SWCNT), (B) Multiwall carbon nanotubes (C) Graphene (D) Polymeric supports.	22
Figure 2.7	The three stages of adsorbate-adsorbent interactions.	43
Figure 2.8	Challenges and role of adsorbents in hydro-harsh environments.	44
Figure 2.9	Remediation performance of conventional and Nano-adsorbents.	52
Figure 3.1	The scheme of hydrothermal reduction.	63
Figure 3.2	Mechanical grades of POCS by US standard sieving.	64
Figure 3.3	Garnet ferrites diffractogram showing 100% phase purity.	68
Figure 3.4	A typical cyclic voltammogram.	75
Figure 3.5	A typical model circuit.	77

Figure 3.6	Model fit in Nyquist plot.	78
Figure 4.1	XRD patterns of the (a) $\text{CuFe}_2\text{O}_4$ (b) $\text{CuCe}_{0.2}\text{Fe}_{1.8}\text{O}_4$ (c) $\text{CuCe}_{0.2}\text{Fe}_{1.8}\text{O}_4$ -rGO.	92
Figure 4.2	FTIR spectra of (a) $\text{CuFe}_2\text{O}_4$ (b) $\text{CuCe}_{0.2}\text{Fe}_{1.8}\text{O}_4$ (c) $\text{CuCe}_{0.2}\text{Fe}_{1.8}\text{O}_4$ -rGO.	94
Figure 4.3	TGA analysis of (a) rGO (b) $\text{CuCe}_{0.2}\text{Fe}_{1.8}\text{O}_4$ -rGO nanocomposites.	95
Figure 4.4	FESEM images (a) $\text{CuFe}_2\text{O}_4$ (b) $\text{CuCe}_{0.2}\text{Fe}_{1.8}\text{O}_4$ (c) $\text{CuCe}_{0.2}\text{Fe}_{1.8}\text{O}_4$ -rGO nanocomposites.	96
Figure 4.5	EDS and elemental mapping in $\text{CuCe}_{0.2}\text{Fe}_{1.8}\text{O}_4$ -rGO nanocomposites.	97
Figure 4.6	Raman spectrum of $\text{CuCe}_{0.2}\text{Fe}_{1.8}\text{O}_4$ -rGO nanocomposites.	99
Figure 4.7	VSM hysteresis loops of (a) $\text{CuFe}_2\text{O}_4$ (b) $\text{CuCe}_{0.2}\text{Fe}_{1.8}\text{O}_4$ -rGO (c) $\text{CuCe}_{0.2}\text{Fe}_{1.8}\text{O}_4$ nanocomposites.	101
Figure 4.8	Mechanical and physical treatments.	104
Figure 4.9	Particle size distribution curve of POCS.	107
Figure 4.10	FTIR spectrum and functional groups peaks. Inset showing the 1200 to 4000 $\text{cm}^{-1}$ .	108
Figure 4.11	FESEMs, micro porous structure of POCS (A) 50 $\mu\text{m}$ (B) 400 $\mu\text{m}$ (C) 500 $\mu\text{m}$ (D) EDX composition.	109
Figure 4.12	The model predicted and experimental results.	111
Figure 4.13	3D response surface plots. RSM 1 Arsenic initial Conc. ( $\text{mg L}^{-1}$ ) and POCS dose (mg) RSM 2 Temp vs POCS dose (mg). RSM 3 Initial pH vs POCS dose (mg) RSM 4 Temp. vs Arsenic initial Conc. ( $\text{mg L}^{-1}$ ). RSM 5 pH vs Arsenic initial Conc. ( $\text{mg L}^{-1}$ ), RSM 6 pH and Temp ( $^{\circ}\text{C}$ ).	114
Figure 4.14	2D Contour plots. CP 1 Arsenic initial Conc. ( $\text{mg L}^{-1}$ ) and POCS dose (mg) CP 2 Temp vs POCS dose (mg). CP 3 Initial pH vs POCS dose (mg) CP 4 Temp. vs Arsenic initial Conc. ( $\text{mg L}^{-1}$ ). CP 5 pH vs Arsenic initial Conc. ( $\text{mg L}^{-1}$ ) and CP 6 pH and Temp ( $^{\circ}\text{C}$ ).	116
Figure 4.15	Molecular structure of Acephate (AP).	119
Figure 4.16	HPLC schematic	120

Figure 4.17	I-1, I-2, I-3, I-4 and I-5 represent Freundlich, Langmuir, Temkin, DR and FH Isotherms respectively.	123
Figure 4.18	A comparison of $Q_e$ predicted by different isotherm models.	123
Figure 4.19	K1, K2, K3 show the 1 <sup>st</sup> , pseudo 2 <sup>nd</sup> and intraparticle diffusion models respectively.	125
Figure 4.20	Comparison among experimental and model predicted results for AP adsorption.	125
Figure 4.21	XRD spectra [A] un-doped $\text{CuFe}_2\text{O}_4$ , [B] doped $\text{CuCe}_{0.1}\text{Fe}_{1.9}\text{O}_4$ , [C] $\text{CuCe}_{0.2}\text{Fe}_{1.8}\text{O}_4$ , [D] $\text{CuCe}_{0.3}\text{Fe}_{1.7}\text{O}_4$ , [E] $\text{CuCe}_{0.4}\text{Fe}_{1.6}\text{O}_4$ , and [F] $\text{CuCe}_{0.5}\text{Fe}_{1.5}\text{O}_4$ adsorbents for fluoride, annealed at 650 °C for 3 h.	131
Figure 4.22	(A) Effect of the applied potential on the current response and (B) Nyquist diagrams of (x=0) un-doped $\text{CuFe}_2\text{O}_4$ (x=0.1), doped $\text{CuCe}_{0.1}\text{Fe}_{1.9}\text{O}_4$ (x=0.2), $\text{CuCe}_{0.2}\text{Fe}_{1.8}\text{O}_4$ (x=0.3), $\text{CuCe}_{0.3}\text{Fe}_{1.7}\text{O}_4$ (x=0.4), and $\text{CuCe}_{0.4}\text{Fe}_{1.6}\text{O}_4$ (x=0.4) $\text{CuCe}_{0.5}\text{Fe}_{1.5}\text{O}_4$ in 0.1 M KCl solution containing 1.0 mM $\text{K}_3[\text{Fe}(\text{CN})_6]$ and $\text{K}_4[\text{Fe}(\text{CN})_6]$ (1:1).	132
Figure 4.23	FTIR overlay spectra of (A) un-doped $\text{CuFe}_2\text{O}_4$ , (B) doped $\text{CuCe}_{0.1}\text{Fe}_{1.9}\text{O}_4$ , (C) $\text{CuCe}_{0.2}\text{Fe}_{1.8}\text{O}_4$ , (D) $\text{CuCe}_{0.3}\text{Fe}_{1.7}\text{O}_4$ , (E) $\text{CuCe}_{0.4}\text{Fe}_{1.6}\text{O}_4$ , and (F) $\text{CuCe}_{0.5}\text{Fe}_{1.5}\text{O}_4$ .	133
Figure 4.24	FESEM images of (A) un-doped $\text{CuFe}_2\text{O}_4$ , (B) doped $\text{CuCe}_{0.1}\text{Fe}_{1.9}\text{O}_4$ , (C) $\text{CuCe}_{0.2}\text{Fe}_{1.8}\text{O}_4$ , (D) $\text{CuCe}_{0.3}\text{Fe}_{1.7}\text{O}_4$ , (E) $\text{CuCe}_{0.4}\text{Fe}_{1.6}\text{O}_4$ , and (F) $\text{CuCe}_{0.5}\text{Fe}_{1.5}\text{O}_4$ prepared in micro-emulsion (w=15).	135
Figure 4.25	Magnetic properties of (A) un-doped $\text{CuFe}_2\text{O}_4$ , (B) doped $\text{CuCe}_{0.1}\text{Fe}_{1.9}\text{O}_4$ , (C) $\text{CuCe}_{0.2}\text{Fe}_{1.8}\text{O}_4$ , (D) $\text{CuCe}_{0.3}\text{Fe}_{1.7}\text{O}_4$ , (E) $\text{CuCe}_{0.4}\text{Fe}_{1.6}\text{O}_4$ , and (F) $\text{CuCe}_{0.5}\text{Fe}_{1.5}\text{O}_4$ .	138
Figure 4.26	Effect of some concomitant anions on fluoride adsorption, $m=0.1\text{ gL}^{-1}$ , $[\text{F}]_0 = 10\text{ mgL}^{-1}$ , $\text{pH}=7.0$ : (A) un-doped $\text{CuFe}_2\text{O}_4$ , (B) doped $\text{CuCe}_{0.2}\text{Fe}_{1.8}\text{O}_4$ , (C) $\text{CuCe}_{0.3}\text{Fe}_{1.7}\text{O}_4$ , and (D) $\text{CuCe}_{0.5}\text{Fe}_{1.5}\text{O}_4$ .	140
Figure 4.27	Response surfaces showing the effects of two variables on fluoride adsorption (A) pH and $\text{F}^{-1}$ ( $\text{mg L}^{-1}$ ), (B) pH and Ads. Dose (mg), (C) $\text{F}^{-1}$ ( $\text{mg L}^{-1}$ ) and Ads. Dose (mg), and (D) Temp. ( $^{\circ}\text{C}$ ) and Ads. Dose (mg).	143
Figure 5.1	Further work plan for future studies.	147

## LIST OF TABLES

Table 2.1	Some common method for Nano-adsorbents preparations.	11
Table 2.2	Hydrothermal method superiority over other method for nanomaterial synthesis.	17
Table 2.3	Waste water treatment with CNTs adsorbents.	28
Table 2.4	Regeneration and reuse of Nano-adsorbents.	31
Table 2.5	Magnetic Adsorbents for hydrological remediation.	34
Table 2.6	Outstanding Nano-adsorbents for heavy metal removal.	38
Table 2.7	Experimental conditions for Nano-adsorbents applications.	39
Table 2.8	General problems and issues of adsorbents	45
Table 2.9	The protective measure for iron oxides	46
Table 2.10	The comparative removal efficiency of remediation techniques.	53
Table 2.11	Adsorbents regeneration methods.	57
Table 3.1	List of chemicals.	61
Table 3.2	Chronology of ion exchange chromatography.	73
Table 3.3	IC measurement conditions.	74
Table 4.1	Crystallite sizes and micro-strain in $\text{CuFe}_2\text{O}_4$ , $\text{CuCe}_{0.2}\text{Fe}_{1.8}\text{O}_4$ , and graphene $\text{CuCe}_{0.2}\text{Fe}_{1.8}\text{O}_4$ nanocomposites.	93
Table 4.2	Magnetic saturation (Ms), remanence (Mr) and coercivity (Hc) of $\text{CuFe}_2\text{O}_4$ , $\text{CuCe}_{0.2}\text{Fe}_{1.8}\text{O}_4$ and graphene - $\text{CuCe}_{0.2}\text{Fe}_{1.8}\text{O}_4$ .	100

Table 4.3	The CCD variables, symbols and levels.	105
Table 4.4	Arsenic adsorption statistical analysis results.	112
Table 4.5	Isotherms results for Acephate.	122
Table 4.6	Acephate Kinetic models results.	124
Table 4.7	Thermodynamics constants.	126
Table 4.8	Crystal sizes and the micro-strain and BET properties of a series of copper ferrites $\text{CuCe}_x\text{Fe}_{2-x}\text{O}_4$ ( $x=0$ to $0.5$ ).	130
Table 4.9	Magnetic properties of the $\text{CuCe}_x\text{Fe}_{2-x}\text{O}_4$ adsorbents by VSM.	136
Table 4.10	Retention times of the selected anions during ion chromatography.	138

## LIST OF EQUATIONS

Equation 2.1	Ionic state of Cr (VI) at acidic p <sup>H</sup>	27
Equation 2.2	Reduction of Cr (VI) to Cr (III).	27
Equation 2.3	Reaction between Cr <sup>3+</sup> and water.	27
Equation 2.4	Cations adsorption.	27
Equation 2.5.	Adsorption capacity of adsorbents.	40
Equation 2.6.	The Quadratic model.	41
Equation 3.1	Uniformity coefficient of adsorbents.	65
Equation 3.2	Coefficient of gradation.	65
Equation 3.3	Debye Scherrer's formula.	67
Equation 3.4	Bragg $\beta hkl$ .	67
Equation 3.5	Relation between anodic and cathodic peak potentials.	76
Equation 3.6	Nernst equation	76
Equation 3.7	Peak current	76
Equation 3.8	Number of moles of samples in redox reaction.	77
Equation 3.9	Adsorption capacity of adsorbents.	79
Equation 3.10	The Quadratic model.	79
Equation 3.11	The Langmuir adsorption model.	81

Equation 3.12.	The maximum adsorption capacity ( $Q_{max}$ ).	81
Equation 3.13	The separation factor.	81
Equation 3.14	Freundlich model.	82
Equation 3.15	Temkin model.	83
Equation 3.16	FH model.	83
Equation 3.17	The surface coverage.	83
Equation 3.18	DR model.	83
Equation 3.19	DR model $\epsilon$ .	84
Equation 3.20	A general reaction.	84
Equation 3.21	Rate law.	85
Equation 3.22	Zero order.	85
Equation 3.23	First order.	86
Equation 3.24	Integration first order equation.	86
Equation 3.25	Rate equation.	87
Equation 3.26	Pseudo-1st order model.	88
Equation 3.27	Pseudo 2nd order model.	88
Equation 3.28	Intra-particle diffusion model.	88
Equation 3.29	Bangham's model.	89

Equation 3.30	Gibbs free energy.	89
Equation 3.31	Enthalpy of adsorption.	89
Equation 3.32	The entropy of adsorption.	89
Equation 4.1	The average crystal size.	92
Equation 4.2	The micro strain of crystals.	92
Equation 4.3	The proposed quadratic model for Arsenic.	110
Equation 4.4	% AP by HPLC method.	120
Equation 4.5	Adsorption capacity with time " $Q_t$ ".	124
Equation 4.6	Reaction in chemical suppressor.	139
Equation 4.7	Fluorides I.C detection.	139
Equation 4.8	The proposed model for Fluorides.	141

## LIST OF SYMBOLS AND ABBREVIATIONS

AC	:	Alternating current
ACN	:	Acetonitrile
Ads	:	Adsorbent
ANOVA	:	Analysis of variance
AP	:	Acephate
ATR	:	Attenuated total reflectance spectroscopy
ASB	:	Aluminum tri-sec-butoxide
BET	:	Brunauer-Emmett- Teller
CE	:	Counter electrode
CNS	:	Central nervous system
CPE	:	Cloud point extraction
CP	:	Contour plots
CTAB	:	Cetyltrimethyl ammonium bromide
$C_u$	:	Uniformity coefficient
$C_z$	:	Coefficient of gradation
CV	:	Cyclic voltammetry
CNT	:	Carbon nanotubes
$D$	:	Crystallite size
3D	:	Three dimensional
DC	:	Direct current
DOE	:	Design of Experiments
DR	:	Dubinín-Radushkevich model
dSPE	:	Dispersive solid phase extraction
DRS	:	Diffuse Reflectance spectroscopy
DLLME	:	Dispersive liquid-liquid micro-extraction
$E^o$	:	Standard electrode potential
EDTA	:	ethylene di-ammine tetra acetic acid
EDS	:	Energy Dispersive X-ray
EIS	:	Electrochemical impedance spectroscopy
$E_{pc}$	:	Cathodic peak potential
$E_{pa}$	:	Anodic peak potential
$E^o_f$	:	Formal electrode potential
EPA	:	Environmental Protection Agency
F	:	Faraday's constant
FH	:	Flory Huggins
FRA	:	Frequency response analysis
FTIR	:	Fourier Transform Infrared Spectroscopy
FWHM	:	Full width at half maximum
GI	:	Galvanized iron
GO	:	Graphene Oxide
GCE	:	Glassy carbon electrode
HDTMA	:	hexadecyltrimethylammonium bromide
HPLC	:	High Performance Liquid Chromatography
HRTEM	:	High resolution transmission electron microscopy
HWPT	:	Household water pre-treatment
I	:	Current
$I_{pc}$	:	Cathodic peak current
IC	:	Ion chromatography

ISC	:	Inner sphere complexes
ICPMS	:	Inductively coupled mass spectrometry
JCPDS	:	Joint Committee on Powder Diffraction Standards
LLE	:	Liquid-Liquid Extraction
LFD	:	Large Field Detector
LOD	:	Limit Of Detection
MALLE	:	Membrane-Assisted Liquid-Liquid Extraction
MOFs	:	Metal Organic Frameworks
MWCNT	:	Multi-Wall Carbon Nanotubes
$M_r$	:	Magnetic Resonance
$M_s$	:	Magnetic Saturation
MS	:	Mild Steel
MPTES	:	Mercaptopropyl triethoxysilane
MCL	:	Maximum Concentration Level
$\eta$	:	Lattice strain
NP	:	Nanoparticle
OSC	:	Outer sphere complexes
OVAT	:	One Variable at a Time
OPA	:	sec-octylphenoxy acetic acid
POCS	:	Palm Oil Clinker Sand
POPs	:	Persistent Organic Pollutants
PDMS	:	Polydimethyl Siloxanes
PXRD	:	Powder X-ray diffraction
Q	:	Charge
QA	:	Quality assurance
QC	:	Quality control
$Q_e$	:	Adsorption capacity
$Q_m$	:	Maximum Adsorption Capacity
R	:	Resistance
$R_{ct}$	:	Electron transfer resistance
rGO	:	Reduced Graphene Oxide
R %	:	Percent removal
$R^2$	:	Correlation coefficient
RA	:	Residuals analysis
RE	:	Reference electrode
RSD	:	Relative standard deviation
RSM	:	Response Surface Method
SPE	:	Solid-phase extraction
SPME	:	Solid-phase micro-extraction
SBSE	:	Stir-bar sorptive extraction
SDME	:	Single-drop micro-extraction
SDS	:	Sodium dodecyl sulfate
SWCNT	:	Single-Wall carbon nanotubes
SMART	:	Storm water Management and Road Tunnel
TAH	:	Tetramethyl ammonium hydroxide
TO	:	Tetraethyl orthosilicate
$t_R$	:	Retention time
UF	:	Ultrafiltration
$\mu m$	:	Micro meter
W	:	Warburg diffusion
WE	:	Working electrode
WHO	:	World health organization

## LIST OF APPENDICES

Appendix A	Kinetic models 1st order, 2nd order, Bangham and intraparticle diffusion.	174
Appendix B	Isotherms Models: Langmuir, Freundlich, DR, FH and Temkin at 313K.	175
Appendix C	Variables and level of Central composite design for fluoride adsorption model.	176
Appendix D	Analysis of variance (ANOVA) for the fluoride quadratic model.	176
Appendix E	Central composite design arrangement and IC response observed and predicted.	177
Appendix F	The number of solutions provided along with the desirability factor.	178
Appendix G	The factors and related coefficient estimate, standard error and confidence intervals.	181
Appendix H	ICPMS response for Arsenic adsorption by POCS adsorbents.	182



been dedicated to overcome the global problems with the application of novel adsorbents (Wang et al., 2005). However, the major challenge is the preparation of green adsorbents, with desirable properties to solve a particular environmental problem (Cevasco et al., 2014). The WOS analysis elaborates that it is a multidisciplinary research attracting parallel attention from chemists, physicists, engineers, environmentalists and geologists.

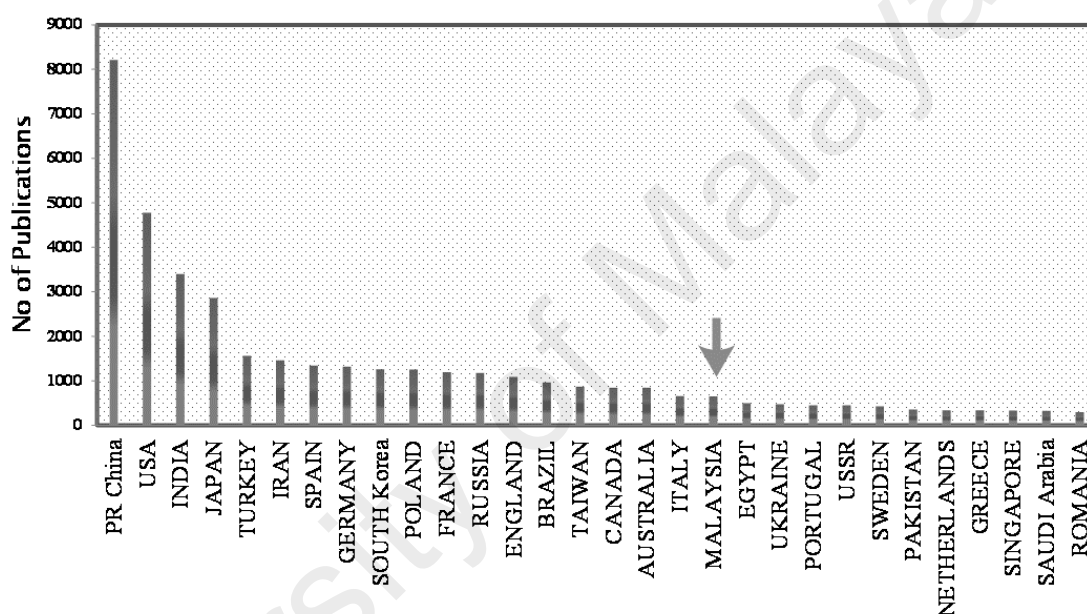


**Figure 1.2. Country wise estimate of increase in the research activity in the area of adsorbents for hydrological remediation.**

## 1.2 Characterizations methods

The detailed characterization and analysis with Fourier Transform Infrared spectroscopy (FTIR) (Perkin Elmer System 2000 series), Raman spectroscopy (Renishaw 2000 system), X-ray Diffraction (XRD) PANalytical Empyrean), equipped with a monochromatic Cu K $\alpha$  radiation source, Energy dispersion spectroscopy (EDS), BET surface area, particle size analyzer, Zeta Potential (ZP), Thermogravimetric analysis (TGA & DTA), Field emission scanning electron microscopy (FESEM), Transmission Electron microscopy (TEM), Nuclear magnetic resonance (NMR), High

performance liquid chromatography (HPLC), ion chromatography (IC), Inductively coupled mass spectroscopy (ICPMS), Electrochemical impedance spectroscopy (EIS), cyclic voltammetry (C.V) and Diffuse Reflectance spectroscopy (DRS) revealed the formation of impurity free adsorbents.

### **1.3 Applications or modelling**

A novel investigation in modelling of adsorptive and catalytic degradation of hydro contaminants using response surface methods (RSM) and central composite design (CCD) method was developed to remove pollutants from hydrological samples. The complex nature of all the interaction was explained by a number of isotherms and kinetic models. Kinetic models: pseudo first order, pseudo second order, Banghams, intra-particle diffusion, and the equilibrium models: Langmuir, Freundlich, Temkin, Dubenin Redushkvich (DR), Flory Huggins (FH) were applied to test for goodness of fit and to explain the adsorption mechanisms.

### **1.4 Problem statement**

Environmental pollution is a global issue and water contamination is one of the major concerns because the occurrence of pollutants is increasing over time. This study concerns application of new series of adsorbents preparation, characterization, applications and modeling for green environment remediation. Society has a need for safe water free from chemical pollutants to avoid health risks and the environment deteriorations. Neither situation can afford to wait for scientists to provide all the answers or to wait for agreement before any actions are taken. The best possible course of action is to make available the advanced adsorbents to environmental specialists. This study followed a roadmap on geochemical modelling that benefits geochemists, hydrologists, engineers and town planners. Most practitioners in the environmental field lack formal training in geochemical modelling at the same time they have to work under

stringent deadline, budget, and regulatory constraints. A lack of understanding of geochemistry and competent research designs may lead to the failure of remediation techniques. Failure in combating pollutants can be resolved by the use of magnetic, energy efficient, economical adsorbents with added recycle and reuse capabilities. Some researches argue that geochemical modelling does not produce practical useful results. Through this study we demonstrate the use of geochemical modelling as a systematic, effective and efficient tool for the solution of environmental problems. The study proposes the use of raw material from indigenous Palm oil industry, magnetic ferrites and graphene supported magnetic ferrites that are rich in functional groups, surface morphology, crystal structure, mechanical strength, thermal properties, electrical and magnetic properties suitable for environmental remediation.

### **1.5 Aims and objectives**

It is a challenge to produce specific and competent types of adsorbent materials for the application in hydrological decontamination strategies. The environmental remediation is dependent on the conditions and starting material used during the preparation of adsorbents. The preparative conditions variables such as ferrites composition, types, time, temperature and medium turbulence along with pH will significantly change the surface morphology, surface area, pore volume, pore size and distribution and interaction functional groups. From the pilot scale to the industrial scale, removal of hydrological pollutants needs to take into consideration the preparation, specifications, intended use, to fully realize the benefits of applying magnetic Nano-adsorbents. The following objectives have been addressed in this work.

1. To prepare, characterize and use adsorbents of natural and synthetic origin from suitable, economical, green and environment friendly sources, by

converting them into particles of suitable specific gravity, fitness modulus and adsorption characteristics.

2. To fabricate composite ferrite materials and enhance the hydro decontamination efficiencies for the optimum removal of heavy metals, anionic species and organophosphorus pesticides.
3. To optimize or model using the equilibrium isotherms including Langmuir, Freundlich, Temkin, Dubinin-Redishkevich (DR), Florry huggins (FH) model.

The methods, instruments and statistical procedures to collect, analyze and interpret the experimental data and findings are presented. The experimental setup used to make magnetic adsorbents via mechanical milling, sol-gel method, micro-emulsions, co-precipitation, various analytical and spectroscopic techniques for adsorbents characterization and environmental applications are described. All experiments are distinctive from each other and in each situation standard procedures were followed for data collection, interpretation and presentation. The experimental parameters were optimized through two strategies: one variable at a time (OVAT) as well as design of experiment (DOE). The adsorption experiments were repeated at least three times to establish the reproducibility of the experimental results. Maximum care is taken in the design, conduct, collection and analysis of experimental results.

## **1.6 Thesis outline**

This thesis presents preparation of adsorbents, characterization and application for green environment remediation. Chapter 1 describes the general introduction on adsorbents, characterization, optimization and modelling, problem statement as well as the aim and objectives. Chapter 2 presents a review of the relevant literature on adsorbents, methods of preparation and the fabrication of nanocomposite ferrites.

Chapter 3 comprises materials and methods used to prepare, characterize and model the application of adsorbents. Chapter 4 discusses a novel series of Graphene based ferrite adsorbent based on the hydrothermal fabrication of copper ferrite. The magnetic adsorbents series are characterized by XRD, Raman, EDX, FESEM and TGA techniques. It is also dedicated to the development of novel POCS adsorbent from abundant indigenous agricultural resource as a green alternative series of adsorbents. This chapter discusses magnetic copper ferrite adsorbent for fluorides removal using design of experiments (DOE). The use of ion chromatography and electrochemical methods is highlighted. Chapter 5 summarizes the thesis, leading to conclusions and future work.

## CHAPTER 2: LITERATURE REVIEW

The success of green environmental remediation is dependent on the reliability of data, design of work, experimentation, application of precise and accurate research methodology. Normally, geological features of the study area are well documented by field observation followed by mechanical, physical and chemical analysis to interpret the causes of a particular environmental problem. In this regards, the geochemical models are efficient and selective in terms of large scale data presentation, three dimensional maps building through the use of vector and raster data. The interpretation of geochemical model identifies the environmental issue and local point pollution resources e.g. industrial waste, hospital waste or house waste. The identified problem is resolved by the application of magnetic Nano-adsorbents by following OVAT or DOE strategies to reduce time, cost and efforts. Well-planned and performed experiments ordinarily give reproducible and reliable data.

The acceptable water quality criterion has a dynamic link with the local environmental conditions, availability of fresh water resources and public health benefits. Public health relies on the supply of water free from toxic substances and harmful pathogens. An appraisal of water supply system indicates the population exposed to fecal contamination because of leakage of the water supply channels and mixing of sewer water adversely affects the good health of consumer communities (Kyle Onda et al., 2013). Usually natural water resources are found to have elevated levels of pathogens and contaminants because of discharge of the municipal, industrial, agrochemicals, agricultural, hospital and households waste into streams, lakes and rivers (Azizullah et al., 2011). Research findings highlights that even occasional consumption of contaminated water may result in severe health effects (Azizullah et al., 2011). The improve public health necessitates the need for a careful and continuous monitoring

program of water resources (Onda et al., 2012). The global pollution problem of the natural resources need to be resolved to enjoy the full benefits of the safe water practice (Reidy et al., 2013). The surroundings effects in these varied environments arises from some basic factor such as pH, temperature fluctuations, high concentration of pollutants, complex nature of interaction among the pollutants and greater volumes of domestic and industrial effluents (Farré et al., 2012). A number of studies has been undertaken to understand the release, transport, transformation and fate of pollutants in the environment (Gao et al., 2013). It appears that a strategic design of pollutants removal is a primary concern to improve present and future public health (Gao et al., 2013).

## **2.1 Green environmental remediation**

The twelve principles of green chemistry provide the grounds for the design and application of green environmental remediation strategies. These guiding principles emphasize the minimum use of energy, solvents and chemicals to protect the natural ecosystems of the planet as shown in **Figure 2.1** (Ashraf et al., 2014). A green route for adsorbents preparation requires least toxic, readily available, renewable raw materials with minimum use of chemicals, energy, processing and minimal side products. The active surface of adsorbents should be self-sufficient to interact with a large amount of the desired adsorbate molecules. The preparation of adsorbents should be monitored continuously to prevent spread of environmental pollutants. The preparation, characterization and application processes should be safe free from explosions or accidents. A long term strategic economic development design calls for environmental protection as a tangible contributor and facilitator of economic development and should not be regarded as an obstacle and burden in the minds of the relevant stake holders. It must be realized that economic growth is essentially linked to clean and protected environment. A win-win goal of environmental conservation and accelerated economic

development must be achieved without sacrificing either of the two in the struggle against global environment pollution.

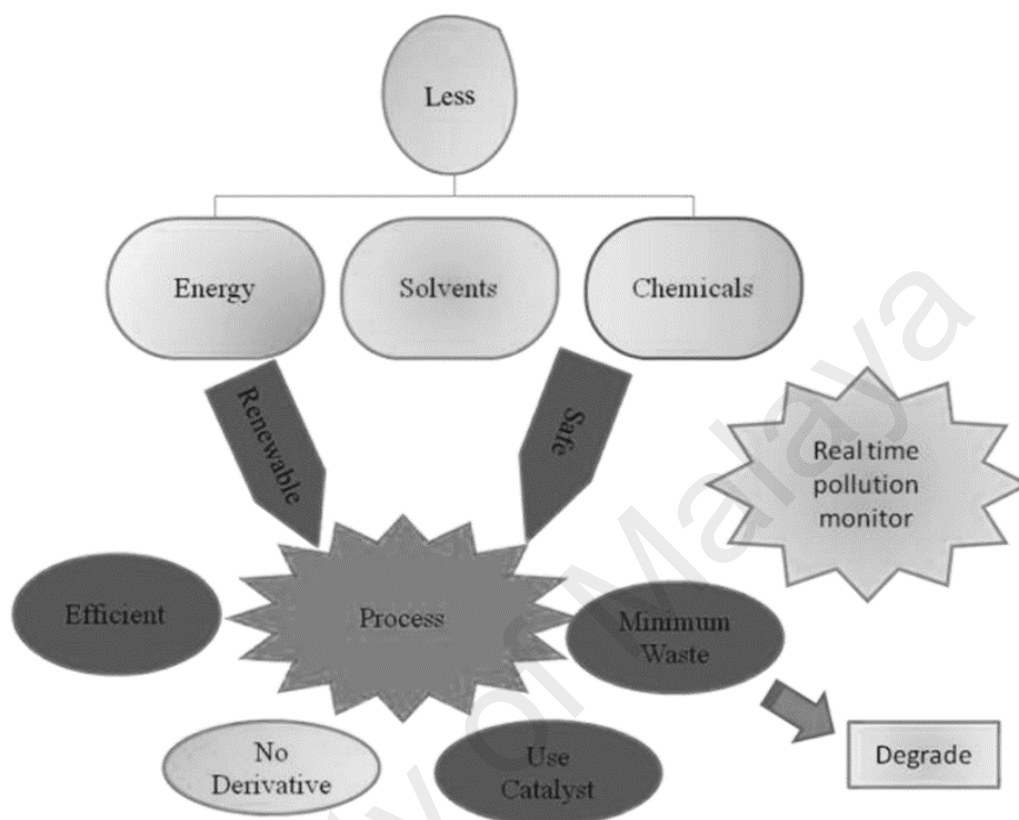


**Figure 2.1 the principles of green environment remediation.**

In the present thesis, the analysis of literature guided to prepare natural and magnetic Nano-adsorbents by green remediation strategies.

## **2.2 Preparation of Nano-adsorbents**

Magnetic adsorbents play a very important role in hydrogeological decontaminations, separation, physical and materials sciences. The superior physical, chemical, thermal, electrical, optical and magnetic properties attract extensive applications in green environmental remediation, removal of pollutants from drinking water, river water and polluted water resources. In this context, preparation of adsorbent is a very important assignment for material scientists. In this work, we have fabricated

the different series of adsorbents by the hydrothermal, sol-gel method, micro-emulsions, co-precipitation, and mechanical milling methods.

Novel classes of adsorbents have become a feasible and achievable objective because of flexible material structure, desirable functionalities, and advancement in nanotechnology (Ramsden, 2011). The use of adsorbents is dependent on their physical, mechanical and chemical properties that can be fine-tuned by an appropriate preparation method (Yu et al., 2008). The current literature about advanced adsorbents emphasize that the fabrication of adsorbent is an important area of research, particularly when carried with a precise control over different physicochemical properties, such as particle size, shape and crystalline structure (Vamvasakis et al., 2015). Because of small size, high active surface area, and porosity, Nano-adsorbents are not only capable of removing pollutants with diverse types, size, hydrophilicity, hydrophobicity and speciation, but also have competitive metal binding capacities. The adsorbents micro-structures can be controlled and optimized along a range of temperature, pH, reactants concentration and variety of preparation methods to facilitate the formation of desired functionalities (**Table 2.1**). The reported preparation methods has many advantages including environment friendliness, high purity products, low cost and size and homogeneity control of the products e.g. monocrystalline magnetic  $\text{Fe}_3\text{O}_4$ ,  $\text{Al}_2\text{O}_3$  and  $\text{TiO}_2$  etc. In accordance with these desirable objectives, generally researchers apply two main approaches, i. top down and ii. Bottom up to design and control the process of synthesis.

**Table 2.1: Some common method for Nano-adsorbents preparations.**

Type of nanomaterial	method	Starting materials	BET surface area (m <sup>2</sup> /g)	Size (nm)	Temp.(K)	p <sup>H</sup>	time (hr)	Ref.
Alumina	Sol gel	ASB: HCL: (CH <sub>3</sub> ) <sub>2</sub> CHOH: C <sub>2</sub> H <sub>5</sub> OH	NA	50	355	9.5	36	(Pacheco et al., 2006)
γ-Al <sub>2</sub> O <sub>3</sub>	Sol-gel	AlCl <sub>3</sub> : NH <sub>3</sub> : CH <sub>3</sub> COOH	292	6	773	NA	72	(Zeng et al., 1998)
γ-Fe <sub>2</sub> O <sub>3</sub>	Sol-gel	FeCl <sub>3</sub> : NaOH: H <sub>2</sub> O <sub>2</sub>	NA	15	353	8	24	(Hu et al., 2007)
NiO	Sol-gel	(CH <sub>3</sub> COO) <sub>2</sub> Ni: C <sub>2</sub> H <sub>5</sub> OH : HOCCOOH	NA	22	383	NA	24	(Thota et al., 2007)
TiO <sub>2</sub>	Sol gel	Ti(SO <sub>4</sub> ) <sub>2</sub> : Fe <sub>2</sub> O <sub>3</sub>	330	6	NA	NA	NA	(Ilisz et al., 2003)
TiO <sub>2</sub> /silica	Sol-gel	TO: C <sub>2</sub> H <sub>5</sub> OH: TiO <sub>2</sub>	360	NA	NA	NA	150	(Pitoniak et al., 2005)
Fe <sub>2</sub> O <sub>3</sub> /Au	Sol-gel	Fe(III) acetyl- acetate: CH <sub>3</sub> COOAu	NA	NA	NA	NA	12	(Wang et al., 2007)
Fe <sub>2</sub> O <sub>3</sub> /silica	Co- condensation	FeCl <sub>3</sub> : silica	470	72	383	3.5	24	(Melerio et al., 2007)
Thiolactic acid coated TiO <sub>2</sub>	Sol gel	TiCl <sub>4</sub> : TLA	NA	40-60	NA	NA	2	(Skubal et al., 2002)
Magnetite	Co- precipitation	FeSO <sub>4</sub> : NaNO <sub>3</sub> : NH <sub>4</sub> OH	116	10-15	273	9.5	0.5	(Wei et al., 2007)
Akageneite [β-FeO-(OH)]	Co- precipitation	FeCl <sub>3</sub> : (NH <sub>4</sub> ) <sub>2</sub> CO <sub>3</sub>	100	2.6	298	8	NA	(Deliyanni et al., 2003)

HDTMA*-coated akageneite	Co-precipitation	FeCl <sub>3</sub> : HDTMA: (NH <sub>4</sub> ) <sub>2</sub> CO <sub>3</sub>	231	4.6	298	8	0.5	(Deliyanni et al., 2006)
MnFe <sub>2</sub> O <sub>4</sub>	Co-precipitation	MnCl <sub>2</sub> : FeCl <sub>3</sub> : NaOH	180	20	673	11	2	(Hu et al., 2007)
Fe <sub>3</sub> O <sub>4</sub>	Co-precipitation	FeCl <sub>3</sub> : HNO <sub>3</sub> : TAH: ethylene glycol	97.7	15	673	NA	4	(Hurt et al., 2006)
γ-Fe <sub>2</sub> O <sub>3</sub>	Co-precipitation	FeCl <sub>2</sub> : HCl	97.7	15	NA	NA	NA	(Uheid et al., 2006)
Ceria nanoparticles coated CNT	Catalytic pyrolysis	C <sub>3</sub> H <sub>6</sub> /H <sub>2</sub>	189	NA	723	9	1	(Peng et al., 2005)
Cyclodextrin-coated CNT	Chemical vapor deposition	C <sub>2</sub> H <sub>2</sub> : β-cyclodextrin: dimethyl formamide	NA	NA	343	NA	24	(Salipira et al., 2007)
MnO <sub>2</sub> -coated CNT	Catalytic pyrolysis	C <sub>3</sub> H <sub>6</sub> : H <sub>2</sub> : Ni: CNT: HNO <sub>3</sub> : MnO <sub>2</sub>	NA	NA	353	NA	24	(Wang et al., 2007)
HNO <sub>3</sub> -modified MWCNT	NA	CNT: HNO <sub>3</sub>	254	NA	413	5	6	(Wang et al., 2007)
			NA	6	413	7	24	(Li et al., 2003)

Note. ASB = aluminum tri-sec-butoxide; HDTMA = hexadecyltrimethylammonium bromide; TAH = Tetramethyl ammonium hydroxide; TO = tetraethyl orthosilicate; NA = not available.

Despite their different mode of work, both type of synthesis techniques are known to improve the manufacturing cost, reduce the need for solvent and minimize waste generation criteria for the green environmental remediation.

### **2.2.1 Top-down approach**

The “top-down” approach mainly refers to slicing or successive breaking down of the bulk materials e.g. POCS, for the formation of nanoparticles. In this approach the shape or structure is optimized by externally controlled devices. One of the method known top down approaches is mechanical milling. (Priyadarshana et al., 2015).

### **2.2.2 Bottom-up approach**

It follows a step by step building of nanomaterial, where a molecular precursor is decomposed with the generation of atoms or molecular segments that further nucleate and result in the formation of fine and mono-dispersed nanomaterial (Byun et al., 2015). It basically requires condensation of atomic or molecular entities in a liquid or gas phase to form adsorbents with nanometer range size distribution. **Figure 2.2** shows a schematic illustration of the two approaches to make the desired adsorbents. The bottom-up approach is more popular for the synthesis of nanomaterial, and is further sub divided into a) liquid phase b) gas phase or c) vapor phase synthesis. The focus in the present discussion is on the liquid-phase synthesis of nanomaterial. The liquid phase adsorbents synthesis is further divided to include hydrothermal or solvothermal, micro emulsion, auto-combustion, sonochemical and sol-gel synthesis. As the materials reported in the subsequent chapters have been synthesized using *Hydrothermal*, *sonochemical* and *microemulsion* methods, these will be discussed in detail in this chapter. The following sections will present the different bottom up approaches to prepare nano adsorbents.

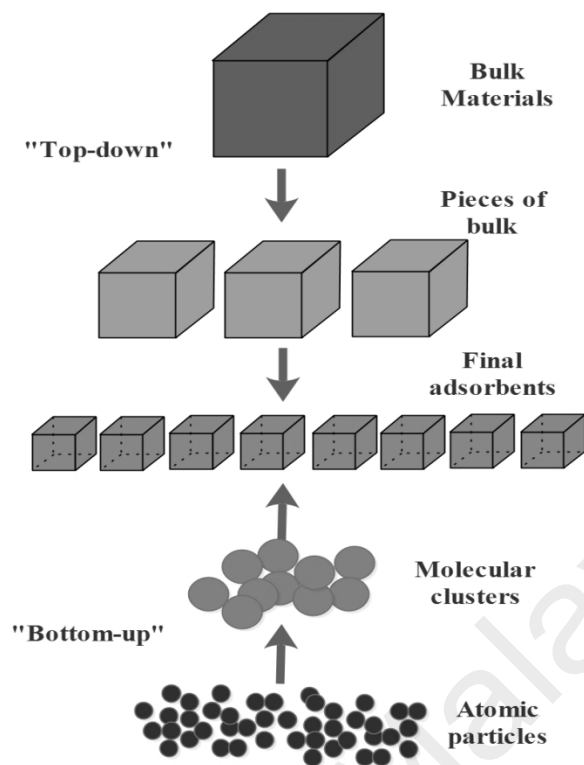


**Figure 2.2. The top-down and bottom-up approach.**

### 2.2.3 Auto-combustion method

It is a method to make nanoparticles with high crystallinity and broad surface areas. During programmed heating regime temperature reached  $\sim 650^{\circ}\text{C}$ , at this stage thermally catalyzed reaction takes place in the presence of redox groups and yield a crystalline product (Mirzaee et al., 2015).

### 2.2.4 Sol-gel process

It is a multi-step process involving the hydrolysis and condensation of alkoxide precursors, the transition of a liquid "sol" to a solid "gel", followed by annealing. The size of sol particles is controlled by altering the synthesis parameters e.g. temp., pH, solvent and surfactants (Amiri, 2015).

### 2.2.5 Micro emulsions

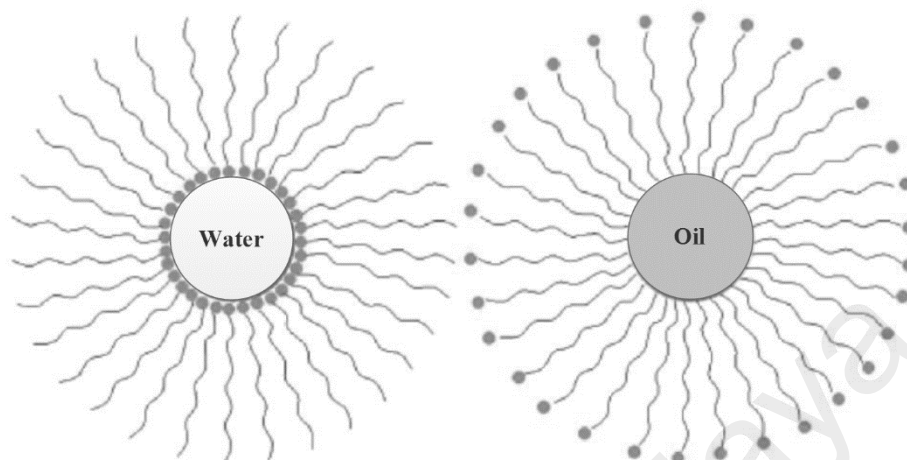


**Figure 2.3. Reverse and normal micelle structure.**

A micro emulsion is a thermodynamically stable isotropic dispersion of polar and non-polar immiscible liquids e.g. water and oil (McClements, 2012). Water is polar and oil is non polar; when mixed together in suitable proportions, two classes are formed i. water in oil (W/O) and ii. Oil in water (O/W) as shown in **Figure 2.3**. A micro emulsion also needs a surfactant to stabilize the interfacial film or surface active molecules. (Rosen et al., 2012). In this current study the micro or Nano emulsion based metal, mixed metal oxides and magnetic ferrites have been prepared and applied for the decontamination of hydrogeological samples.

### 2.2.6 Hydrothermal fabrication

“Hydrothermal” was first introduced by a British Geologist, Sir Roderick Murchison (1792-1871), to explain the action of water at raised temperature and pressure that causes variations in the earth’s crust and forms several minerals and rocks (Kondalkar et al., 2015). A number of minerals, ore deposits were created after hydrothermal process in the presence of water, high temperature and pressures. An in depth understanding of mineral creation in an environment of water, temperature and pressure gave birth to hydrothermal fabrication method. In 1970, hydrothermal method was defined as the

growth of nanoparticles from aqueous solutions in ambient conditions (Byrappa et al., 2012). Later in 1973, it was redefined as the heterogeneous system for recrystallization in superheated aqueous solutions at elevated pressures (Ingebritsen et al., 1999). Similarly, it was also defined as heterogeneous chemical reaction in aqueous solvent or a mineralizer above 100 °C temperature and a pressure above 1 atmosphere (Byrappa et al., 2007). All these definitions are acceptable in material synthesis, but at this stage the exact low limits for the temperature and pressure have not been defined. Many studies have reported hydrothermal temperature higher than 100 °C and pressure >1 atm. In accordance with all these reported hydrothermal conditions, hydrothermal fabrication procedure is described as a heterogeneous reaction, in the company of aqueous or non-aqueous solvent in a closed container e.g. autoclave and Teflon lined stainless steel above room temperature and 1 atm pressure.

Hydrothermal synthesis has been a commonly employed technique for the synthesis of nanomaterial. This technique exploits the solubility of almost all the metal salts in water and then the recrystallization of nanoparticles at elevated temperatures and pressures. Owing to the different structure of water at elevated temperature and very high vapor pressure, solubility and reactivity of molecules changes and water plays a crucial role in the transformation of precursors into products (Byrappa et al., 2007). Different reaction conditions including temperature, time, concentration of reactants and the amount of catalysts can be optimized to maintain nucleation rate and uniform particles size distribution.

Hydrothermal method has several advantages as compared to other methods (**Table 2.2**). Hydrothermal synthesis of nanomaterial in the laboratory needs a reaction vessel, called an autoclave. For the synthesis of metal and mixed metals nanomaterial, very corrosive salt are used over a long time. The autoclave must be constructed with

corrosion resistant materials e.g. Carbon tubes or Teflon lined stainless steel. Autoclave is sealed after addition of all the metallic salts and reagents and placed in an oven at programmed temperature. As the reaction temperature rises, it also increases the pressure inside the Carbon tube/ Teflon necessary for the formation of nanomaterial.

**Table 2.2: Hydrothermal method superiority over other method for nanomaterial synthesis.**

#	Advantages
1	One pot synthesis, close system, less instrumentation, energy and labor.
2	Green, environment friendly, no release of toxic effluents.
3	Generation of high pressure, require low temperature or reduce activation energy.
4	Better stoichiometric control, avoids volatilization of reactants.
5	Offer better options to control nanoparticles size and morphology.

### 2.2.7 Sono-chemical technique

Sonochemistry concerns understanding of ultrasound waves for the formation of acoustic cavitation i.e. formation, growth and implosive collapse of bubbles in liquids. Interestingly, without the use of high temperature, pressure and long-time ultrasound waves efficiently convert precursors into products (Figure 2.4). The theory behind is that ultrasound initiates severe momentary conditions that result in the formation of hot spots with a tremendous rise in temperature above 5000 K, pressure above 1000 atm and heating/ cooling rates around  $1.0 \times 10^{11} \text{ K.S}^{-1}$  (Xiao et al., 2013). The acoustic cavitation plays a vital role during the fabrication of nanomaterial. In a liquid medium, the speed of sound is 1000 to 1500 m/s, wavelength 10 cm to 100  $\mu\text{m}$  and frequency 20 kHz to 15 MHz, which is greater than the molecular scale. The ultrasound has no direct interaction with the precursor but it interacts indirectly by the formation of bubbles,

growth and collapse, generating severe temporary environment with high temperature and pressure for the production of nanomaterials.

The mechanism involved in the ultrasonic synthesis explains the whole scenario for the synthesis of nanomaterial. When a liquid containing precursors is fed to ultrasound treatment, a chemical reaction starts by different mechanisms, as shown in **Figure 2.4**. Primary reaction takes place inside the collapsing bubbles at elevated temperature with the production of free metal atoms after bond dissociations. The free atoms diffuse into the liquid phase, then nucleate and form nanomaterial under appropriate template or stabilizers present in the solution. The non-volatile precursors undergo secondary reaction with the free radicals, outside the collapsing bubbles. The free radicals diffuse into liquid phase to initiate a series of reaction and reduction of metal positive ions ( $M^{n+}$  where,  $n=1,2$  or  $3$ ). The low cost and speedy reaction kinetics enhances the performance of various phase transfer catalysis and improve the catalytic activity.

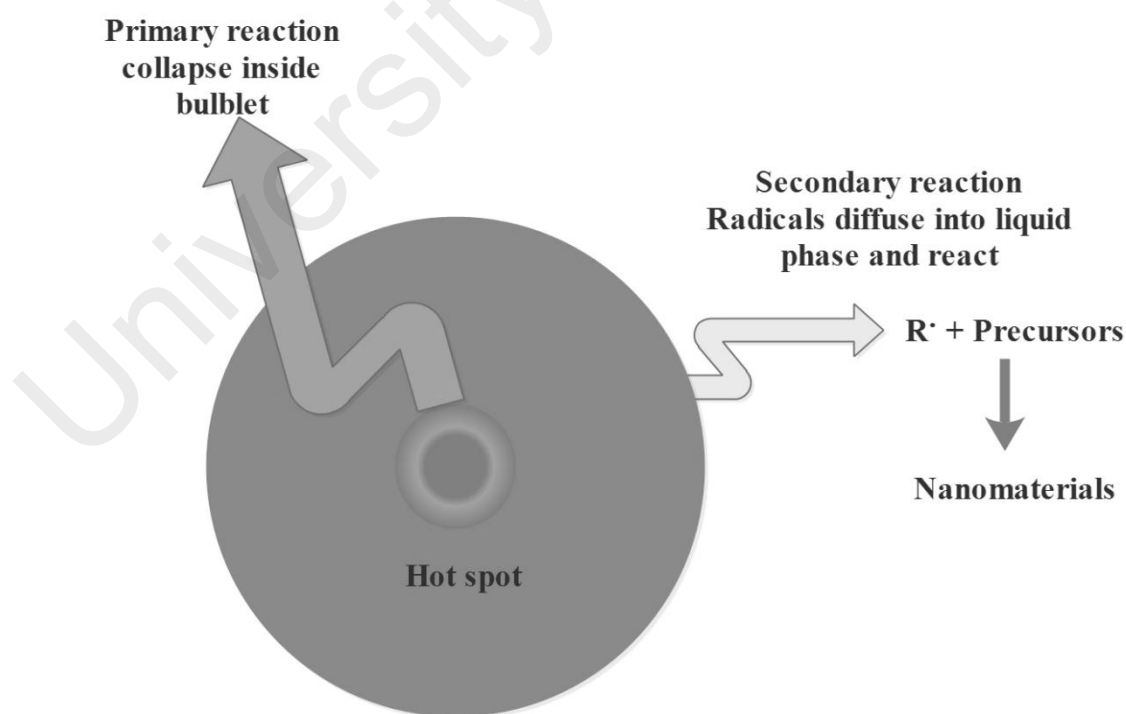


**Figure 2.4. Sonochemical primary and secondary reactions for the formation of nanomaterial.**

### **2.2.8 Agro-industrial waste for environmental remediation**

The increasing interest in the use of agricultural and industrial wastes is because of the dual benefits. It is thought to remove the pollution causing waste and solves the problem of solid waste pollution but also it become an addition revenue resource by converting waste into products (Rehman et al., 2015). From chemical functional groups perspectives these waste are found to be rich in diverse types of functional groups and can be converted into activated carbons, clinkers and sands. The choice of agro-industrial adsorbents is mainly dependent on the processing cost, purity, bulk availability, renewable resources and consistency. Large amount of agricultural residues are annually generated and cause anxiety of environmental pollution to the production managers. From environmental point of view, innocuous dealing of these agro-industrial residues deserve immediate research.

### **2.2.9 Palm oil clinker sand (POCS)**

Palm oil industry generated large amount of waste biomass in the form of empty fruit bunch (EFB), palm shell (PS) and fibrous residues. Nearly 110 million tons of non-oil agricultural mass is produced from palm oil industry each year. Normally, this waste is burnt in boilers to produce steam energy. After calcination in the boiler unit, the unburnt waste biomass is left as waste. This waste has a very fine texture, and is used to produce activated carbons. Each year nearly 4 million tons of palm ash is produced in Malaysia. However, an uncontrolled forest burning, the palm ash is spread into the environment and become a source of air pollution in the region. It calls for a revision in our understanding this abundant natural resource. A properly managed utilization leads to zero waste generation and lot of revenue is generating that makes it a profitable business. On the contrary, un-managed burning of trees only causes environmental pollution **Figure 2.5**.



**Figure 2.5. Burning of old Palm oil trees for Land clearance.**

#### **2.2.10 Properties of adsorbents**

In commercial application, an adsorbent is designed and developed with the anticipated properties. It is expected to own selective, specific, stable and suitable physicochemical properties such as surface morphology, pore size, pore volume, surface area, chemical functional groups, and an option for regeneration and reuse in continuous removal systems (Aksu et al., 2002; Da'na et al., 2011). A review of the currently used green, smart and efficient adsorbent shows a number of classes and types of adsorbents from diverse origins. Among these, silica and carbon-based materials with composite structures have been found to be suitable adsorbents for water treatment techniques (Rehman et al., 2015). The primary property is to taking advantage of the electrostatic attractions between the composite materials and wastes that can be reversed with the use of a suitable regeneration reagent for economic extended re-applications. The other interesting aspects is the separation after use or the recycling of used adsorbents. In this situation several metal oxides having magnetic properties for easy separation (Rehman

et al., 2015). After adsorption process start it has been observed these magnetic metal oxides began to act as catalysts and synergistically improve the decontamination ability of the designed systems (Rehman et al., 2015). Diverse morphologies have been prepared and used to remove toxic substances from the environment. A number of studies were reported for the preparation, characterization and application of unique micro-structure adsorbents and catalysts with dissimilar morphologies that competently remove the environmental contaminations (Sahoo et al., 2014; Su et al., 2014; Xiao et al., 2013). It is noted that uniform, highly dispersed with a suitable support materials e.g. *Nano*-graphene sheets or carbon nanotubes improved adsorbents as compared to bulk forms probably due to surface areas and surface controlled interaction (Rehman et al., 2015). More research interest has risen in magnetic materials as they can be easily directed and separated by a magnetic field and they can be systematically assembled with other materials. By developing the magnetic characteristics in the *Nano*-structured and transition metal oxides, it is thinkable to design water treatment materials that are less cost and high adsorption capacity. The justification behind the research and development of these contaminant removal techniques is because of the increasing concentration of contaminants and failure to achieve the desired level of safe water in the event of stringent water quality standards. The techniques like coagulation, flocculation, and precipitation are generally unsuccessful to remove dissolved contaminants because of the availability of the universal reagents that is suitable for dissimilar contaminants (Trivedi, 2004). The water chlorination and ozone treatments are effective for killing pathogens but some degradation products formed in this process remain as such in the treated water (Camel et al., 1998). The biological processes, bio-filtration, and soil aquifer treatment, have been shown to reduce the concentration of compounds that are biodegradable and/or readily bind to quench particles.

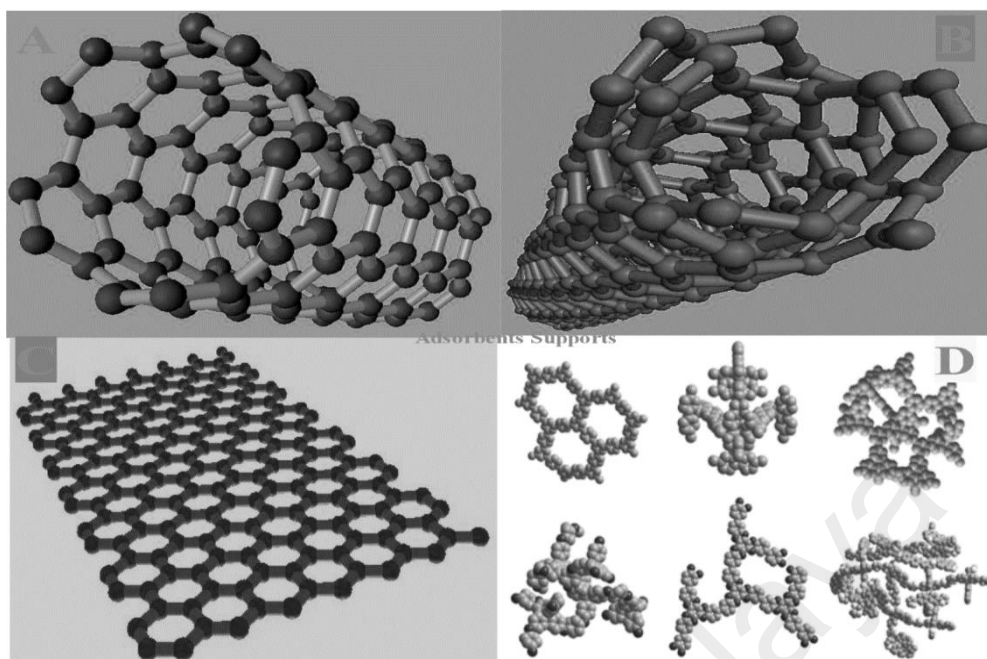


**Figure 2.6. Adsorbents large surface area supports (A) Single wall carbon nanotubes (SWCNT), (B) Multiwall carbon nanotubes (C) Graphene (D) Polymeric supports.**

The commonly used adsorbents such as activated carbons remove organic or inorganic contaminants in water, but the removal efficiency is low and requires longer contact time, suffers inactivation by organic species, and contaminant resuspensions (Gupta, 1998). The advance water treatment processes such as Reverse osmosis (RO) and Nano-filtration (NF) membranes offer effective barriers for the rejection of contaminants, while microfiltration and ultrafiltration (UF) membranes provide sharp removal for contaminants with specific properties (Dhakras, 2011). Researchers apply concentration and clean-up techniques in order to improve sensitivity and limits of detection (LOD) and to eliminate some potentially interfering compounds (Smuleac et al., 2011). We observed in the literature, some researchers also applied liquid-liquid extraction (LLE), solid-phase extraction (SPE), solid-phase micro-extraction (SPME), stir-bar sorptive extraction (SBSE), single-drop micro-extraction (SDME), membrane-assisted liquid-liquid extraction (MALLE), dispersive liquid-liquid micro-extraction (DLLME) and cloud point extraction (CPE) as micro-extraction techniques for water treatment. Similarly, dispersive solid phase extraction (dSPE), a promising sample pre-

treatment technique to disperse and collect by centrifugations (Abu Qdais et al., 2004; Diallo et al., 2005; Savage et al., 2005).

The bio-adsorbent from agro-based industries exemplify a renewable and bulk raw materials resource to design adsorbents for water treatment. Materials of agricultural origin for example palm oil waste, have been reported to be the preferred to design low cost decontamination systems (Rehman et al., 2015). These low cost adsorbents offer an alternative to these traditional methods used for the wastewater treatment. More research is driven by the fact that these are relatively inexpensive, non-hazardous, left as waste in agro process based industries worldwide. The main benefit over other treatment materials includes, low cost, high volume, reuse options, universal availability and comparable efficiency (Rehman et al., 2015).

#### **2.2.11 Fine-tuned Nano-adsorbents**

The increasing trend in planning for the application of Nano-adsorbents is accelerated by the environmental friendly nature and improved efficiencies. Nano-adsorbents develop exceptional properties, particle sizes, large surface area, and chemical functional groups for interactions. The properties can be fine-tuned by chemical doping with metals for specific applications, capping and protection with suitable inert supports and synthesis of composites, offering more competent and compatible systems for environment applications. The primary objective of these modifications is to fulfil the desire for green, compatible and selective water treatment systems for the specific contaminants (Ashraf et al., 2014; Smuleac et al., 2011). The Nano-adsorbents using magnetically active properties have gain more interest owing to the energy reduction due to simple separation from open system e.g. river or ocean water. The next sub-section describes the application of magnetic Nano-adsorbents for hydro-decontamination strategies.

### 2.2.12 Magnetic separation

The attractive energy efficient separation by utilizing magnetic properties of adsorbents is the key to the success of these adsorbents. Lately, magnetic adsorbents with high adsorption capacity have been developed and applied for the treatment of contaminants, such as fluoride, nitrate, sulfate, arsenate and phosphate in water (Rehman et al., 2015). The magnetic adsorbents are generally iron, copper, cobalt and nickel transition metals oxides (Hua et al., 2012). The fine tuning of compositions and geometric configurations leads the production of adsorbents with unique properties (Rao et al., 2012). The low adsorption affinity for the pollutants is demanding area to research for better adsorbents that are stable, easily separable, reasonable adsorption capacities for competent removal efficiency. Presently, high adsorption capacities are reachable by composite formation but it requires a compromise between the magnetic properties and adsorption capacities (Rehman et al., 2015). In this regard, various composite formation strategies such as the doping of magnetic materials with some suitable dopant materials incorporates the desirable features and practical solutions (Tang et al., 2015; Wong et al., 2015; Yu et al., 2015). The new generations of *nano*-materials, metal organic frameworks (MOFs) have been produce for the same energy efficient objectives. The MOFs involve an organic ligand to coordinate a metallic center, forming a highly porous and specific surface that not only supports magnetic separation but also improves adsorption capacities and scope of applications as magnetic adsorbents, catalysts, sensors and directed drug delivery systems (Wang et al., 2015; Yu et al., 2014). From application point of view the major challenges for these novel materials in the field of hydrology are discussed in the following sub-section.

### 2.2.13 Graphene and carbon nanotubes

The different allotropic form of carbon e.g. graphene, carbon nanotubes, have achieved considerable applications for the remediation of the aquatic environment (Stankovich et al., 2006). The reason for their extended applications is assigned to the desirable electrical, mechanical and morphological properties (Geim et al., 2007). Impressed by these properties, carbon nanotubes have been applied as Nano-adsorbents not only for removing a variety of pollutants such as heavy metals and organic compounds but also for purifying drinking water (Geim, 2009). It must be remembered that the  $\pi$  electron system graphene or CNTs need to be stabilized by desirable functional groups modification to improve the removal of the desired pollutants (Wang et al., 2007). It is widely known that acidic pretreatments improve the surface functional groups and lead to improve adsorption capacities (Castro Neto et al., 2009). For these reasons, various researchers have tried to modify these carbon supports by using different oxidizing acids. For instance, nitric acid for functionalization of multiwall carbon nanotubes for lead removal from water (**Table 2.3**). The characterization of the modified tubes indicated the formation of carboxylic and hydroxyl functionalities on the surface that were thought to improve the adsorption capacities through functional groups electrostatic interactions.

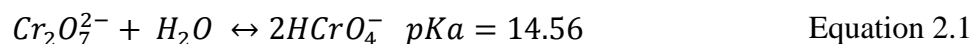
Graphene has been the focus of many research worldwide and has attracted the attention of scientists and researchers due to its useful applications in several fields (Geim et al., 2007). Graphene has exceptional physical, chemical, and mechanical properties, a capability to form composites in combination with various organic and inorganic functionalities (Castro Neto et al., 2009; Mcallister et al., 2007; Tian et al., 2012). Previous studies applied metal oxides or sulfides to construct required graphene nanocomposites (Tian et al., 2012). The present tendency is to study the combined effects of two or more substances, and to achieve graphene nanocomposites with better

properties (Geim, 2009; Tian et al., 2012). It is also highlighted that graphene plays an important role in magnetic and catalysis applications (Sun et al., 2013; Zhang et al., 2014), and also improves flexibility in morphology, phase, size, and uniform distribution. In addition, graphene is used as a promising alternative to multiwall carbon nanotubes (MWCNTs) and single-wall carbon nanotubes (SWCNTs) (Mcallister et al., 2007) because of its  $SP^2$  hybridization bonds of carbon atoms, effect on electromagnetic properties, chemical inertness, thermal conductivity, structural flexibility and adsorption properties (Fu et al., 2014; Santhosh et al., 2014; Xu et al., 2013). Magnetic composite of graphene are of the carbon type selective materials used as electrochemical sensors, electromagnetic wave absorbers and adsorbents applications (Balandin et al., 2008; Dreyer et al., 2010; Huang et al., 2006; Stankovich et al., 2006; Wang et al., 2014; Zhang et al., 2014). More recent application of graphene magnetic ferrites nanocomposite comprise the design of better catalytic reduction systems, novel composites industrial process catalysts, Nobel metals catalysts and energy storage devices (Ding et al., 2013; Fu et al., 2012; Zhang et al., 2014; Zhang et al., 2015). An attractive field is application of these novel nanocomposites to make non enzymatic glucose sensors because of attractive magnetic separation, electronic, thermal and catalytic properties (Zhang et al., 2015; Zhao et al., 2014).

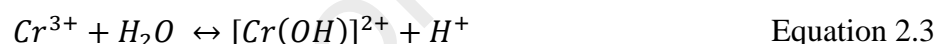
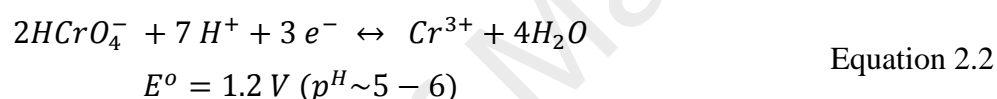
However, in another study it was observed that acidic pretreatments bring about a decrease in surface area due to blockage of pores openings by the oxygen containing functional groups (Lu et al., 2006). The acidic oxidation process was reported to promote hydrophilic character of the Nano-adsorbents, due to this reason the modified Nano-adsorbent exhibit greater adsorption capacities for environmental pollutants (Kurniawan et al., 2012). The adsorptive removal of heavy metals was proposed to involve the ion exchange mechanisms and affected by the solution  $pK_a$  values. For

example, in acidic pH range Cr (VI) was predominantly in  $\text{HCrO}_4^-$  for than  $\text{Cr}_2\text{O}_7^{2-}$  form

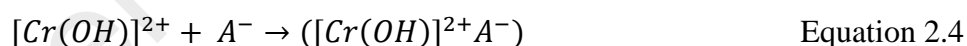
**Equation 2.1.**



The graphene or CNTs supported nanomaterials rich in carboxylic or hydroxyl groups become the source of electron donation to the solution, reducing Cr (VI) to Cr (III) oxidation state as shown by **equation 2.2**. It can be seen from this redox equation that an abundance of  $\text{H}^+$  ions favor the formation of  $\text{Cr}^{3+}$  oxidation state, it further reaction with water and form a complex cation as shown in **equation 2.3**.



The cations formed get adsorbed on the negatively charged adsorption sites present on the Nano-adsorbent surface as shown by the **equation 2.4**.



The electron donating functional groups on the adsorbents surface act as Lewis bases and the cationic or heavy metals pollutants due to their electron accepting properties act as Lewis acids. The cost of these novel interventions in wastewater treatment can be considerably lowered through a vigilant regeneration and reuse strategy for Nano-adsorbents. **Table 2.3** present some commonly used adsorbents for waste water treatment with carbon nanotubes or modified carbon nanotubes. The BET surface area of MWCNT range from 130-600  $\text{m}^2\text{g}^{-1}$  which is quite suitable to adsorb a number of metals e.g. Ni (II), Pb (II), Cr (VI) and Co (II). It is also observed that MWCNT show better adsorption results as compared to SWCNT, but after  $\text{NaClO}$  treatments the SWCNT show better adsorption of Ni (II) (Lu et al., 2006).

**Table 2.3 Waste water treatment with CNTs adsorbents.**

Nano-adsorbent	BET surface area (m <sup>2</sup> g <sup>-1</sup> )	Particle size (nm)	Dose (g L <sup>-1</sup> )	Type of pollutants	Conc. Of pollutant (mgL <sup>-1</sup> )	time (min)	pH	R (%)	Ads. capacity (m <sup>g</sup> g <sup>-1</sup> )	Ref.
MWCNT	307	10	0.5	Ni (II)	60	720	8-11	NA	38.46	(Lu et al., 2006)
MWCNT	130	10	10	Cr (VI)	0.1	720	5.5	98	NA	(Pillay et al., 2009)
MWCNT	162	NA	NA	Pb (II)	20	60	3.5	NA	7.2	(Wang et al., 2007)
MWCNT	211	2.6	0.5	Pb (II)	60	120	7	NA	26	(Wang et al., 2007)
MWCNT	600	10	5	Co (II)	10	240	9	50	NA	(Tuzen et al., 2008)
HNO <sub>3</sub> treated MWCNT	NA	6	0.5	Pb (II)	10	240	5	99	97.08	(Li et al., 2003)
HNO <sub>3</sub> treated MWCNT	NA	6	0.5	Cu (II)	10	240	5	98	24.49	(Li et al., 2003)
HNO <sub>3</sub> treated MWCNT	NA	6	0.5	Cd (II)	10	240	5	90	10.86	(Li et al., 2003)
HNO <sub>3</sub> treated MWCNT	600	10	5	Co (II)	10	240	9	90	2.6	(Li et al., 2003)
HNO <sub>3</sub> treated MWCNT	254	NA	NA	Pb (II)	20	60	3.5	75	91	(Li et al., 2003)
MnO <sub>2</sub> coated MWCNT	275	2.6	0.5	Pb (II)	60	120	7	98	78.7	(Wang et al., 2007)

NaClO treated MWCNT	307	10	0.5	Ni (II)	60	720	8-11	NA	7.53	(Lu et al., 2006)
SWCNT	397	10	0.5	Ni (II)	60	720	8-11	NA	9.22	(Lu et al., 2006)
NaClO treated SWCNT	397	10	0.5	Ni (II)	60	720	8-11	NA	47.85	(Lu et al., 2006)
Ceria nanoparticles coated CNT	189	NA	5	As (V)	20	1440	3	80	20	(Peng et al., 2005)
Cyclodextrin coated CNT	NA	NA	2	p-nitrophenol	10	1440	NA	99	NA	(Salipira et al., 2007)

Peng et al. applied Ceria nanoparticles decorated CNTs for the adsorptive removal of As (V), with 80 % removal efficiency (Peng et al., 2005). The cyclodextrin coated CNT has also been used for the adsorptive removal of p-nitro phenol (Salipira et al., 2007). The literature shows that still there is a tremendous potential for the generation of new libraries of adsorbents using the carbon based adsorbents.

The green aspect in these adsorbents arises due to their ability to regenerate after each application cycle. **Table 2.4**, show a number of eluents used to regenerate adsorbents. It was observed that in most of such type of studies an acid or base solution of known concentrations were used to recover the adsorbent for the next cycle (Pillay et al., 2009). In general, the applications of magnetic Nano-adsorbents for hydrological remediation do not generate secondary waste. After exhaustion, the spent adsorbents can be regenerated for reuse without and loss of adsorption capacities. The comparison of desorption efficiencies of various adsorbents indicates a range from 30 % to 100 % (Deliyanni et al., 2007; Uheida et al., 2006). The heavy metals e.g. Cr (VI) and As (V) were successfully desorbed with basic solution (NaOH). However, other metals e.g. Cu (II) and Co (II) were desorbed at the acidic pH using either HCl or HNO<sub>3</sub>. Moreover, researcher also applied EDTA to remove the adsorbed Cu (II) ions on the surface of magnetic ketoglutaric (Zhou et al., 2009).

**Table 2.4 Regeneration and reuse of Nano-adsorbents.**

Nano-adsorbent	Pollut.	Conc.(mg L <sup>-1</sup> )	Eluent	Conc. Of Eluent (mM)	pH	Desorp. time (min)	Desorp. (%)	Ref
MWCNT	Cr (VI)	0.1	Na OH	100	6.0	300	100	(Pillay et al., 2009)
$\beta$ -FeO(OH)	As (V)	10	Na OH	NA	12	NA	75	(Deliyanni et al., 2003)
$\beta$ -FeO(OH)	Zn (II)	50	NA	NA	6.5	NA	99	(Deliyanni et al., 2007)
$\gamma$ -Fe <sub>2</sub> O <sub>3</sub>	Cr (VI)	100	Na OH	10	2.5	60	98	(Hu et al., 2007)
$\gamma$ -Fe <sub>2</sub> O <sub>3</sub>	Co (II)	17.25	H NO <sub>3</sub>	NA	NA	10	86	(Uheida et al., 2006)
Fe <sub>3</sub> O <sub>4</sub>	Co (II)	17.25	H NO <sub>3</sub>	NA	4	120	30	(Uheida et al., 2006)
Fe <sub>3</sub> O <sub>4</sub>	Cu (II)	200	H Cl	NA	1.5	5	93	(Banerjee et al., 2007)
coated Fe <sub>3</sub> O <sub>4</sub>	Cu (II)	200	H Cl	NA	1.5	5	93	(Banerjee et al., 2007)
HDTMA coated	PO <sub>4</sub> <sup>3-</sup>	20	NA	NA	12	1440	100	(Deliyanni et al., 2007)
nanoparticle coated CNT	As (V)	20	NaOH	100	3	NA	94	(Peng et al., 2005)
Magnetic ketoglutaric	Cu (II)	200	Na <sub>2</sub> EDTA	100	6	30	92	(Zhou et al., 2009)

MnFe <sub>2</sub> O <sub>4</sub>	Cr (VI)	100	NaOH	10	N A	NA	75	(Hu et al., 2007)
MgFe <sub>2</sub> O <sub>4</sub>	Cr (VI)	100	NaOH	10	N A	NA	95	(Hu et al., 2007)
ZnFe <sub>2</sub> O <sub>4</sub>	Cr (VI)	100	NaOH	10	N A	NA	95	(Hu et al., 2007)
CuFe <sub>2</sub> O <sub>4</sub>	Cr (VI)	100	NaOH	10	N A	NA	92	(Hu et al., 2007)
NiFe <sub>2</sub> O <sub>4</sub>	Cr (VI)	100	NaOH	10	N A	NA	97	(Hu et al., 2007)
CoFe <sub>2</sub> O <sub>4</sub>	Cr (VI)	100	NaOH	10	N A	NA	98	(Hu et al., 2007)

#### 2.2.14 Metal oxides and magnetic ferrites

Apart from graphene or CNTs electron donor supports, metallic oxides and magnetic ferrites are widely researched and applied for the treatment of contaminated hydrosphere. The magnetic ferrites Nano-adsorbents offer various advantages over the nonmagnetic Nano-adsorbents. The superiority is contributed to the energy efficient separation and effective remediation of pollutants. The properties are tailored by optimizing composition to fit the requirements of a specific application, enhancing the adsorption capacities for heavy metals or anionic species. The iron oxide such as magnetite (Fe<sub>3</sub>O<sub>4</sub>) and maghemite ( $\gamma$ -Fe<sub>3</sub>O<sub>4</sub>) are widely used as magnetic oxides for water treatment. Magnetite has cubic inverse spinel structure where iron occupies the octahedral and tetrahedral sites while oxygen atoms occupying face centered regions of the cube. These structural sites can be tailored and offer a novel series of Nano-

adsorbents. For instance, Cr (VI) was removed by application of these magnetic forms of iron oxide. Interestingly, the use of manganese ferrites ( $\text{MnFe}_2\text{O}_4$ ) enabled the minimum levels of contaminants in the treated waters which was not achievable as described in the previous section (Hu et al., 2007). For instance, 5 g/ L dose of manganese ferrite at acidic pH (2) was reported to remove 100 mg/L of Cr within a short period of time (60 min). Similarly, other ferrites such as  $\text{MgFe}_2\text{O}_4$ ,  $\text{Zn Fe}_2\text{O}_4$ ,  $\text{Cu Fe}_2\text{O}_4$ ,  $\text{Ni Fe}_2\text{O}_4$  and  $\text{Co Fe}_2\text{O}_4$  having comparable particle sizes (~20 nm) but different BET surface areas were reported to remove heavy metals within comparable reaction times. It was noted that chitosan coated magnetic ferrites have almost doubled the removal performance of these magnetic Nano-adsorbents. The magnetic Nano-adsorbents have been successfully researched and used to remove As (V), Co(II), Cr (VI), Co (II), Pb (II), Cr (III), Mn (II), Cu (II), Co (II) and Zn (II) along a range of acidic, neutral and basic conditions.

**Table 2.5** comprises a number of input parameters to control the adsorption efficiencies of various magnetic adsorbents. It is clear that iron oxides are mostly used to remove As (V), Co (II), Cr (VI), Co (II) and Pb (II) ions from aqueous solutions. Some authors also used materials e.g. gum Arabic, chitosan, zeolites, alumina to make new adsorbents for the better removal of metals (Banerjee et al., 2007). The effect of various transition metals ferrites were compared to account the relative efficiencies of Cr (VI). The comparison show that  $\text{MnFe}_2\text{O}_4$  showed 100 %, removal followed by 89% and 62 % for  $\text{Mg Fe}_2\text{O}_4$  and  $\text{Zn Fe}_2\text{O}_4$  respectively.

**Table 2.5 Magnetic Adsorbents for hydrological remediation.**

Nano-adsorbent	Particle diameter (nm)	BET (m <sup>2</sup> g <sup>-1</sup> )	D (gL <sup>-1</sup> )	Target pollut.	Conc. (mg L <sup>-1</sup> )	T (min)	p <sup>H</sup>	Temp (K)	R (%)	Q <sub>e</sub>	Ref.
Fe <sub>3</sub> O <sub>4</sub>	25	245	0.1	As (V)	20	NA	6.7	NA	98	5.64	(Hristovski et al., 2007)
γ-Fe <sub>2</sub> O <sub>3</sub>	10	97.7	2.5	Co (II)	17.25	15	7.1	295	85	NA	(Uheida et al., 2006)
γ-Fe <sub>2</sub> O <sub>3</sub>	NA	NA	0.5	Cr (VI)	100	30	2.5	298	85	19.4	(Hu et al., 2007)
Fe <sub>3</sub> O <sub>4</sub>	10	97.7	2.5	Co (II)	17.25	15	7.1	295	99	Na	(Uheida et al., 2006)
Fe <sub>3</sub> O <sub>4</sub>	NA	NA	4	Pb (II)	20	50	5.5	303	72	260	(Wang et al., 2009)
Fe <sub>3</sub> O <sub>4</sub>	NA	NA	4	Cr (III)	20	50	5.5	303	38	240	(Wang et al., 2009)
Fe <sub>3</sub> O <sub>4</sub>	Na	NA	4	Mn (II)	20	50	5.5	303	11	127	(Wang et al., 2009)
Fe <sub>3</sub> O <sub>4</sub>	13	Na	4	Cu (II)	200	2	2-6	573	NA	17.6	(Banerjee et al., 2007)
Gum Arabic											
Fe <sub>3</sub> O <sub>4</sub>	13	NA	5	Cu (II)	200	2	2-6	573	NA	38.5	(Banerjee et al., 2007)
Chitosan											
Fe <sub>3</sub> O <sub>4</sub>	13.5	NA	21	Cu (II)	1150	1	5	300	NA	21.5	(Chang et al., 2005)
Chitosan											
Fe <sub>3</sub> O <sub>4</sub>	13.5	NA	20	Co (II)	1500	60	5.5	298	NA	27.5	(Chang et al., 2005)
β-FeO(OH)	2.6	330	1	Zn (II)	50	1170	6.5	298	99	27.6 1	(Deliyanni et al., 2007)
β-FeO(OH)	2.6	330	1	Cd (II)	10	1440	6.0	338	90	66.7 2	(Deliyanni et al., 2005)
β-FeO(OH)	2.6	330	0.5	PO <sub>4</sub> <sup>3-</sup>	10	1440	7	338	NA	59.6 2	(Deliyanni et al., 2007)

$\beta$ -FeO(OH)	2.6	330	0.5	Cr (VI)	50	432	5.5-6.5	298	90	80	(Lazari dis et al., 2005)
HDTMA $\beta$ -FeO(OH)	4.6	231	0.5	As (III)	30	1440	NA	298	NA	84	(Deliy anni et al., 2006)
HDTMA $\beta$ -FeO(OH)	4.6	231	0.5	PO <sub>4</sub> <sup>3-</sup>	10	1440	7	338	NA	451	(Deliy anni et al., 2007)
Fe(II) zeolite	4	21	10	As (V)	20	1440	5-8	293	95	22.5	(Dous ova et al., 2006)
Alumina	50	NA	3.5	Hg (II)	94	42	NA	NA	100	NA	(Pache co et al., 2006)
MnFe <sub>2</sub> O <sub>4</sub>	20	180	5	Cr (VI)	100	60	2	298	100	NA	(Hu et al., 2007)
MgFe <sub>2</sub> O <sub>4</sub>	20	70.3	5	Cr (VI)	100	60	2	298	89	NA	(Hu et al., 2007)
ZnFe <sub>2</sub> O <sub>4</sub>	20	79.6	5	Cr (VI)	100	60	2	298	62	NA	(Hu et al., 2007)
CuFe <sub>2</sub> O <sub>4</sub>	20	93.8	5	Cr (VI)	100	60	2	298	49	NA	(Hu et al., 2007)
NiFe <sub>2</sub> O <sub>4</sub>	20	101.2	5	Cr (VI)	100	60	2	298	32	NA	(Hu et al., 2007)
CoFe <sub>2</sub> O <sub>4</sub>	20	55.1	5	Cr (VI)	100	60	2	298	20	NA	(Hu et al., 2007)
ZrO <sub>2</sub>	20	45	0.1	As (V)	20	NA	6.7	NA	85	3.97	(Hristo vski et al., 2007)
NiO	10	80	0.1	As (V)	20	NA	8.4	NA	98	NA	(Hristo vski et al., 2007)

NA = not available

### 2.2.15 Comparing adsorbents performance

The efficiency and effectiveness of the Nano-adsorbents was studied in comparison to the conventional adsorbents to collect useful information to construct future water purification systems. In this regards, the experimental parameters such as sample solution pH, required adsorbent dose, adsorbates concentration, temperature (K) and reaction time were compared to assess the performance of the Nano-adsorbents. Table 2.6 presents some adsorbents with high percent removal efficiency for the desired environmental pollutants. For instance, the nitric acid treated MWCNT has far better adsorption capacity for Pb (II) as compared to MnO<sub>2</sub> coated MWCNT (Li et al., 2003; Wang et al., 2007). The reason for such a difference of adsorption performance may be ascribed to the generation of negative centers on the surface of MWCNT for effective adsorptive interaction with metal cations. In batch adsorption studies times also plays important role as it controls the steps involved during adsorption. In case of nitric acid treatment four hours reaction time provide more adsorption capacity than MnO<sub>2</sub> treated adsorbent as only two hours were allowed to complete the adsorption process. In former case the BET surface area was not reported while the second study reported a large BET surface area as shown in the Table 2.1. The adsorbent particle sizes has shown contradictory effect e.g. the particle size of MnO<sub>2</sub>-MWCNT is smaller than HNO<sub>3</sub>-MWCNT but the percent removal and adsorption capacities are better in the second case. The zero valent iron (Fe (0)) has more BET surface area than Kaolinite supported Fe (0) Nano-adsorbent that provide 98 % adsorptive removal of Co (II) cations (Uzum et al., 2009; Uzum et al., 2008). The incorporation of kaolinite with nZVI leads to increase particle size from 8 to 300 nm as given in **Table 2.6**. Although nZI alone has more surface area, still the Kaolinite supported nZVI adsorbent has almost doubled adsorption capacity as it results in a 99 % removal efficiency of Co (II) of 100 mgL<sup>-1</sup> initial concentration as compared to nZVI with 98 % removal of Co (II) with only 50

mgL<sup>-1</sup>, when the remaining experimental conditions were reported similar in the individual studies (Uzum et al., 2009; Uzum et al., 2008). MCM 41 adsorbent has 99 % removal efficiency for Cs with an initial concentration 2 mgL<sup>-1</sup>. The outstanding adsorption capacity 179 mg g<sup>-1</sup> may be related to the BET surface area as shown in the Table 2.6.

The occurrence of Arsenic (As) in the surface or ground water at an increasing rate is currently reported all over the world (Arcibar-Orozco et al., 2014; Smith et al., 2000). It is estimated in different studies that As is affecting more than 100 million people all over the world with increasing problem of polluted waters (Arcibar-Orozco et al., 2014; Dixit et al., 2003). The World Health Organization (WHO) Arsenic established maximum allowable limit is 10µgL<sup>-1</sup>(Bilici Baskan et al., 2010). The arsenic chemistry elaborates that it is found in two oxidation states i.e. 3<sup>+</sup> and 5<sup>+</sup> (Anirudhan et al., 2013; Dixit et al., 2003). The oxidation states are interchangeable with a relative change in environmental pH, temperature, concomitant ionic species and oxidation reduction conditions (Anirudhan et al., 2013; Bilici Baskan et al., 2010). Due to this reason one form of Arsenic which is less toxic at present, can transform into more toxic state with a change in environmental (Wang et al., 2014). There are different strategies to remove Arsenic beyond permissible level in water supplies (Sen Gupta et al., 2009; Singh et al., 2015; Trois et al., 2015). Adsorption is reported to be effective, efficient, easy, economical and accessible technology (Anirudhan et al., 2013; Naseri et al., 2014).

**Table 2.6 Outstanding Nano-adsorbents for heavy metal removal.**

Adsorbents	BET (m <sup>2</sup> g <sup>-1</sup> )	size (nm)	Dose (gL <sup>-1</sup> )	Metal	Conc. (mg L <sup>-1</sup> )	Time (min)	pH	R (%)	Ads. Capacity (m <sup>g</sup> g <sup>-1</sup> )	Ref.
HNO <sub>3</sub> treated MWCNT	NA	6	0.5	Pb (II)	10	240	5	99	97.08	(Li et al., 2003)
MnO <sub>2</sub> coated MWCNT	275	2.6	0.5	Pb (II)	60	120	7	98	78.74	(Wang et al., 2007)
Fe <sub>2</sub> O <sub>3</sub>	25	245	0.1	As (V)	20	NA	6.7	98	5.64	(Hristovski et al., 2007)
Akaganetite (β-FeO(OH))	2.6	330	1	Zn (II)	50	1170	6.5	99	27.61	(Deliyanni et al., 2007)
Fe (0)	14.2	80	20	Co (II)	50	45	10	98	99	(Uzum et al., 2008)
Kaolinite supported Fe (0)	9.6	300	5	Co (II)	100	45	10	99	NA	(Uzum et al., 2009)
Arginine modified TiO <sub>2</sub>	45	NA	1.3	Hg (II)	150	32	NA	100	NA	(Skubal et al., 2002)
PAMAM dendrimer	NA	NA	2.5	Cu (II)	10	270	7	100	NA	(Diallo et al., 2005)
MCM 41	900	NA	5	Cs	2	120	NA	99	179	(Lin et al., 2005)

**Table 2.7** compares Nano-adsorbents working conditions such as pH, reaction time, initial concentration of pollutants and adsorbent dose for the effect on percent removal and adsorption capacities. The acid treated carbon nanotubes adsorbents were compared to remove lead in acidic pH condition. As it can be seen, the increase in initial

concentration from 10 to 20 mg L<sup>-1</sup> has a negative effect on percent removal as it decreases from 99 % to 75 % in these two comparative studies (Li et al., 2003; Lu et al., 2006).

**Table 2.7 Experimental conditions for Nano-adsorbents applications.**

Adsorbents	BET (m <sup>2</sup> g <sup>-1</sup> )	Size (nm)	Dose	Pollut.	Conc. (mgL <sup>-1</sup> )	T (hr)	pH	R%	Q <sub>e</sub>	Ref.
HNO <sub>3</sub> treated MWCNT	NA	6	10	Pb (II)	10	4	5	99	97	(Li et al., 2003)
HNO <sub>3</sub> treated MWCNT	254	NA	NA	Pb (II)	20	1	3.5	75	91	(Lu et al., 2006)
Fe (0)	14.2	80	20	Co (II)	50	0.7 5	10	98	99	(Uzum et al., 2008)
Activated carbon	987	NA	4	Zn (II)	60	120	7	Na	20	(Leyva Ramos et al., 2002)
Industrial by products	107	0.1	10	Ni (II)	249	8	4	90	32	(Gupta, 1998)
Industrial by-products	32	NA	2	Pb (II)	200	24	5.5	NA	32	(Feng et al., 2004)
Industrial by products	32	NA	2	Cu (II)	200	24	5.5	NA	29	(Feng et al., 2004)
Agricultural waste	Na	NA	9	Cu (II)	126	NA	5	73	10	(Kadirvelu et al., 2001)
Agricultural waste	592	NA	0.4	Ni (II)	40	1	4	80	63	(Kadirvelu et al., 2001)

The other reason of this decline may be reduce reaction time or the use of more acidic pH in the later study. This highlights the importance of experimental conditions on the overall performance of Nano-adsorbents. Industrial by products offer an economical alternate raw source of Nano-adsorbent. Industrial by products were compared to remove Ni (II), Pb (II) and Cu (II) (Feng et al., 2004; Gupta, 1998). The adsorbent show comparable adsorption capacity for Ni (II) and Pb (II) but a decline of Cu (II) adsorption. Similarly, agricultural waste was reported to have better adsorption capacity for Cu (II) but less than that of industrial byproducts (Kadirvelu et al., 2001). In another study, a large BET surface area (592 (m<sup>2</sup>g<sup>-1</sup>)) removed 63 mg g<sup>-1</sup> of Ni (II). The superior adsorption capacity of agricultural waste over the industrial by products (**Table 2.7**) supports the further studies to produce better adsorbents with large BET surface area, functional groups, particle size with a competitive affinity for pollutants.

## 2.3 Modelling adsorption

### 2.3.1 Design of experiments

Central composite design (CCD), using the Stat ease 9.0 software, was selected to plan for the adsorption experiments. The experiments were performed as suggested by the software. Adsorption capacity ( $Q_e$  mg.g<sup>-1</sup>) was calculated by following (Shanmugaprakash et al., 2013).

$$Q_e = \frac{(C_o - C_e)V}{m} \quad \text{Equation 2.5}$$

Where,  $C_o$  and  $C_e$  stand for initial and equilibrium adsorbate concentration (mgL<sup>-1</sup>) respectively,  $V$  is the total volume of solution in liters and  $m$  is the mass of adsorbent (g). Adsorption experiments were repeated to check for systematic variations to determine standard deviation and reproducibility of results. Four variables viz. adsorbate initial conc. (mgL<sup>-1</sup>), pH, temp and Adsorbent (Ads. mg) in the range of 300-

500 mgL<sup>-1</sup>, 3.0 to 9.0, 20 to 40 and 400 to 600 (mg) respectively. In this work, **Equation 2.6**, shows the selected quadratic model (Rehman et al., 2015).

$$Q_e = \beta_o + \sum_{i=1}^k \beta_i x_i + \sum_{i=1}^k \beta_{ii} x_i^2 + \sum_{i=1}^{k-1} \sum_{j=2}^k \beta_{ij} x_i x_j + \varepsilon \quad i \neq j \quad \text{Equation 2.6}$$

Where  $\beta_o$  is a constant coefficient,  $\varepsilon$  symbolizes error,  $x_i$  and  $x_j$  are independent variables,  $\beta_i$ ,  $\beta_{ii}$  and  $\beta_{ij}$  represent coefficients of linear, quadratic and interaction effects respectively. The data for each experiment was checked for the goodness of fit into the statistical models. The verification of models was carried out by statistical tests i.e. analysis of variance (ANOVA), residuals analysis (RA), scaling residuals (SR) and prediction error sum of squares (PRESS) (Naseri et al., 2014). The verified and validated models were applied to optimize the four input variables and to maximize output i.e. fluoride, nitrates, nitrites, sulphates, phosphates, arsenic, cadmium, nickel, iron and related heavy metals adsorption capacity.

### 2.3.2 Response surface methodology

Design of experiments (DOE) strategy is found as a superior method as compared to one variable at a time “OVAT it strategy”, enables deeper insight into interactions among pre-selected experimental variables (Rehman et al., 2015). The DOE strategy applies collaborating experiments to minimize implementation cost of research and development (Rehman et al., 2015). Normally, multiple interactions of variables and non-linear behavior of adsorption process constitute a complex mechanism (Dora et al., 2013). Until now, response surface methodology (RSM) is a competitive modeling tool to analyze and present complex nonlinear relationships among variables either alone or in combination and their synergistic or antagonistic effects on adsorption (Simsek et al., 2013). Principle of RSM is to use polynomial equations in a programmed range to discover optimum values and the best system response (Roy et al., 2014). All significant

experimental variables are co-varied over a pre-selected range to find combined interactive effects and finally uniting all interaction results to build a mathematical model (Rehman et al., 2015). Model can be implemented to improve adsorption performance, reducing number of experiments and eradicating statistically insignificant variables.

### 2.3.3 Adsorption Kinetics

Kinetics is the science which deals with the mechanisms and rates of chemical reactions, and ideally kinetic models should be incorporated into geochemical models, along with thermodynamics. From a thermodynamic study of a reaction we are unable to say anything about how fast salt will dissolve in water. However there are complex reaction taking place in the hydrosphere and it is important to know the kinetics of these reactions to understand the complex interaction and mechanisms. **Figure 2.7**, shows the three well known stages of adsorbate adsorbent interaction. The rate of these entire steps controls the overall kinetics. The step taking more time to complete is known as the slowest or the rate determining step. While identification of rate determining steps offers an option to tailor the adsorption process. Adsorption kinetics provides useful information about the mechanism of adsorption but also the speed of adsorption reaction. A number of kinetic models are normally used to interpret the adsorption mechanism e.g. pseudo-second order reaction, pseudo-first order reaction and intraparticle diffusion models.

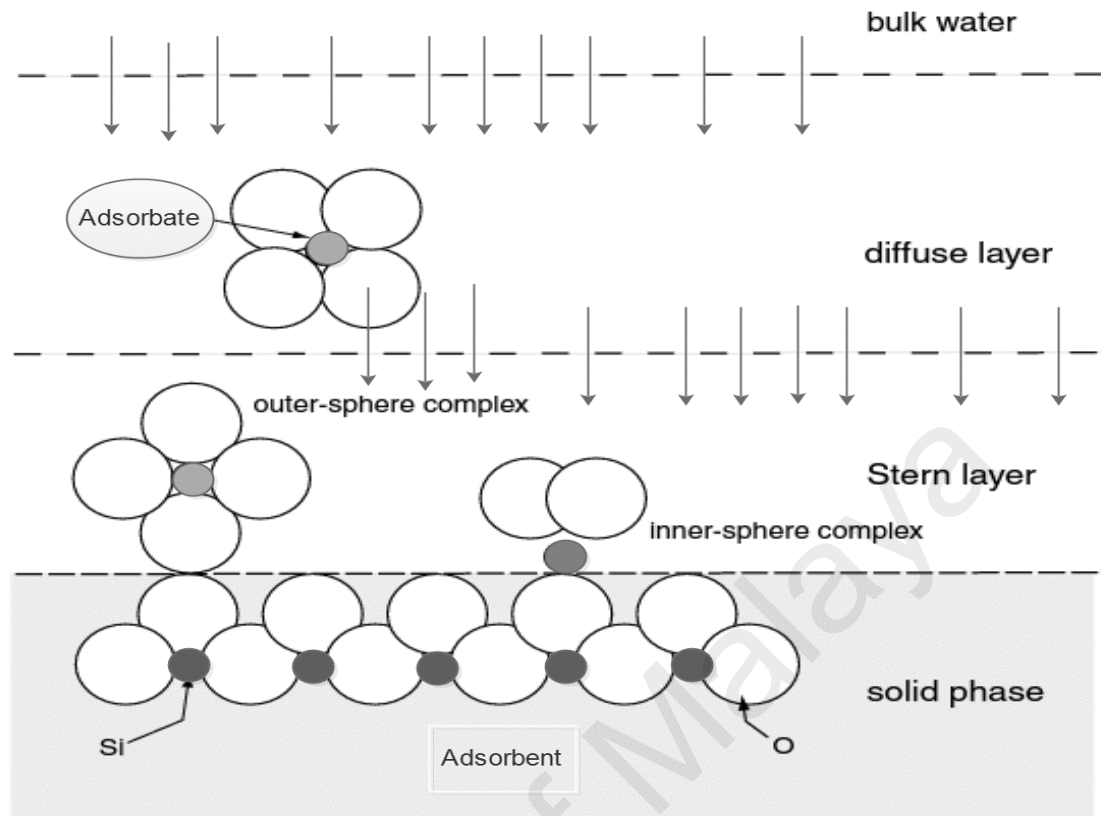


**Figure 2.7. The three stages of adsorbate-adsorbent interactions.**

For the design of an effective hydro-decontamination system we need to know the rate of chemical reaction taking place i.e. the rate of adsorption. With reference to geochemical modelling, we do not attempt to explain in detail the broad field of chemical kinetics, but just enough to understand the basics of kinetics. Several kinetic models are implemented to examine the experimental data to decide on the nature, intensity and mechanism of the adsorption process. The speed of adsorption was evaluated by employing four kinetic models: pseudo-first order, pseudo-second order, intraparticle diffusion and Banghams. The overall adsorption rate is proportional to the driving force and the concentration gradient in the case of the first order, while in the case of the second order, it is proportional to the square of driving force.

#### **2.4 Challenges and role of adsorbents in remediation**

Hydrology is concerned with the water properties, resources, resource conditions, and water movement in relation to land along the dynamic environments (Dingman,

2015). While hydrological connectivity is determined by the presence of waterways, hydraulic infrastructure, soil type, topography and geology to facilitate flow of water across the land. Distribution pattern of water have a great influence on homing success, the level of gene flow and population structure (Olsen et al., 2010). Environmental fluctuations associated with water composition has a direct effect on all the depending living beings e.g. fish, plants and the primary, secondary and tertiary consumers (Chaparro et al., 2015). The global climate change, population increase, damming of rivers, water abstractions and more water pollutants have exerted multiple pressures on the water resources, aquatic and land ecosystem (Karthe et al., 2015). Occasionally, the hydrological samples contain elevated levels of fluorides, nitrates, sulfates, phosphates, chlorates, bromates, perchlorates and a number of heavy metals cause of serious environmental issues and adverse impacts on public health (Bohlke et al., 1995; Kröger et al., 2009; Pluta, 2001). Each geological regions have characteristic water availability and water quality parameters, including turbidity, temperature, total dissolved solids (TDS), pH, inorganic ions and organics and number of anthropogenic sources (Orem et al., 2011).

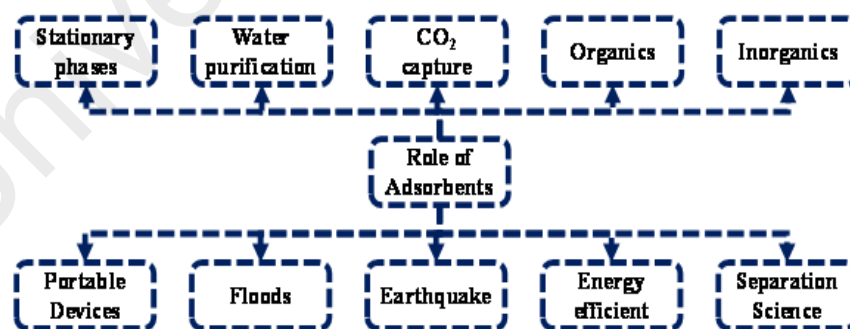


**Figure 2.8. Challenges and role of adsorbents in hydro-harsh environments.**

The geological regions are unique and require some specific modification in the water treatment systems. The environmental conditions have an influence on role of adsorbents, stationary phases, water pollutants and CO<sub>2</sub> capture, removal of organic and

inorganic species in routine or emergency situations as shown in **Figure 2.8**. For example biological contamination and inactivation through biological fouling results in decreased removal efficiency. A thorough understanding of the hydrosphere is compulsory to design, manage and realize the global socio-economic developments (Ruddell et al., 2015). The global water scarcity is an urgent and well-recognized problem. The concept of water scarcity appears related with water quantity and quality (Jiang, 2009; Zeng et al., 2013). However, without considering water quality criterion the assessments and estimates of water scarcity is less precise and water quality has become a critical factor with increasing number of pollutants (Zeng et al., 2013). **Table 2.8** present current problem and issue with the use of adsorbents.

**Table 2.8. General problems and issues of adsorbents (Karthe et al., 2015).**

#	<i>Problem/ issues</i>
1	<i>Effect of environmental acidity, basicity and alkalinity.</i>
2	<i>Temperature fluctuations in different geological regions of the world.</i>
3	<i>Increased concentration of persistent organic pollutant (POPs).</i>
4	<i>The biological contamination, inactivation of systems through fouling.</i>
5	<i>Non-selectivity of specific problem contaminants in some regions.</i>
6	<i>The binding with non-interest species in the environmental matrix</i>
7	<i>The prevalence of physical parameters in aquatic systems.</i>
8	<i>The diversified nature of environmental industrial effluents</i>
9	<i>The leaching of metal ions from the protective coatings</i>

## **2.5 Research advancement in adsorbents protections**

A number of research advancements have been observed in the literature in the past decade. **Table 2.9** presents some of the current research advancements in iron derived adsorbents and protective measures as a contribution to advance the used or these magnetic adsorbents under harsh environments. A common observation is the

aggregation of magnetic nanoparticles which leads to reduce efficiency as the effective surface area is reduce by this behaviour of Nano-adsorbents.

**Table 2.9 The protective measure for iron oxides.**

#	Research advancement	Adsorbent	Protective measure	Contribution	Ref.
1	Preventing aggregations	Iron oxide	SDS surface coatings	enhanced Arsenic immobilizations efficiency	(Kim et al., 2012)
2	Reduce particle size	Iron oxide	SDS surface coatings	enhanced Arsenic immobilizations efficiency	(Kim et al., 2012)
3	Stability of magnetic particles in acidic environments	Iron oxide	sec-octylphenoxy acetic acid (OPA)	Lanthanides removal system	(Zhu et al., 2011)
4	Introducing affinity for nanoparticles	Iron oxide	polydimethyl siloxanes (PDMS)	enhance hydrocarbon adsorption	(Konieczny et al., 2008)
5	Environment friendly adsorbent	iron oxide	iron oxide coated with humic acid	efficient removal of heavy metals	(Campos et al., 2011)
6	Smart scavenger of Hg (II)	gold	coating gold particles with citrate	avoids the addition of reducing agents	(Ojea-Jiménez et al., 2012)
7	Thiol-functionalization	Iron oxide	3-mercaptopropyltriethoxysilane (MPTES)	adsorption of cadmium, lead and copper ions	(Chen et al., 2012)
8	Ionic liquids in hydrodecontaminations	Iron oxide	Imidazolium based ionic liquid (IL)	reactive black dye	(Poursaberi et al., 2013)
9	Protected adsorbents	Iron oxide	Prussian blue (K <sub>4</sub> [Fe(CN) <sub>6</sub> ])	removal of radioactive cesium (Cs)	(Thammawong et al., 2013)

Kim et al. reported that this issue can be resolved by the use of nanoparticle surface coating with surfactants e.g. SDS coating (Kim et al., 2012). Secondly, this development was also reported to reduce the effective particles size that enabled an enhanced heavy metal immobilization from aqueous samples. Similarly, the problem of stability in acidic environments were resolved by protective coating with sec-octylphenoxy acetic acid (OPA) (Zhu et al., 2011). Konieczny et al found that magnetic nanoparticles affinity for hydrocarbons removal can be amplified by coating with polydimethyl siloxanes (PDMS) (Konieczny et al., 2008). The environmental friendly humic acids (HA) coated Nano-adsorbents were developed to fulfill the decontamination challenge by heavy metals pollution (Campos et al., 2011).

The use of reducing agents to prepare magnetic Nano-adsorbents makes these methods environment non-friendly. This issue was resolved by coating gold particles with citrate for making environment friendly mercury smart scavengers by avoiding the use of chemical reducing agents (Ojea-Jiménez et al., 2012). Thiol functionalization of iron nanoparticles by mercaptopropyl triethoxysilane (MPTES) provide suitable magnetic modified Nano-adsorbent for heavy metals removal e.g. Cd, Pb and Cu (Chen et al., 2012). Imidazolium based Ionic liquids were also reported to protect magnetic Nano-adsorbents for organic dye removal from hydrological samples (Poursaberi et al., 2013). Protected magnetic Nano-adsorbents have been also used for the remediation of radioactive waste by the Prussian blue coatings (Thammawong et al., 2013).

The issues related to compatibility problems of nanotechnology materials with natural environments include matrix effects from environmental range of pH, temperature, alkalinity, hardness, organics, inorganics, biological contaminants, increase in industrial effluents and functionality loss with the extended use Table 2.8. Aqueous streams with beyond permissible levels of heavy metals is regarded as one of

the most common problem in Malaysia (Fakhru'l-Razi et al., 2009). The attractive energy efficient separation of magnetic adsorbents has been explored to open new developments in the field of adsorbents for environmental treatment systems. Magnetic anion exchange resin for the removal of reactive blue dye were considered superior due to the easy magnetic separation (Shuang et al., 2011). The current literature review provides an overview that how we can overcome some of the challenges by a careful planning of adsorption system and protecting the magnetic Nano-adsorbents for an extended use and stability to overcome the hydro-harsh condition that adversely affect the separation efficiency, adsorption capacities in the extended adsorption/ desorption cycles.

### **2.5.1 Socio-economic development and public health**

The socio-economic development and improved public health is linked with the supply of safe water. The rapid industrialization, urbanization and exponential increase in population imposes burden to sustainability of limited natural resources. Earth hydrosphere is facing evolving challenges by rigorous contamination from development activities (Smith et al., 2000). The desire for improve living standards have highlighted the needs for quantity and quality safe water. The awareness has risen gradually with time to improve the quality of water to improve quality of life. The statistics about population with access to safe water assumes ideal situations as they rely on perceived fact while ignoring the ground realities (Onda et al., 2012). The superfluous underestimate mislead the severity of water contamination problems, concerning public health. The reason behind may be the difference in pollution levels or range of contaminants concentration as indicator of the water quality in different geological regions based on the availability of water. As the water flows across urban water supply system it is continuously exposed to contaminants because of leakage or accidental rupture of water pipes. Therefore, a continuous monitoring system is necessary to

monitor the fault of a particular water resource over the course of time. A continuous attention and care is mandatory for better public health and social development (Onda et al., 2012). The safe water usage practice is obligatory to realize the health gains from water quality interventions. The distorted hygiene practices with even occasional consumption of untreated drinking water results in the adverse public health issues. A similar effort is the use of portable water treatment system at homes (Brown et al., 2012). The household water pre-treatment (HWPT) is believed to prevent 500 disability adjusted life years (DALYs) per 100,000 persons per year. The declining percentages of HWPT tend to reduce the predicted health benefits (Brown et al., 2012). The fecal contaminations of drinking water is a common cause of water-borne diseases (Kyle Onda et al., 2013). World Health Organization (WHO) has documented various drinking water quality parameters to assign safe status to consumer water. The improper disposal of municipal, industrial wastes and indiscriminate applications of agrochemicals challenges water quality. The Microbial or chemical pollutants remain the main concern for better public health (Azizullah et al., 2011). It is crucial to minimize the contamination of underground water, rivers, and lakes for the collective survival of community members. The development of Nano-adsorbents offers the possibility to resolve or greatly ameliorate the current problems plaguing water quality (Qu et al., 2012).

Surface and ground water resources are often found to have elevated levels of contaminants beyond the safe water quality level (Smith et al., 2000). The problem of municipal and industrial waste, the massive output of agrochemicals from agricultural practices, and natural disasters have become the main causes of declining water quality (Azizullah et al., 2011). The present science desires to development chlorine-free biocides to selectively target disease causing bacteria and viruses in water (Savage et al., 2005). The desalination of saline water, recovery of toxic and valuable metals,

contaminants including perchlorate, pharmaceuticals, endocrine disrupters and chiral compounds concerns present and future studies (Savage et al., 2005).

### **2.5.2 Resources scarcity**

The basic problem is depletion of natural resources, massive exploration and rapid changes in geochemistry. This situation is worsening by the increasing water demand of population and the present pollution crisis. Further studies are mandatory to provide some practical solutions for the changing definition of water scarcity. The all form of life on the planet Earth gets benefits from the environment in the form of water, food and shelter. Since the beginning of life the Earth is the nursery in which life developed over billions of years (Postel et al., 2012). The natural hiccups in the environment occur from time to time, but life continue to survive. There are two types of issues; the natural and our own made environmental problem. The man made alteration in the environments are thought to impose threat to the survival of life (Stevens, 1997). The Earth provides the life support system and we must use it wisely not only for our survival but also for coming generations (Young et al., 2009). At the present time we have no other option to live on some other planets than Earth (Raymond et al., 2004). There is a desire to preserve and protect the natural resources for sustainable health and development. The contamination causes of hydrosphere must be checked and resolved to carry forward the safe environment for future generation. Adsorbents purifying and protecting materials have risen as a renewable, green and workable solution to protect the natural hydrosphere. The expanding use of resources and industrial development is necessary to fulfil the needs of increasing population but socio-economic development must comply with the green environment for sustainable public health.

## 2.6 Comparative hydrological remediation

A number of remediation techniques are compared to evaluate the competency of respective decontaminations strategies reported in the literature. The abundantly available calcium hydroxide provides basic pH medium to precipitate Mn (II) with a 99.3 % removal efficiency (Charerntanyarak, 1999). A comparison with coagulation with pol ferric sulfate for Cu (II) removal shows that the previous technique require 10 mg L<sup>-1</sup> optimum dose to remove 1.09 mg L<sup>-1</sup> while the later technique need more dose 25 g L<sup>-1</sup>. As it is clear the later technique requires more adsorbent dose to accomplish a 99 % removal of Cu (II) from hydrological samples. Nevertheless, the second technique remove 20 mg L<sup>-1</sup> of Cu (II) that is far high concentration of pollutant as compared to the previous technique (Li et al., 2003). The role of ionic surfactants to remove Zn (II) cations from hydrological samples is compared by the use of surfactant 105 and sodium dodecyl sulfate (SDS) in two separate studies (Matis et al., 2004; Zouboulis et al., 2003). In these two flotation methods the SDS surfactant displayed better removal of Zn (II) as compared to Surfactant 105, as it remove 0.05 mg L<sup>-1</sup>(**Table 2.10**). Interestingly, the synthetic zeolites demonstrated 100 % removal efficiency for Cr (III), Ni (II) and Zn (II). As compared to ultrafiltration the nanofiltration with polyamide remove 200 mgL<sup>-1</sup> of Cd (II) with a 99 % removal efficiency (Abu Qdais et al., 2004; Juang et al., 2000). The reverse osmosis techniques was compared to remove Cu (II) and Ni (II) metal cations with a ES20 membrane (Ozaki et al., 2002). Similarly, membrane electrolysis provided 99.6 % removal efficiency for Cr (VI) by iron rotary with 130 mg L<sup>-1</sup> pollutants initial concentration in basic pH 8.5 (Martinez et al., 2004). Table 2.10 also compared metals removal efficiency of adsorption technique for Pb (II), Zn (II), Hg (II) and Co (II), with different adsorbent dosages ranging from 0.5 g to 5.0 g. It can be seen from the comparison results that with the use of more adsorbent dosage the percent removal efficiency increases linearly because of the availability of more surface sites for interaction

with the hydrological pollutants (Deliyanni et al., 2007; Skubal et al., 2002; Uzum et al., 2009; Wang et al., 2007). **Figure 2.9** provide a clear picture of the relative remediation performance in terms of adsorption capacities. The available activated carbon, industrial by products and agricultural waste has comparable adsorption capacities for heavy metals. On the other side advanced supports e.g. MWCNT, MCM-41 and magnetic nZVI are demonstrating the high adsorption capacity as compared to conventional adsorbents. It clearly supports the use of advance materials for further research as it is evident from the literature review study.

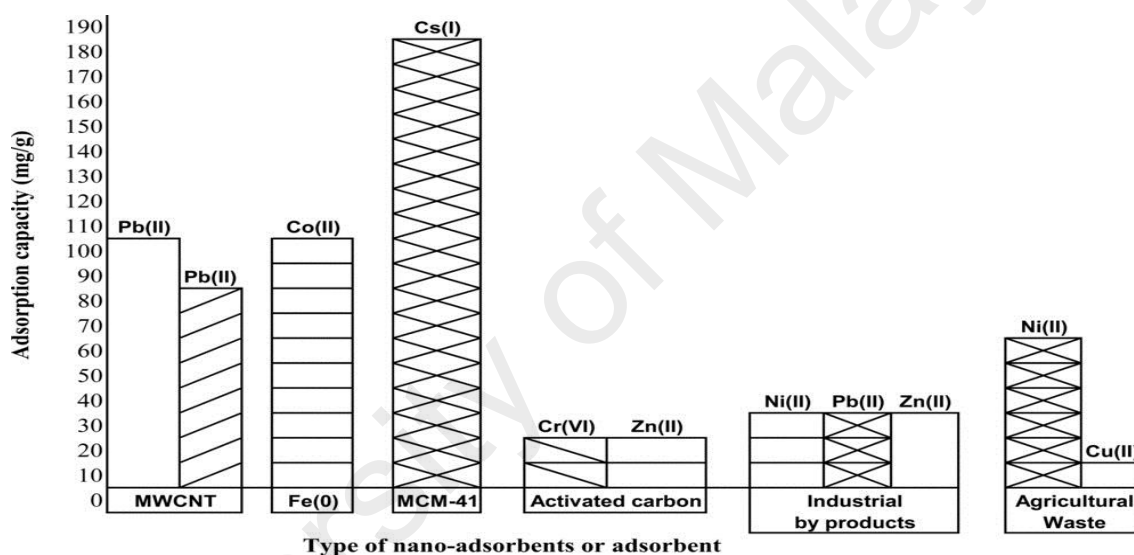


**Figure 2.9 Remediation performance of conventional and Nano-adsorbents.**

**Table 2.10 The comparative removal efficiency of remediation techniques.**

Remediation technique	Environ. Pollutant	Remediation source	dose (gL <sup>-1</sup> )	Conc. (mg L <sup>-1</sup> )	pH	R (%)	Reference
Chemical precipitation	Mn (II)	Ca (OH) <sub>2</sub>	10	1.085	11	99.30	(Chareerntanyarak, 1999)
Coagulation	Cu (II)	Poly ferric sulfate	25	20	10-11.5	99	(Li et al., 2003)
Floatation	Zn (II)	Surfactin 105	0.04	50	6	100	(Zouboulis et al., 2003)
Floatation	Zn (II)	SDS	0.05	50	7-9	100	(Matis et al., 2004)
Ion exchange	Cr (III)	zeolite	2.5	100	NA	100	(Alvarez-Ayuso et al., 2003)
Ion exchange	Ni (II)	Synthetic zeolite	2.5	100	NA	100	(Alvarez-Ayuso et al., 2003)
Ion exchange	Zn (II)	zeolite	2.5	100	NA	100	(Alvarez-Ayuso et al., 2003)
Ultra-filtration	Cu (II)	YMI	NA	79	8.5-9.5	100	(Juang et al., 2000)
Nanofiltration	Cd (II)	Polyamide	NA	200	4-11	99	(Abu Qdais et al., 2004)
Reverse osmosis	Cu (II)	ES20	NA	50	7-9	100	(Ozaki et al., 2002)
	Ni (II)	ES20	NA	50	7-9	100	(Ozaki et al., 2002)
Membrane electrolysis	Cr (VI)	Iron rotary	NA	130	8.5	99.60	(Martinez et al., 2004)
Adsorption	Pb (II)	MnO <sub>2</sub> coated MWCNT	0.5	60	7	98	(Wang et al., 2007)
Adsorption	Zn (II)	Akaganetite	1	50	6.5	99	(Deliyanni et al., 2007)
Adsorption	Co (II)	Kaolinite supported Fe (0)	5	100	10	99	(Uzum et al., 2009)
Adsorption	Hg (II)	Arginine modified TiO <sub>2</sub>	1.33	150	NA	100	(Skubal et al., 2002)

## 2.7 The competitive adsorption technique

The competency or preference of adsorption over other techniques relies on the involvement of surface phenomenon that can be fine-tuned to remove contaminants or the dissolved solutes from samples e.g. Industrial wastewater, polluted river and drinking water. Desorption is the process to remove adsorbed solute on the surface of adsorbent by the use of a suitable elution solvents e.g. acids, bases, ionic liquids, organic solvents or technique such as sonication, microwave or calcination. The opportunity to desorb contaminants from the surface of adsorbents paves the way to recycle and reuse of adsorbents. Water treatment techniques apply adsorbents as an effective, alternative and practical solution to remove contaminants (Crini, 2006). The extended applications include product purification, storage or capturing organics, chromatographic stationary phases, and removal of pollutants (Hicks et al., 2008; Rehman et al., 2015; Wang et al., 2011; Xu et al., 2002). The need-based adsorbents have sparked interest throughout the scientific community along with an allusive challenge of competency and stability during harsh environmental conditions (Jeremias et al., 2012; Zhang et al., 2011). The rational design of adsorbents with prolonged stability in environmental stress conditions has lead towards the curiosity and search for more adsorbents (Masters et al., 2011). The manifestation of unforeseen disasters, such as earthquakes, floods and mega natural disasters highlight the need for straightforward adsorbents (Mahmood et al., 2011). The interest to make smart, portable water treatment devices with minimal energy consumption follows the developments in separation sciences applications (Baig et al., 2011; Mwabi et al., 2011). Water crisis in different geological regions of the planet has called for research to ensure superior adsorption capacity, magnetic separation and prolonged stability (Chaturvedi et al., 2012). Fortunately, the synthetic revolution in Nano-adsorbents and advanced characterization

techniques provide deep insights into the modified Nano-adsorbents (Rehman et al., 2015). Future research is dedicated to collective consequences from water chemistry, nanoparticles characteristics and their coating condition, performance of supports and adsorbents (Crini, 2015). We realize that the adherence to green approaches in pollutants removal techniques provides the roadmap for the future developments (Husain et al., 2015; Rezaei et al., 2015).

The feasibility of adsorption desorption cycles depends on the nature of adsorbent-adsorbate interaction. For example, there are two types of complex formation (a) Inner sphere complexes (ISC) (b) Outer sphere complexes (OSC). In case of ISC formation intense chemical bonding takes place and recycling is more challenging and require stringent desorption conditions or chemical, while in case of OSC the surface phenomenon is governed by the dominant physical forces of attraction holding the participants together through relatively weaker forces (Huang et al., 2008). In OSC the reuse and regeneration process is exercised to maintain the overall cost by reusing the materials over extended period of times (Loganathan et al., 2013). The regeneration and reuse of Nano-adsorbents is one of the crucial aspects as it controls the economy of the hydro-decontamination technologies. Many researchers has attempted to regenerate and recycle Nano-adsorbents, as it become the hot spot of the separation sciences. An understanding of the mechanism and chemistry of separation reactions helps to bring out novel ways to regeneration and reuse. Recent literature shows the use of various reagents such as acids, alkalis and chelating agents for application in the regeneration of adsorbents for extended economical usage. A comparison between the past and present research indicates, various number of studies reported on adsorbent that can be recycled several times for recycling and reuse (**Table 2.11**). The number of time a specific adsorbent recycles seems to be dependent on the stability of the adsorbent. The ferri-hydrate adsorbent demonstrated an unchanged efficiency even after 50 times of

regeneration and reuse cycles by controlling the pH of the medium to regenerate the adsorbents (Edwards et al., 1989). The graphene hydrogel and hydro-talcites were studied upto 10 regenerations with pH control, salt solution and organic solvent such as ethanol (Gao et al., 2013; Kuzawa et al., 2006). The chelating agents such as ethylene di-ammine tetra acetic acid (EDTA) can be used to regenerate magnetic bio-char based adsorbent for six consecutive cycles, however the adsorbent efficiencies were reported to decreased after each cycle (Wang et al., 2015). Normally, pH control of the solution by the use of appropriate amounts of acids or alkalis can be used to regenerate a number of adsorbent such as Chitin based adsorbents, cement adsorbents, clay adsorbents, chitosan, maghemite, zeolites and functionalized silica (Han et al., 2009; Hu et al., 2005; Kamble et al., 2007; Kundu et al., 2005; Liu et al., 2000; Mandal et al., 2009; Thakre et al., 2015). Organic solvents (e.g. n-hexane) were used to dissolve organic pollutants such as dyes and the organics adsorbed on the surface and regeneration of the exhausted adsorbents on the simple principal of solvent extraction (Ma et al., 2013). Asghar et al. reported an electrochemical regeneration method for un-treated and treated graphite based adsorbents (Asghar et al., 2013). At the anode, the oxidation of adsorbed dye acid violet 17 leads to the regeneration.

The high regeneration efficiency (100%) was reported over five adsorption/regeneration cycles for the un-treated and treated graphite. Besides this method involve the formation of several breakdown products during electrochemical oxidation of organic dye (Asghar et al., 2013).The most important aspect in regeneration and reuse strategy is a wise reuse of the desorbed concentrated amounts of organic or inorganic pollutants along with the recycled adsorbents. The best way of disposal management is to avoid Nano-toxicology and reuse of the desorbed pollutant in the relevant industry for the manufacture of various commodities (Ali, 2012). The regenerated metals may be reused in the metal processing industries.

**Table 2.11 Adsorbents regeneration methods.**

#	Type of adsorbents	Regeneration method	No of reuse (times)	Effect on efficiency	Ref.
1	Ferri-hydride	pH control	50	unchanged	(Edwards et al., 1989)
2	Hydro-talcite	Salt and pH control	10	decreased	(Kuzawa et al., 2006)
3	Functionalized Silica	pH	03	decreased	(Liu et al., 2000)
4	Zeolites	pH	03	decreased	(Han et al., 2009)
5	Graphene composite	Annealing	05	unchanged	(Geng et al., 2012)
6	Maghemite	pH	06	unchanged	(Hu et al., 2005)
7	Graphene hydrogels	pH and ethanol	10	decreased	(Gao et al., 2013)
8	Chitosan	pH	03	decreased	(Kamble et al., 2007)
9	Porous desiccants	Microwave	-	-	(Inglis et al., 1989)
10	Activated carbons	Microwave	06	Increased	(Ania et al., 2004)
11	Super adsorbent polymer	Photo catalytic	-	decrease	(Dhodapkar et al., 2007)
12	Clay	pH	05	decreased	(Mandal et al., 2009)
13	Graphene composite	ethylene glycol	05	Decreased	(Sun et al., 2011)
14	Zeolite	Microwave	03	slight decrease	(Han et al., 2010)
15	Phosphate adsorbent	Ion exchange	20	decrease	(Urano et al., 1992)
17	Chitin base adsorbent	pH	-	decrease	(Thakre et al., 2015)
18	Activated carbon	Ethanol/ NaCl	05	Suppressed	(Du et al., 2015)
19	Magnetic bio char	EDTA	06	decrease	(Wang et al., 2015)

## **2.8 Summary of the literature review**

Magnetic and Nano-adsorbents have been proven as effective measure for treating contaminated environment for green environment remediation. The high chemical consumption and treatment cost is reduced by the application of renewable adsorbents resources. The research of novel series of adsorbents by a number of preparation routes provides a solution to meet the increasing safe water requirement of the population. The poor socioeconomic conditions and generation of large volume of industrial and agricultural waste are the major challenges of the present time. The CCD modelling tools can be applied to model the adsorption process. The application of kinetic studies provides some basic information regarding the speed of pollutants removal during field applications. The emergence of novel composite adsorbents by the composite with grapheme oxide and carbon nano tubes offers practical advantages in adsorbent applications. A large number of composites formats were reviewed to compare the relative percent removal efficiency of some of the advance forms of adsorbents in this study.

### CHAPTER 3: RESEARCH METHODOLOGY

The success of green environmental remediation is dependent on the reliability of data, design of work, experimentation, application of precise and accurate research methodology. Normally, geological features of the study area are well documented by field observation followed by mechanical, physical and chemical analysis to interpret the causes of a particular environmental problem. In this regards, the geochemical models are efficient and selective in terms of large scale data presentation, three dimensional maps building through the use of vector and raster data. The interpretation of geochemical model identifies the environmental issue and local point pollution resources e.g. industrial waste, hospital waste or house waste. The identified problem is resolved by the application of magnetic Nano-adsorbents by following OVAT or DOE strategies to reduce time, cost and efforts. Well-planned and performed experiments ordinarily give reproducible and reliable data.

This chapter describes the materials as well as the methodology used in the study. The sampling methods, research instruments and statistical procedures to collect, analyze, interpret the data and findings are also presented. The experimental setup used to make magnetic Nano-adsorbents via mechanical milling, sol-gel method, micro-emulsions, co-precipitation, various analytical and spectroscopic techniques for adsorbents characterization and hydrogeological applications are described. All experiments are distinctive from each other and in each situation standard procedures were followed for data collection, interpretation and presentation. The experimental parameters were optimized through two strategies: one variable at a time (OVAT) as well as design of experiment (DOE). The adsorption experiments were repeated at least three times to establish the reproducibility of the experimental results. Maximum care is

taken in the design, conduct, collection and analysis of experimental results. The following section will discuss the materials and methods employed in this study.

### **3.1 Materials**

In this work, the AR grade reagents with high purity were used as listed in **Table 3.1**. Acetonitrile (ACN), Water and Methanol of HPLC grade were purchased from Merck, Germany, and used for making Acephate aqueous solutions and for HPLC method. Throughout the experiments, all glassware was cleaned with 20% nitric acid and repeatedly washed with deionized water, followed by drying at 373K in an oven for 5 h. The samples of required concentrations were prepared by diluting the stock solution. The buffers of pH (1–3), (4–6) and (7–10) were prepared by mixing an appropriate volume of 0.1M solutions of HCl–KCl, CH<sub>3</sub>COOH–CH<sub>3</sub>COONa and H<sub>3</sub>BO<sub>3</sub>–NaOH, respectively [D. Perrin 1974]. In this work, deionized water (18.2 MΩ-cm at 25 °C) was used for preparing working and standard solutions.

### **3.2 Preparation of magnetic adsorbents**

Magnetic adsorbents play a very important role in hydrogeological decontaminations, separation, physical and materials sciences. The superior physical, chemical, thermal, electrical, optical and magnetic properties attract extensive applications in green environmental remediation, removal of pollutants from drinking water, river water and polluted water resources. In this context, preparation of adsorbent is a very important assignment for material scientists. In this work, we have fabricated the different series of adsorbents by the hydrothermal, sol-gel method, micro-emulsions, co-precipitation, and mechanical milling methods.

**Table 3.1: List of chemicals**

Name	Formula	Company	Purity (%)
Copper nitrate	$\text{Cu}(\text{NO}_3)_2$	Merck	>99
Ferrous nitrate	$\text{Fe}(\text{NO}_3)_2$	Merck	>99.5
Ferric nitrate	$\text{Fe}(\text{NO}_3)_3$	Merck	>99.5
Potassium Ferro cyanide	$\text{K}_4[\text{Fe}(\text{CN})_6]$	Merck	>99.5
Potassium Ferri cyanide	$\text{K}_3[\text{Fe}(\text{CN})_6]$	Merck	>99.5
Sodium hydroxide	$\text{NaOH}$	Merck	>99.5
Potassium chloride	$\text{KCl}$	Merck	>99.5
Ammonium hydroxide	$\text{NH}_4\text{OH}$	Merck	>99.5
Sulphuric acid	$\text{H}_2\text{SO}_4$	Merck	>99.5
Hydrochloric acid	$\text{HCl}$	Merck	>32
Nitric acid	$\text{HNO}_3$	Merck	>69.5
Phosphoric acid	$\text{H}_3\text{PO}_4$	Merck	>75.5
Potassium di-chromate	$\text{K}_2\text{Cr}_2\text{O}_7$	Merck	>99.5
Carbon flakes	$\text{C}$	Sigma Aldrich	>99.5
Cerium ammonium nitrate	$(\text{NH}_4)_2\text{Ce}(\text{NO}_3)_6$	Merck	>99.5
Monosodium phosphate	$\text{NaH}_2\text{PO}_4$	Merck	>99.5
Disodium phosphate	$\text{Na}_2\text{HPO}_4$	Merck	>99.5
Acephate	$\text{C}_4\text{H}_{10}\text{NO}_3\text{PS}$	Merck	>99.5
Methylene blue	$\text{C}_{16}\text{H}_{18}\text{N}_3\text{SCl}$	Merck	>99.5
Methyl orange	$\text{C}_{14}\text{H}_{14}\text{N}_3\text{NaO}_3\text{S}$	Merck	>99.5
n-hexane	$\text{C}_6\text{H}_{12}$	Merck	>99.5
Boric acid	$\text{H}_3\text{BO}_3$	Merck	>99.5
Acetic acid	$\text{CH}_3\text{COOH}$	Merck	>99.5
hexadecyl-trimethyl-ammonium bromide (CTAB)	$\text{C}_{19}\text{H}_{42}\text{NBr}$	Merck	>97.0
Phenosephranine	3, 7-Damino-5-phenylphenazinium chloride	Sigma Aldrich	>99.5
Gadolinium nitrate hexahydrate	$\text{Gd}(\text{NO}_3)_3 \cdot 6\text{H}_2\text{O}$	Sigma Aldrich	>99.5

### 3.2.1 Co-precipitation method for the preparation of $\text{CuCe}_{0.2}\text{Fe}_{1.8}\text{O}_4$

The pre-weighed quantities of  $\text{Fe}(\text{NO}_3)_3 \cdot 9\text{H}_2\text{O}$  (12.338 g/250 cm<sup>3</sup>),  $\text{Cu}(\text{NO}_3)_2$  (3.1089 g/250 cm<sup>3</sup>), and  $(\text{NH}_4)_2\text{Ce}(\text{NO}_3)_6$  (2.1 g/250 cm<sup>3</sup>) were separately dissolved in deionized water. All solutions were kept in a 2.0 dm<sup>3</sup> beaker and magnetically stirred at 330 K. NaOH (5.0 M) was poured dropwise, with stirring, as a precipitation reagent at 60°C. The ageing of the precipitates was completed by keeping them overnight at ambient temperature. The precipitates were centrifuged, washed, and dried at 110°C in the electrical oven for 24 h. The dried precipitates were annealed by heating in an electric furnace at 800°C for 500 min at a rate of 5°C per min<sup>-1</sup>.

### 3.2.2 Micro-emulsion method for $\text{CuCe}_x\text{Fe}_{2-x}\text{O}_4$ (x=0 to 0.5).

A transparent microemulsion (1.0 dm<sup>3</sup>) was prepared by sonicating hexadecyl-trimethyl-ammonium bromide (CTAB) in cyclohexane, 1-propanol and water. The calculated amounts of respective abovementioned salts were dissolved by magnetic stirrer at 60 °C. The basic solution of ammonium hydroxide ( $\text{NH}_4\text{OH}$ ) was drop wise added along with stirring to achieve pH 8.0. The precipitated ferrites were kept overnight at ambient temperature. The removal of unreacted or unwanted surfactants were accomplished through repeated washing using 85% methanol. The products were dried in an air electric furnace operating at 570 °C for 3.0 h at a rate of 5 °C min<sup>-1</sup>. As a final point, the dried products were ground in a quartz mortar and pestle into very fine powder for series of experiments with these adsorbents.

### 3.2.3 Hydrothermal reductive fabrication of $\text{CuCe}_{0.2}\text{Fe}_{1.8}\text{O}_4\text{-rGO}$

Graphene sheets were prepared using a modified Hummer's method (Azarang et al., 2015). The process began with the oxidation of graphite flakes by adding sulfuric acid and phosphoric acid (4:1 v/v) at room temperature. A weighed quantity of potassium permanganate ( $\text{KMnO}_4$ ) was added slowly, and then continuously stirred with a magnetic stirrer for three days to complete the oxidation process. The chemical oxidation reaction was stopped by the addition of hydrogen peroxide ( $\text{H}_2\text{O}_2$ ), along with ice cubes, to keep the temperature to a minimum, which immediately formed yellow precipitates. A neutral pH condition was achieved by successively washing the precipitates with hydrochloric acid (HCl) several times to yield the final product: exfoliated graphene oxide (GO). For the preparation of the graphene-based  $\text{CuCe}_{0.2}\text{Fe}_{1.8}\text{O}_4$  nanocomposites, graphene oxide (GO) (10.0 mg) was dissolved into  $50.0\text{ cm}^3$  of deionized water and sonicated for about 20 min to obtain a clear solution. Similarly,  $\text{CuCe}_{0.2}\text{Fe}_2\text{O}_4$  nanoparticles were dissolved in water by sonication, and mixed into the GO solution as shown in **Figure 3.1**. The above-mentioned solutions were transferred into a Teflon-lined stainless steel autoclave and heated for 480 min at a heating rate of  $5^\circ\text{C}$  per min in an electrical heating furnace. Following this, it was cooled, centrifuged and washed several times with deionized water. The graphene-based  $\text{CuCe}_{0.2}\text{Fe}_{1.8}\text{O}_4$  nanocomposites were then dried in an oven at  $60^\circ\text{C}$  overnight.

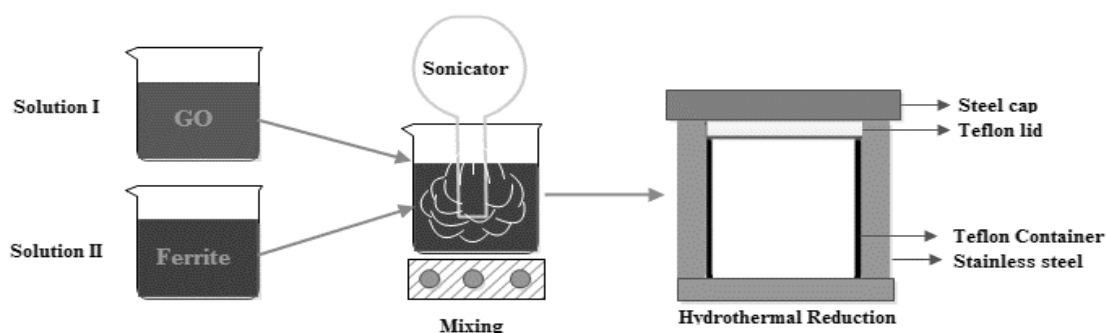


**Figure 3.1.** The scheme of hydrothermal reduction.

### 3.2.4 Mechanical milling to form grades of POCS

Mechanical milling was used to prepare three grades of POCS:

- i. Well graded
- ii. Uniformly graded and
- iii. Gap graded adsorbents from palm oil industrial waste.

The factory rejected waste materials were fed to a mechanical mill to obtain the particles of various sizes, followed by the separation of each type of particles according to the US standards sieving process. A standard criteria for well graded POCS is illustrated as in **Figure 3.2**.

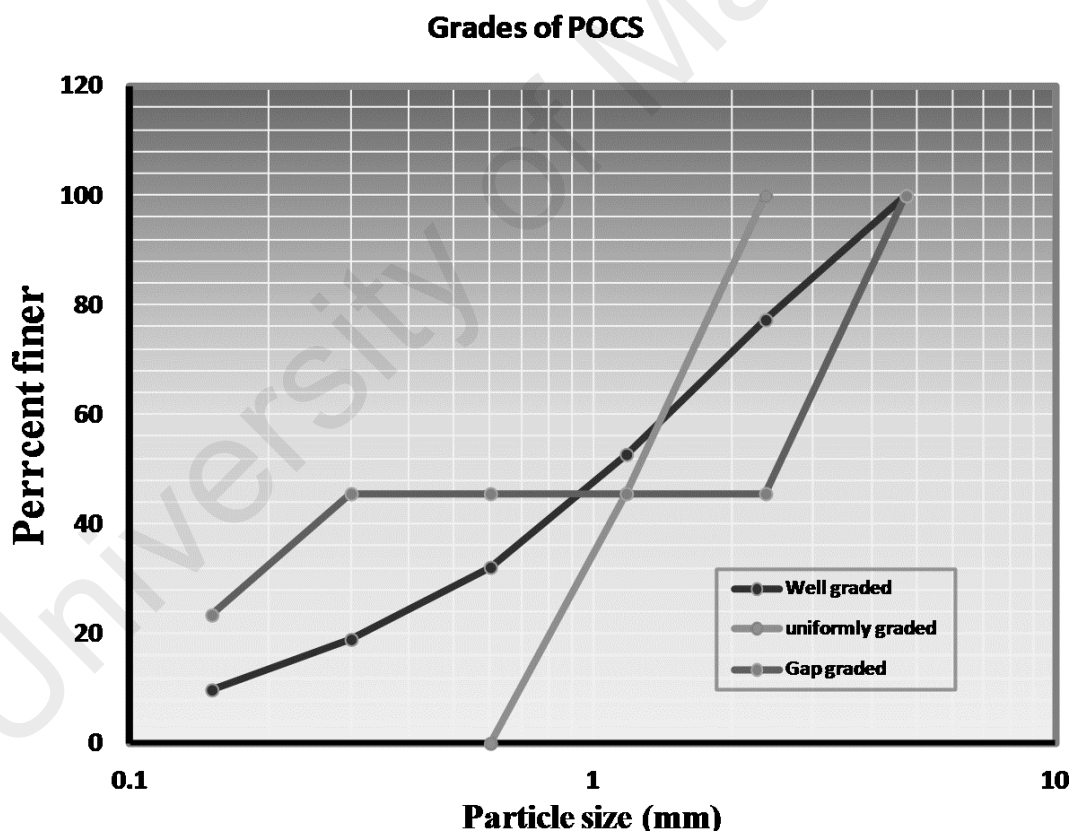


Figure 3.2. Mechanical grades of POCS by US standard sieving.

**Equation 3.1.** Uniformity coefficient of adsorbents.

$$C_u = \frac{D_{60}}{D_{10}}$$

Equation 3.1

Where  $C_u$  is the uniformity coefficient of the particles and should be greater than 4-6,  $D_{10}$ ,  $D_{60}$  corresponds to particles diameter of 10 % or 60 % finer respectively and is accepted as the effective size. The effective size of adsorbent particles is a good measure to estimate the hydraulic conductivity and drainage (Das, 2010). In Fig. 3.2, the blue curve represents the adsorbents with well graded adsorbents particles (0.1 mm to 5.0 mm). The coefficients  $C_u$  and  $C_z$  for the blue curve are 10.67 and 1.13 respectively satisfy the criterion for well graded adsorbents particles prepared by the mechanical milling process. The second criteria for well graded adsorbents is the coefficient of gradation ( $C_z$ )

**Equation 3.2.** Coefficient of gradation.

$$C_z = \frac{D_{30}^2}{D_{60} \times D_{10}}$$

Equation 3.2

The desirable range of  $C_z$  for the adsorbent particles is between 1-3. The POCS (red curve) shows a very narrow range of particle size from 0.6mm to 2.3mm. The value of coefficients  $C_u$ ,  $C_z$  is 2.28 and 0.77 respectively. From these values it is clear that the particles have different sizes with a gap represented by a linear trend. The POCS (green curve) consists of nearly uniform particles as shown by the graph. The high value of ( $C_u \sim 29$ ) and least value of ( $C_z \sim 0.11$ ) conforms to the uniformly graded adsorbents.

### **3.3 Characterization of fabricated Nano-adsorbents**

The successful chemical synthesis of Nano-adsorbents can be judged by the yield and the homogeneity of the product. The materials performance is certified by using analytical and spectroscopic techniques. The characterization of Nano-adsorbents is an important part in the determination of functional groups, shape, size, phase purity, optical band gap and chemical composition. In the present work, the synthesized adsorbents are calcined at dissimilar temperatures and are structurally characterized by different spectroscopic and analytical techniques such as powder X-ray diffraction (XRD), X-ray photoelectron emission spectroscopy (XPS), Raman Spectroscopy, thermogravimetric analysis (TGA), scanning electron microscopy (SEM)/ energy-dispersive X-ray spectroscopy (EDS), High resolution transmission electron microscopy (HRTEM), Fourier transform infrared spectroscopy (FTIR) and ultraviolet– visible spectroscopy (UV-Vis).

#### **3.3.1 Powder X-ray diffraction (XRD)**

Powder XRD method is commonly exploited for characterization of Nano-adsorbents. In this method the materials to be analyzed is grinded to a very fine powder by a quartz mortar pestle and spread on the sample holder to feed into the beam of monochromatic X-rays. Each particle in the sample is a tiny crystal randomly oriented with respect to the incident X-rays. The tiny crystals reflect light at different 2-theta scale depending on the lattice plans (Chung, 1974). The reflected beam position and intensity is recorded for comparison with a known standard. This comparison delivers the information regarding the crystallinity, crystalline size, crystal stress or crystal strain, solid solutions and amorphous content of the sample. XRD is used to confirm the formation of solid state reaction, purity of phases, lattice constants, inter-planar distances, composition of elements at the octahedral and

tetrahedral sites (Suryanarayana et al., 2013).

Mathematically, the average crystallite sizes can be determined by using the Debye-Scherrer's formula **Equation 3.3**.

$$D = \frac{K\lambda}{\beta_{hkl}\cos\theta} \quad \text{Equation 3.3}$$

Where, D is the crystal size perpendicular to the reflection plane, K is the unit cell geometry dependent constant and its value is typically between 0.85-0.99,  $\lambda$  is the wavelength of X-rays radiations by the equipment (1.5418 Å),  $\beta_{hkl}$  is the broadening of the diffraction line measured at half the line maximum intensity (full width at half maxima; FWHM) and  $\theta$  is the angle between the incident X-rays and the reflection plane ( $2\theta/2$ ). The Bragg  $\beta_{hkl}$  can be written as **Equation 3.4**.

$$\beta_{hkl} = (B_{hkl} - b) \quad \text{Equation 3.4}$$

Where,  $\beta_{hkl}$  is the broadening measured on the X-ray pattern, and b is the broadening error of the equipment, a typical of each instrument. The X-ray powder diffraction spectra determines the lattice constants, phase nature, purity and crystal structure of synthesized magnetic Nano-adsorbents. The XRD analysis was performed using PANalytical X-ray diffraction model Almelo, The Netherlands equipped with HighScorePlus (Version: 3.0d (3.0.4 and License Number 10003698, Chemistry department, University of Malaya) software for data processing and analysis. The samples were finely grinded before placing on the sample holder with a gentle tapping to make a uniform powder layers. The sample holder was placed in the labelled samples vertical stage for identification. A continuous  $2\theta$  scan mode from 10o-95 o was used for whole range scan. A divergence slit ensure that the X-rays

focused only on the sample. The diffractograms were matched with the Joint Committee on Powder Diffraction Standards (JCPDS) PDF 1 database 2.6 to confirm the identity of samples (**Figure 3.3**).

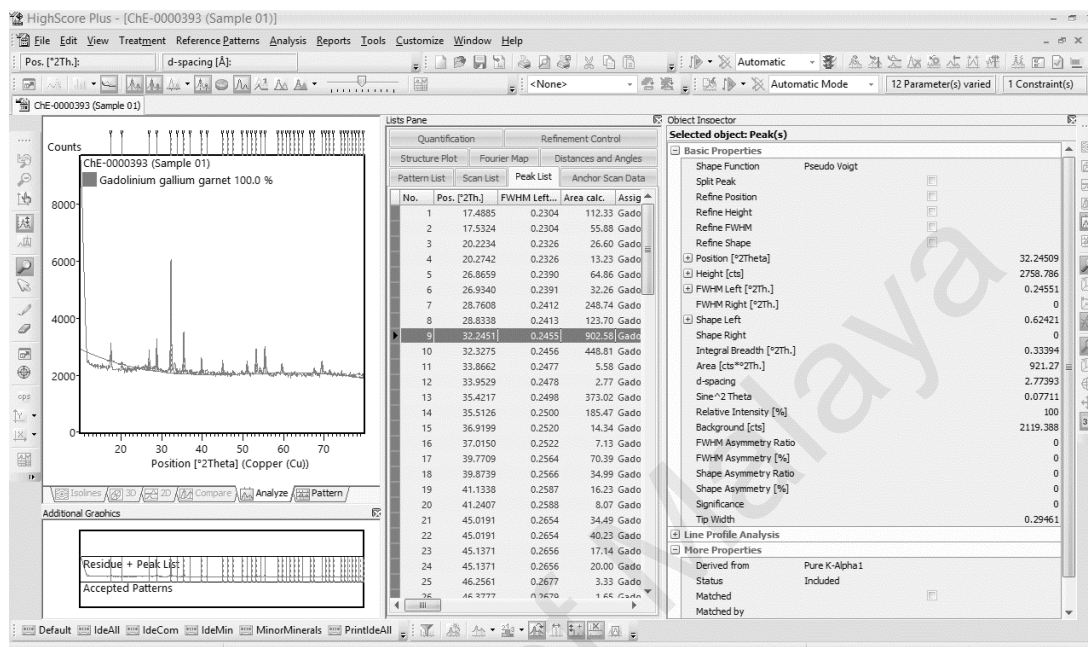


**Figure 3.3. Garnet ferrites diffractogram showing 100% phase purity.**

### 3.3.2 Thermogravimetric analysis

Thermogravimetric analysis (TGA) is an analytical technique that employs thermobalance to monitor changes in the weight of a sample as the temperature increases in the preselected programmed temperature range e.g. 50 °C to 900 °C. The thermogram is the graph that shows the pattern of weight loss. Each downfall in the thermogram indicates a degradation of sample, evaporation of water, decomposition or formation of certain phases. The thermogram is used to evaluate quantity of components, weight loss and thermal effects during the conversion of precursors to final metal oxides Nano-adsorbents.

The thermal strength of the magnetic Nano-adsorbents was assessed by using a computer programmed thermobalance equipped with a supply of inert gas (N<sub>2</sub>), located at the central equipment facility, chemistry department university of

Malaya. An approximate weight (~10 to 50 mg) of each materials was taken into the ceramic cup and placed inside the thermobalance followed by a lid on the top to provide an isolated environment. The software options were selected dynamically from ambient to 900°C at a heating rate of 10 °C min<sup>-1</sup> under nitrogen gas with a flow rate of 20 ml min<sup>-1</sup>. For second sample the thermobalance automatically cools down to room temperature before being heated again from ambient to 900°C at a heating rate of 2 °C min<sup>-1</sup> with the same gas flow rate.

### **3.3.3 Electron microscopic analysis**

Electron microscopy analysis tender structural information along a range of magnifications as compared to a simple light microscope from 10  $\mu\text{m}$  to 0.2 nm, specifically for the minute quantity or tiny fragment of magnetic Nano-adsorbents particles at a time when optical microscopes are unable to image it to any further extent. The modern electron microscopes work in either transmission or reflection mode to view the particles of magnetic Nano-adsorbents. The primary principle or plan of each operative approach are discussed as follows.

#### **3.3.3.1 Scanning electron microscopy (SEM)**

Scanning electron microscopy (SEM) is one of the versatile and well known exploratory techniques (Tung et al., 2009). Compared to the old-fashioned optical microscope, an electron microscope offers high magnifying capability, high resolution, and inspection of Nano-adsorbents or simplicity of sample preparation. Electrons fired by an electron gun enter the surface of the sample and produce several low energy secondary electrons. The intensity of the secondary electrons is governed by the surface features and nature of the sample. Consequently, image is constructed by determining the secondary electron as a function of the location of the incidental electron beam (Cahn et al., 2013).

In addition to secondary electrons, backscattered electrons, Energy Dispersive X-ray (EDS) analysis delivers useful information about the magnetic Nano-adsorbents particle sizes, distribution and aggregation. In case of backscattered electrons imaging the intensity of the backscatter electron, generated by electron bombardment is correlated to the atomic number of the element, revealing the identity of the constituents' elements and percent composition of the magnetic Nano-adsorbents. The fingerprints X-rays emitted from the component elements aid in deduction of elemental information of the magnetic Nano-adsorbents. It also serves chemical elements mapping along the entire surface and a semi quantitative analysis. At present, these analytical techniques are frequently used for non-destructive surface analysis, material characterization and wide applications in research and industry.

### **3.3.3.2 High resolution transmission electron microscopy**

HRTEM is an indispensable technique for nanomaterials and nanotechnology for the determination of fine structure, shape and lattice properties at a very high resolution. In this technique, transmitted or forward-scattered electron beam interacts with a solid particles, creating a number of elastic or inelastic scattering. Further, the beam passes through a succession of lenses that determines the image resolution. The source electron beam is produced by current heating of cathode filament. TEM requires high vacuum for the travelling of electrons from cathode to anode. A supporting accelerating voltage is applied between 50 to 150 kV, to control the electrons and image resolution. The higher accelerating voltage provides shorter electron waves for high image resolution of the samples particles. The accelerated electrons reach to the bottom anode, following a similar way to that of light in an optical microscope. The electrons are focused by a condenser onto the object, where they are partially deflected after collision with the nanoparticles. The degree of

deflection varies according to the electron density of the nanoparticles. Generally, the greater the mass of the particles, the greater is the degree of electrons deflection. The scattered electrons are collected on an objective lens creating an image that is magnified by an additional system of lenses. The final processed image is visible on the computer screen, ready for saving into image file formats. In the present study, LEO-Libra 120 (Germany) transmission electron microscope is used to study the morphology of the products.

### 3.3.3.3 Surface analysis of Magnetic Nano-adsorbents

The surface morphology of the samples was studied by using a Quanta 200 FEI FESEM instrument and EDS was used to analyze the chemical composition of the sample surface. The powder samples were adhered to the aluminium sample holder using a small piece of carbon conductive tape before they are loaded into the sample chamber of the instrument. The air evacuation in chamber was performed before analysis. The EDS were analyzed using INCA-Suite version 4.02 software. The detailed parameters of the measurement were as follow:

---

Working distance	:	8-10 mm
Vacuum mode	:	High vacuum
Accelerating voltage	:	5 kV
Spot size	:	2.5 – 3 $\mu\text{m}$
Detector	:	Large Field Detector (LFD)

---

For measurement of the elemental composition of the samples the acceleration voltage was focused on the sample dispersed on carbon tape fixed on sample holder. The TEM specimens were prepared by dropping the samples on a copper grid. For the size measurement and phase identification, images of representative areas of the sample were taken at different magnifications with a CCD

camera.

### **3.3.4 Fourier Transform Infrared Spectroscopy (FTIR)**

Fourier Transform Infrared Spectroscopy (FTIR) is an analytical technique used to identify the functional groups present in the sample (Stuart, 2005). The FTIR spectrophotometer is used to measure the absorption of various infrared light wavelengths by the material of interest. The infrared absorption bands are used to identify a specific functional group. The early-stage IR instrument dispersive infrared light through a prism or a grating monochromator (Sheppard, 2006). The scanning rate of these pioneers' instruments was slow requiring more time for the analysis of samples. The latest Fourier Transform Infrared (FTIR) spectrometer work faster. A typical FTIR spectrometer obtains infrared spectra by collecting an interferogram of a sample signal with an interferometer, which measures all of infrared frequencies simultaneously (Stuart, 2005). The acquired interferogram is digitized by Fourier transform function to build an output FTIR spectrum (Stuart, 2005). The infrared light can be categorized as far infrared ( $4\sim 400\text{ cm}^{-1}$ ), mid infrared ( $400\sim 4,000\text{ cm}^{-1}$ ) and near infrared ( $4,000\sim 14,000\text{ cm}^{-1}$ ). When an infrared ray interacts with the sample chemical bonds oscillate, stretch or contract. A chemical functional group in the sample adsorbs infrared radiation of a specific wave number range irrespective of the structure of the rest of the molecule. Therefore, IR spectroscopy identifies various functional groups in a Nano-adsorbents.

#### **3.3.4.1 Sample preparation & analysis**

The FTIR spectrum was recorded in the transmittance mode using a Bruker-optic spectrometer with a resolution of  $4\text{ cm}^{-1}$ . A small amount of Nano-adsorbent was placed on the holder to directly interact with FTIR laser light. All the FTIR spectra were recorded at a rate of 32 scan data accumulation in a  $400\sim 4000\text{ cm}^{-1}$

range.

### 3.3.5 Ion Chromatography

The beginning of the ion chromatography or the ion exchange chromatography techniques is thought to be around the middle of the twentieth century. The “Manhattan project” considerably provides better insights about ion exchangers and their applications (1935 to 1950). The theoretical model to explain the ion exchange phenomenon was developed during the fifties and sixties. **Table 3.2**, lists the chronology of ion exchange chromatography.

**Table 3.2. Chronology of ion exchange chromatography (Kolb et al., 2001)**

Year	Development	Developers
1850	Soil as an ion exchanger for cations e.g. $\text{NH}_4^+$ , $\text{Ca}^{2+}$ , $\text{Mg}^{2+}$ .	Thomas & Way
1935	Sulfonated and aminated condensation polymers e.g. formaldehyde and phenols.	Adams, Holmes
1942	Sulfonated polystyrene/ divinyl benzene resins as cation exchangers (Manhattan-Project)	d'Allelio
1947	Animated polystyrene/ divinyl benzene resins as anion exchangers	McBurney
1953	Ion exclusion chromatography	Wheaton, Baumann
1957	Macroporous ion exchangers	Corte, Meyer, Kunin et al.
1959	Basic theoretical principle of IC	Helfferich
1967-70	Peculiar ion exchangers	Horvath, Kirkland
1975	Ion exchange chromatography with conductivity detection with a “stripper”.	Small, Stevens, Baumann
1979	Conductivity without “stripper”.	Gjerde, Fritz, Schmuckler
1976-80	Ion pair chromatography	Waters, Bidlingmeier, Horvath et al.

The introduction of continuous detectors and high pressures offered a performance jump from normal pressure liquid chromatography to high pressure or high performance liquid chromatography (HPLC). At present IC is a competitive tool to study the anionic and cationic contaminants in hydrological samples and drinking water.

### 3.3.5.1 IC Measurement conditions

Anhydrous  $\text{Na}_2\text{CO}_3$  (191 mg) and  $\text{NaHCO}_3$  (143 mg) were weighed on analytical balanced and dissolved in deionized water with 20 mL of acetone to make up the final volume 1L. The IC operation conditions are listed in **Table 3.3**.

**Table 3.3 IC measurement conditions**

Column	Metrosep A Supp 4
Flow rate of mobile phase	1.0 cm <sup>3</sup> / min
Pressure	5.5 MPa
Analysis time	30 min
Sample size	20 $\mu\text{L}$
Regeneration media for suppressor	50 mmol/ L $\text{H}_2\text{SO}_4$ , ultra-pure water

### 3.3.6 Electrochemical methods

#### 3.3.6.1 Cyclic voltammetry

The cyclic voltammetry (CV) measures the potential of working electrode in a cyclic manner by switching between the positive and negative direction of the applied potential. A typical plot between current and applied potential is known as cyclic voltammogram (**Figure 3.4**). A cyclic voltammogram is plotted by immersing the three electrode system (reference, counter and working electrode) into a background electrolyte solution of known concentration and measuring response with Auto lab

instruments. A proper potential range (window) is selected to study the effect of working electrode potential on the electro-active species.

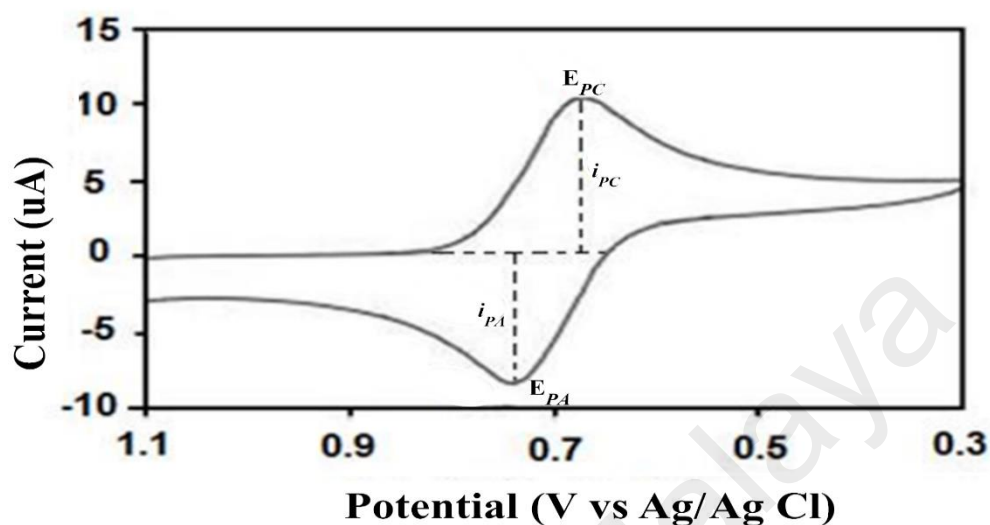


**Figure 3.4** A typical cyclic voltammogram.

As the potential of working electrode immersed in a redox couple e.g. 0.1 M KCl solution containing 1.0 mM  $K_3[Fe(CN)_6]$  and  $K_4[Fe(CN)_6]$  (1:1), becomes negative, the reduction process takes place at the electrode surface and vice versa in a cyclic fashion. During reduction half cycle the uncharged species get electron and become negatively charged until a potential is reached when all the species have been reduced, at this stage a maximum current peak also known as cathodic current peak ( $i_{PC}$ ) is observed as shown in **Figure 3.4**. Further increase negative cathodic potential has declined the current due to reduction of all the species. During the oxidation half cycle, the reduced species are oxidized by applying reverse anodic potential. Similar to the  $i_{PC}$  as stage of maximum anodic current is reached ( $i_{PA}$ ) but in opposite direction.

Consider a typical redox couple R and R-. If the electrode system is fully reversible and diffusion of the species i.e. the uncharged species (R) is the rate controlling step and there are well separated anodic and cathodic peak potential calculated by **Equation 3.5**.

$$E_{PA} - E_{PC} = \frac{59}{n} V \quad \text{Equation 3.5}$$

Where “n” is the number of electrons exchanged during the redox reaction. The Nernst equation is commonly used to measure the standard electrode potential ( $E^o$ ) of the reversible R/R- redox system (**Equation 3.6**). It is also known as the mid peak potential between the cathodic and anodic peak potentials.

$$E = E^o + \left\{ \frac{59}{n} \right\} \log\left(\frac{a_R}{a_{R^{n-}}}\right) \quad \text{Equation 3.6}$$

Where  $a_R$  and  $a_{R^{n-}}$  represents, the activities of oxidation and reduction products respectively. When activities are exchanged with concentration in equation 3.6, the standard electrode potential ( $E^o$ ) is named as the formal or conditional electrode potential ( $E^o_f$ ), it is characteristic for a specific redox reaction. There are certain redox reaction in which diffusion is not the rate slowing step and electrode reaction in non-reversible. In these type of reaction over potential is used as the reaction driving force to continue the chemical reaction. In such situations the applied over potential creates more peak separation than estimated. The peak current ( $I_p$ ) can be calculated by **Equation 3.7**.

$$I_p = \frac{dQ}{dt} = \frac{dN}{dt} nF \quad \text{Equation 3.7}$$

Where Q, F and N stands for the flowing charge in coulombs per second, Faraday constant and the number of moles of sample involved in the redox reaction at the glassy carbon electrode surface. The number of moles of sample can be calculated by rearranging equation 3.7. The amount of sample adsorbed ( $\text{mol cm}^{-2}$ ) can be calculated by dividing the number of moles by the surface area of the working electrode. **Equation 3.8**, number of moles of samples in redox reaction.

$$N = \frac{Q}{nF}$$

Equation 3.8

### 3.3.6.2 Electrochemical Impedance Spectroscopy (EIS)

EIS measures the current flowing through a working electrode of an electrochemical cell by applying an alternating current (AC) of 5 to 10 mV. The electrochemical process at the electrode-electrolyte interface is treated as an electronic circuit containing a combination of capacitors and resistors as shown in **Figure 3.5**. The solution resistance ( $R_s$ ) is placed in series with the parallel combination of the electrical double layer capacitance ( $C_{dl}$ ) and an impedance of the reaction of interest, consisting of charge transfer resistance ( $R_{ct}$ ) and Warburg diffusion element ( $W$ ). Following a hit and trial method the experimental data is fitted into a model circuit available in NOVA software, and can be modified manually according to the need of the work.

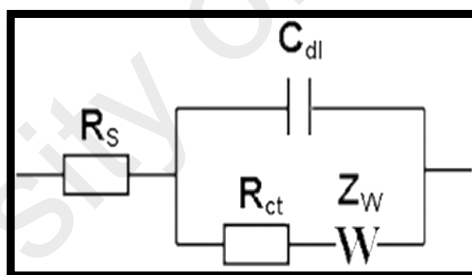


**Figure 3.5** A typical model circuit.

Nyquist plot represent the EIS data with distinct regions of charge transfer by the first half circle followed by the mass transfer region under the Warber diffusion control, as observed in the low frequencies. The  $R_{ct}$  values are calculated from the diameter of the semicircle in the Nyquist plot as shown in **Figure 3.6**.

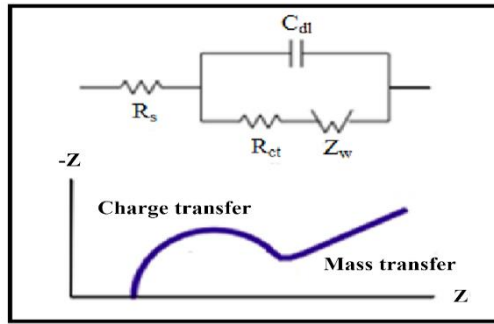


**Figure 3.6 Model fit in Nyquist plot.**

### 3.4 Nano-ferrites applications

Nanoferrites are made for a variety of purposes and the purpose characteristically edict the content and precursors.

#### 3.4.1 Nano-ferrites

Sample preparation is a critical step before physic-chemical analysis. The target molecules are usually present at very low concentration while interfering substances are usually present at higher concentrations. The quality of samples is ensured by taking different replicates samples from each bulk. Therefore, the target molecules need to be enriched; at the same time, the interfering substances need to be removed. A variety of functionalized materials such as activated carbons, silica, polymeric materials, nanoparticles, ferrites and biomass derived adsorbents have been used for the selective capture and enrichment of samples. Sample enrichment units are fabricated using these materials to suit the analysis needs of particular sample.

#### 3.4.2 Analysis techniques

The heavy metals analysis procedure involve inductively coupled plasma mass spectroscopic (ICP-MS) analysis for multiple metals analysis e.g. Ca, Mg, Pb, As, and Cr. A high performance liquid chromatography (HPLC) method was employed to separate and measure the amount of organic pollutant acephate. The amounts of anionic species e.g.  $F^-$ ,  $Cl^-$ ,  $NO_3^-$  and  $SO_4^{2-}$  were estimated by ion

chromatography.

### 3.5 Modelling adsorption

#### 3.5.1 Response Surface Model

The statistical models i.e. response surface standard method of experimental design was followed to study the effect of linear, interaction and quadratic effects of experimental factors. According to the selected DOE method, a central composite design (CCD) option was chosen in the Stat Ease 9.0 software. The modelling of adsorption process was carried out based on the designed experiments by the software to study the individual as well as the group effects of the factors selected for the present study. The experiments were repeated to determine any systematic or nonsystematic errors of the present adsorption system. The adsorbent adsorption capacity ( $Q_e$  mg.g<sup>-1</sup>) was calculated by **Equation 3.9** (Shanmugaprakash et al., 2013).

$$Q_e = \frac{(C_o - C_e)V}{m} \quad \text{Equation 3.9}$$

Where,  $C_o$  and  $C_e$  stand for initial and equilibrium adsorbate concentration (mgL<sup>-1</sup>) respectively,  $V$  is the total volume of solution in liters and  $m$  is the mass of adsorbent (g). Adsorption experiments were repeated to check for systematic variations to determine standard deviation and reproducibility of results. Four variables are Adsorbate initial conc. (mgL<sup>-1</sup>), pH, temp and Adsorbent (Ads. mg) in the range of 300-500 mgL<sup>-1</sup>, 3.0 to 9.0, 20 to 40 and 400 to 600 (mg) respectively. In this work, **equation 3.10** is used for the selected quadratic model (ZHANG ET AL., 2015).

$$Q_e = \beta_o + \sum_{i=1}^k \beta_i x_i + \sum_{i=1}^k \beta_i x_i^2 + \sum_{i=1}^{k-1} \sum_{j=2}^k \beta_{ij} x_i x_j + \varepsilon \quad i \neq j \quad \text{Equation 3.10}$$

Where  $\beta_o$  is a constant coefficient,  $\varepsilon$  represents error,  $x_i$  and  $x_j$  are

independent variables,  $\beta_i$ ,  $\beta_{ii}$  and  $\beta_{ij}$  represent coefficients of linear, quadratic and interaction effects respectively. The adsorption data of each experiment were analyzed and fitted into the quadratic models. The models were verified by statistical tests i.e. analysis of variance (ANOVA), residuals analysis (RA), scaling residuals (SR) and prediction error sum of squares (PRESS) (Naseri et al., 2014). The verified and validated models were applied to optimize the four input variables and to maximize output i.e. fluoride, nitrates, nitrites, sulphates, phosphates, arsenic, cadmium, nickel, iron and related heavy metals adsorption capacity.

### 3.5.2 Isotherms

Adsorbate-adsorbent interaction can also be presented in the form of isotherm, by plotting of the equilibrium concentration of ions in the exchanger or the solid phase versus equilibrium concentrations of the same ions in the co-existing solution phase. The design of hydro-decontamination system requires a thorough analysis of the adsorption capacity ( $Q_e$ ) of each adsorbent and the percent removal ( $\%R$ ) efficiency. The adsorption process is taken to be completed in four steps i.e. bulk diffusion, film diffusion, pore diffusion and chemical reaction. First, the sorbate molecules travel from the solution to the sorbent surface where they diffuse through the boundary layer to the surface of the material. Then, these sorbate molecules diffuse into the interior of the particles where they chemically react with active sites on the surface of the sorbent. To verify the physical adsorption in the sorbent network and chemical interaction in the dye molecules during the adsorption process, several equilibrium models have been known to be used (Kyzas et al., 2015; Kyzas et al., 2015; Świetlik et al., 2015). The basic purpose of these equilibrium isotherms is to provide an insight into the molecular interaction. The suitability of a particular isotherm is decided based on the correlation coefficient ( $R^2$ ) which is ideally 1, while

the other parameter is the degree of agreement between the experimental results and the isotherms predicted results. These parameters help to assess and decide on the success rate of a particular hydro-decontamination system and on the viability of the process for a specific contaminant at certain geological locations.

### 3.5.2.1 Langmuir Isotherm for monolayer adsorption

This model assumes an ideal localized monolayer adsorption phenomena on the surface of adsorbents. Each adsorbent has a fixed number of sites while each site can adsorb only one adsorbate ion or molecule. As all sites are uniform so the energy of adsorption is the same throughout the adsorbent surface. The linear Langmuir adsorption model (Gimbert et al., 2008), is given as **equation 3.11**.

$$\frac{C_e}{Q_e} = \frac{1}{K_L} + a_L \frac{C_e}{K_L} \quad \text{Equation 3.11}$$

The Langmuir constants,  $K_L$  and  $a_L$  are related to the adsorption energy and the binding force between adsorbent and adsorbate. The maximum adsorption capacity ( $Q_m$ ) can be calculated from the ratio of these constants. The maximum adsorption capacity ( $Q_{max}$ ) **Equation 3.12**.

$$Q_{max} = \frac{K_L}{a_L} \quad \text{Equation 3.12.}$$

The dimensionless separation factor ( $R_L$ ) **Equation 3.13**, explains the nature of adsorption process. It can be calculated using: The separation factor.

$$R_L = \frac{1}{1 + K_L C_e} \quad \text{Equation 3.13.}$$

When  $R_L$  equals to zero it means irreversible adsorption process, a value from zero to one indicates favorable adsorption, while a value of more than one represents

unfavorable process.

### 3.5.2.2 Freundlich isotherm for heterogeneous adsorption

The Freundlich model explains the heterogeneous adsorption process at the adsorbate-adsorbent interface showing multilayer adsorption. Multiple adsorption is characteristic of adsorbents with affinities for the toxic substances due to their better surface morphology, porous structure and range of surface functional groups. This model assumes exponential distribution of surface active sites and energetics of adsorption systems. The primary adsorption sites are occupied first by the adsorbate molecules that forms a layer on which the secondary or tertiary layers of adsorbate are formed. However, the limitation of this model is that as the number of layers increases the adsorption-desorption phenomenon takes place in these systems. The Freundlich model (Crini et al., 2007) is illustrated as **Equation 3.14**.

$$\ln q_e = \ln K_F + \frac{1}{n} \ln C_e \quad \text{Equation 3.14.}$$

Where,  $q_e$ , is the equilibrium amount of adsorbate (mg g<sup>-1</sup>);  $K_F$ , the Freundlich constant associated with the degree of adsorption;  $1/n$ , the heterogeneous factor related to the intensity of adsorption. A value of  $1/n$  greater than unity represents the physical adsorption.

### 3.5.2.3 Temkin Isotherm for energetics of adsorption

Temkin isotherm assumes that the heat of the adsorption process for all the molecules present in an adsorbed layer decreases linearly with surface coverage. It helps to calculate the energetics of the system and provides an insight on the exothermic and endothermic nature of the adsorption process. It can also be used to calculate the free energy of the system, entropy and enthalpy of the system.

According to the Temkin model, adsorption is characterized by a uniform distribution of binding energies up to some maximum value. The linear form of this model is given as **Equation 3.15**:

$$q_e = B_t \ln K_T + B_t \ln C_e \quad \text{Equation 3.15}$$

Where  $K_T$  is the equilibrium binding constant corresponding to the maximum binding energy, and  $B_t = RT/B$  is related to the heat of adsorption. The value of  $K_T$  and  $B_t$  are obtained from the intercept and slope of the plot of  $q_e$  versus  $\ln C_e$  respectively.

#### 3.5.2.4 Flory Huggin (FH) model for degree of surface coverage

The FH model accounts for the degree of surface coverage that is characteristic of adsorbate and adsorbent. The linear form of the FH equation is represented by:

$$\log \frac{Q}{C_i} = \log K_{FH} + n \log(1 - Q) \quad \text{Equation 3.16}$$

Where  $Q$  is the degree of surface coverage, which can be calculated by the following:

$$Q = 1 - \frac{C_e}{C_i} \quad \text{Equation 3.17}$$

Where  $n$  is the number of adsorbate molecules occupying the adsorption sites,  $K_{FH}$  is the equilibrium constant. The  $n$  and  $K_{FH}$  constants can be calculated from the slope and intercept of the curve  $\log Q/C_i$  versus  $\log(1-Q)$ .

#### 3.5.2.5 Dubinin-Radushkevich (D-R) isotherm

The linear form of Dubinin Rudushkevish (Dubinin et al., 1947) model is given as **Equation 3.18**.

$$\ln Q_e = \ln X_m - K_{DR} \varepsilon^2 \quad \text{Equation 3.18}$$

The value of  $X_m$  represents the monolayer sorption capacity ( $\text{mg g}^{-1}$ ); it can be calculated from the intercept of the plot between  $\ln Q_e$  and  $\varepsilon^2$ .

**Equation 3.19:** DR model  $\varepsilon$ .

$$\varepsilon = RT \ln \left( 1 + \frac{1}{C_e} \right) \quad \text{Equation 3.19}$$

### 3.5.3 Adsorption Kinetics

For the design of an effective hydro-decontamination system we need to know the rate of chemical reaction taking place i.e. the rate of adsorption. With reference to geochemical modelling, we do not attempt to explain in detail the broad field of chemical kinetics, but just enough to understand the basics of kinetics. Several kinetic models are implemented to examine the experimental data to decide on the nature, intensity and mechanism of the adsorption process. The speed of adsorption was evaluated by employing four kinetic models: pseudo-first order, pseudo-second order, intraparticle diffusion and Banghams. The overall adsorption rate is proportional to the driving force and the concentration gradient in the case of the first order, while in the case of the second order, it is proportional to the square of driving force.

#### 3.5.3.1 Rate law

A rate law is a statement about how the rate of a reaction depends on the concentration of the participating species (Reactants). If we think at the molecular level, imagine molecules colliding with one another. The overall reaction rate is controlled by the number and orientation of collisions and the number and type of

molecules interacting. Let say we have a general reaction as in **Equation 3.20**.



Where A, B, C and D are the chemical formulae, and a, b, c and d are the stoichiometric coefficients. The rate of reaction can be written as **Equation 3.21**:

$$R = \frac{d\xi}{dt} k \cdot C_A^{n_A} C_B^{n_B} C_C^{n_C} D_D^{n_D} \quad \text{Equation 3.21}$$

The variable  $\xi$  is called the reaction progress variable and the proportionality constant, k, is called the rate constant. The exponents  $n_A, n_B, \dots, n_D$  are either integers or decimals and are used to calculate the order of a reaction. If  $n_A$  is 1, the reaction is designated as first order and if 2 as second order. The sum of exponents gives the overall order of the reaction. Rate laws are determined by analyzing one or more reactant or product as a functional of time as the reaction proceeds, and then fitting the results to see what theoretical model fits the data.

### 3.5.3.2 Zero order

A reaction is zero order if the rate of reaction is independent of substrate concentration, so the rate of reaction is constant. A plot of concentration vs. time will thus give a straight line. For example, bacterial reduction of sulfate in marine environments, where variables other than sulfate are constant (Gattuso et al., 1998).

**Equation 3.22.** Zero order

$$-\frac{dC}{dt} = k \quad \text{Or} \quad C_t = C_i - k \cdot t \quad \text{Equation 3.22}$$

Where  $C_i$  and  $C_t$  are the reactants concentration at  $t=0$  and  $t=t$  respectively.

### 3.5.3.3 First order

A first order reaction proceeds at a rate that depends only on the concentration of A as shown below. The more quantity of the reactant A, the more product is formed and vice versa.



For example, the burning of methane in the air will continue only for as long as it is available. If all exponents in **Equation 3.22**, are zero except of  $n_A = 1$ , then the rate law becomes:

$$\frac{d\xi}{dt} = \frac{dC_A}{dt} = k \cdot C_A \quad \text{Equation 3.23}$$

For example, decay of radioactive elements is a first order reaction. Suppose  $C_A = C$  and  $C = C^\circ$ , when  $t=0$ , then **Equation 3.20**, can also be simplified in the following forms (Zhu et al., 2002).

$$\begin{aligned} \int_{C^\circ}^C \frac{dC}{C} &= -k \int_0^t dt \\ \ln \frac{C^\circ}{C} &= kt \\ \ln C &= \ln C^\circ - kt \\ C &= C^\circ e^{-kt} \end{aligned} \quad \text{Equation 3.24}$$

These forms show the various ways to plot data to see if they fit first order rate law. For example, a plot of  $\ln (C^\circ/C)$  vs.  $t$  will contribute a straight line with a slope equals to the rate constant for change in reactants concentration.

### 3.5.3.4 Second order

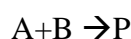
The bimolecular collisions reaction are generally second order. For example:



The rate law is proportional to the concentration of the reactants and the concentration of products has no effect on the rate of reaction. There are a number of other rate laws, but this will suffice to give an idea of the procedures. However, due to the complexity of chemical reactions, understanding them in terms of their fundamental mechanisms is not easy to achieve.

### 3.5.3.5 Pseudo order reactions

In the natural environment, we observe complex reactions that are not zero, first or second order but they partially follow the order criteria and are named as pseudo order reactions. Let us consider a reaction where A and B react to form a product (P).



The rate equation for this general reaction can be written as **Equation 3.25**.

$$\text{Rate} = k. [A]^1[B]^1 \quad (\text{Overall order} = 2) \quad \text{Equation 3.25}$$

Now suppose we perform an experiment in which  $[A] = 0.01 \text{ mol dm}^{-3}$  and  $[B] = 0.100 \text{ mol dm}^{-3}$ , i.e. B is 10 times more concentrated. After completion of the reaction, the concentration of reactant B remaining will be  $[B] = 0.099 \sim 0.100 \text{ mol dm}^{-3}$  i.e. the concentration of B remains unchanged.

For experiments where  $[B] \gg [A]$ , or  $[B] = \text{constant}$ , **Equation 3.25** becomes:

$$\text{Rate} = k. [A]^1[B]^0 \quad \text{or} \quad \text{Rate} = k. [A]^1$$

The experimental results show that the reaction is first order instead of second order as determined by chemical equation. Such type of reaction in which a reactant is much more concentrated than the other, the concentrated reactant is made to have no effect on the rate law, resulting in an overall pseudo order reactions.

### 3.5.3.6 Pseudo-First Order Kinetic Model

The pseudo-first order kinetic model is widely used to predict the adsorption mechanism. The linear form of the pseudo-first order model is given by **Equation 3.26**.

$$\ln(q_e - q_t) = \ln q_e - k_1 t \quad \text{Equation 3.26}$$

Where  $k_1$ , is the first-order rate constant of adsorption, while  $q_e$  and  $q_t$  are the maximum amount adsorbed at equilibrium and at time  $t$ , respectively. The linear plots of  $\ln(q_e - q_t)$  versus  $t$  yield straight lines. The values of  $k_1$  ( $\text{min}^{-1}$ ) and  $q_e$  ( $\text{mg g}^{-1}$ ) can be calculated from the slope and intercept of the pseudo first order linear plots.

### 3.5.3.7 Pseudo second order model

The linear form of the pseudo-second-order model is given by **Equation 3.27**:

$$\frac{t}{q_t} = \frac{1}{k_2 q_e^2} + \frac{t}{q_e} \quad \text{Equation 3.27}$$

Where  $k_2$  ( $\text{g mg}^{-1} \text{min}^{-1}$ ) is the rate constant of pseudo-second order kinetic equation, which can be calculated from the intercept of the linear plot of time versus  $t/q_t$ . The equilibrium adsorption capacity ( $q_e$ ) can be calculated from the slope.

### 3.5.3.8 Intraparticle Diffusion Model

The intraparticle diffusion model was used to evaluate the experimental data to see the possibility of intraparticle diffusion as the rate limiting step. It is given as:

**Equation 3.28:** Intra-particle diffusion model.

$$q_t = k_{id} t_{\frac{1}{2}} + I \quad \text{Equation 3.28}$$

Where  $k_{id}$  ( $\text{mg g}^{-1} \text{min}^{-1/2}$ ) is the intra-particle diffusion rate constant and  $I$  is the boundary layer effect ( $\text{mg g}^{-1}$ ). The value of  $I$  is directly proportional to the boundary layer thickness. According to **Equation 3.28**, the plot of  $q_t$  versus  $t_{1/2}$  should be a straight line with a slope  $K_{id}$  and intercept  $I$  when the mechanisms follow the intra-particle diffusion model.

### 3.5.3.9 Banghams's Model

The hydro-decontamination kinetic data was evaluated with Banghams's equation (**Equation 3.29**) to determine the slowest or the rate-controlling step during the adsorption process.

$$\log\left(\log\left(\frac{C_0}{C_0 - q_t m}\right)\right) = \log\left(\frac{k_o m}{2.303 V}\right) + \alpha \log(t) \quad \text{Equation 3.29}$$

Where  $V$  is the volume of solution (l) and  $\alpha$  and  $k_o$  are constants.

### 3.5.4 Thermodynamics

The study of adsorption reaction dependent on temperature gives valuable information about the change in free energy, enthalpy and entropy during adsorption. The values of adsorption energies ( $\Delta G$ ,  $\Delta H$  and  $\Delta S$ ) are calculated using the following equations.

$$\Delta G = -RT \ln K_L \quad \text{Equation 3.30}$$

$$\ln \frac{K_2}{K_1} = -\frac{\Delta H}{R \left(\frac{1}{T_2} - \frac{1}{T_1}\right)} \quad \text{Equation 3.31}$$

$$\Delta G = \Delta H - T\Delta S \quad \text{Equation 3.32}$$

## CHAPTER 4: RESULTS AND DISCUSSIONS

This chapter describes the results and discussion related to the main phases of this study. In the phase I, adsorbent characterization results are discussed. While in the phase II, application and modelling results are presented. The following sub-section describes the characterization of adsorbents, followed by application for green environment remediation.

### 4.1 Characterization results of $\text{CuCe}_{0.2}\text{Fe}_{1.8}\text{O}_4\text{-rGO}$ .

The characterization of adsorbents is an important step in the exploration of surface active functional groups, shape and size of particles, phase purity, optical band gap and chemical composition. In the present work, the synthesized adsorbents were characterized by different spectroscopic and analytical techniques. The crystal structure, crystallite size and lattice strain of the  $\text{CuFe}_2\text{O}_4$ ,  $\text{CuCe}_{0.2}\text{Fe}_{1.8}\text{O}_4$  ferrite nanoparticles, and graphene-based  $\text{CuCe}_{0.2}\text{Fe}_{1.8}\text{O}_4$  nanocomposites were observed by an X-ray diffractometer (XRD, PANalytical Empyrean), equipped with a monochromatic Cu K $\alpha$  radiation source. Fourier transform infrared spectroscopy (FTIR) was carried out on a Perkin Elmer System 2000 series spectrophotometer (USA) between 4000-400  $\text{cm}^{-1}$ . Thermogravimetric analysis (TGA) was used to examine the graphene and graphene-based  $\text{CuCe}_{0.2}\text{Fe}_{1.8}\text{O}_4$  nanocomposites. Energy dispersion spectroscopy (EDS), elemental mapping, and Field Emission Scanning Electron Microscopy (FESEM) were applied to study the elemental composition, the surface distribution of the elemental components, and particle size and distribution. Raman spectroscopy, (Renishaw 2000 system) was performed using a green laser operating at 532 nm and room temperature. The magnetic hysteresis loops of  $\text{CuFe}_2\text{O}_4$ ,  $\text{CuCe}_{0.2}\text{Fe}_{1.8}\text{O}_4$ , and graphene-based  $\text{CuCe}_{0.2}\text{Fe}_{1.8}\text{O}_4$  nanocomposites were recorded on a Vibrating Sample Magnetometer (VSM).

#### 4.1.1 XRD analysis

**Figure 4.1** shows the XRD patterns of the  $\text{CuFe}_2\text{O}_4$ ,  $\text{CuCe}_{0.2}\text{Fe}_{1.8}\text{O}_4$  ferrite nanoparticles, and graphene-based  $\text{CuCe}_{0.2}\text{Fe}_{1.8}\text{O}_4$  nanocomposites. We observed the single-phase structure of  $\text{CuFe}_2\text{O}_4$  that was obtained at  $800^\circ\text{C}$  and was indexed using JCPDS#034-425. **Figure 4.1 (b)** displays the diffraction patterns of the  $\text{CuCe}_{0.2}\text{Fe}_{1.8}\text{O}_4$  ferrite nanoparticles. The structure shows the major peak (311), while two other peaks represent the  $\text{CeO}_2$  peaks, and was indexed using JCPDS#043-1002 (Fig. 2b). The second phases were observed by adding  $\text{Ce}^{3+}$  content into the  $\text{CuFe}_2\text{O}_4$  ferrite. However, by increasing the  $\text{Ce}^{3+}$  ( $x > 0.2$ ), more peaks of  $\text{CeO}_2$  and  $\text{Ce}_2\text{O}_3$  can be seen, which may be the result of the larger ionic radii of  $\text{Ce}^{3+}$  ( $1.020\text{\AA}$ ) as compared to  $\text{Fe}^{3+}$  ( $0.645\text{\AA}$ ) (Wu et al., 2014). Thereby, we have investigated the second phase in the  $\text{CuCe}_{0.2}\text{Fe}_{1.8}\text{O}_4$  spinel ferrite structure. After the addition of graphene, similar developments were observed when looking at  $\text{CuCe}_{0.2}\text{Fe}_{1.8}\text{O}_4$ . In fact, due to the inherent low crystalline structure of graphene, the typical peaks of graphene were absent in the XRD patterns (**Figure 4.1 (c)**). However, a slight increase in the peak increases with the introduction of graphene, which was noticed with the crystallite refinement and lattice microstrain decrement. During the formation of the  $\text{CuCe}_{0.2}\text{Fe}_{1.8}\text{O}_4$  spinel ferrite structure,  $\text{Ce}^{3+}$  ions were dissolved in the medium to form a solid solution. Annealing at  $800^\circ\text{C}$ , this forced the  $\text{Ce}^{3+}$  ions to migrate into the crystal structure, spaces or grain boundary sites. The large ionic radius of  $\text{Ce}^{3+}$ , as compared to  $\text{Fe}^{3+}$  (Wu et al., 2014), offered a relative space interference to viable vacant crystal or interstitial sites in copper ferrites. Consequently, the excess  $\text{Ce}^{3+}$  ions oxidized into  $\text{Ce}^{4+}$  at this temperature and appeared as a separate phase in the XRD spectra.

XRD scientists have developed various theoretical models to assess these structural features through the mathematical analysis of XRD patterns. In this study, the average

crystallite size and micro strain of the samples were calculated using Equation 4.1 and Equation 4.2 respectively (Ebrahimi-Kahrizsangi et al., 2010):

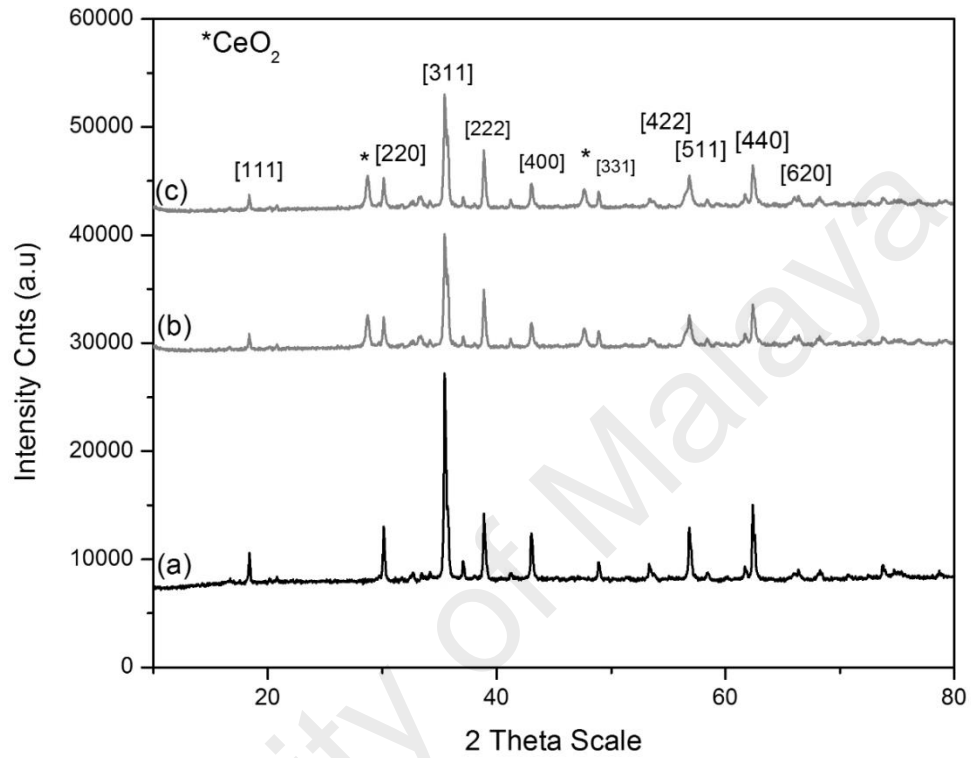


**Figure 4.1. XRD patterns of the (a)  $\text{CuFe}_2\text{O}_4$  (b)  $\text{CuCe}_{0.2}\text{Fe}_{1.8}\text{O}_4$  (c)  $\text{CuCe}_{0.2}\text{Fe}_{1.8}\text{O}_4\text{-rGO}$ .**

Equation 4.1. The average crystal size.

$$D_{\text{ave}} = \frac{k\lambda}{(B_{\text{obs}} - B_{\text{std}})(\cos\theta)} \quad \text{Equation 4.1}$$

Equation 4.2. The micro strain of crystals.

$$E^2 = \frac{(B_{\text{obs}}^2 - B_{\text{std}}^2)}{(4\tan\theta)^2} \quad \text{Equation 4.2}$$

Where B stands for the difference in the fundamental profile width between a standard and an unknown sample, and thus describes structural expansion. However, K, the crystal shape coefficient (0.9-1.0),  $\lambda$ ,  $D_{\text{ave}}$ , E, and  $\theta$  were the wavelength of the X-

ray (0.15406 nm), average crystallite size, mean lattice distortion (lattice strain), and Bragg's angle ( $^{\circ}$ ) respectively.

**Table 4.1. Crystallite sizes and micro-strain in  $\text{CuFe}_2\text{O}_4$ ,  $\text{CuCe}_{0.2}\text{Fe}_{1.8}\text{O}_4$ , and graphene  $\text{CuCe}_{0.2}\text{Fe}_{1.8}\text{O}_4$  nanocomposites.**

Ferrites	Crystallite size ( $D$ nm)	Lattice strain ( $\eta$ ,%)
$\text{CuFe}_2\text{O}_4$	$28 \pm 2.1$	$0.424 \pm 0.021$
$\text{CuCe}_{0.2}\text{Fe}_{1.8}\text{O}_4$	$50 \pm 1.3$	$0.251 \pm 0.017$
$\text{CuCe}_{0.2}\text{Fe}_{1.8}\text{O}_4$ -rGO	$59 \pm 1.7$	$0.211 \pm 0.019$

The important features of  $\text{CuFe}_2\text{O}_4$  and  $\text{CuCe}_{0.2}\text{Fe}_{1.8}\text{O}_4$  spinel ferrites in the presence and absence of graphene were compared (**Table 4.1**). In this case,  $\text{CuFe}_2\text{O}_4$  ferrite has a crystallite size of  $28 \pm 2.1$  nm and a lattice micro strain of  $0.424 \pm 0.021$ . In the absence of rGO, the average crystallite size of the  $\text{CuCe}_{0.2}\text{Fe}_{1.8}\text{O}_4$  was  $50.5 \pm 1.3$  nm and the lattice micro strain was  $0.251 \pm 0.017$ . However, with the creation of rGO, we observed a slight increase in the average crystallite size ( $59.3 \pm 1.3$  nm) and lattice micro strain ( $0.211 \pm 0.019$ ). We noticed that the crystallite size increased with the introduction of both  $\text{Ce}^{3+}$  matter and rGO. We furthermore observed that the combination of rare earth ions and graphene with a  $\text{CuFe}_2\text{O}_4$  spinel structure would also affect the physical forms, functional groups, morphologies and magnetic properties.

#### 4.1.2 FTIR functional groups

**Figure 4.2** details the comparative FTIR functional groups of the  $\text{CuFe}_2\text{O}_4$ ,  $\text{CuCe}_{0.2}\text{Fe}_{1.8}\text{O}_4$  ferrite nanoparticles and graphene-based  $\text{CuCe}_{0.2}\text{Fe}_{1.8}\text{O}_4$  nanocomposites. Fig. 3a displays the distinguishing absorption peaks of a typical  $\text{CuFe}_2\text{O}_4$  ferrite (Rehman et al., 2015). Fig. 3b shows the depletion of  $3360 \text{ cm}^{-1}$  bands, while the appearance of  $1470 \text{ cm}^{-1}$  clearly indicates the creation of  $\text{CuCe}_{0.2}\text{Fe}_{1.8}\text{O}_4$ . The involvement of  $\text{CuFe}_2\text{O}_4$  functional groups with the arriving Ce is seen in the complete

vanishing of the FTIR band from  $876\text{ cm}^{-1}$  to  $1230\text{ cm}^{-1}$ . The distinctive of the doped ferrite band at  $574\text{ cm}^{-1}$  also indicates the formation of the desired spinel structure (Rehman et al., 2015). The absorption band near  $1390\text{ cm}^{-1}$  and  $1470\text{ cm}^{-1}$  matches to the carbonyl stretch ( $-\text{C}=\text{O}$ ) of the carboxylic acid group and in-plane vibrations of the  $\text{sp}^2$  carbons ( $-\text{C}=\text{C}-$ ) associated with the deoxygenation of GO (Ji et al., 2014). The FTIR analysis of the  $\text{CuCe}_{0.2}\text{Fe}_{1.8}\text{O}_4$  ferrite nanoparticles and graphene  $\text{CuCe}_{0.2}\text{Fe}_{1.8}\text{O}_4$  nanocomposites showed an powerful and characteristic band at  $549\text{ cm}^{-1}$  of the ferrites, indicating the tetrahedral and octahedral sub-lattices in the prepared samples (Borhan et al., 2013; Zhang et al., 2014).

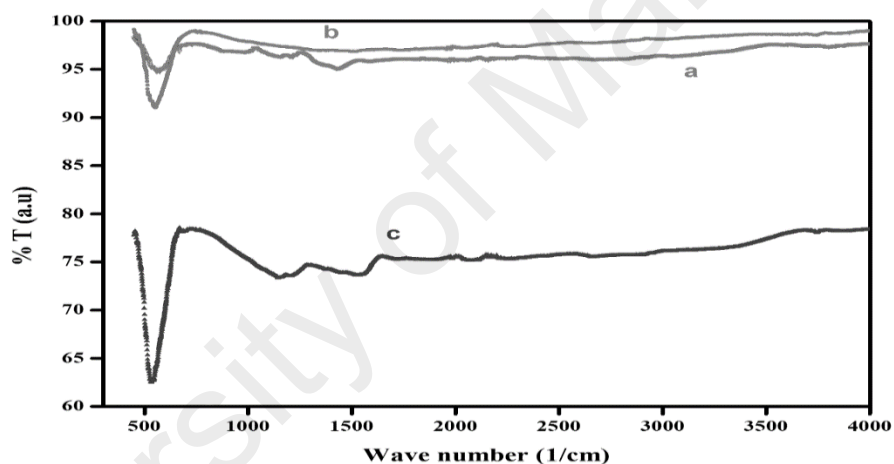


**Figure 4.2.** FTIR spectra of (a)  $\text{CuFe}_2\text{O}_4$  (b)  $\text{CuCe}_{0.2}\text{Fe}_{1.8}\text{O}_4$  (c)  $\text{CuCe}_{0.2}\text{Fe}_{1.8}\text{O}_4\text{-rGO}$ .

#### 4.1.3 Thermogravimetric analysis (TGA)

The graphene sheets act as a filler to improve the mechanical, electrical and magnetic properties of the nanocomposites (Mcallister et al., 2007). The rapid loss of mass at  $200^\circ\text{C}$  parallels to the decomposition of functional groups containing oxygen in the rGO (Ghadim et al., 2014). In contrast, the graphene-based  $\text{CuCe}_{0.2}\text{Fe}_{1.8}\text{O}_4$  nanocomposites showed only a slight weight loss at  $380^\circ\text{C}$ . The value of  $\Delta Y$  (Figure 4.3) measured the amount of graphene as  $\sim 0.5$  mg of graphene per gram of the  $\text{CuCe}_{0.2}\text{Fe}_{1.8}\text{O}_4$  nanocomposites. In addition, TGA also measures the graphene substance in the

nanocomposites. We noted that the rGO decomposition peak was absent and that the decomposition of the graphene-based  $\text{CuCe}_{0.2}\text{Fe}_{1.8}\text{O}_4$  nanocomposites shifted to a higher temperature ( $380^\circ\text{C}$ ). This indicates the structural strength of the nanocomposites, which may be due to the incorporation of graphene and the forerunner  $\text{CuCe}_{0.2}\text{Fe}_{1.8}\text{O}_4$ .

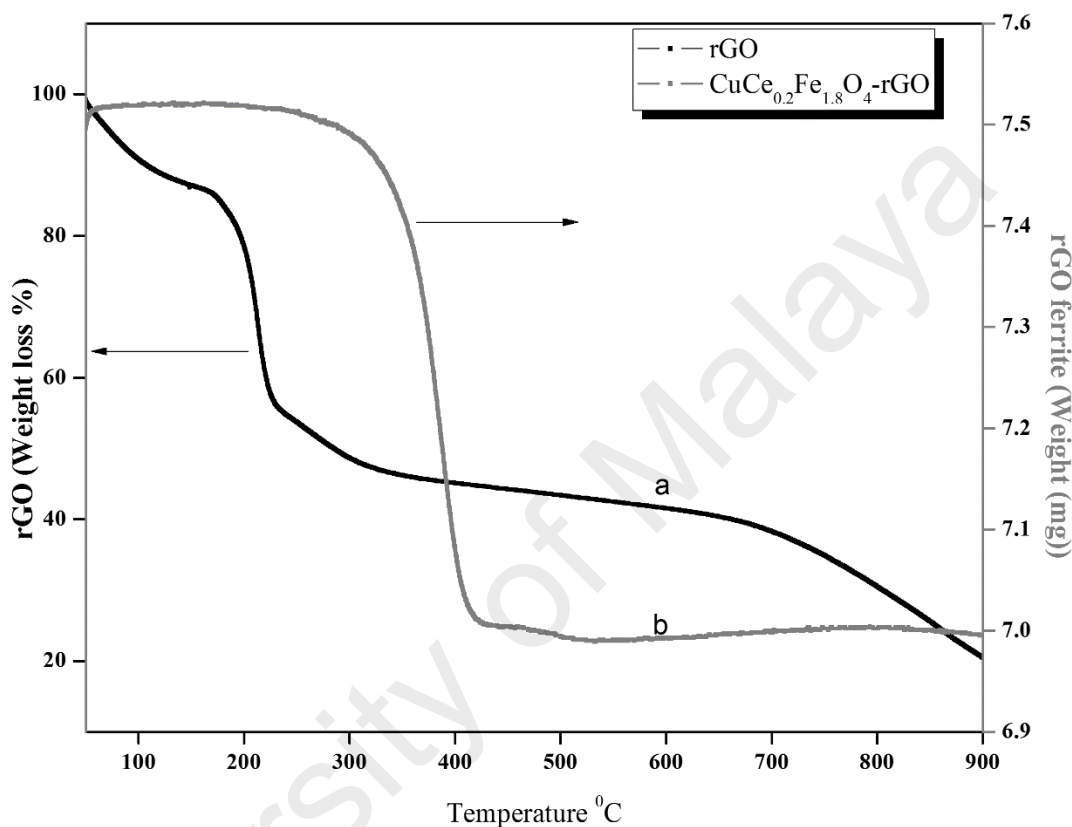


**Figure 4.3.** TGA analysis of (a) rGO (b)  $\text{CuCe}_{0.2}\text{Fe}_{1.8}\text{O}_4$ -rGO nanocomposites.

#### 4.1.4 Morphology and microstructural analysis

The **Figure 4.4** shows FESEM images of graphene,  $\text{CuFe}_2\text{O}_4$ ,  $\text{CuCe}_{0.2}\text{Fe}_{1.8}\text{O}_4$ , ferrite nanoparticles and graphene-based  $\text{CuCe}_{0.2}\text{Fe}_{1.8}\text{O}_4$  nanocomposites. Fig. 5a demonstrates the agglomerated  $\text{CuFe}_2\text{O}_4$  nanoparticles. However, the  $\text{CuCe}_{0.2}\text{Fe}_{1.8}\text{O}_4$  ferrite nanoparticles have less agglomeration as compared with  $\text{CuFe}_2\text{O}_4$ , which may be the result of additional  $\text{Ce}^{3+}$  content. This change in behavior is credited to the van der Waals interactions seen in the specific large surfaces of the fine particles. From a nanochemistry point of view, neighboring nanoparticles sharing a common

crystallographic orientation may collide with each other, which produces coalescence (Balaz, 2008). Therefore, the adjacent primary particles appear to aggregate, yielding larger secondary particles. In addition, owing to their nanometer size, the nanoparticles collide and coalesce in a fashion that again results in bigger particles. This phenomenon may eventually cause agglomeration in the fabricated samples. In agreement with Fig. 5b, the average size of the inter- and intra-agglomerate pores were 300 and 30 nm, respectively.

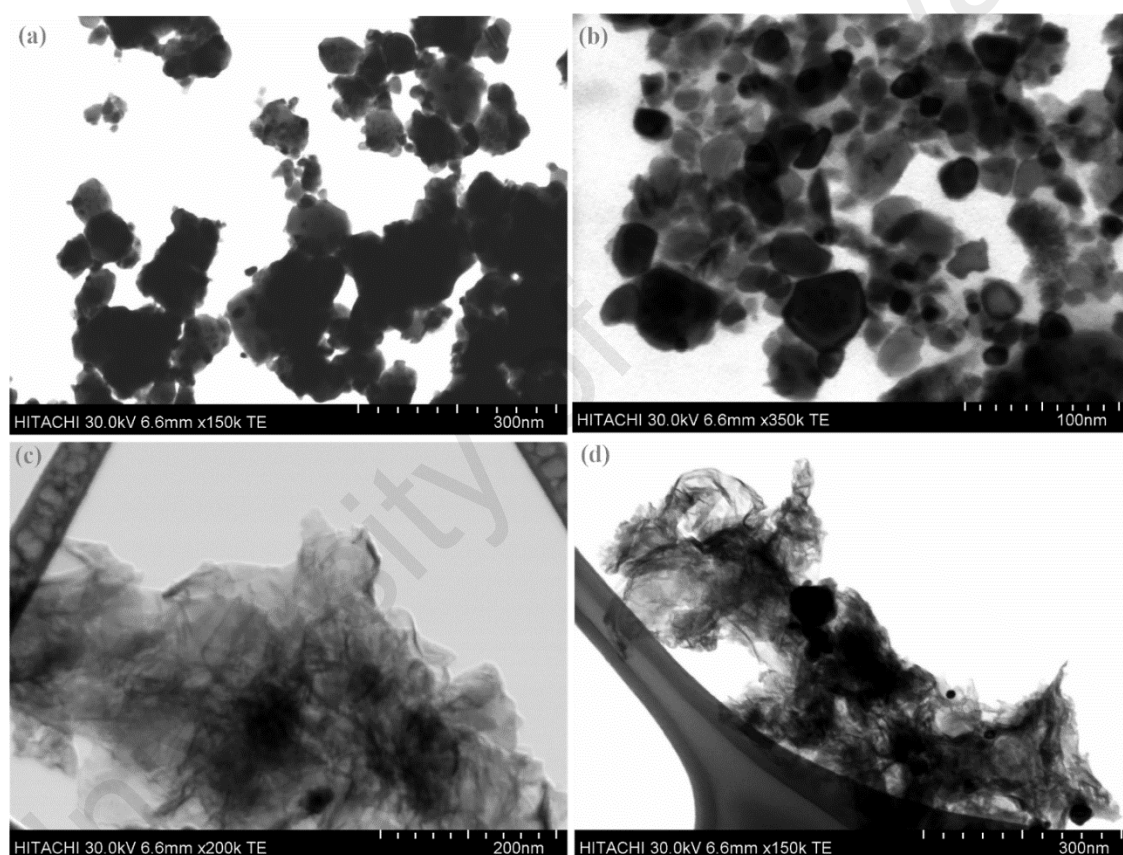


**Figure 4.4. FESEM images (a) CuFe<sub>2</sub>O<sub>4</sub> (b) CuCe<sub>0.2</sub>Fe<sub>1.8</sub>O<sub>4</sub> (c) CuCe<sub>0.2</sub>Fe<sub>1.8</sub>O<sub>4</sub>-rGO nanocomposites.**

It is clear that the intra-agglomerate pore sizes are relatively smaller than the inter-agglomerate pore sizes. On the other hand, in the presence of graphene, the CuCe<sub>0.2</sub>Fe<sub>1.8</sub>O<sub>4</sub> nanoparticles were adsorbed on the graphene sheets in the synthetic process (Fig. 5c). Similar to the CuCe<sub>0.2</sub>Fe<sub>1.8</sub>O<sub>4</sub> nanoparticles, the graphene-based CuCe<sub>0.2</sub>Fe<sub>1.8</sub>O<sub>4</sub> nanocomposites indicated a high tendency to agglomerate (Fig. 5d). The various processing parameters, such as the mixing speeds, intensity, and time, affected

the extent of agglomeration. Here, during co-precipitation and hydrothermal synthesis, the rate of particle collision increased and the resultant particles aggregated into larger particles. The average grain size of the  $\text{CuCe}_{0.2}\text{Fe}_{1.8}\text{O}_4$  nanoparticles was  $43\pm 2$  nm. In addition, the graphene sheets, with some wrinkles and folds, possessed a large aspect ratio, which is the main factor behind the intensification of the contact area with the ferrites phases.

#### 4.1.5 EDS and elements maps

The EDS study and the relative distribution of the constituent elements provided exemplification of the XRD results, as shown in Fig. 6. The percentage (%) of the individual elements in the present composite was: 36.72, 29.49, 17.86, 12.30, and 3.63, of Fe, O, Cu, Ce and C respectively. We observed the carbon peak with a relative percentage of elements in the EDS full-scale profile of the sample. Interestingly, the EDS results show carbon peaks that were not prominent in the XRD spectrum (**Figure 4.5**). The EDS results also disclose nonappearance of any impurities during the followed synthesis route.

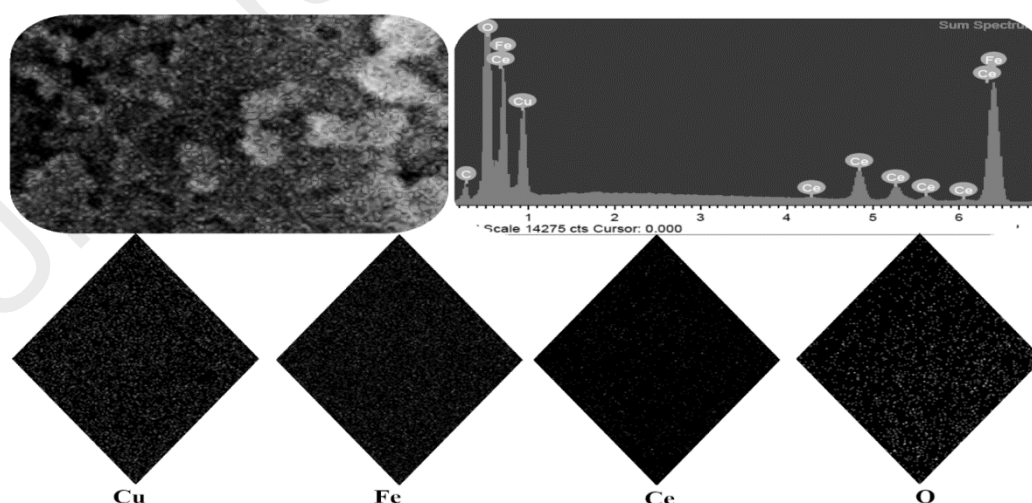


**Figure 4.5. EDS and elemental mapping in  $\text{CuCe}_{0.2}\text{Fe}_{1.8}\text{O}_4$ -rGO nanocomposites.**

The elemental mapping shows a uniform distribution of the constituent elements carbon, copper, cerium, oxygen, and iron all over the nanocomposites (Fig. 6). The

results confirmed the formation of the graphene ferrite's uniform microstructure through the hydrothermal process.

#### 4.1.6 Raman Spectroscopy

The Raman spectroscopy, a powerful analysis tool is used to distinguish between the GO and rGO (Mondal et al., 2015; Wu et al., 2009; Zhang et al., 2014). Raman is a non-destructive structural scrutinizing tool for the analysis of graphene based materials (Ferrari et al., 2006; Meidanchi et al., 2014). The precursor graphite shows in phase vibrations because of the highly ordered graphaite lattice (G band) and disorder graphite edges (D band) at  $1575\text{ cm}^{-1}$  and  $1355\text{ cm}^{-1}$  respectively (**Figure 4.6**) (Calizo et al., 2007; Ferrari et al., 2006). The D band is credited to the lattice defect induced phonon, and G band refers to the C-C bond increase or contraction in the hexagonal carbon conformations (Shahid et al., 2014; Shahid et al., 2015). In contrast, the GO and rGO has well defined D and G bands near  $1343\text{ cm}^{-1}$  and  $1596\text{ cm}^{-1}$  (Kudin et al., 2008). A small bump in Raman spectrum near  $2685\text{ cm}^{-1}$  allotted to the 2D band in rGO associated with the reduced number of re-stacking because of the incorporation of ferrites during the hydrothermal process (Akhavan, 2015). The 2D band also suggest the construction of exfoliated rGO sheets from the dense multilayer GO (Calizo et al., 2007). It is also because of the spacer role of the Nano ferrites as confirmed by the FESEM. The Raman shift of G band of rGO also demonstrates the “self-healing” properties of the rGO (Cui et al., 2015). These observations support the successful transformation of Go to rGO during the hydrothermal process. Moreover the intensity ratio of the D to G band ( $I_D/I_G$ ) is another Raman parameter that is related with the degree of disorder and interatomic size of the  $Sp^2$  hybridized carbons (Meidanchi et al., 2014; Shahid et al., 2015). The  $I_D/I_G$  ratio for rGO (1.064) is higher than GO (0.88), suggesting the formation of partially ordered crystal structures and relatively stronger bonding (Bacsa et al., 2015) . The Raman spectroscopic analysis results also

complements the thermal analysis (TGA & DTA) associated to the relative stability of the nanocomposites because of the additional  $\pi$  bonding stability in the doubly bonded carbons in rGO (Chia et al., 2015).

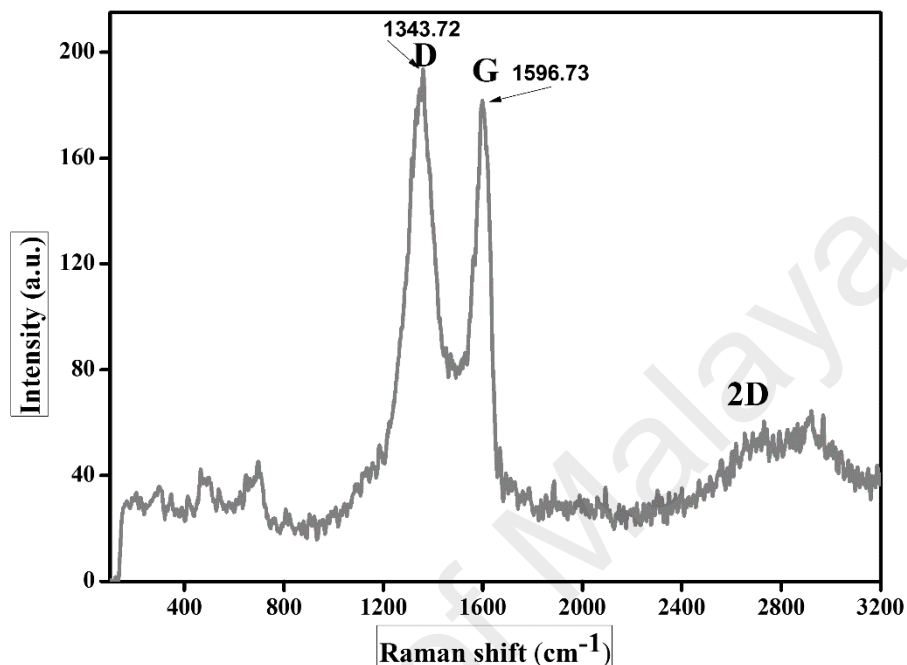


**Figure 4.6.** Raman spectrum of  $\text{CuCe}_{0.2}\text{Fe}_{1.8}\text{O}_4$ -rGO nanocomposites.

#### 4.1.7 Magnetic hysteresis loops

**Figure 4.7(a-c)** shows the hysteresis loops of the  $\text{CuFe}_2\text{O}_4$ , graphene-based  $\text{CuCe}_{0.2}\text{Fe}_{1.8}\text{O}_4$  nanocomposites, and  $\text{CuCe}_{0.2}\text{Fe}_{1.8}\text{O}_4$  nanoparticles, which were measured at room temperature ( $25 \pm 0.6^\circ\text{C}$ ) with a maximum applied field from -12000 to 12000 Oe. The hysteresis loops revealed the magnetic properties, such as saturation, magnetization, remanence and coercive force, of the prepared samples. We observed that the  $\text{CuCe}_{0.2}\text{Fe}_{1.8}\text{O}_4$  nanoparticles demonstrated an increase in magnetic remanence ( $M_r$ ), as compared with the  $\text{CuFe}_2\text{O}_4$  and graphene-based  $\text{CuCe}_{0.2}\text{Fe}_{1.8}\text{O}_4$  nanocomposites. The  $\text{CuCe}_{0.2}\text{Fe}_{1.8}\text{O}_4$  nanoparticles show a relatively large magnetic saturation ( $M_s$ ). The intrinsic and extrinsic factors contributed to the noteworthy improvements in both  $M_r$  and  $M_s$  in the presence of  $\text{Ce}^{3+}$  and graphene. The extrinsic factors depend on the morphology, density, and grain size of the nanoparticles (Potts et

al., 2011), whereas the intrinsic factors, such as the relative occupation of the sub-lattice sites, contributed to the magnetism in the Nano ferrites (Raju et al., 2014). The shape and width of the hysteresis loops depends on the method of preparation, composition, and the spreading of metals cations at the tetrahedral and octahedral sites, in addition to the spin canting and crystallite size (Borhan et al., 2013). The synthesis processes for the nanocomposites were the same, however, the incorporation of graphene in the  $\text{CuCe}_{0.2}\text{Fe}_{1.8}\text{O}_4$  nanocomposites increased the tetrahedral and octahedral distribution of the metal cations, changed the surface morphology, and decreased the crystal strains (Rehman et al., 2015). Consequently, these magnetic properties revealed a remarkable improvement in the nanocomposites, which could be attributed to the presence of  $\text{Ce}^{3+}$  and rGO. It must be added that a variation in the coercive field ( $H_c$ ) directly depended on the surface spin disorder (Kostopoulou et al., 2014). The FESEM images illustrated the homogenous distribution of the  $\text{CuCe}_{0.2}\text{Fe}_{1.8}\text{O}_4$  nanoparticles over the graphene sheets, which in turn revealed that inactive magnetic behavior reduces magnetization. Therefore, the saturation and remanence decreased when compared to the  $\text{CuCe}_{0.2}\text{Fe}_{1.8}\text{O}_4$  nanoparticles. The decrease in  $H_c$  for the graphene-based  $\text{CuCe}_{0.2}\text{Fe}_{1.8}\text{O}_4$  nanocomposites confirmed that rGO reduced the surface spin disorder.

**Table 4.2** lists the squareness ratio ( $M_r/M_s$ ) of the individual ferrite samples. The squareness ratio increased after the combination of  $\text{Ce}^{3+}$  in the  $\text{CuFe}_2\text{O}_4$ , whereas it decreased with the supplement of graphene in the  $\text{CuCe}_{0.2}\text{Fe}_{1.8}\text{O}_4$ .

**Table 4.2. Magnetic saturation ( $M_s$ ), remanence ( $M_r$ ) and coercivity ( $H_c$ ) of  $\text{CuFe}_2\text{O}_4$ ,  $\text{CuCe}_{0.2}\text{Fe}_{1.8}\text{O}_4$  and graphene -  $\text{CuCe}_{0.2}\text{Fe}_{1.8}\text{O}_4$ .**

Ferrites	$H_c$ (Oe)	$M_r$ (emu/g)	$M_s$ (emu/g)	$M_r / M_s$
$\text{CuFe}_2\text{O}_4$	1044	11.38	15.53	0.73
$\text{CuCe}_{0.2}\text{Fe}_{1.8}\text{O}_4$	690	24.41	30.13	0.81
$\text{CuCe}_{0.2}\text{Fe}_{1.8}\text{O}_4$ -rGO	910	19.96	25.32	0.79

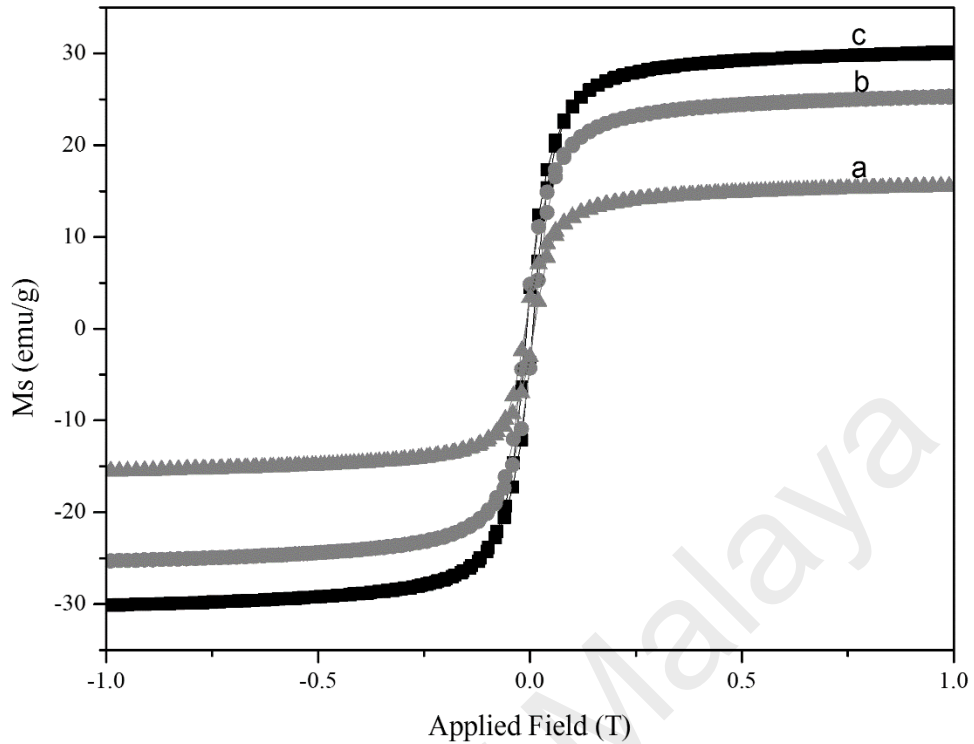


**Figure 4.7. VSM hysteresis loops of (a)  $\text{CuFe}_2\text{O}_4$  (b)  $\text{CuCe}_{0.2}\text{Fe}_{1.8}\text{O}_4\text{-rGO}$  (c)  $\text{CuCe}_{0.2}\text{Fe}_{1.8}\text{O}_4$  nanocomposites.**

The decreasing behavior of the coercivity shows an improvement in the soft magnetic character of the nanocomposites. The magnetic properties of the  $\text{CuCe}_{0.2}\text{Fe}_{1.8}\text{O}_4$  ferrites were controlled by the  $\text{Fe}^{3+}\text{-Fe}^{3+}$  interaction and spin coupling of 3d valance electrons (Dixit et al., 2012). It was noted that the incorporation of graphene in the  $\text{CuCe}_{0.2}\text{Fe}_{1.8}\text{O}_4$  improved the magneto-static interactions (Domingo et al., 2012). The magnetic squareness ratio was less than one ( $>1$ ), indicating the paramagnetic characters of the prepared nanocomposites.

In this study, the  $\text{CuCe}_{0.2}\text{Fe}_{1.8}\text{O}_4$  ferrite nanoparticles and the  $\text{CuCe}_{0.2}\text{Fe}_{1.8}\text{O}_4$  nanocomposites with graphene showed higher magnetic saturation levels and lower levels of coercivity as compared to the original  $\text{CuFe}_2\text{O}_4$  ferrite. This may be because of the better morphology, increased magnetic moments, and domain wall migration of the  $\text{CuCe}_{0.2}\text{Fe}_{1.8}\text{O}_4/\text{graphene}$  nanocomposites (Dutta et al., 2006; Niaz Akhtar et al., 2014). Furthermore, it was observed that the paramagnetic behavior of the  $\text{Ce}^{3+}$  ions would

lessen the resistance between the domain walls and weaken the exchange interactions, which correspond to a decrease in the coercivity in the ferrites. Further study of the VSM curves indicated a relatively  $H_c$  higher values as compared to magnetic ferrites and magnetic saturation was less than 49 emu/g (Nguyen et al., 2014). A similar high  $H_c$  (~1095 Oe) was found in the magnetic ferrites prepared by a micro-emulsion method (Rashad et al., 2015). However, Rao et al. found relatively reduced  $H_c$  (575.2 Oe) but relatively lower  $M_s$  (10.47 emu/g) and  $M_r$  (5.38 emu/g) values for  $\text{CuFe}_2\text{O}_4$  thin films prepared by spray pyrolysis deposition technique (Rao et al., 2015). The magnetic behavior can be explained on the grounds of the development of two independent domains at tetrahedral and octahedral sites (A & B sites) that demonstrate ferromagnetic nature through magnetic coupling interactions (Rao et al., 2015). A manganese substituted ferrite ( $\text{Mn-CuFe}_2\text{O}_4$ ) prepared by bio template medium and simple evaporation method also exhibited comparable  $H_c$  (492 Oe) and  $M_s$  (10.42 emu/g) (Ranjith Kumar et al., 2014). Based on these results, it is apparent that the  $\text{CuCe}_{0.2}\text{Fe}_{1.8}\text{O}_4$  nanoparticles and  $\text{CuCe}_{0.2}\text{Fe}_{1.8}\text{O}_4/\text{graphene}$  nanocomposites act as potential candidates for superior catalysts, switching, electromagnetic wave absorbers and adsorbents for environmental remediation.

Magnetic graphene nanocomposites were fruitfully prepared using a facile co-precipitation hydrothermal reduction method. We assessed the structural, morphological, thermal, and magnetic properties using XRD, FTIR, TGA, FESEM, and VSM techniques, respectively. The magnetic Nano-composite showed improved thermal stability, which can extend its application under more severe temperature conditions. However, nanocomposites have a large crystallite size and large crystal strains as compared to  $\text{CuFe}_2\text{O}_4$  ferrites. The FESEM results indicate the distribution of the  $\text{CuCe}_{0.2}\text{Fe}_{1.8}\text{O}_4$  ferrite constituent elements across the graphene surface. The  $\text{CuCe}_{0.2}\text{Fe}_{1.8}\text{O}_4\text{-rGO}$  magnetic nanocomposites demonstrated an improvement in its

magnetic, thermal and energy efficient separation properties. These improved magnetic nanocomposites provide the basis for a broad range of applications and lead towards a better understanding of energy storage, electromagnetic wave absorbers, chemical process catalysts, electrochemical sensors and adsorbents for pollutants removal technologies.

#### **4.2 Characterization results of Palm oil waste clinker sand.**

The need of specific and competent adsorbents is increasing to remove heavy metals or to maintain permissible levels in drinking water. The excellent experimental results in comparison to external studies confirmed the relative importance of POCS based arsenic removal system for a green environment remediation approach. The reuse or recycle approach in industrial mega production industries is one of the most pertinent desires to re-utilize the enormous volume of solid waste (Ahmad et al., 2011; Dias et al., 2007; Hameed et al., 2009; Roig et al., 2006). Production managers always think about alternative strategies to reuse waste by-products and accomplish goal of “zero waste”(Li et al., 2007; Zaman et al., 2013). This is normally the case in palm oil industry in Malaysia and neighboring countries, where oil palm shell and fibers is produced in large amounts during oil extraction process (Ahmad et al., 2011). The generated waste left after incineration of shell and fiber is researched for conversion into useful adsorbents. At present, nearly 2.6 million tons of waste is a great challenge asking for reutilization of waste resource along with environmental sustainability(Hameed et al., 2009). Providentially, the industrial waste is recycled after suitable mechanical, chemical and physical treatments. The recycle process helps in resources preservation, energy efficient processing and environment friendly waste disposal (Ahmmad et al., 2014; Hameed et al., 2009; Ryan et al., 2000).

#### 4.2.1 POCS mechanical and physical treatments

The samples were grinded and forwarded to fractionation and separation process. The US standard sieves of different pore sizes were used to make different mechanical grades. Each fraction was washed with distilled water to remove color and fine particles. The POCS particles were dried in an electrical heating oven at ambient temperature overnight. The fine grades were obtained after regrinding and sieving with a 12.00-4.75 mm mesh size (Fig. 4.8).

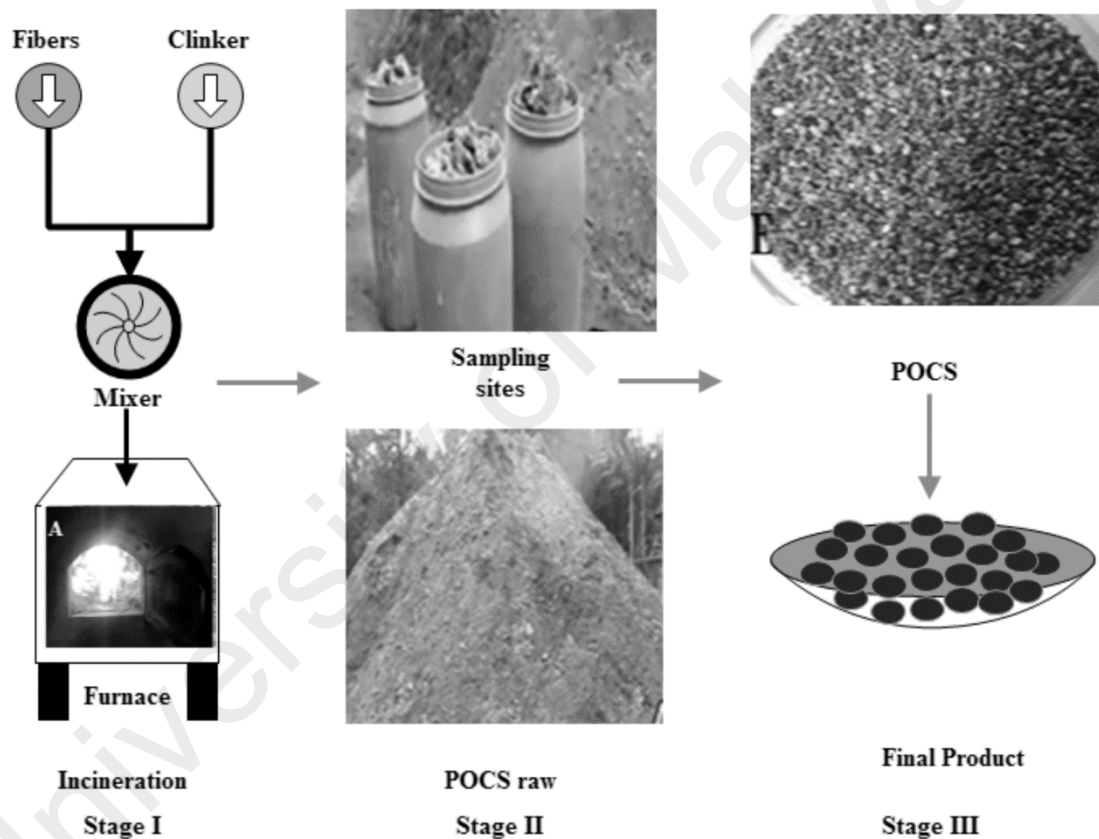


Fig. 4.8. Mechanical and physical treatments.

#### 4.2.2 Application of POCS for As adsorption

The adsorption experiments were planned to achieve maximum POCS adsorption potential. Table 4.3 shows the factors names, codes and levels used to make design matrix.

**Table 4.3. The CCD variables, symbols and levels.**

Variables	Symbol	Level				
		Low	Mean	High	- $\alpha$	+ $\alpha$
POCS, mg	X1	500	750	1000	250	1250
As, mg L <sup>-1</sup>	X2	100	175	250	25	325
T, °C	X3	25	35	45	15	55
pH	X4	4	6.5	9	15	115

The experimental data was collected as advised and designed by CCD, the equilibrium arsenic concentration ( $Q_e$ ) was calculated by using equation 2.1 (Shanmugaprakash et al., 2013). The reproducibility of experimental adsorption capacity was ascertained by repeating the experiments to account for standard deviation. The applied method is robust and beneficial over the arsine gas generation method, as it required no extra reagents to produce gaseous phase arsenic (arsine gas). The selected quadratic model provided better insight into complex correlated, interacting adsorption variables. It assisted to identify the most influencing as well as least influencing variables (Roy et al., 2014). The interactive effects of four important variables were discovered to describe the arsenic adsorption. The designated graphical models clearly visualize and predict maximum arsenic adsorption. The value of each model coefficients was expended to explain important relationships among independent and dependent variables.

The experimental adsorption capacity was analyzed and model fitted to discover the goodness of fit of the proposed model. Successively, model was tested by statistical tests e.g. analysis of variance (ANOVA), residuals analysis (RA), scaling residuals (SR) and prediction error sum of squares (PRESS) (Smith et al., 2000). The verified and validated model was used to augment input process variables and to maximize output

i.e. arsenic adsorption. The decided statistical model was also validated by supplementary experiments.

#### **4.2.3 Batch adsorption**

Arsenic adsorption study was performed in a batch mode of experiments. The pre-weighed POCS (mg) was taken into the conical flask, 20 cm<sup>3</sup> of analyte (As) of known concentration was added and pH adjusted with drops of 0.01M HCl or 0.01M NaOH respectively. Each sample flask was shaken (200 rpm) for 1 h, filtered through a PTFE SIMPLEPURE (0.22 μm) micro filter, and collected into ICPMS ampoules for subsequent analysis.

#### **4.2.4 POCS Particle size distribution**

**Fig. 4.9** shows PSD curve correlating particle size with percent finer. It was observed that POCS has a fitness modulus, specific gravity and water absorption of 3.09, 2.01 and 3.75 % respectively. These results indicated that POCS as a well graded material. The PSD analysis was used to differentiate particle with appropriate features for arsenic adsorption. Previously it was reported that the particle size has a direct effect on degree of contact with desired adsorbate (arsenic) (Kim et al., 2013). The very fine particles possess relatively large surface area and offer better contact with arsenic (Kim et al., 2013). However, these very fine ultra-small particles were found to be unsuitable due to difficult separation and blockage of filter during early viability studies. The small diameter of particles offer extremely slows down speed of water molecules and causes an impractical separation process. Accordingly, 600 μm particle size was selected for further studies. The selected particles were found appropriate owing to porous networking structures, specific gravity, fitness modulus and water absorption properties (Ahmmad et al., 2014) .

#### 4.2.5 Functional groups analysis

FTIR study provides useful functional groups information regarding arsenic and POCS surface interactions during adsorption process. Surface interactions are due to presence of surface functional groups.

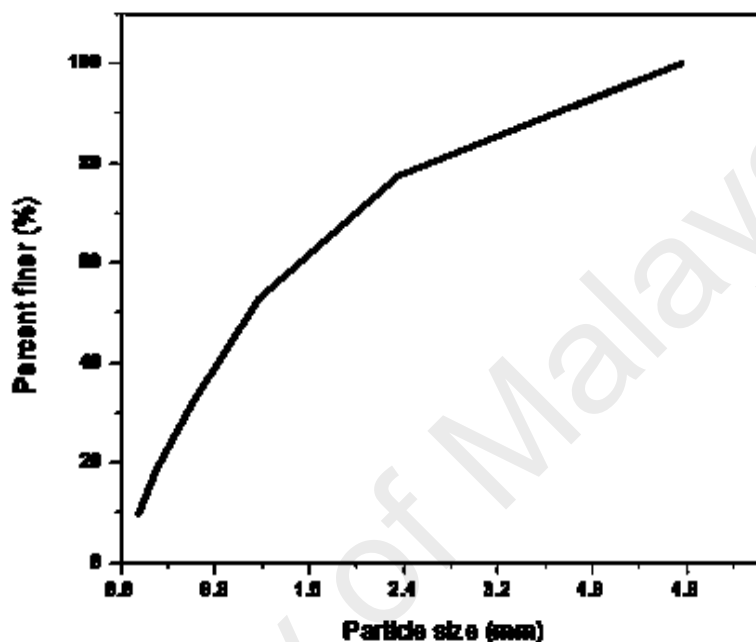


Fig. 4.9. Particle size distribution curve of POCS.

The surface of POCS indicated a number of interesting functional group that possibly become the reason for enhanced arsenic adsorption despite its porous networking structures (Ferraro, 2012).

**Figure 4.10** it can be seen that finger print region of IR spectrum contains a dominant and distinct peaks at  $1022\text{ cm}^{-1}$ . It can be attributed to a number of metals/nonmetals oxides generated during calcinations process in a boiler. Previous studies observed a relative proportion of various metals, nonmetal and their respective oxides (Ahmmad et al., 2014). These mixed oxides are responsible for improved arsenic adsorption. A similar observations has been reported for a role of metal oxide for interaction with arsenic during adsorption process (Ferraro, 2012). Due to abundant

oxides, peaks of other functional groups look weak and negligible at a first glance. However, we selected a separate IR region from 1500 to 4000  $\text{cm}^{-1}$  to account for other functionalities, responsible for a higher arsenic uptake during current adsorption process.

**Figure 4.10** (inset)). Interestingly, the selected IR region shows peaks for other functional groups for arsenic. Particularly, FTIR spectrum shows peaks at 518  $\text{cm}^{-1}$  (C-Br), 538  $\text{cm}^{-1}$  (C-Cl), 621  $\text{cm}^{-1}$  (N-H), 692  $\text{cm}^{-1}$  (C-H), 710  $\text{cm}^{-1}$  (C=C), 728-795  $\text{cm}^{-1}$  aromatic (C=C), 800  $\text{cm}^{-1}$  (C-H), 1022  $\text{cm}^{-1}$  (C-N), 1056  $\text{cm}^{-1}$  (Metal-O), 1160  $\text{cm}^{-1}$  (C=O), 1426  $\text{cm}^{-1}$  (C=C), 1623  $\text{cm}^{-1}$  (C=N), 2106 (C $\equiv$ N), 2500-3000  $\text{cm}^{-1}$  (C-H), 3176  $\text{cm}^{-1}$  (N-H), 3219-3366  $\text{cm}^{-1}$  (O-H). The functional groups study results verified the role of multiple functional groups on adsorbent surface.

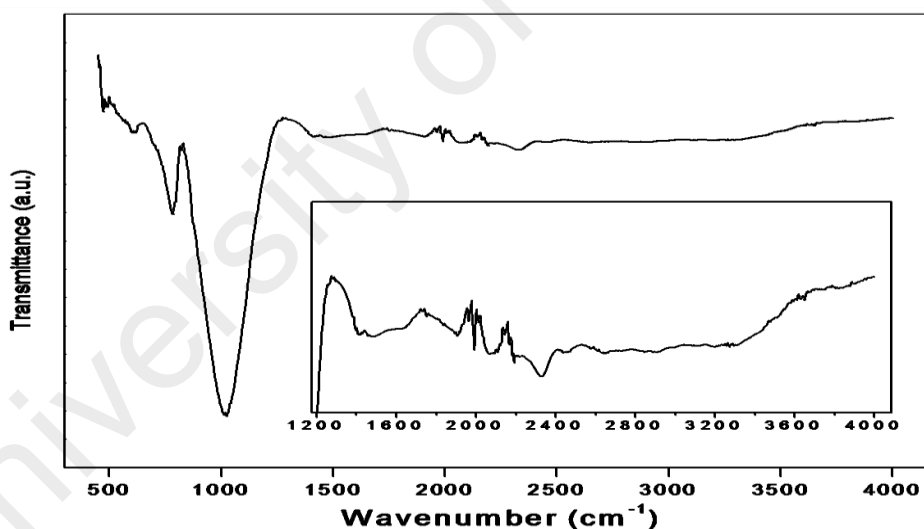


**Figure 4.10.** FTIR spectrum and functional groups peaks. Inset showing the 1200 to 4000  $\text{cm}^{-1}$ .

#### 4.2.6 FESEM and EDX analysis

Figure 4.11 represents POCS surface morphology by FESEM. It can be seen that there are pores of various sizes and diameters. Figure 4.11 (A) shows small scattered fine particles and semi hexagonal type of pores on the porous networking surface. The surface pore can be classified by further exploration of FESEM at different area into the micrometer pores of small, medium and extra-large sizes (Figure 4.11 B & C). The FESEM results visualize a heterogeneous adsorbent surface that is more suitable for interactions and capture of arsenic. The elemental analysis of the selected area were scanned and analyzed by energy dispersive X-rays (EDS). Figure 4.11 D provides the relative percentage of elements e.g. silicon, oxygen, carbon, potassium, calcium, magnesium, and aluminum 34.5, 31.6, 13.3, 12.6, 5.2, 2.1 and 0.8 weight % respectively.

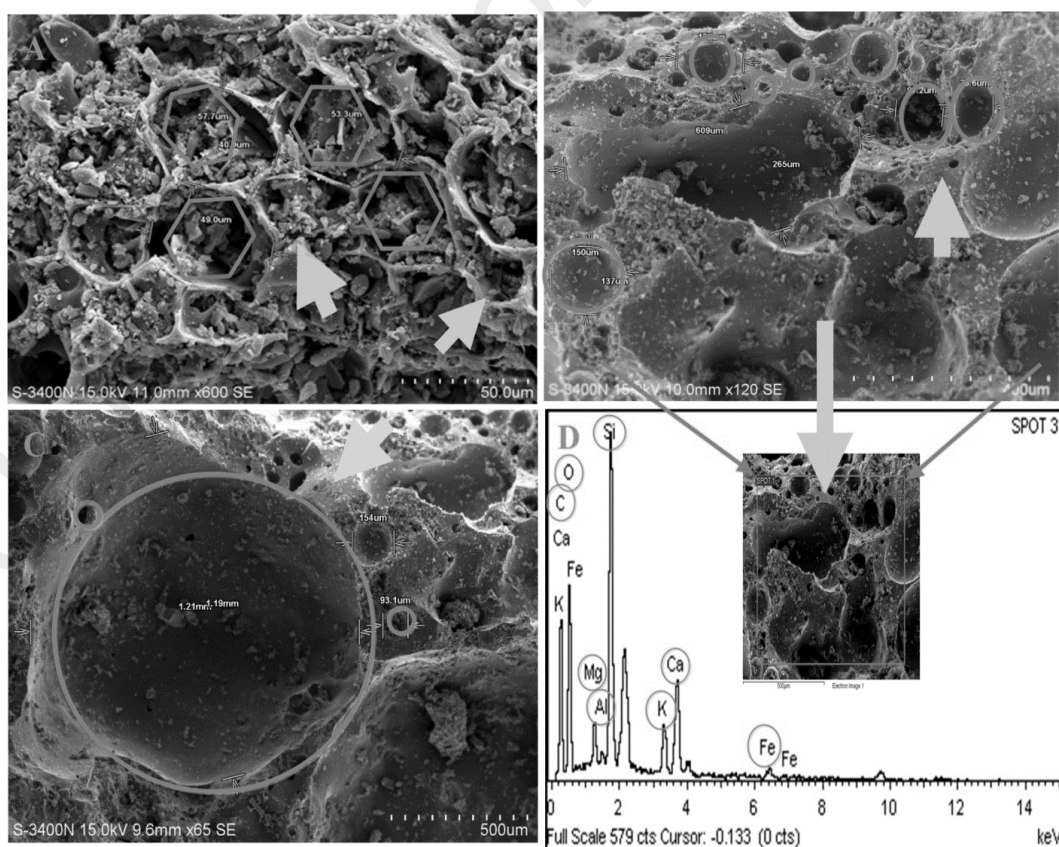


**Figure 4.11. FESEMs, micro porous structure of POCS (A) 50  $\mu\text{m}$  (B) 400  $\mu\text{m}$  (C) 500  $\mu\text{m}$  (D) EDX composition.**

The FESEM surface and elemental analysis indicated that the indigenous POCS was rich in a number of mixed metals, nonmetals and related oxides. Moreover, the attractive functional groups like carbonyl (-C=O), cyano (-CN), hydroxyl (-OH) and amide (-NH) groups (FTIR results) are very interesting for adsorption interactions.

#### 4.2.7 A quantitative comparison of efficiencies

The adsorption capacities were compared and analyzed by an external comparative study by comparing a number of adsorbents. For illustration, Ferrous ions laden Apricot stone activated carbon ( $Q_e = 5.91 \text{ mg g}^{-1}$ ) (Tuna et al., 2013.), Ferric ions and Apricot stone activated carbon ( $Q_e = 5.74 \text{ mg g}^{-1}$ ) (Tuna et al., 2013.), the mesoporous alumina ( $Q_e = 39.06 \text{ mg g}^{-1}$ ) (Han et al., 2013), precipitated zeolites (ZNa-Fe) ( $Q_e = 6.73 \text{ mg g}^{-1}$ ) (Simsek et al., 2013), Aluminum(III) zeolites (ZNa-Al) ( $Q_e = 3.79 \text{ mg g}^{-1}$ ) (Simsek et al., 2013), and a thermally treated Iron on activated carbon ( $Q_e = 4.56 \text{ mg g}^{-1}$ ) (Nieto-Delgado et al., 2012). It became clear through the present comparative study that POCS has a better adsorption capacity. The relative measure of  $q_e$  provides a basic scale to recognize these new adsorbents and the prospective future application in adsorption based remediation techniques.

#### 4.3 Modelling adsorption.

The proposed model for arsenic adsorption by POCS is: **Equation 4.3**. The proposed quadratic model for Arsenic.

$$Q_e = +15.82 + 1.63 * X_1 + 1.84 * X_2 + 0.82 * X_3 + 3.12 * X_4 + 0.04 * X_1^2 - 0.17 * X_1X_3 + 0.85X_1X_4 - 0.25X_2X_3 - 0.67 * X_2X_4 - 0.34X_3X_4 - 0.94 * X_1^2 - 1.03 * X_2^2 - 0.57 * X_3^2 - 1.65 * X_4^2 \quad \text{Equation 4.3}$$

Where the coded variables X1, X2, X3 and X4 represent POCS (mg), As ( $\text{mgL}^{-1}$ ), Temp. ( $^{\circ}\text{C}$ ) and pH respectively. The influence of variables is sorted out by comparing the coefficients obtained by the ANOVA test. The comparative values explain the significance of respective variables. Generally, a positive regression coefficient

symbolizes synergistic effect while a negative sign indicates opposite effect (Badkar et al., 2013). Fischer variation (F-value) and Probability values (p-value) and correlation coefficient ( $R^2$ ) were compared to find out the adequacy of the proposed model. Table 4.4 procures tests applied on the present quadratic model for Arsenic.

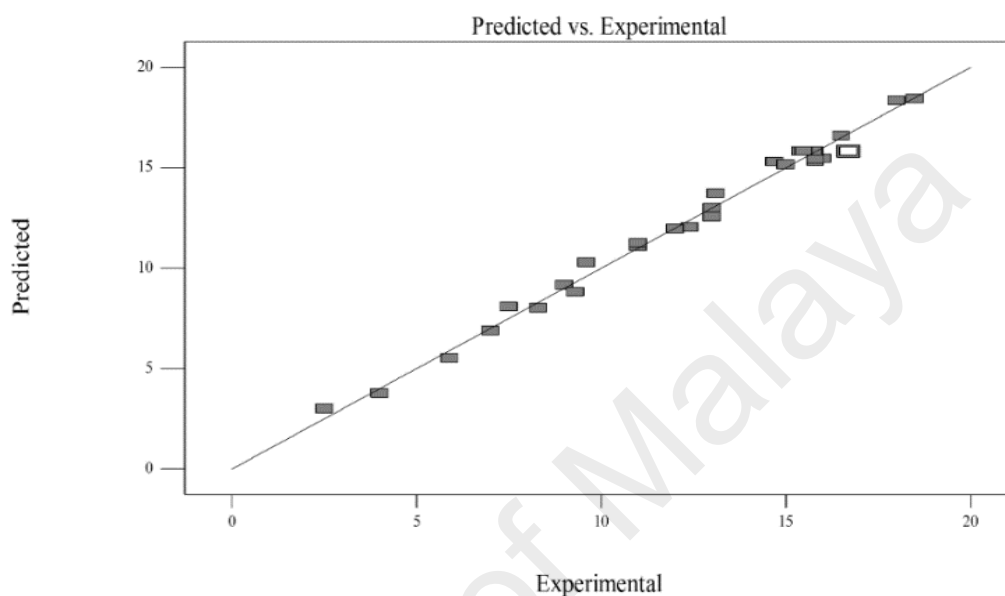


**Figure 4.12. The model predicted and experimental results.**

The lack of Fit test with F-value 1.660 implies that model “Lack of Fit” is insignificant as compared to pure error. The model predicted  $R^2$ -value of 0.96 is in reasonable agreement with adjusted  $R^2$  of 0.98. **Figure 4.12**, the correlation between experimental and predicted system response. The adequate precision test measures signal to noise ratio and the desirable value of precision is greater than 4.0. The Arsenic adsorption quadratic model proposed showed an adequate precision 39.22. It confirms that proposed model for managing optimum arsenic adsorption is adequately precise.

#### 4.3.1.1 The variables influence on model response

The linear and quadratic terms were compared to elaborate the effect of each process variable. A term p-value greater than 0.1 indicates an insignificant term. In this perspectives, POCS dose ( $X_1$ ) F-value 203.2 and p-value less than 0.1, and the corresponding quadratic term ( $X_1^2$ ) F-value 78.16 indicates a remarkable decrease of

the F-value. It can be interpreted as an increase in POCS has resulted in a decrease in its effect on  $Q_e$ , during fixed pH, temperature and arsenic initial concentration ( $\text{mg L}^{-1}$ ). Similarly, linear term of As initial concentration ( $X_2$ ) has F-value 254.0 and p less than 0.0001.  $X_2^2$  has F-value 93.4 and p less than 0.0001. It means that both linear and quadratic terms for initial concentration are significant.

**Table 4.4. Arsenic adsorption statistical analysis results.**

Source of variation	df	SS	MS	F	P-value
Regression	14	514.63	36.76	118.44	< 0.0001
Residual error	15	4.66	0.31	-	-
Lack of Fit (model error)	10	3.58	0.36	1.66	0.299
Pure Error (replicate error)	5	1.08	0.22	-	-
Total	29	519.28	-	-	-
$R^2$	0.991				

Abbreviations: df= degree of freedom; SS=sum of squares; MS= mean squares.

Moreover, the relative values show that initial concentration beyond optimum has resulted in a declined arsenic adsorption. Temperature linear term ( $X$  has F-value 50.01 and p less than 0.0001 while quadratic term ( $X_3^2$ ) has F-value 28.25 & p less than 0.0001. These comparative values of respective statistical terms indicate a relatively lesser effects of temperature as compared to other variables in present design of experiment. The most prominent variable was pH ( $X_4^2$ ) in this study. The variable pH showed a relatively higher impact on adsorption as can be seen in its relatively high F-value 745.6. The quadratic term of pH was still dominant on other variables. A comparison among linear and quadratic terms describes the relative influence of linear and quadratic terms for the variables competitive role during adsorption. It is beauty of

RSM design of study as it explain combined effects of interactive variable, as compared to OVAT strategy of experiments (Witek-Krowiak et al., 2014).

#### 4.3.1.2 RSM 3D plots

**Figure 4.13** portrays the response surfaces (RSM 1 to 6) the three dimensional model presentation to discover the optimum adsorption. It is interesting that the response surface method not only explains shared effects but also support optimum variable ranges for optimum adsorption. **Figure 4.13** (RSM 1) shows a combined effect of arsenic initial concentration ( $\text{mgL}^{-1}$ ) and POCS dosage (mg). It is observed that arsenic initial concentration has more influence on  $Q_e$  as compared to adsorbent dose. For instance, POCS dose in the range from 500 to 1000 mg at a fixed pH 4.0 and temp.  $25^\circ\text{C}$  increases Arsenic  $Q_e$  from 4.0 to 5.9  $\text{mg g}^{-1}$ . Conversely, an increase in initial concentration of from 100 to 250  $\text{mg L}^{-1}$  (pH 4.0 and temperature  $25^\circ\text{C}$ ) bring about a double increase of  $Q_e$  from 4.0 to 9.0  $\text{mg g}^{-1}$ . The RSM 1 projected maximum  $Q_e \sim 18.0 \text{ mg g}^{-1}$  with 1.0 g adsorbent dosage and 250  $\text{mg L}^{-1}$  arsenic. **Figure 4.13** (RSM 2) depicts effects of temperature and POCS dose on Arsenic. The RSM 2 shows direct influence from temperature on  $Q_e$ , indicating an endothermic reaction during the arsenic adsorption. Relatively, it shows lesser effect. E.g. during fixed adsorbent dose, pH and initial concentration, temperature increase from 15 to  $55^\circ\text{C}$  resulted in a slow increase in  $Q_e$  from 12.0 to 15.0  $\text{mg g}^{-1}$ . RSM 3  $Q_e$  increases regularly with pH and dose. The variable range of pH exhibited leading role as compared to dose of adsorbent in this study. E.g. at a fixed dose 1.0 g, temperature  $45^\circ\text{C}$  and initial concentration the  $\text{pH}$  increase resulted in a dramatic increase in  $Q_e$  from 13.0 to 18.5  $\text{mg g}^{-1}$ . **Figure 4.13** (RSM 4) displays the effect of temperature and initial concentration. It shows that an increase in arsenic concentration goes linearly with  $Q_e$  when other variables were held constant. **Figure 4.13** (RSM 3) uncovers the combined i.e. pH and POCS dose effect.

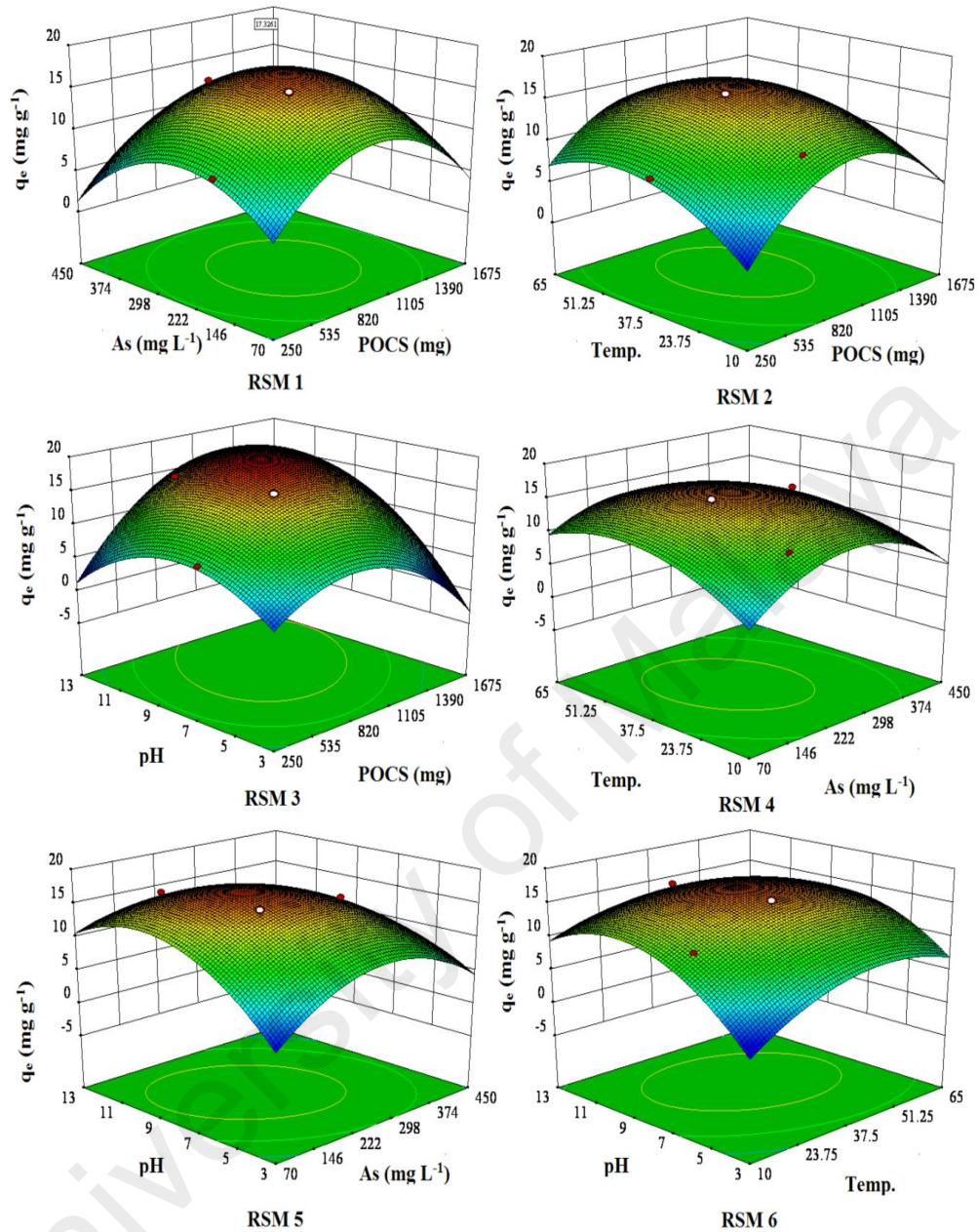


**Figure 4.13. 3D response surface plots. RSM 1 Arsenic initial Conc. ( $\text{mg L}^{-1}$ ) and POCS dose (mg) RSM 2 Temp vs POCS dose (mg). RSM 3 Initial pH vs POCS dose (mg) RSM 4 Temp. vs Arsenic initial Conc. ( $\text{mg L}^{-1}$ ). RSM 5 pH vs Arsenic initial Conc. ( $\text{mg L}^{-1}$ ) RSM 6 pH and Temp ( $^{\circ}\text{C}$ ).**

From The relative increase in  $Q_e$  can be credited to the higher number of effective collisions and high concentration. Likewise, temperature provides the kinetic energy for more effective collisions and improved adsorption. The two process variables work for a better  $Q_e$ . However after optimum a further increase in both variables decreases  $Q_e$  as understood in RSM 4. The reason for decrease in  $Q_e$  is attributed to the increased

velocity of molecules and a widening of pores at elevated temperatures. **Figure 4.13** (RSM 5) illustrates an effect of pH and arsenic initial concentration on  $Q_e$ . In an experiment with POCS 750 mg, arsenic initial concentration 175 mg L<sup>-1</sup> and temperature 35°C an increase in pH from 6.5 to 11.5 changes  $Q_e$  from 16.7 to 15.81 mg g<sup>-1</sup>. The results indicated that at elevated concentration, increase in pH has comparatively slighter effect on adsorption process. Figure 4.13 (RSM 6) shows the effect of pH and temperature at a static POCS dose and arsenic concentration. The response surface also explains optimum  $Q_e$  within a dynamic range of pH and temperature. The response surfaces optimizations experiments results explain the connections among selected variables and the synergistic effects on adsorption. The model presented a suitable design to realize optimum adsorption efficiency by controlling the ranges of the respective input variables.

#### 4.3.1.3 2D adsorption contour plots (CPs)

Figure 4.14 shows the 2D CPs (1 to 6) regarding optimum area of adsorption for batch mode adsorption design based on CCD strategy. The CPs explain the common influence of two variables on adsorption (Bilici Baskan et al., 2010; Roy et al., 2014). In this study, the CP1 displays the effect of POCS dose (mg) and As (mg L<sup>-1</sup>). A regular increase in  $Q_e$  with a corresponding change in dose and concentration variables can be seen from this design. Nevertheless, outside optimum contour lines yet again display area with a  $Q_e$  drop from the optimum (Figure 4.14 CP1). The CP1 likewise shows a middle red zone area of the contours circles for a maximum of  $Q_e$  17.3 mg g<sup>-1</sup>. The CP2 proves the effect of dose (mg) and temperature whereas the other variable are kept constant. The middle red zone shows a maximum  $Q_e$  followed by yellow, green and blue areas in a decreasing order. The CP3 portrays the effect of dose (mg) and pH at a constant As initial concentration (mg L<sup>-1</sup>) and temperature.

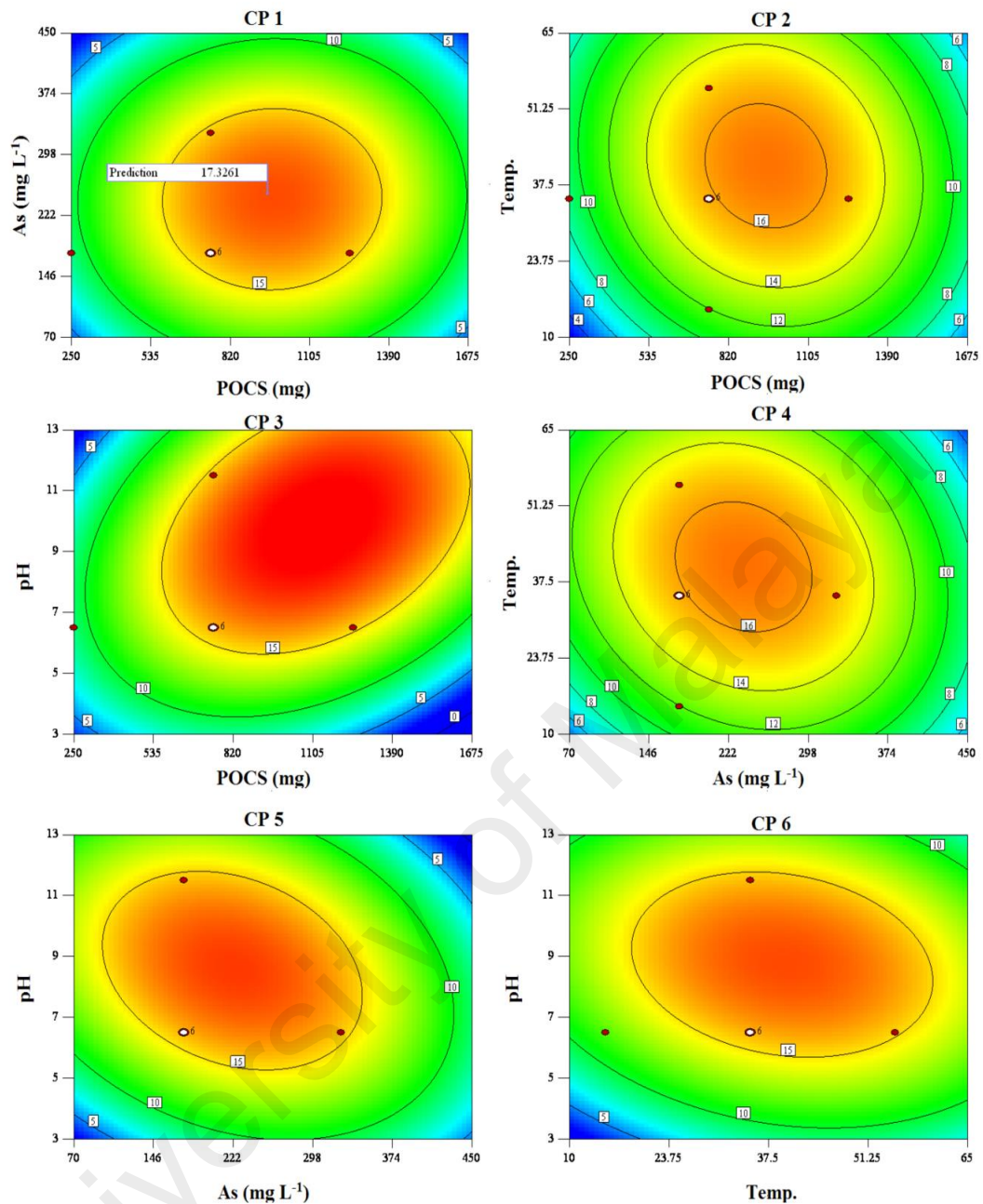


**Figure 4.14. 2D Contour plots. CP 1 Arsenic initial Conc. (mg L<sup>-1</sup>) and POCS dose (mg) CP 2 Temp vs POCS dose (mg). CP 3 Initial pH vs POCS dose (mg) CP 4 Temp. vs Arsenic initial Conc. (mg L<sup>-1</sup>). CP 5 pH vs Arsenic initial Conc. (mg L<sup>-1</sup>) and CP 6 pH and Temp (°C).**

Remarkably, CP3 exhibits a fairly large red zone. It means that we can optimize along a broad range of these variables. The CP4 offers the collective outcome of concentration and temp. It is obvious that CP4 has a reduced red zone but approximately equal to that CP2. It can be ascribed to a relatively lesser influence of

temperature in this study. The CP5 reveals a synergistic consequence of pH and As concentration. The responsible adsorption variables has proved to be the most influencing as the effect on broad red zone is clear from CP5. Finally, the CP6 presents the reasonable effects of pH and temp. Once more time the pH stands out as a dominant adsorption variable as it broadened area of middle contour considerably. Arsenic adsorption results visibly detailed the effects of four variables to accomplish optimum adsorption.

From the results of DOE strategy for Arsenic adsorption we deduced following conclusions: The indigenous POCS bears suitable adsorbent properties for Arsenic e.g. water absorption, specific gravity and fitness modulus. The selected dimensions of the adsorbent possess rich surface functional groups along with the micro porous networking that supports outstanding adsorption. All the selected variables influence the adsorption and were found statistically significant process variables. The strong correlations between predicted and experimental results proves the accuracy and precision of the model. RSM and CPs visualize the effect of variables on the Arsenic adsorption in 3D and 2D fashion respectively. The model finding suggest that a systematic environmental management strategy with indigenous renewable adsorbents resources can be designed to reuse and recycle abundant volumes of agro industrial waste.

#### **4.4 Modelling Acephate adsorption.**

The green natural abundant resource from palm oil industry is a versatile material with diversified functional groups, pore structure, mechanical strength and ability to form various grades of natural adsorbents. Impressed by its natural properties, various experimental parameters and their effect on adsorption of acephate have been studied for their impact to remove an organophosphorous group's pesticides from hydrological

samples. The present study only focused on the three main types of models i.e. i. Isotherms models ii. Kinetic models and iii. Thermodynamics models. The equilibrium adsorption data is subjected to various adsorption isotherms (Langmuir, Freundlich, Flory-Huggins (FH), Dubinin-Radjuvic (DR) and Temkin). Pseudo-first order, second order and intraparticle diffusion kinetic models are used for kinetic studies.

The frequent application of pesticides is being exercised in most of the agricultural countries to control the crops damages by pests. However the proper care to protect the natural environments from unwise or accidental discharge of these toxic molecules into aquifer raises our concern to protect natural environment. There are many classes of pesticides but we selected organophosphorous group (OPPs) of pesticides and more specifically Acephate (AP) (Figure 4.15). The AP is known to cause toxic effects in vertebrates, for example, affecting central nervous system (CNS) (Aragay et al., 2012), respiratory (Tian et al., 2012) and reproductive systems (Salameh et al., 2003) and also adverse genetic changes in the genetic code (DNA) (Singh et al., 2011). The AP is an insecticide for controlling the sucking and biting insects. However its discharge into waters, air and soil is a serious cause of environment quality degradation over time. At present various technologies for pollutants removal e.g. liming, photo-degradation, catalytic degradation have been implemented including adsorption as the superior choice due to the availability of adsorbents and reuse and recycle capabilities. Adsorption is a versatile technique having many practical advantages over the other water treatment techniques. It exploits interplay of complex phenomenon that is sorbate-sorbent interactions, surface phenomenon, matrix matching effects, electrostatic effects, types of bonding.

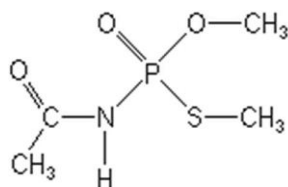


**Figure 4.15 Molecular structure of Acephate (AP).**

The role of ultrasound assisted rapid mixing of sorbate and sorbent molecules leads to many faster steps involved in chemical kinetics (Entezari et al., 2005). The use of ultrasound increases the mass transfer rate by reducing diffusion resistance (Schueller et al., 2001; Zheng et al., 2005). The present study explores the use of ultrasound assisted rapid mixing to facilitate the different steps of adsorption that is bulk diffusion, film diffusion, pore diffusion and chemical binding with the sorbent (POC) (Renault et al., 2008). Acephate was only chosen to develop isotherms i.e. Langmuir, Freundlich, Dubinin-Radushkevich and Florry Huggin model. The Isotherms were developed at two distinct temperatures i.e. 293 K and 313 K respectively. The detailed parameter are given in Table 4.5 “Isotherm results for Acephate. Moreover the model results are completely discussed in sub-section 4.5.3, along with all the experimental parameters in details. It was also exercised to study the Kinetics model i.e. Pseudo-first order, Pseudo-second order and intra-particle diffusion model recommended model for such type of studies. The recommended model were only selected after careful consideration of the current literature to support such type of studies. Moreover the full details of the each model parameters are clearly mentioned in Table 4.6 and fully discussed in sub-section 4.5.4.

#### **4.4.1 HPLC for acephate**

The POC was taken in a glass vial along with the addition of small quantity of HPLC mobile phase in a ratio H<sub>2</sub>O-ACN (20:80). The known amount of AP was placed in the ultrasonic bath for the pre-determined optimized time interval. After that it was taken out, filtered out the solid sorbent particles and immediately injected into HPLC (D-Star

Instruments 8424 Quary Rd., VA 20110–800-DSTAR12), equipped with a Mightysil RP-18, GP 250-4.6 (5µm) column and UV–Vis detector, at 215 nm wavelength (**Figure 4.16**).The percent of Acephate (% AP) can be obtained using the following **Equation 4.4**:

$$\% \text{ AP} = \frac{\text{Area of sample peak}}{\text{Area of Std. peak}} \times \frac{\text{Wt. of Standard}}{\text{Wt. of Sample}} \times \% \text{ Purity of Std.} \quad \text{Equation 4.4}$$

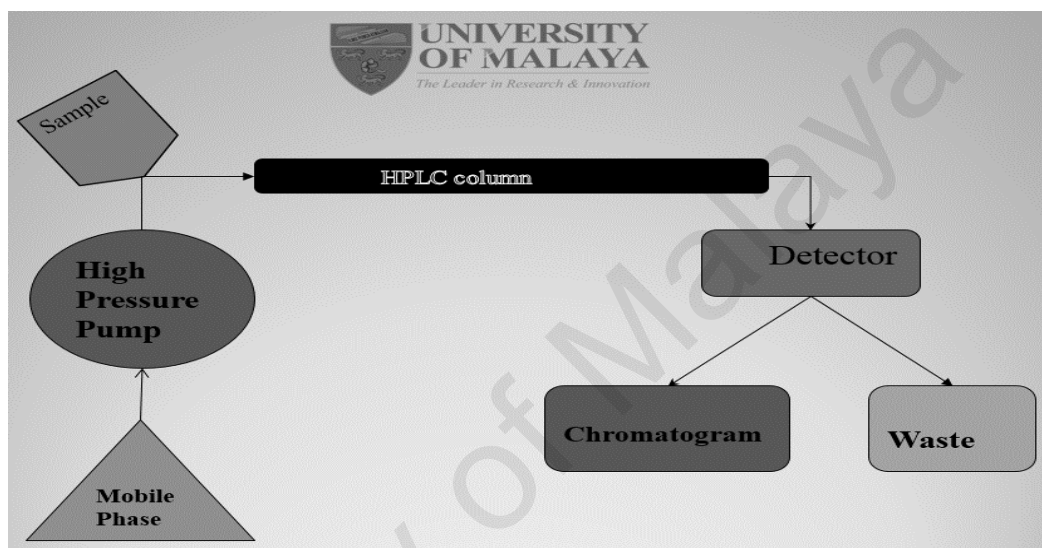


**Figure 4.16 HPLC schematic**

#### 4.4.2 Sonication time optimization

An Ultrasonic bath with temperature control conditions was used to study sonication effects. The sonication time was optimized with 1.0 mL Acephate (100 mgL<sup>-1</sup>), taken in a vial with fixed amount of POC adsorbent. The sorption was determined after different time intervals. The time based studies of AP revealed initially the AP uptake was relatively faster, it became slower towards the equilibrium point. It is explained, at the start of sorption, there were more vacant surface sites on POC available for AP adsorption.

#### 4.4.3 Isotherm models for acephate

The chemical equilibrium was studied using 0.01g of POC, varying the initial AP from 25 mgL<sup>-1</sup> to 300 mgL<sup>-1</sup>, pH 3.0 and temperature at 293K and 313K.. Chemical equilibrium studies were performed at 293 K and 313K at pH 3.0, dose 0.01g, initial concentration of acephate 25-300mgL<sup>-1</sup> with 3.0 min sonication time and the results are given in the Table 4.5. Langmuir parameters  $Q_{max}$ ,  $K_L$ ,  $R_L$  and  $a_L$  are given in Table 4.5. The factor  $a_L$  decreases with increase in temperature representing a decrease in sorption capacity with temperature as shown in Figure 4.17. The  $R_L$  parameter describes whether the adsorption process is favorable: The  $R_L$  parameter is less than 1 but greater than 0, indicating the feasible sorption process. The Freundlich parameter  $n$  and  $K_F$  are in good agreement with the Langmuir parameter  $R_L$ ,  $K_L$  and  $a_L$ . It is clear from Table 4.5, that the value of Temkin constants  $K_T$  and  $B_T$  decreases with an increase in temperature, indicating an exothermic sorption process. The DR isotherms adsorption energy indicated the exothermic adsorption as the value of  $E$  decreases from 201.779 KJ mol<sup>-1</sup> to 148.278 KJ mol<sup>-1</sup> with an increase in temperature from 293K to 313K.

**Table 4.5 Isotherms results for Acephate.**

Isotherm model	Temperature	
	293K	313 K
Langmuir		
$Q_{max}$ (mg/g)	11.228	10.667
$K_L$ (L/g)	0.651	0.323
$a_L$ (L/mg)	0.0295	0.0251
$R_L$	0.0548	0.0854
$R^2$	0.994	0.991
Freundlich		
n	3.2	1.9
$K_F$ (mg/g)	2.57	2.29
$R^2$	0.895	0.901
Temkin		
$K_T$ (L/g)	0.332	0.198
$B_t$ (mg/g)	5.24	4.04
$R^2$	0.9472	0.9321
Dubinin-Radushkevich		
$X_m$ (mg/g)	9.517	8.341
B	3.1E-05	1.9E-05
E (KJ/mol)	301.8	160.3
$R^2$	0.9605	0.9521
FH Model		
n	2.1418	3.3459
$K_{FH}$	0.0357	0.0286
$R^2$	0.8761	0.8978

The FH model parameter for the extent of adsorbate surface coverage also supported the previous results as the value of “n” model parameter increase from 2.142 to 3.36 with a corresponding increase of temperature.

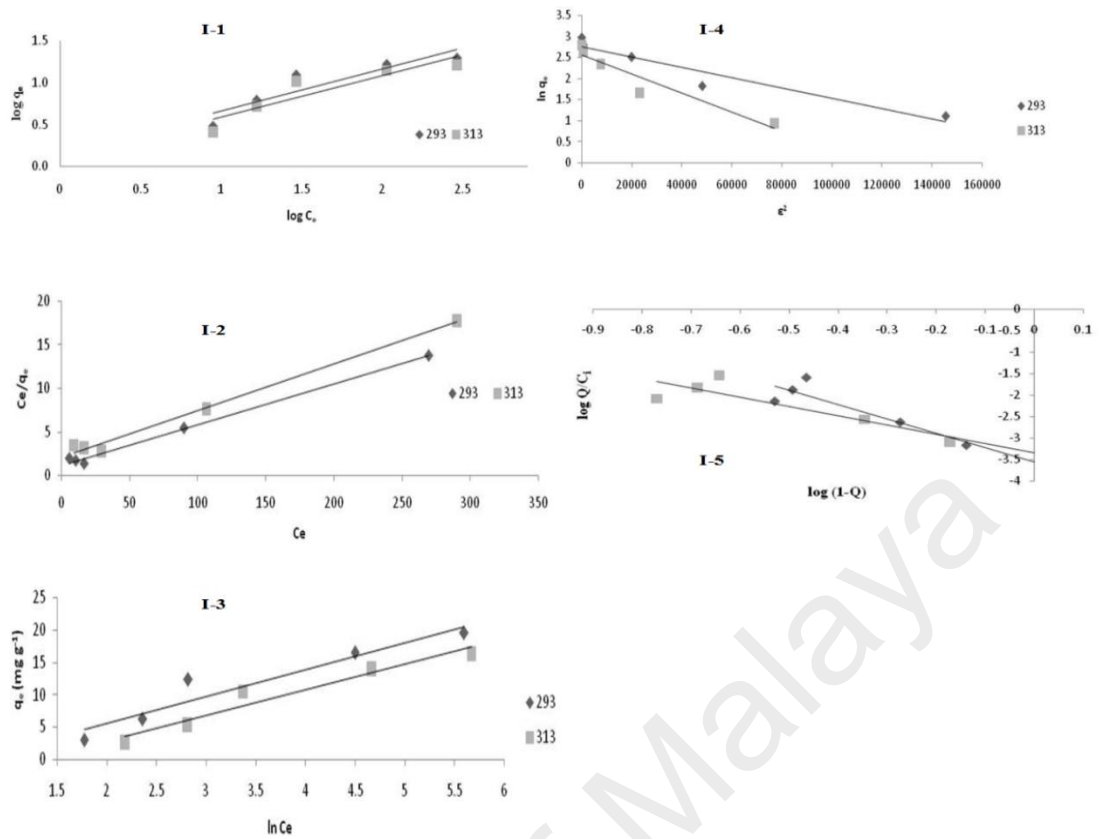


Figure 4.17 I-1, I-2, I-3, I-4 and I-5 represent Freundlich, Langmuir, Temkin, DR and FH Isotherms respectively.

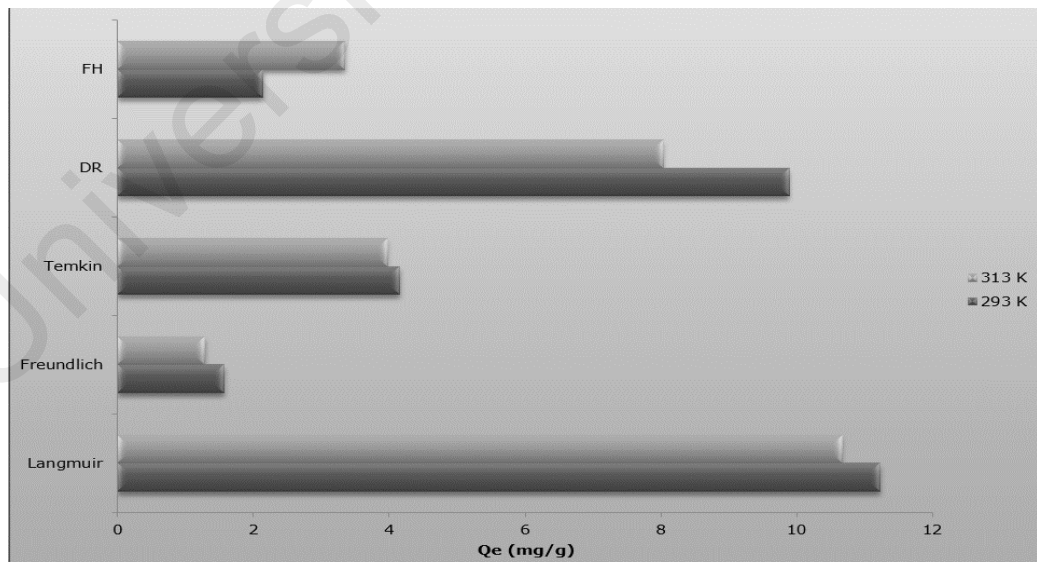


Figure 4.18 a comparison of  $Q_e$  predicted by different isotherm models.

#### 4.4.4 Kinetics models for Acephate

The Kinetic experiments were performed at 293K and 313K using the 100 mgL<sup>-1</sup> of acephate, 0.01g of adsorbent dose, pH 3.0 with different sonication time intervals. The adsorption capacity at any time interval “t” was determined by: **Equation 4.5**, adsorption capacity with time “ $Q_t$ ”.

$$Q_t = \frac{(C_o - C_t)V}{m} \quad : \text{Equation 4.5}$$

**Table 4.6 Acephate Kinetic models results.**

Kinetic model	Temperature	
	293K	313 K
Pseudo-first-order		
$Q_e$ (exp.)/mg g <sup>-1</sup>	11.607	11.081
$K_1$ (min <sup>-1</sup> )	0.014	0.015
$R^2$	0.978	0.969
Pseudo-second-order		
$Q_e$ (model)/mg g <sup>-1</sup>	12.427	12.280
$k_2$ (g mg <sup>-1</sup> min <sup>-1</sup> )	0.0014	0.001
$h$ /mg g <sup>-1</sup> min <sup>-1</sup>	0.3058	0.287
$t_{1/2}$ / min	169.183	165.730
$R^2$	0.998	0.996
Intraparticle diffusion		
$I$ (model)/mg g <sup>-1</sup>	5.040	4.642
$K_{id}$ (g mg <sup>-1</sup> min <sup>-1</sup> )	0.508	0.509
$R^2$	0.925	0.966

The value of constants  $K_2$  ( $\text{g}\cdot\text{mg}^{-1}\cdot\text{min}^{-1}$ ) and  $Q_e$  ( $\text{mg}\cdot\text{g}^{-1}$ ) are given in the **Table 4.6**. According to correlation coefficient values, the 2<sup>nd</sup> order model is more suitable to the Acephate adsorption kinetic data than that of the first order model. **Table 4.6** shows that the value of  $Q_e$  decreases by increasing the temperature. It is an established fact that the value of intraparticle parameter “I” is directly proportional to the boundary layer thickness (Bekçi et al., 2008). The Value of I (**Table 4.6**) shows a deviation of model curve from origin which means that surface adsorption and intraparticle diffusion steps are operating simultaneously during the adsorption process **Figure 4.19**.

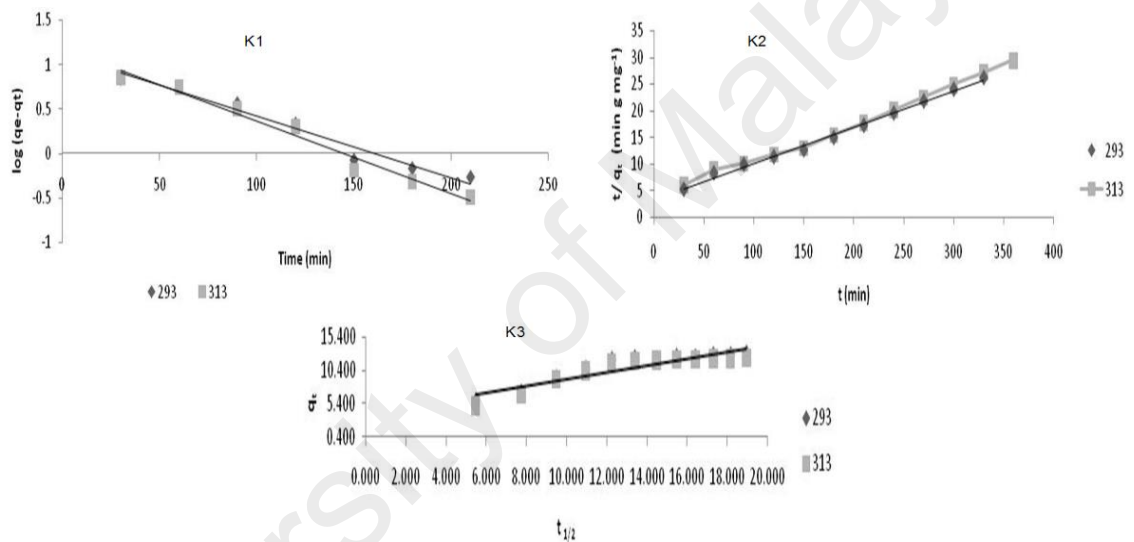


**Figure 4.19, K1, K2, K3 show the 1<sup>st</sup>, pseudo 2<sup>nd</sup> and intraparticle diffusion models respectively.**

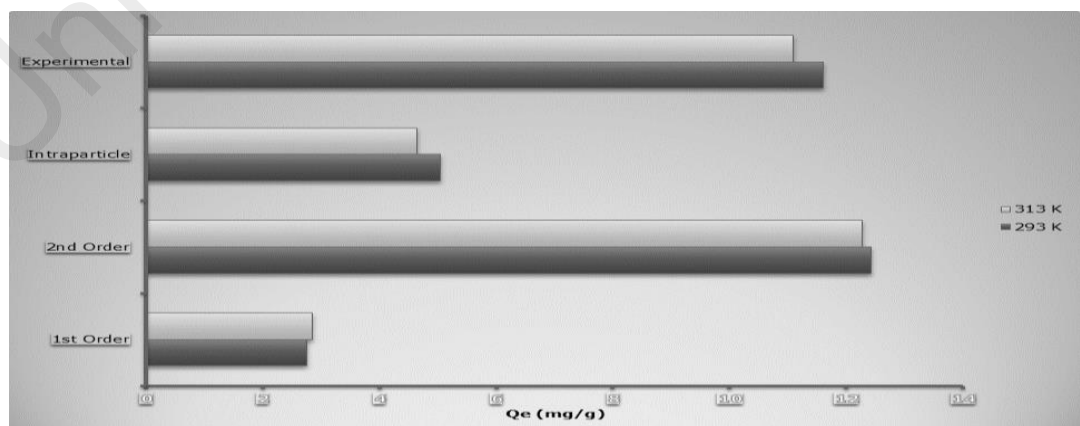


**Figure 4.20. Comparison among experimental and model predicted results for AP adsorption.**

From **Figure 4.21**, A simple  $Q_{e(exp)}$  and  $Q_{e(model)}$  graphical comparison highlights that the pseudo 2<sup>nd</sup> order kinetic model better fits and explains the AP adsorption.

#### 4.4.5 Thermodynamics of Acephate adsorption

**Table 4.7** presents the thermodynamics at the selected temperature i.e. 293K and 313K. The negative value of Gibb's free energy ( $\Delta G$ ) represents the spontaneous adsorption process. The negative values of  $\Delta H$  show the exothermic nature of adsorption process. It can be seen that the entropy of the system show a decrease, that support the hypothesis that adsorption decreases the degree of system disorder ( $\Delta S$ ).

**Table 4.7 Thermodynamics constants**

Temp (K)	Sorbent	$\Delta G$ [kJ mol <sup>-1</sup> ]	$\Delta H$ [kJ mol <sup>-1</sup> ]	$\Delta S$ [kJ mol <sup>-1</sup> K <sup>-1</sup> ]
293	POC	-0.5309	-22.5902	-0.0757
313	POC	-1.9926	-22.5902	-0.0703

The present results conclude the sorption of Acephate (AP) onto POC using batch mode of experiments performed at different experimental condition. The HPLC technique was used to estimate the AP concentration in the sample obtained after sorption batch experiments. The HPLC results were examined using different isotherm model. The best fit model based upon the correlation coefficient was Langmuir followed by the DR model. The sorption kinetics results were fitted into pseudo 1<sup>st</sup> order, pseudo 2<sup>nd</sup> order and Intraparticle diffusion models. Among the studied models, the pseudo 2<sup>nd</sup> order better fitted the AP sorption data. The thermodynamic results illustrated the nature of the sorption to be spontaneous, exothermic with a reduction in the entropy of the system.

#### 4.5 Fluoride remediation using doped and un-doped magnetic ferrites.

Fluoride is an essential element for health as it prolongs dental life to offer resistance to the acids that are formed by bacteria feeding on the teeth trapped food. A proper

washing of teeth and regular tooth brush activities is a simple solution to overcome dental decay or plaque formation. Fluoride consumption is reportedly increasing beyond maximum permissible limits that is believed to cause health problems (Bain et al., 2012; Gonzalo et al., 2012; Shen et al., 2003). The maximum allowable concentration level (MCL) of 1.5 mg/L fluorides has been recommended by World Health Organization (WHO). The drinking of lots of fluorides results into impaired growth, intelligence, arthritis, skeletal deformations, osteoporosis and even cancer in severe cases (Kang et al., 2011; Ma et al., 2014; Onyango et al., 2004; Velazquez-Jimenez et al., 2013; Yadav et al., 2007). The present problem of fluorides access in consumer water give an idea to make an adsorptive removal strategy using some series of magnetic ferrites.

However, some problems remain in the development of adsorbents for fluoride adsorption, such as instability, matrix effects, mechanical strength and poor adsorption capacity. Therefore, more efforts should be devoted towards new classes of adsorbents with high de-fluoridation capacity. In recent times, magnetic adsorbents with competent adsorption capacities and environmental friendly properties have been designed, developed and applied for the treatment of anionic waste products, such as fluoride, nitrate, sulfate, arsenate and phosphate. The magnetic adsorbents include magnetic materials, such as iron, copper, cobalt and nickel oxides (Hua et al., 2012). The flexible geometric structures of transition metal oxides allows the manufacture of adsorbents with exceptional properties (Rao et al., 2012). The cubic close packed geometry of  $\text{CuFe}_2\text{O}_4$  offer two types of sites, i.e., tetrahedral sites (A) and octahedral sites (B) (Gadkari et al., 2009). The electrical and magnetic properties depend on the position of each metal on each site. These sites play a deciding role in the electromagnetic properties (Ahmed et al., 2006). Ferrites exhibit the trade of electrons during Fe-Fe interaction, causing polarizations and electrical conductivity (Ahmed et al., 2006). However, doping rare earth cations alters the electrical, magnetic and physical

properties (Kobayashi et al., 2002; Zhao et al., 2008). For instance, Cerium (Ce) is a unique single electron system; it enables particle dispersion, which is an anticipated and expected property for an adsorbent. Cerium also promotes a larger number of active functional sites, surface area, and a larger pore size and pore volume. These improvements expedite the adsorbate-adsorbent interactions because the adsorbate can straightforwardly diffuse and reach the active sites for adsorption.

The ion chromatographic (IC) parting and detection method for quantifying anions provides numerous benefits. First, only a small amount of sample (20  $\mu$ L) is required, which permits for the separation of associated ions, depending on the retention times ( $t_R$ ). Second, aligned ion suppressor controls the conductivity by suppressing the concomitant ions, in this manner causing high conductivity. Third, a number of anions can be concurrently spotted and quantified in a single run due to the specific interaction and partition amid the stationary phase and the mobile phase. Besides, IC separation is a highly specific, selective, reproducible, robust and cost-effective method.

Electric, magnetic and dielectric behavior of ferrites is a function of structural properties (Ahmed et al., 2015; Larbi et al., 2015; Larbi et al., 2014). Therefore XRD, ATR and FESEM are especially used for adsorbent characterization. High penetrating power, X-rays provides important information regarding structural properties of the matter. Every material is distinctive due to its size of atoms, arrangement of atoms and ability to scatter X-rays. Since no two atoms have exactly same size and X-ray scatter ability, the intensities of diffracted beam will be only one of its kinds for every material. This individuality helps to identify the structure and determine the structural parameters of the material (Gadkari et al., 2009). Multiphase structure, crystallite sizes and crystal strains of  $\text{CuCe}_x\text{Fe}_{2-x}\text{O}_4$  were observed by XRD, (PANanalytical's Emprean), equipped with a monochromatic *Cu K $\alpha$*  radiation source. Ferrites surface morphology, particle

size distribution were studied by FESEM. FTIR analysis was performed on a Perkin Elmer System 2000 series spectrophotometer (USA) between 4000-400  $\text{cm}^{-1}$ . Magnetic hysteresis loops were recorded on VSM. BET specific surface area study of the samples was carried out on the basis of nitrogen adsorption desorption isotherms measured at 77K using a BELSORP-max nitrogen adsorption equipment (Japan Inc.). CV and EIS experiments were carried out on Autolab PGSTAT 302N and NOVA 1.10 software for the analysis of data.

#### **4.6 Characterization of doped and undoped magnetic ferrites**

##### **4.6.1 XRD analysis**

In the absence of cerium ( $x=0.0$ ), all of the identified peaks match with copper ferrite ( $\text{CuFe}_2\text{O}_4$ ), indicating the creation of spinel-type  $\text{CuFe}_2\text{O}_4$  (Mexmain, 1971). After the addition of Ce ( $x=0.1$ ), some additional peaks of low intensity appeared in the XRD spectra corresponding to  $\text{CeO}_2$  (Wyckoff, 1963). The accumulation of cerium into the pristine copper ferrite showed distinct variation in the percentages of the respective phases. The organized increase in dopant concentration ( $x$ ) caused in a gradual increase in the intensity of the  $\text{CeO}_2$  peaks. Moreover, we observed a decline in the (311) peak. A judgment among the crystallite sizes divulges a regular fall of crystallite size with a gradual increase in dopant (Ce). **Table 4.8** shows that while doping copper ferrites with Ce reduced the crystallite sizes of pristine ferrite.

**Table 4.8. Crystal sizes and the micro-strain and BET properties of a series of copper ferrites  $\text{CuCe}_x\text{Fe}_{2-x}\text{O}_4$  ( $x=0$  to  $0.5$ ).**

Property	x=0.0	x=0.1	x=0.2	x=0.3	x=0.4	x=0.5
BET Surface area ( $\text{m}^2/\text{g}$ )	70	75	79	83	88	92
Crystallite sizes $D$ (nm)	72	50	34	30	20	18
Average pore size (nm)	38	34	30	25	20	17
Pore volume ( $\text{cm}^3/\text{g}$ )	0.44	0.4	0.38	0.34	0.29	0.26
Lattice strain $\eta$ (%)	0.17	0.25	0.38	0.42	0.64	0.69

This decrease was attributed to the formation of secondary phases (Khandekar et al., 2013). This decrease was also supported by a relative increase in the lattice parameters. Accordingly, the  $\text{Ce}^{3+}$  ions were oxidized to  $\text{Ce}^{4+}$  at this temperature and appeared as a separate phase in the XRD spectrum (Figure 4.21).

The surface properties, surface area, and pore size and volume of the adsorbents were analyzed via BET. [Table 4.8] indicates that a measured increase in dopant concentration ( $x$ ) parallels to an increase in the BET surface area. Cerium oxide likely constrains the growth of larger particles because of its high dispersion (Zhao et al., 2008). The BET results indicate that during adsorption, more fluoride can interact with the available active sites that are created by doping in these magnetic ferrites.

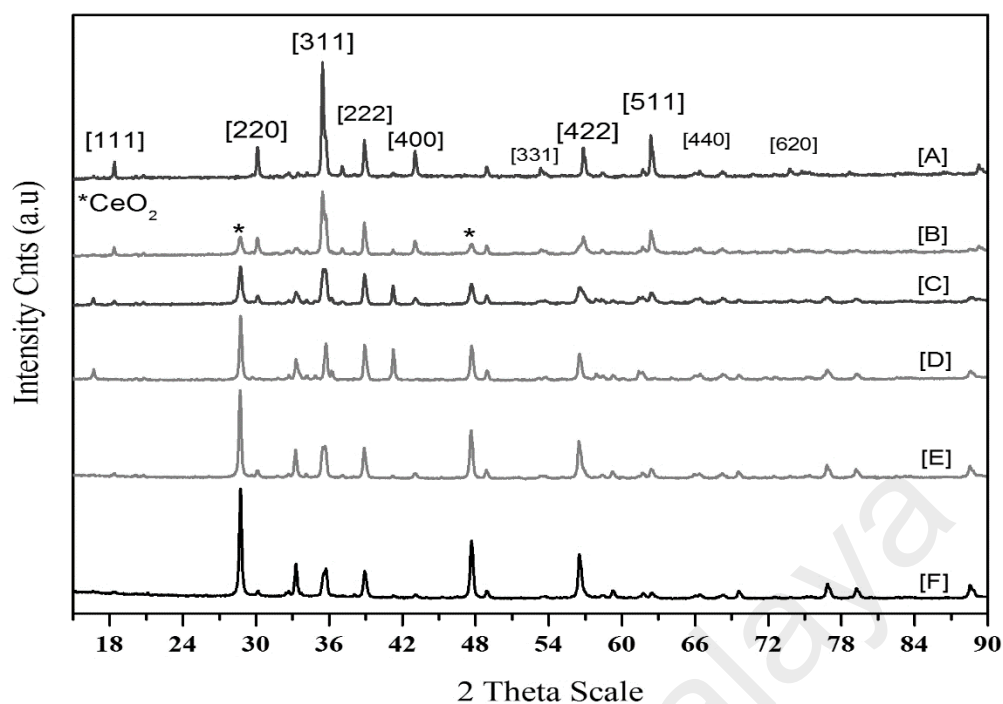


**Figure 4.21. XRD spectra [A] un-doped  $\text{CuFe}_2\text{O}_4$ , [B] doped  $\text{CuCe}_{0.1}\text{Fe}_{1.9}\text{O}_4$ , [C]  $\text{CuCe}_{0.2}\text{Fe}_{1.8}\text{O}_4$ , [D]  $\text{CuCe}_{0.3}\text{Fe}_{1.7}\text{O}_4$ , [E]  $\text{CuCe}_{0.4}\text{Fe}_{1.6}\text{O}_4$ , and [F]  $\text{CuCe}_{0.5}\text{Fe}_{1.5}\text{O}_4$  adsorbents for fluoride, annealed at  $650^\circ\text{C}$  for 3 h.**

#### 4.6.2 Electro-analytical results

The electrochemical properties of ferrite modified electrodes were studied using electrochemical impedance spectroscopy (EIS) (**Figure 4.22**). The EIS technique measures the charge transfer resistance ( $R_{ct}$ ) and parting efficiency between the holes and electrons. The studied  $R_{ct}$  is a critical factor in the charge separation efficiency. The arc radius shrinkages from  $x=0$  to  $x=0.2$ , which indicates higher charge resistance with higher Ce content. According to the hopping mechanism, changes in the mobility of the charge carriers lead to the transmission of current by hopping from one iron atom to the next (Rezlescu et al., 2000). When cerium is doped in the place of iron, the resistivity of the sample is found to increase. This behavior can be explained by the greater resistivity of cerium ( $74.4 \times 10^{-8}\Omega\text{ m}$ ) compared with iron ( $8.57 \times 10^{-8}\Omega\text{ m}$ ) (Lamarca et al. (2005). Further increase in the Ce dopant in the range of  $x=0.3$  to  $x=0.5$  again uncovers that larger semicircles are associated with the higher amounts of  $R_{ct}$ . The LSV analysis was used to study the electrochemical properties of the adsorbents.

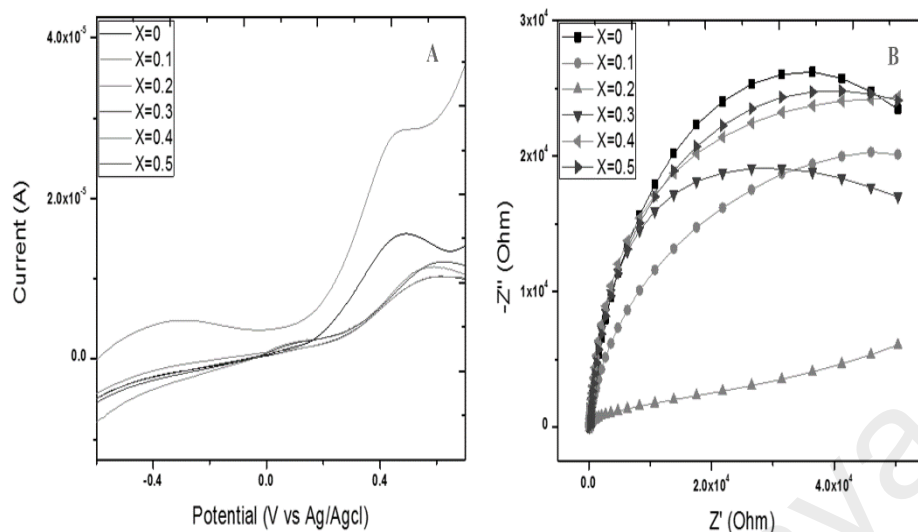


**Figure 4.22.** (A) Effect of the applied potential on the current response and (B) Nyquist diagrams of ( $x=0$ ) un-doped  $\text{CuFe}_2\text{O}_4$  ( $x=0.1$ ), doped  $\text{CuCe}_{0.1}\text{Fe}_{1.9}\text{O}_4$  ( $x=0.2$ ),  $\text{CuCe}_{0.2}\text{Fe}_{1.8}\text{O}_4$  ( $x=0.3$ ),  $\text{CuCe}_{0.3}\text{Fe}_{1.7}\text{O}_4$  ( $x=0.4$ ), and  $\text{CuCe}_{0.4}\text{Fe}_{1.6}\text{O}_4$  ( $x=0.5$ )  $\text{CuCe}_{0.5}\text{Fe}_{1.5}\text{O}_4$  in 0.1 M KCl solution containing 1.0 mM  $\text{K}_3[\text{Fe}(\text{CN})_6]$  and  $\text{K}_4[\text{Fe}(\text{CN})_6]$  (1:1).

Ferrite with  $x=0.2$  exhibited the maximum photocurrent response, followed by  $x=0.1$ . The photo-electrochemical activity is well known to be determined by the light harvesting capacity and the separation of electron-hole pairs (Zhang et al., 2014). Generally, a high value of the photocurrent indicates that the sample has a strong ability to generate and transfer the photo-excited charger carrier under irradiation. The EIS and LSV results confirm that the ferrite adsorbents can be used as photo-catalysts and photo-electrode materials in addition to their excellent adsorbent properties.

#### 4.6.3 FTIR of spinel ferrites

The inter-metallic ionic mode of vibration in FTIR spectroscopy analysis provides information regarding the ions involved in the formation of the crystal lattice (Borhan et al., 2013; Zhang et al., 2014). The characteristic peaks of the spinel structure observed in the range of  $560$  to  $580\text{ cm}^{-1}$  are attributed to Fe-O stretching vibration at the tetrahedral site (Figure 4.23). FTIR functional groups were compared in pristine and Ce-doped ferrites. All Ce-doped ferrites have distinct peaks near  $850\text{ cm}^{-1}$  and  $1440\text{ cm}^{-1}$

<sup>1</sup>. The additional functionality is thought to be responsible for the electrostatic interaction with the adsorbate to enhance the overall fluoride adsorption. The hydroxyl and sulfate groups are clearly involved in the fluoride adsorption. The abundance of these groups in the Ce-doped ferrite may be the main reason for the high fluoride uptake.

#### 4.6.4 FESEM results

“When  $x=0.0$ , we observe normally sized  $\text{CuFe}_2\text{O}_4$  nano-crystals ( $\sim 74$  nm) with uniform morphology along with some agglomerations of larger size ( $\sim 180$  nm). This behavior was due to the large specific surface of the fine particles for van der Waals interactions. From a Nano chemistry perspective, adjacent nanoparticles that share a common crystallographic orientation may collide with each other, which leads to coalescence (Balaz, 2008) because adjacent primary particles attach to each other and form aggregates.

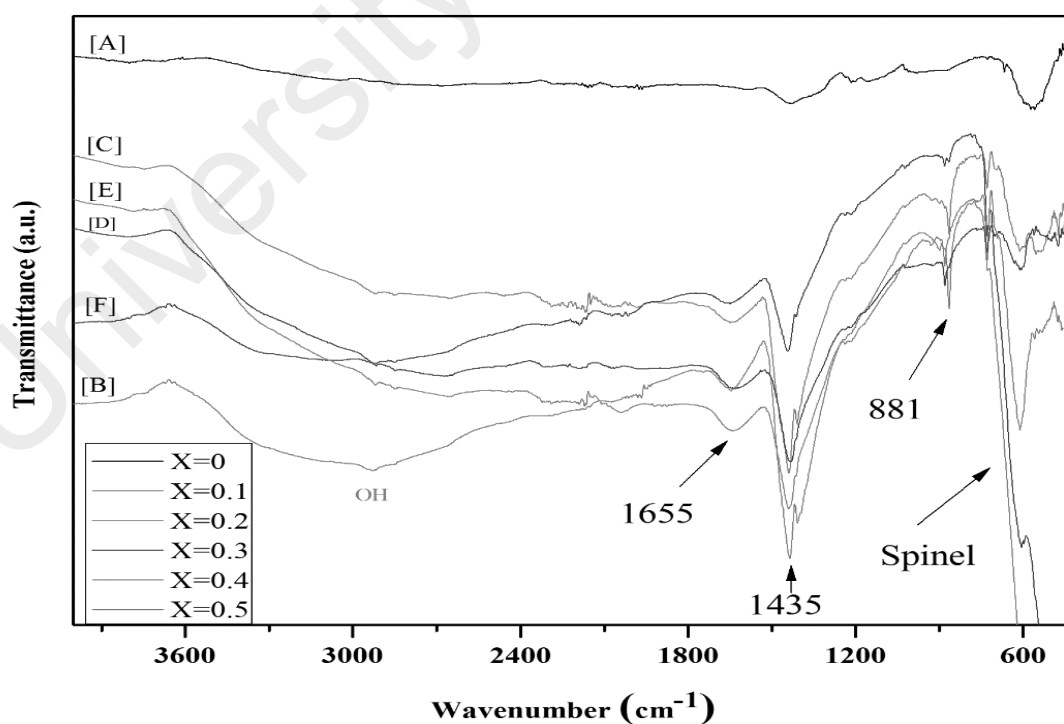


**Figure 4.23. FTIR overlay spectra of (A) un-doped  $\text{CuFe}_2\text{O}_4$ , (B) doped  $\text{CuCe}_{0.1}\text{Fe}_{1.9}\text{O}_4$ , (C)  $\text{CuCe}_{0.2}\text{Fe}_{1.8}\text{O}_4$ , (D)  $\text{CuCe}_{0.3}\text{Fe}_{1.7}\text{O}_4$ , (E)  $\text{CuCe}_{0.4}\text{Fe}_{1.6}\text{O}_4$ , and (F)  $\text{CuCe}_{0.5}\text{Fe}_{1.5}\text{O}_4$ .**

In addition, due to the nanometer-scale sizes, these particles continue to collide and coalesce to form even larger particles. This phenomenon may eventually cause agglomeration in the fabricated ferrites. The agglomeration is affected by various processing parameters, such as speed, intensity and mixing time. Relatively smaller sizes were observed with further addition of ceria ( $x=0.1$  to  $x=0.5$ ). Moreover, the addition of ceria particles was found to increase the surface area by allowing for maximum dispersion and retarding large grain growth (**Figure 4.24**). These results complement the XRD results and provide evidence of an increased surface area, which can facilitate better fluoride adsorption. These results also agree with those of other studies, indicating that doping lanthanides delays particle grain growth (Ishaque et al., 2015; Khandekar et al., 2013). The observed incremental diminution in grain morphology via the orderly doping of ceria promotes fluoride adsorption.

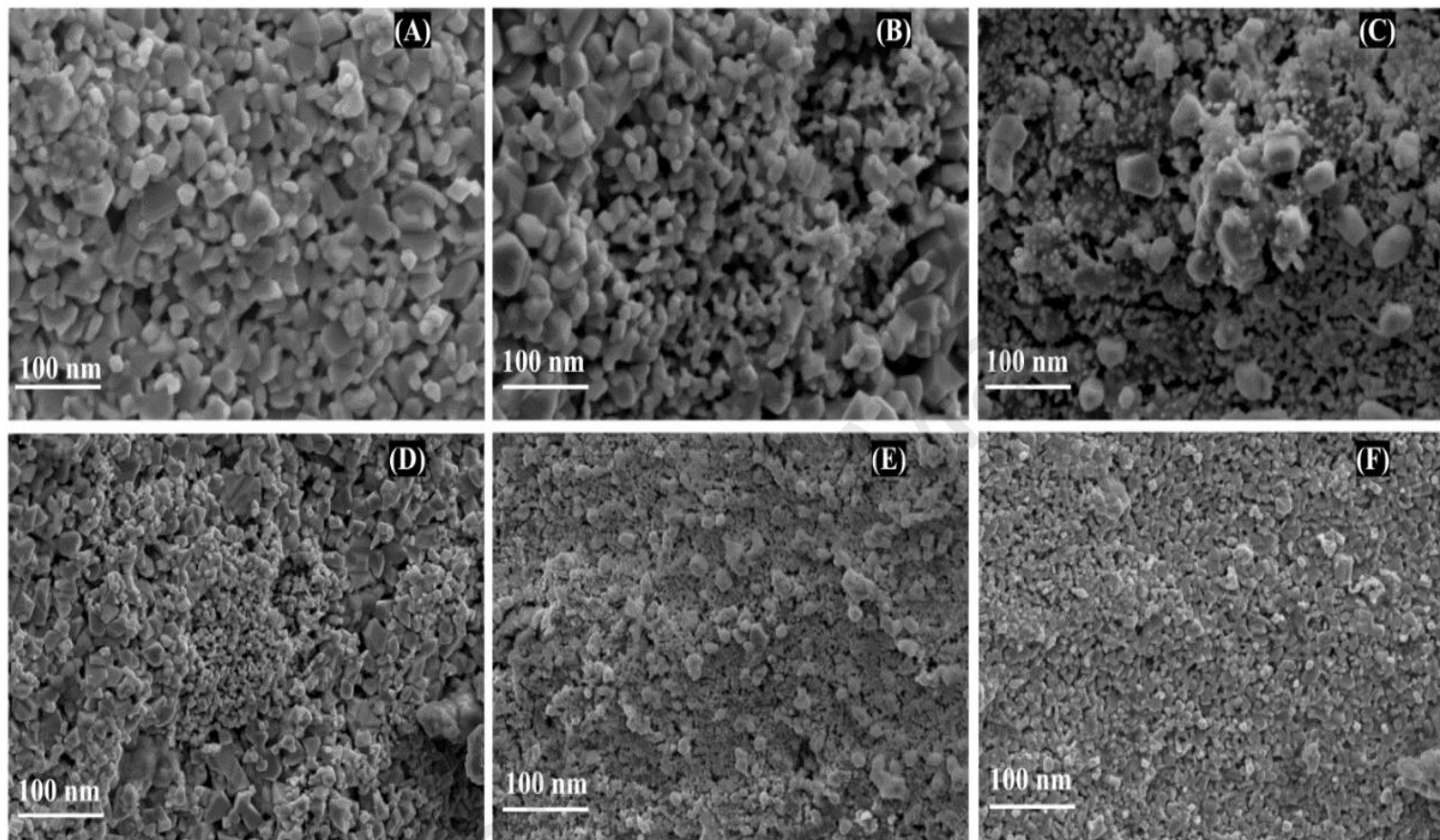


**Figure 4.24. FESEM images of (A) un-doped  $\text{CuFe}_2\text{O}_4$ , (B) doped  $\text{CuCe}_{0.1}\text{Fe}_{1.9}\text{O}_4$ , (C)  $\text{CuCe}_{0.2}\text{Fe}_{1.8}\text{O}_4$ , (D)  $\text{CuCe}_{0.3}\text{Fe}_{1.7}\text{O}_4$ , (E)  $\text{CuCe}_{0.4}\text{Fe}_{1.6}\text{O}_4$ , and (F)  $\text{CuCe}_{0.5}\text{Fe}_{1.5}\text{O}_4$  prepared in micro-emulsion ( $w=15$ ).**

#### 4.6.5 Magnetic properties

The value of the squareness ratio (SQ) was analyzed by dividing the value of the magnetic remanence (Mr) by the magnetic saturation (Ms) (Appendix E). The SQ value reflects the magneto-crystalline anisotropy and the super-exchange interactions of the ferrite series (Chinnasamy et al., 2003).  $\text{CuFe}_2\text{O}_4$  exhibits a SQ value of 0.13 ( $x=0.0$ ), but after Ce doping, this value increases in the cases of  $x=0.1$  and  $x=0.2$ . Note that the incorporation of Ce reduced the magneto-static interactions (Domingo et al., 2012). However, the further supplement of Ce exhibits a regular declining inclination from  $x=0.3$  to  $x=0.5$ . This phenomenon indicates that the local canting effect is taking control over the surface canting effects associated with crystallite size and coercivity (Wahba et al., 2015). The relative change in Mr and Ms with Ce content has exactly the same trend, as expected from the SQ values for each member of the series **Table 4.9**.

**Table 4.9. Magnetic properties of the  $\text{CuCe}_x\text{Fe}_{2-x}\text{O}_4$  adsorbents by VSM.**

Magnetic parameters	0.0	0.1	0.2	0.3	0.4	0.5
Coercivity (T)	0.007	0.009	0.010	0.01	0.009	0.004
Ms (emu/g)	30.14	25.31	15.53	13.01	11.65	8.89
Mr (emu/g)	4.34	3.89	3.09	2.50	2.11	0.82
SQ	0.14	0.15	0.20	0.19	0.18	0.09

The Hc value is obviously increasing with the quantity of dopant ( $x$  from  $x=0.0$  to  $x=0.2$ ), and further doping results in a regular decline (from  $x=0.3$ ; the maximum decrease occurs when  $x=0.5$ ), which is credited to extrinsic and intrinsic factors. The extrinsic factors depend on the density, morphology and grain size (Potts et al., 2011). The intrinsic factors, such as relative occupation of sub-lattice sites, contributed to the magnetism in the nano-ferrites (Raju et al., 2014). The shape and width of the hysteresis loops depend on the method of preparation, composition, and distribution of the metal

cations at the tetrahedral and octahedral sites, the spin canting and the crystallite size (Borhan et al., 2013). The values of  $M_r$  and  $M_s$  exhibit a regular decline. This behavior could be described by the decrease of  $D$  from 73 nm to 18 nm, and the respective increase in the Ce content at the B-sites. Because the magnetic moment of Ce is less than that of Fe, theoretically, increasing the Ce content will reduce the  $M_s$  monotonically (Petrovic et al., 2001; Wahba et al., 2015). Generally, rare-earth elements have a strong anisotropic subsystem with a adequately high anisotropic exchange constant for iron (Gornostaeva et al., 2013). Thermal excitation breaks the Kondo state, which causes a gradual recovery of magnetic moments (Buschow, 2005).

$Ce^{3+}$  magnetic moments are managed by direct or indirect exchange interaction, namely RKKY interaction facilitated by conduction electrons (Fikáček et al., 2013). Appropriately strong exchange interaction produces a magnetically ordered ground state. However, in the case of  $x=0.3$ , a dominance of the Kondo interaction occurs, which results in a nonmagnetic ground state. A variation in the coercive field ( $H_c$ ) directly depends on the surface spin disorder (Kostopoulou et al., 2014). The decrease in  $H_c$  of the present series affirmed the reduced surface spin disorder. The magnetic properties of the ferrites are controlled by Fe-Fe interaction via the spin coupling of 3d valance electrons (Dixit et al., 2012). The present decrease in coercivity is assigned to morphology-increased magnetic moments and domain wall migration (Niaz Akhtar et al., 2014). The lower values of  $M_r$  and  $M_s$  are due to the oxidation of cerium into diamagnetic states (Dutta et al., 2006). However, the present decrease in magnetic character has little effect on the fluoride adsorption capacity, but it affects the magnetic separation capability due to the change in its morphology, crystal structure and related electromagnetic properties.

#### 4.6.6 Ion chromatography separation results

The anions were identified and quantified based on their retention time ( $t_R$ ) when performing Ion chromatography (IC), as presented in Table 4.10. Anion calibration standards of 1, 5 and 10  $\text{mgL}^{-1}$  were run to develop a calibration method. The  $t_R$  values of standards and samples were compared and quantified with MagICNet™1.0. In suppressed ion chromatographic separation, an ion suppressor was inserted between the separating column and the detector to reduce the inherent conductivity of the eluent for improved anion detection. The reactions involved with the chemical suppressor are represented by the following equation (Eith et al., 2001).

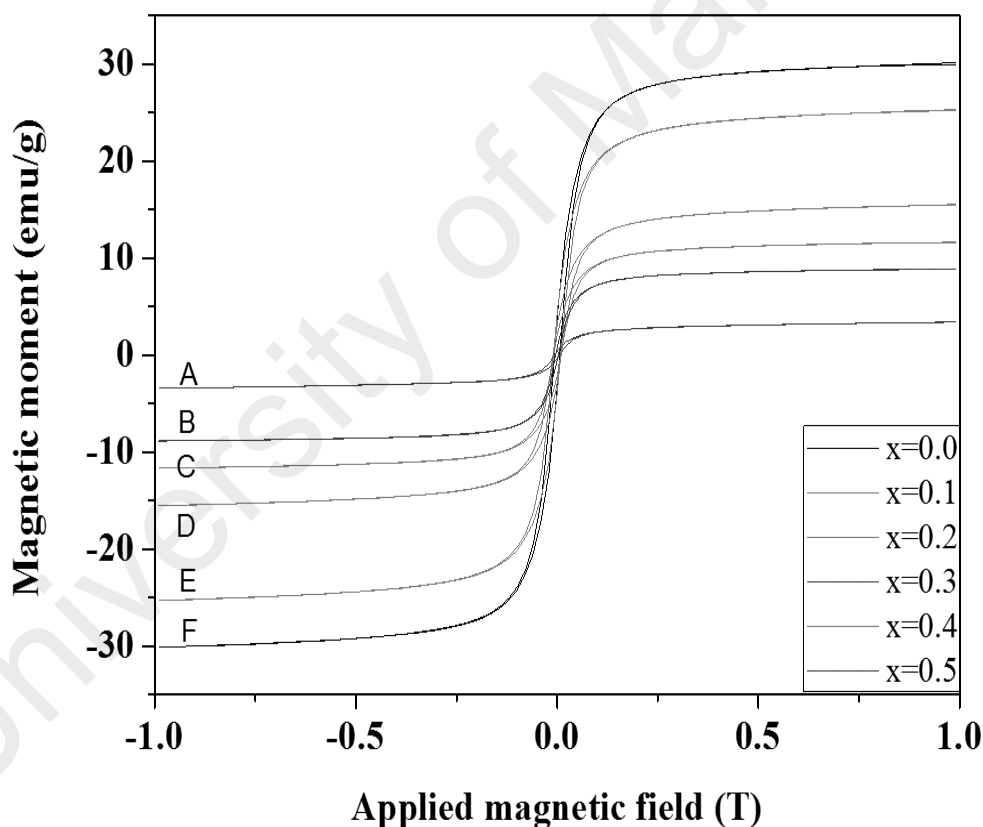


**Figure 4.25.** Magnetic properties of (A) un-doped  $\text{CuFe}_2\text{O}_4$ , (B) doped  $\text{CuCe}_{0.1}\text{Fe}_{1.9}\text{O}_4$ , (C)  $\text{CuCe}_{0.2}\text{Fe}_{1.8}\text{O}_4$ , (D)  $\text{CuCe}_{0.3}\text{Fe}_{1.7}\text{O}_4$ , (E)  $\text{CuCe}_{0.4}\text{Fe}_{1.6}\text{O}_4$ , and (F)  $\text{CuCe}_{0.5}\text{Fe}_{1.5}\text{O}_4$ .

**Table 4.10.** Retention times of the selected anions during ion chromatography.

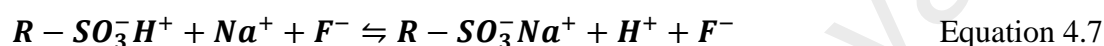
Anions	$\text{F}^-$	$\text{Cl}^-$	$\text{NO}_3^-$	$\text{SO}_4^{2-}$
$t_R$	4.05	5.54	8.87	16.60

Na<sup>+</sup> ions coming in mobile phase are substituted with H<sup>+</sup> ions, reducing the conductivity of the background electrolyte, as represented by **Equation 4.46**. The anion in sample, e.g., F<sup>-</sup> remains unchanged by the suppressor, detected and quantified by IC system, as represented by **Equation 4.57**.

**Equation 4.4.** Reaction in chemical suppressor



**Equation 4.5.** Fluorides for I.C detection.



#### 4.6.7 Effect of competing anions

Concomitant anions, such as chlorides, bicarbonate, nitrate, sulfate and arsenate, commonly exist in surface and ground water. Because these anions compete with fluorides for adsorbent active sites, their influence on fluoride adsorption was experimentally studied under different concentrations (0.1, 1.0 and 10 mM). In addition, arsenate (As), which is a concomitant anion of widespread concern, was studied at four different concentrations (2, 5, 10 and 30 mgL<sup>-1</sup>). The results show that to fluoride adsorption was affected by the presence of competitive anions. The red, orange, yellow, green and blue areas highlight the degree of adverse effect, with red indicating the greatest effect and blue indicating the least effect on fluoride adsorption (**Figure 4.26**). In summary, by using a straightforward doping of cerium into magnetic ferrite, we fruitfully fabricated a series of novel magnetic adsorbents for fluoride adsorption and water remediation technology. Compared with un-doped parent material, superior results were obtained, and the present enhancement in adsorption behavior contributed to the active functional groups created after doping, the increased surface area with appropriate porosity and the electro-magnetic properties.

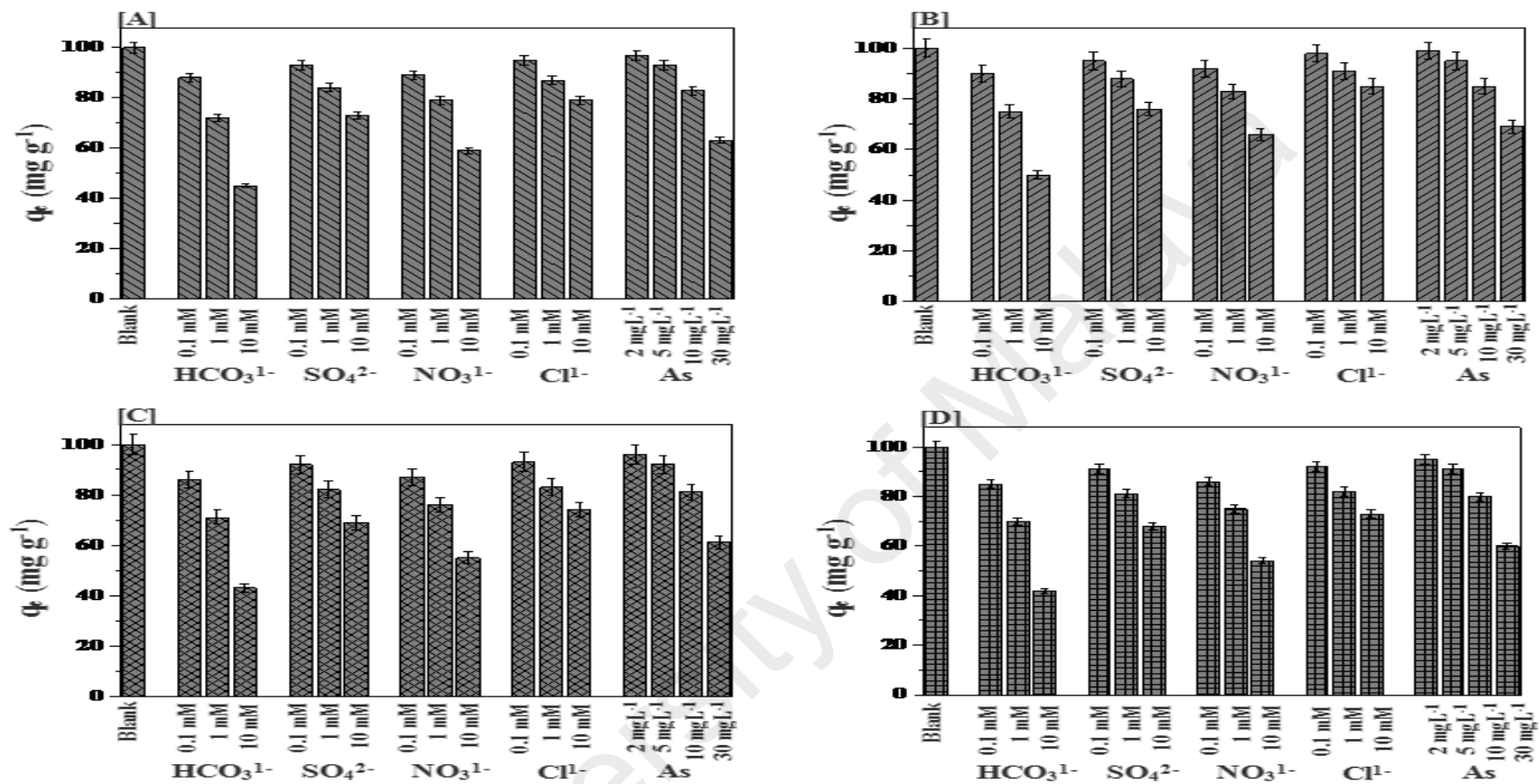


Figure 4.26. Effect of some concomitant anions on fluoride adsorption,  $m=0.1 \text{ g L}^{-1}$ ,  $[F]_0 = 10 \text{ mg L}^{-1}$ ,  $\text{pH}=7.0$ : (A) un-doped  $\text{CuFe}_2\text{O}_4$ , (B) doped  $\text{CuCe}_{0.2}\text{Fe}_{1.8}\text{O}_4$ , (C)  $\text{CuCe}_{0.3}\text{Fe}_{1.7}\text{O}_4$ , and (D)  $\text{CuCe}_{0.5}\text{Fe}_{1.5}\text{O}_4$ .

However, the presence of some coexistent species that are usually found in high concentration in industrial effluents reduced the efficiency of the present series of adsorbents due to competition for adsorbent active sites, which led to a decline in fluoride removal. The series of ferrite adsorbents for fluoride adsorption open new vistas for a broad range of applications and may lead to better insights into energy efficient magnetic adsorbents, electrochemical sensors and photo catalysts for environment remediation.

#### 4.7 Fluoride adsorption Model.

The fluoride adsorption is given by **Equation 4.8**. The results of ANOVA test were used to compare the coefficients values for each factor. In this model, positive value of a coefficient symbolizes a synergistic effect, whereas a negative value indicates an opposite effect (Badkar et al., 2013).

**Equation 4.8.** The proposed model for Fluorides.

$$\begin{aligned}
 q_e = & +139.71 + 14.29 * X_1 + 15.31 * X_2 + 6.99 * X_3 + 28.31 * X_4 + 0.67 * \\
 & X_1X_2 - 1.11 * X_1X_3 + 6.73X_1X_4 - 1.38X_2X_3 - 6.25 * X_2X_4 - 3.35X_3X_4 - 7.40 * \\
 & X_1^2 - 8.60 * X_2^2 - 4.71 * X_3^2 - 14.40 * X_4^2
 \end{aligned}
 \tag{Equation 4.8}$$

Where  $X_1$ ,  $X_2$ ,  $X_3$  and  $X_4$  are the coded variables for pH,  $F^{-1}$  ( $\text{mgL}^{-1}$ ), Temp. ( $^{\circ}\text{C}$ ) and ferrite dose (mg), respectively. The adequacy of the model was ensured and compared by Fischer variation (F-value), probability values (p-value) and the correlation coefficient ( $R^2$ ). The lack of fit value of the model of 0.74 was insignificant relative to the pure error. The predicted  $R^2$  value of 0.9988 was in reasonable conformity with an adjusted  $R^2$  of 0.9994. The adequate precision of the model is a measure of the signal-to-noise ratio. A ratio greater than 4 is desirable. In the present case, a ratio of 194.5

indicates an adequate signal. The effect of variables was analyzed by comparing the values of the linear, quadratic and interaction terms. The pH linear term ( $X_1$ ) with an F-value of 2112.63 indicates the significant role of pH in fluoride adsorption. However, the pH quadratic term ( $X_1^2$ ) has an F-value of 2239.4, which is greater than that of the linear term and indicates a positive role of pH increase in the selected range on fluoride adsorption. An optimum fluoride adsorption was achieved at neutral pH, as shown in **(Figure 4.27)** (RSM A, B and C).

According to the speciation of fluoride, it exists as a HF species instead of ionic ( $F^{-1}$ ), which may be the reason for the reduced adsorption under acidic conditions (Yu et al., 2015). According to the electrostatic interaction mechanism, a comparatively stronger attraction is observed at a pH below 6.12. However, pH is not the only factor that controls the fluoride adsorption. In the same way, the linear and quadratic terms of the fluoride initial concentration are significant during fluoride adsorption. An increase in the fluoride initial concentration improved the rate of adsorption. However, increasing the fluoride concentration beyond the optimum reduces the fluoride adsorption, as shown in **(Figure 4.27)** (RSM A and D). The linear and quadratic terms of temperature ( $X_3$  and  $X_3^2$ ) indicate a decrease in fluoride adsorption at elevated temperatures. The most prominent variable was adsorbent dose ( $X_4$ ), which has a significant influence on fluoride adsorption. This influence can be explained by the adsorbent dose being directly related with the number of active sites for fluoride adsorption.

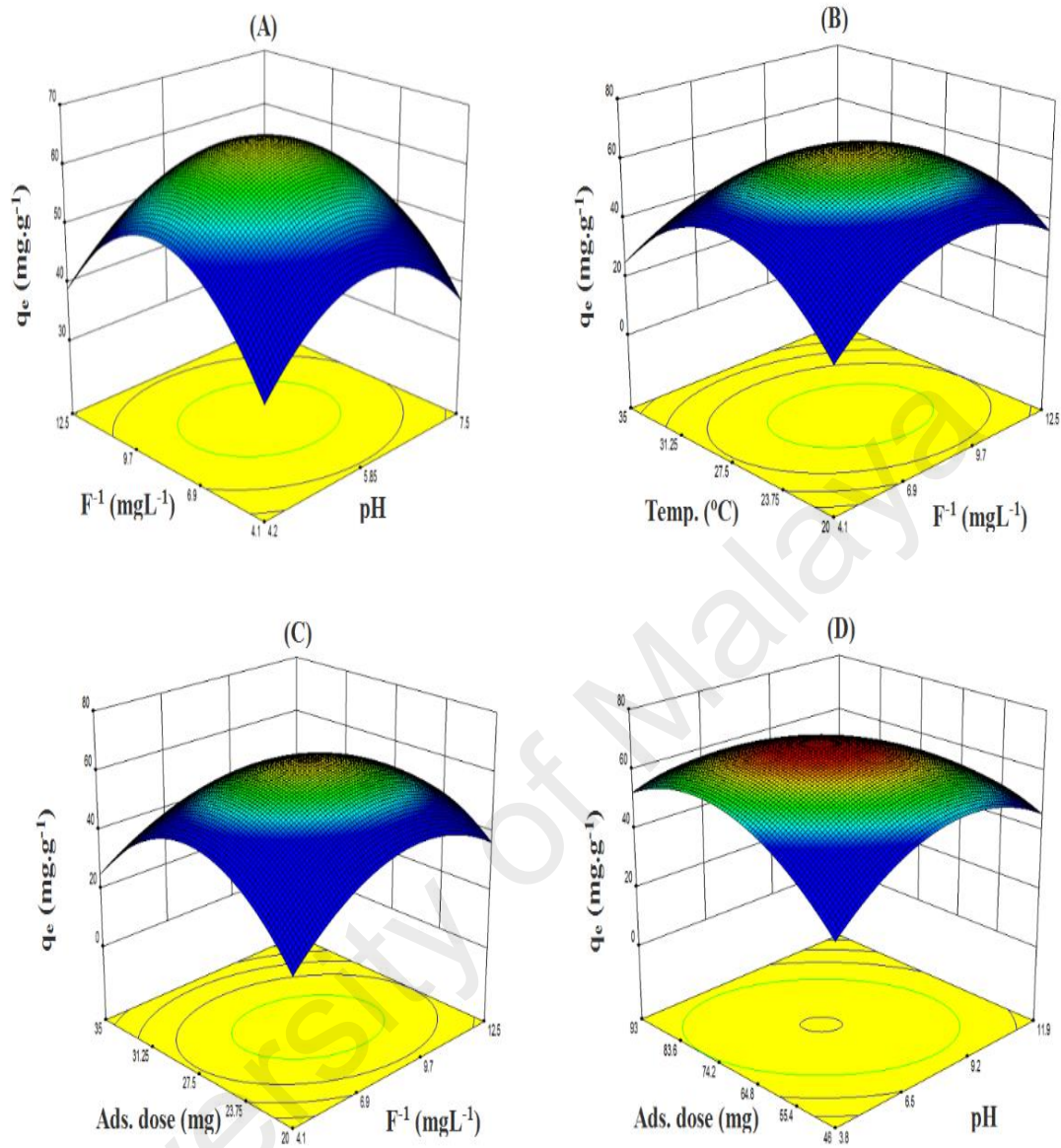


**Figure 4.27.** Response surfaces showing the effects of two variables on fluoride adsorption (A)  $\text{pH}$  and  $F^{-1}$  ( $\text{mg}\cdot\text{L}^{-1}$ ), (B)  $\text{pH}$  and  $\text{Ads. Dose}$  ( $\text{mg}$ ), (C)  $F^{-1}$  ( $\text{mg}\cdot\text{L}^{-1}$ ) and  $\text{Ads. Dose}$  ( $\text{mg}$ ), and (D)  $\text{Temp.}$  ( $^{\circ}\text{C}$ ) and  $\text{Ads. Dose}$  ( $\text{mg}$ ).

## CHAPTER 5: CONCLUSIONS

### 5.1 Conclusions

In response to the worldwide environmental contamination contributed by both natural and anthropogenic sources, two different sources of Nano-adsorbents, indigenous Palm oil waste and synthetic magnetic ferrites, have been prepared, characterized and applied for green environment remediation. Studies on adsorbents are of prime importance to understand the characteristics of the adsorbate-adsorbents interactions and their efficiency in the removal of hydrological contaminants for the potential remediation of the hydrosphere. The natural abundantly available palm oil clinker waste was researched for its versatile surface morphology, green origin and magnetic separation and application as a renewable resource of natural adsorbent. The mechanical, physical and chemical treatment were applied to impart the desired characteristics to the waste biomass.

The primary objective was to convert waste into wealth resource for the betterment of the agricultural sector that is facing a pollution challenge from the enormous volumes of bio-waste. A series of adsorbents were prepared based on particle size distribution, specific gravity, pore size, pore volume and fitness modulus by standard methods. The reproducibility of experimental adsorption capacity was ascertained by repeating the experiments to account for standard deviation. The present procedure is robust and advantageous over arsine gas generation method, as it required no extra reagents to produce gaseous phase arsenic (arsine gas). The analysis of the adsorption capacity data was subjected to mathematical modelling. The selected quadratic model provided better insight into complex correlated, mutually influencing system variables. Unique series of natural and magnetic Nano-adsorbents were prepared and tested for the hydro decontamination of heavy metals, organophosphorous pesticides, organic dyes and anionic water contaminants. The Nano-adsorbents were investigated for the crystal

structure, functional groups, thermal stability, morphology and magnetic properties. Graphene was found to have distinct effects on the surface morphology, crystallite size, lattice strain, and thermal stability of magnetic Nano-adsorbents.

The average crystallite size and grain size were found to increase, whereas the lattice strain decreased, with the use of graphene. The Vibrating Sample Magnetometer (VSM) results indicated that the saturation magnetization and coercivity followed a declining trend owing to the separation of magnetic centers in the nanocomposite. The fabricated composite ferrite materials were evaluated to enhance the hydro decontamination efficiencies for the maximum removal of arsenic, fluorides species along with acephate (AP), by using the preferred Design of Experiment (DOE) strategy. The adsorption data was analyzed by isotherm models e.g. Langmuir, Freundlich, Temkin, Dubinin-Redishkevich (DR), Florry huggins (FH). The present thesis corroborates the efficiency of Nano-adsorbents under single and dynamic competent environmental conditions. The adsorption mechanisms was elaborated by the interpretation of pseudo 1st order kinetic model, pseudo 2nd order and Bhangam's model. Present work provides a solution for pollution abatement through the use of novel classes of natural, synthetic and modified magnetic ferrite adsorbents. It also presents the use of the latest computer software for strategic application of magnetic Nano-ferrites to reuse industrial waste and remove toxic pollutants from water.

## **5.2 Recommendation**

Further research for future environmental applications relies on the few continuous natural resources of adsorbents. The proposed sources of adsorbents can be utilized for energy free separations or green environment remediation. In case of catastrophic accidents such as earthquake, floods and distress, these classes of adsorbents provide a low cost and energy saving alternate solution to provide efficient water decontamination

systems. Palm oil industry waste can be reprocessed and exported to the town planners, situation managers and community users looking for economical adsorbents to protect and purify water, air and soil. Novel series of adsorbents designed and used for making nanocomposites with emerging base materials such as graphene and nanotubes of carbon have long future impacts on public health and social developments. The use of the DOE strategy resolves the execution and implementation issues e.g. time, efforts and cost in research and development. The statistically well planned experiments yield better insight and interaction among the competing process variables responsible for controlling the adsorption capacities of the Nano-adsorbents. The use of POCS and magnetic Nano-adsorbents may be extended for industrial process catalysis, reduce byproducts and protect moisture or air sensitive materials e.g. medicines (**Figure 5.1**). Pollutants in the hydrosphere have a direct negative impact on public health and our combined socio-economic development. The aftermaths of hydrosphere contaminations embrace toxic waste production, equipment degradation, increased risk to the health and safety of humans, plants and animals. Henceforward, pollutants in the hydrosphere require contaminants removal technologies to circumvent the negative consequences of polluted environments. Nevertheless, the studies of specific magnetic Nano-adsorbents are still in need of the collaboration from the related agricultural and environmental businesses.

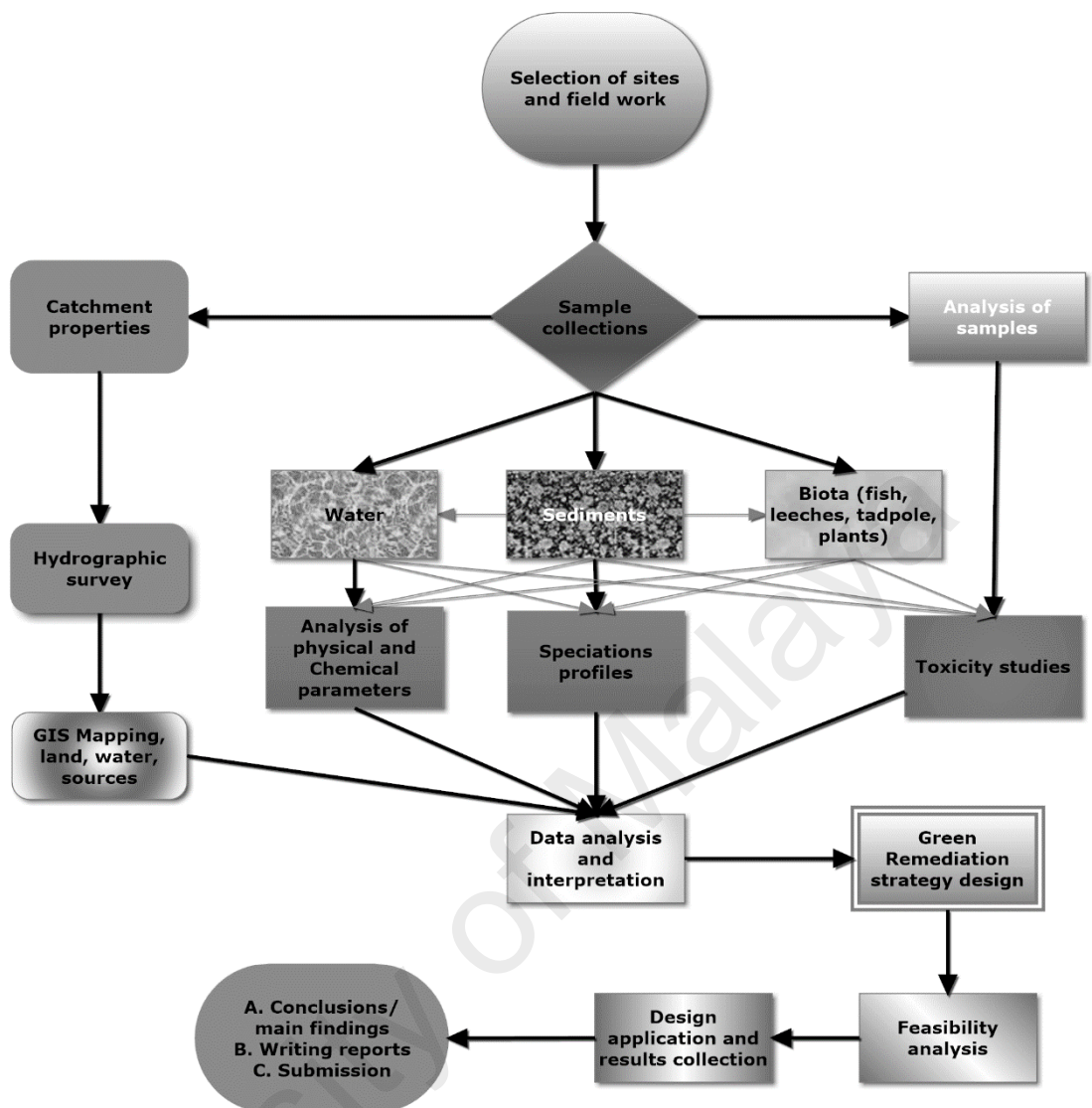


**Figure 5.1 Further work plan for future studies.**

## REFERENCES

- Abu Qdais, H., & Moussa, H. (2004). Removal of heavy metals from wastewater by membrane processes: a comparative study. *Desalination*, 164(2), 105-110.
- Ahmad, T., Rafatullah, M., Ghazali, A., Sulaiman, O., & Hashim, R. (2011). Oil palm biomass-based adsorbents for the removal of water pollutants--a review. *J. Environ. Sci. Health C Environ. Carcinog. Ecotoxicol. Rev.*, 29(3), 177-222.
- Ahmed, M. A., Ateia, E., & Salem, F. M. (2006). Spectroscopic and electrical properties of Mg-Ti ferrite doped with different rare-earth elements. *Physica B: Condensed Matter*, 381(1-2), 144-155.
- Ahmed, M. A., Mansour, S. F., & Ismael, H. (2015). A comparative study on the magnetic and electrical properties of MFe<sub>12</sub>O<sub>19</sub> (M=Ba and Sr)/BiFeO<sub>3</sub> nanocomposites. *Journal of Magnetism and Magnetic Materials*, 378(0), 376-388.
- Ahmmad, R., Jumaat, M. Z., Bahri, S., & Islam, A. B. M. S. (2014). Ductility performance of lightweight concrete element containing massive palm shell clinker. *Constr. Build. Mater.*, 63(0), 234-241.
- Akhavan, O. (2015). Bacteriorhodopsin as a superior substitute for hydrazine in chemical reduction of single-layer graphene oxide sheets. *Carbon*, 81, 158-166.
- Aksu, Z., Gönen, F., & Demircan, Z. (2002). Biosorption of chromium(VI) ions by Mowital®B30H resin immobilized activated sludge in a packed bed: comparison with granular activated carbon. *Process Biochemistry*, 38(2), 175-186.
- Ali, I. (2012). New Generation Adsorbents for Water Treatment. *Chemical Reviews*, 112(10), 5073-5091.
- Alvarez-Ayuso, E., & Garcia-Sanchez, A. (2003). Removal of heavy metals from waste waters by vermiculites. *Environmental Technology*, 24(5), 615-625.
- Ania, C. O., Menéndez, J. A., Parra, J. B., & Pis, J. J. (2004). Microwave-induced regeneration of activated carbons polluted with phenol. A comparison with conventional thermal regeneration. *Carbon*, 42(7), 1383-1387.
- Anirudhan, T. S., Divya, L., & Parvathy, J. (2013). Arsenic adsorption from contaminated water on Fe(III)-coordinated amino-functionalized poly(glycidylmethacrylate)-grafted TiO<sub>2</sub>-densified cellulose. *Journal of Chemical Technology & Biotechnology*, 88(5), 878-886.
- Aragay, G., Pino, F., & Merkoçi, A. (2012). Nanomaterials for Sensing and Destroying Pesticides. *Chemical Review*, 112(10), 5317-5338.
- Arcibar-Orozco, J. A., Josue, D.-B., Rios-Hurtado, J. C., & Rangel-Mendez, J. R. (2014). Influence of iron content, surface area and charge distribution in the arsenic removal by activated carbons. *Chemical Engineering Journal*, 249, 201-209.

- Asghar, H. M. A., Hussain, S. N., Roberts, E. P. L., Campen, A. K., & Brown, N. W. (2013). Pre-treatment of adsorbents for waste water treatment using adsorption coupled-with electrochemical regeneration. *Journal of Industrial and Engineering Chemistry*, 19(5), 1689-1696.
- Ashraf, M. A., Ullah, S., Ahmad, I., Qureshi, A. K., Balkhair, K. S., & Abdur Rehman, M. (2014). Green biocides, a promising technology: current and future applications to industry and industrial processes. *Journal of the Science of Food and Agriculture*, 94(3), 388-403.
- Azarang, M., Shuhaimi, A., Yousefi, R., & Jahromi, S. P. (2015). One-pot sol-gel synthesis of reduced graphene oxide uniformly decorated zinc oxide nanoparticles in starch environment for highly efficient photodegradation of Methylene Blue. *RSC Adv.*, 5(28), 21888-21896.
- Azizullah, A., Khattak, M. N. K., Richter, P., & Häder, D.-P. (2011). Water pollution in Pakistan and its impact on public health — A review. *Environ Int.*, 37(2), 479-497.
- Bacsa, R. R., Cameán, I., Ramos, A., Garcia, A. B., Tishkova, V., Bacsa, W. S., Jourdain, V. (2015). Few layer graphene synthesis on transition metal ferrite catalysts. *Carbon*, 89, 350-360.
- Badkar, D., Pandey, K., & Buvanashakaran, G. (2013). Development of RSM- and ANN-based models to predict and analyze the effects of process parameters of laser-hardened commercially pure titanium on heat input and tensile strength. *Int. J. Adv. Manuf. Technol.*, 65(9-12), 1319-1338.
- Baig, S. A., Mahmood, Q., Nawab, B., Shafqat, M. N., & Pervez, A. (2011). Improvement of drinking water quality by using plant biomass through household biosand filter – A decentralized approach. *Ecological Engineering*, 37(11), 1842-1848.
- Bain, R. E., Gundry, S. W., Wright, J. A., Yang, H., Pedley, S., & Bartram, J. K. (2012). Accounting for water quality in monitoring access to safe drinking-water as part of the Millennium Development Goals: lessons from five countries. *Bull World Health Organ*, 90(3), 228-235A.
- Balandin, A. A., Ghosh, S., Bao, W., Calizo, I., Teweldebrhan, D., Miao, F., & Lau, C. N. (2008). Superior Thermal Conductivity of Single-Layer Graphene. *Nano Letters*, 8(3), 902-907.
- Balaz, P. (2008). *Mechanochemistry in nanoscience and minerals engineering*. Berlin, Heidelberg: Springer.
- Banerjee, S. S., & Chen, D. H. (2007). Fast removal of copper ions by gum arabic modified magnetic nano-adsorbent. *Journal of Hazardous Materials*, 147(3), 792-799.
- Barua, A., Kriebel, C. H., & Mukhopadhyay, T. (1995). Information technologies and business value: An analytic and empirical investigation. *Information systems research*, 6(1), 3-23.

- Bekçi, Z., Özveri, C., Seki, Y., & Yurdakoç, K. (2008). Sorption of malachite green on chitosan bead. *Journal of Hazardous Materials*, 154(1–3), 254-261.
- Benedetti, R., Piersimoni, F., & Postiglione, P. (2015). Survey Data Collection and Processing *Sampling Spatial Units for Agricultural Surveys* (pp. 219-237): Springer.
- Bilici Baskan, M., & Pala, A. (2010). A statistical experiment design approach for arsenic removal by coagulation process using aluminum sulfate. *Desalination*, 254(1-3), 42-48.
- Bohlke, J. K., & Denver, J. M. (1995). Combined use of groundwater dating, chemical, and isotopic analysis to resolve the history and fate of nitrate contamination in 2 agricultural watersheds, Atlantic coastal-plan, Maryland. *Water Resources Research*, 31(9), 2319-2339.
- Borhan, A. I., Iordan, A. R., & Palamaru, M. N. (2013). Correlation between structural, magnetic and electrical properties of nanocrystalline Al<sup>3+</sup> substituted zinc ferrite. *Materials Research Bulletin*, 48(7), 2549-2556.
- Brown, J., & Clasen, T. (2012). High Adherence Is Necessary to Realize Health Gains from Water Quality Interventions. *PLoS ONE*, 7(5), e36735.
- Burby, R. J., Deyle, R. E., Godschalk, D. R., & Olshansky, R. B. (2000). Creating hazard resilient communities through land-use planning. *Natural hazards review*, 1(2), 99-106.
- Buschow, K. J. (2005). *Concise encyclopedia of magnetic and superconducting materials*. Netherlands: Elsevier.
- Byrappa, K., & Adschiri, T. (2007). Hydrothermal technology for nanotechnology. *Progress in Crystal Growth and Characterization of Materials*, 53(2), 117-166.
- Byun, Y., & Coskun, A. (2015). Bottom-up Approach for the Synthesis of a Three-Dimensional Nanoporous Graphene Nanoribbon Framework and Its Gas Sorption Properties. *Chemistry of Materials*, 27(7), 2576-2583.
- Cahn, R. W., & Lifshitz, E. (2013). *Concise encyclopedia of materials characterization*. USA, Elsevier.
- Calizo, I., Balandin, A. A., Bao, W., Miao, F., & Lau, C. N. (2007). Temperature Dependence of the Raman Spectra of Graphene and Graphene Multilayers. *Nano Letters*, 7(9), 2645-2649.
- Camel, V., & Bermond, A. (1998). The use of ozone and associated oxidation processes in drinking water treatment. *Water Research*, 32(11), 3208-3222.
- Campos, A. F. C., Aquino, R., Cotta, T. A. P. G., Tourinho, F. A., & Depeyrot, J. (2011). Using speciation diagrams to improve synthesis of magnetic nanosorbents for environmental applications. *Bulletin of Materials Science*, 34(7), 1357-1361.
- Castro Neto, A. H., Peres, N. M. R., Novoselov, K. S., & Geim, A. K. (2009). The electronic properties of graphene. *Reviews of Modern Physics*, 81(1), 109-162.

- Cevasco, G., & Chiappe, C. (2014). Are ionic liquids a proper solution to current environmental challenges? *Green Chemistry*, 16(5), 2375-2385.
- Chang, Y. C., & Chen, D. H. (2005). Preparation and adsorption properties of monodisperse chitosan-bound Fe<sub>3</sub>O<sub>4</sub> magnetic nanoparticles for removal of Cu(II) ions. *Journal of Colloid and Interface Science*, 283(2), 446-451.
- Chaparro, G., Fontanarrosa, M. S., Cataldo, D., & O'Farrell, I. (2015). Hydrology driven factors might weaken fish predation effects on zooplankton structure in a vegetated warm temperate floodplain lake. *Hydrobiologia*, 752(1), 187-202.
- Charerntanyarak, L. (1999). Heavy metals removal by chemical coagulation and precipitation. *Water Science and Technology*, 39(10-11), 135-138.
- Chaturvedi, S., & Dave, P. N. (2012). Removal of iron for safe drinking water. *Desalination*, 303, 1-11.
- Chen, S. B., & Wang, M. (2012). Removal of Cd, Pb and Cu from Water Using Thiol and Humic Acid Functionalized Fe<sub>2</sub>O<sub>3</sub> Nanoparticles. *Advanced Materials Research*, 518, 1956-1963.
- Chen, Z., Yan, Q., Zhang, L., Peng, L., & Han, H. (2015). Using Map-Based Interactive Interface for Understanding and Characterizing Crime Data in Cities *Advances in Swarm and Computational Intelligence* (pp. 479-490): Springer.
- Chia, J. S. Y., Tan, M. T. T., Khiew, P. S., Chin, J. K., & Siong, C. W. (2015). A bio-electrochemical sensing platform for glucose based on irreversible, non-covalent pi-pi functionalization of graphene produced via a novel, green synthesis method. *Sensors and Actuators B: Chemical*, 210, 558-565.
- Chinnasamy, C. N., Senoue, M., Jeyadevan, B., Perales-Perez, O., Shinoda, K., & Tohji, K. (2003). Synthesis of size-controlled cobalt ferrite particles with high coercivity and squareness ratio. *Journal of Colloid and Interface Science*, 263(1), 80-83.
- Chung, F. H. (1974). Quantitative interpretation of X-ray diffraction patterns of mixtures. I. Matrix-flushing method for quantitative multicomponent analysis. *Journal of Applied Crystallography*, 7(6), 519-525.
- Clegg, P., Bruciatelli, L., Domingos, F., Jones, R., De Donatis, M., & Wilson, R. (2006). Digital geological mapping with tablet PC and PDA: A comparison. *Computers & Geosciences*, 32(10), 1682-1698.
- Crini, G. (2006). Non-conventional low-cost adsorbents for dye removal: A review. *Bioresource Technology*, 97(9), 1061-1085.
- Crini, G., Peindy, H. N., Gimbert, F., & Robert, C. (2007). Removal of C.I. Basic Green 4 (Malachite Green) from aqueous solutions by adsorption using cyclodextrin-based adsorbent: Kinetic and equilibrium studies. *Separation and Purification Technology*, 53(1), 97-110.
- Cui, W., Ji, J., Cai, Y.-F., Li, H., & Ran, R. (2015). Robust, anti-fatigue, and self-healing graphene oxide/hydrophobically associated composite hydrogels and

- their use as recyclable adsorbents for dye wastewater treatment. *J. Mater. Chem. A*, 3(33), 17445-17458.
- Da'na, E., & Sayari, A. (2011). Adsorption of copper on amine-functionalized SBA-15 prepared by co-condensation: Equilibrium properties. *Chemical Engineering Journal*, 166(1), 445-453.
- Das, B. M. (2010). *Principles of geotechnical engineering* (5th ed.). Cengage Learning India Private Limited., New Delhi, India.
- Deliyanni, E. A., Bakoyannakis, D. N., Zouboulis, A. I., & Matis, K. A. (2003). Sorption of As(V) ions by akaganeite-type nanocrystals. *Chemosphere*, 50(1), 155-163.
- Deliyanni, E. A., & Matis, K. A. (2005). Sorption of Cd ions onto akaganeite-type nanocrystals. *Separation and Purification Technology*, 45(2), 96-102.
- Deliyanni, E. A., Nalbandian, L., & Matis, K. A. (2006). Adsorptive removal of arsenites by a nanocrystalline hybrid surfactant-akaganeite sorbent. *Journal of Colloid and Interface Science*, 302(2), 458-466.
- Deliyanni, E. A., Peleka, E. N., & Lazaridis, N. K. (2007). Comparative study of phosphates removal from aqueous solutions by nanocrystalline akaganeite and hybrid surfactant-akaganeite. *Separation and Purification Technology*, 52(3), 478-486.
- Deliyanni, E. A., Peleka, E. N., & Matis, K. A. (2007). Removal of zinc ion from water by sorption onto iron-based nanoadsorbent. *Journal of Hazardous Materials*, 141(1), 176-184.
- Dhodapkar, R., Rao, N. N., Pande, S. P., Nandy, T., & Devotta, S. (2007). Adsorption of cationic dyes on Jalshakti®, super absorbent polymer and photocatalytic regeneration of the adsorbent. *Reactive and Functional Polymers*, 67(6), 540-548.
- Diallo, M. S., Christie, S., Swaminathan, P., Johnson, J. H., & Goddard, W. A. (2005). Dendrimer enhanced ultrafiltration. 1. Recovery of Cu(II) from aqueous solutions using PAMAM dendrimers with ethylene diamine core and terminal NH<sub>2</sub> groups. *Environmental Science & Technology*, 39(5), 1366-1377.
- Dias, J. M., Alvim-Ferraz, M. C. M., Almeida, M. F., Rivera-Utrilla, J., & Sanchez-Polo, M. (2007). Waste materials for activated carbon preparation and its use in aqueous-phase treatment: A review. *Journal of Environmental Management*, 85(4), 833-846.
- Ding, Y., Zhu, L., Wang, N., & Tang, H. (2013). Sulfate radicals induced degradation of tetrabromobisphenol A with nanoscaled magnetic CuFe<sub>2</sub>O<sub>4</sub> as a heterogeneous catalyst of peroxymonosulfate. *Applied Catalysis B: Environmental*, 129, 153-162.
- Dingman, S. L. (2015). *Physical hydrology*., Waveland press, USA.

- Dixit, G., Pal Singh, J., Srivastava, R. C., & Agrawal, H. M. (2012). Magnetic resonance study of Ce and Gd doped NiFe<sub>2</sub>O<sub>4</sub> nanoparticles. *Journal of Magnetism and Magnetic Materials*, 324(4), 479-483.
- Dixit, S., & Hering, J. G. (2003). Comparison of Arsenic(V) and Arsenic(III) Sorption onto Iron Oxide Minerals: Implications for Arsenic Mobility. *Environmental Science & Technology*, 37(18), 4182-4189.
- Domingo, N., Bellido, E., & Ruiz-Molina, D. (2012). Advances on structuring, integration and magnetic characterization of molecular nanomagnets on surfaces and devices. *Chem Soc Rev*, 41(1), 258-302.
- Dora, T. K., Mohanty, Y. K., Roy, G. K., & Sarangi, B. (2013). Adsorption studies of As(III) from wastewater with a novel adsorbent in a three-phase fluidized bed by using response surface method. *J. Environ. Chem. Eng.*, 1(3), 150-158.
- Dousova, B., Grygar, T., Martaus, A., Fuitova, L., Kolousek, D., & Machovic, V. (2006). Sorption of As-V on alumino silicates treated with Fe-II nanoparticles. *Journal of Colloid and Interface Science*, 302(2), 424-431.
- Dreyer, D. R., Park, S., Bielawski, C. W., & Ruoff, R. S. (2010). The chemistry of graphene oxide. *Chem Soc Rev*, 39(1), 228-240.
- Du, Z., Deng, S., Chen, Y., Wang, B., Huang, J., Wang, Y., & Yu, G. (2015). Removal of perfluorinated carboxylates from washing wastewater of perfluorooctanesulfonyl fluoride using activated carbons and resins. *Journal of Hazardous Materials*, 286, 136-143.
- Dubinin, M., & Radushkevich, L. (1947). Equation of the characteristic curve of activated charcoal. *Chem. Zentr*, 1(1), 875.
- Dutta, P., Pal, S., Seehra, M. S., Shi, Y., Eyring, E. M., & Ernst, R. D. (2006). Concentration of Ce<sup>3+</sup> and Oxygen Vacancies in Cerium Oxide Nanoparticles. *Chemistry of Materials*, 18(21), 5144-5146.
- Ebrahimi-Kahrizsangi, R., Nasiri-Tabrizi, B., & Chami, A. (2010). Synthesis and characterization of fluorapatite-titania (FAP-TiO<sub>2</sub>) nanocomposite via mechanochemical process. *Solid State Sciences*, 12(9), 1645-1651.
- Edwards, M., & Benjamin, M. M. (1989). Regeneration and Reuse of Iron Hydroxide Adsorbents in Treatment of Metal-Bearing Wastes. *Journal (Water Pollution Control Federation)*, 61(4), 481-490.
- Eith, C., Kolb, M., Seubert, A., & Viehweger, K. H. (2001). Practical Ion Chromatography. *Metrohm Ltd., Herisau, Switzerland*.
- Eldrandaly, K. A. (2006). A COM-based expert system for selecting the suitable map projection in ArcGIS. *Expert Systems with Applications*, 31(1), 94-100.
- Entezari, M. H., Heshmati, A., & Sarafraz-yazdi, A. (2005). A combination of ultrasound and inorganic catalyst: removal of 2-chlorophenol from aqueous solution. *Ultrasonics Sonochemistry*, 12(1-2), 137-141.

- Esbensen, K. H., & Ramsey, C. A. (2015). QC of Sampling Processes—A First Overview: From Field to Test Portion. *Journal of AOAC International*, 98(2), 282-287.
- Fakhru'l-Razi, A., Pendashteh, A., Abdullah, L. C., Biak, D. R. A., Madaeni, S. S., & Abidin, Z. Z. (2009). Review of technologies for oil and gas produced water treatment. *Journal of Hazardous Materials*, 170(2–3), 530-551.
- Farré, M., Kantiani, L., Petrovic, M., Pérez, S., & Barceló, D. (2012). Achievements and future trends in the analysis of emerging organic contaminants in environmental samples by mass spectrometry and bioanalytical techniques. *Journal of Chromatography A*, 1259(0), 86-99.
- Feng, D., van Deventer, J. S. J., & Aldrich, C. (2004). Removal of pollutants from acid mine wastewater using metallurgical by-product slags. *Separation and Purification Technology*, 40(1), 61-67.
- Ferrari, A. C., Meyer, J. C., Scardaci, V., Casiraghi, C., Lazzeri, M., Mauri, F., Geim, A. K. (2006). Raman Spectrum of Graphene and Graphene Layers. *Physical Review Letters*, 97(18), 187401.
- Fikáček, J., Prokleška, J., Prchal, J., Custers, J., & Sechovský, V. (2013). Nature of the magnetic ground state in the mixed valence compound CeRuSn: a single-crystal study. *Journal of Physics: Condensed Matter*, 25(41), 416.
- Fowkes, F. M. (1964). Attractive forces at interfaces. *Industrial & Engineering Chemistry*, 56(12), 40-52.
- Fu, M., Jiao, Q., Zhao, Y., & Li, H. (2014). Vapor diffusion synthesis of CoFe<sub>2</sub>O<sub>4</sub> hollow sphere/graphene composites as absorbing materials. *Journal of Materials Chemistry A*, 2(3), 735.
- Fu, Y., Chen, Q., He, M., Wan, Y., Sun, X., Xia, H., & Wang, X. (2012). Copper Ferrite-Graphene Hybrid: A Multifunctional Heteroarchitecture for Photocatalysis and Energy Storage. *Industrial & Engineering Chemistry Research*, 51(36), 11700-11709.
- Gadkari, A. B., Shinde, T. J., & Vasambekar, P. N. (2009). Structural analysis of Y<sup>3+</sup>-doped Mg–Cd ferrites prepared by oxalate co-precipitation method. *Materials Chemistry and Physics*, 114(2-3), 505-510.
- Gao, H., Sun, Y., Zhou, J., Xu, R., & Duan, H. (2013). Mussel-Inspired Synthesis of Polydopamine-Functionalized Graphene Hydrogel as Reusable Adsorbents for Water Purification. *ACS Applied Materials & Interfaces*, 5(2), 425-432.
- Gao, Y., Luo, Z., He, N., & Wang, M. (2013). Metallic nanoparticle production and consumption in China between 2000 and 2010 and associative aquatic environmental risk assessment. *Journal of Nanoparticle Research*, 15(6), 1-9.
- Gattuso, J. P., Frankignoulle, M., Bourge, I., Romaine, S., & Buddemeier, R. W. (1998). Effect of calcium carbonate saturation of seawater on coral calcification. *Global and Planetary Change*, 18(1–2), 37-46.
- Geim, A. K. (2009). Graphene: Status and Prospects. *Science*, 324(5934), 1530-1534.

- Geim, A. K., & Novoselov, K. S. (2007). The rise of graphene. *Nature Material*, 6(3), 183-191.
- Geng, Z., Lin, Y., Yu, X., Shen, Q., Ma, L., Li, Z., Wang, X. (2012). Highly efficient dye adsorption and removal: a functional hybrid of reduced graphene oxide-Fe<sub>3</sub>O<sub>4</sub> nanoparticles as an easily regenerative adsorbent. *Journal of Materials Chemistry*, 22(8), 3527-3535.
- Ghadim, E. E., Rashidi, N., Kimiagar, S., Akhavan, O., Manouchehri, F., & Ghaderi, E. (2014). Pulsed laser irradiation for environment friendly reduction of graphene oxide suspensions. *Applied Surface Science*, 301(0), 183-188.
- Gimbert, F., Morin-Crini, N., Renault, F., Badot, P.-M., & Crini, G. (2008). Adsorption isotherm models for dye removal by cationized starch-based material in a single component system: Error analysis. *Journal of Hazardous Materials*, 157(1), 34-46.
- Gleick, P. H. (2000). A look at twenty-first century water resources development. *Water International*, 25(1), 127-138.
- Gonzalo, C., & Camargo, J. A. (2012). Fluoride bioaccumulation in the signal crayfish *Pacifastacus leniusculus* (Dana) as suitable bioindicator of fluoride pollution in freshwater ecosystems. *Ecological Indicators*, 20(0), 244-251.
- Gornostaeva, O. V., Lamonova, K. V., Orel, S. M., & Pashkevich, Y. G. (2013). Magnetic properties of Ce<sup>3+</sup> ion in iron-containing oxypnictide CeFeAsO. *Low Temperature Physics*, 39(4), 343.
- Groshong, R., Jr. (2006). Location and Attitude *3-D Structural Geology* (pp. 33-61): Springer Berlin Heidelberg.
- Gu, B., Schmitt, J., Chen, Z., Liang, L., & McCarthy, J. F. (1994). Adsorption and desorption of natural organic matter on iron oxide: mechanisms and models. *Environmental Science & Technology*, 28(1), 38-46.
- Gupta, V. K. (1998). Equilibrium uptake, sorption dynamics, process development, and column operations for the removal of copper and nickel from aqueous solution and wastewater using activated slag, a low-cost adsorbent. *Industrial & Engineering Chemistry Research*, 37(1), 192-202.
- Hameed, B. H., Tan, I. A., & Ahmad, A. L. (2009). Preparation of oil palm empty fruit bunch-based activated carbon for removal of 2,4,6-trichlorophenol: optimization using response surface methodology. *J. Hazard. Mater.*, 164(2-3), 1316-1324.
- Han, C., Pu, H., Li, H., Deng, L., Huang, S., He, S., & Luo, Y. (2013). The optimization of As(V) removal over mesoporous alumina by using response surface methodology and adsorption mechanism. *J. Hazard. Mater.*, 254-255, 301-309.
- Han, R., Wang, Y., Sun, Q., Wang, L., Song, J., He, X., & Dou, C. (2010). Malachite green adsorption onto natural zeolite and reuse by microwave irradiation. *Journal of Hazardous Materials*, 175(1-3), 1056-1061.
- Han, R., Zou, L., Zhao, X., Xu, Y., Xu, F., Li, Y., & Wang, Y. (2009). Characterization and properties of iron oxide-coated zeolite as adsorbent for removal of

- copper(II) from solution in fixed bed column. *Chemical Engineering Journal*, 149(1-3), 123-131.
- Hicks, J. C., Drese, J. H., Fauth, D. J., Gray, M. L., Qi, G., & Jones, C. W. (2008). Designing Adsorbents for CO<sub>2</sub> Capture from Flue Gas-Hyperbranched Aminosilicas Capable of Capturing CO<sub>2</sub> Reversibly. *Journal of the American Chemical Society*, 130(10), 2902-2903.
- Hristovski, K., Baumgardner, A., & Westerhoff, P. (2007). Selecting metal oxide nanomaterials for arsenic removal in fixed bed columns: From nanopowders to aggregated nanoparticle media. *Journal of Hazardous Materials*, 147(1-2), 265-274.
- Hsu, L., Martin, R. L., McElroy, B., Litwin-Miller, K., & Kim, W. (2015). Data management, sharing, and reuse in experimental geomorphology: Challenges, strategies, and scientific opportunities. *Geomorphology*.
- Hu, J., Chen, G., & Lo, I. M. C. (2005). Removal and recovery of Cr(VI) from wastewater by maghemite nanoparticles. *Water Research*, 39(18), 4528-4536.
- Hu, J., Lo, I. M. C., & Chen, G. H. (2007). Comparative study of various magnetic nanoparticles for Cr(VI) removal. *Separation and Purification Technology*, 56(3), 249-256.
- Hu, J., Lo, I. M. C., & Chen, G. H. (2007). Performance and mechanism of chromate (VI) adsorption by delta-FeOOH-coated maghemite (gamma-Fe<sub>2</sub>O<sub>3</sub>) nanoparticles. *Separation and Purification Technology*, 58(1), 76-82.
- Hua, M., Zhang, S., Pan, B., Zhang, W., Lv, L., & Zhang, Q. (2012). Heavy metal removal from water/wastewater by nanosized metal oxides: A review. *Journal of Hazardous Materials*, 211-212(0), 317-331.
- Huang, X., Jiao, L., Liao, X., & Shi, B. (2008). Adsorptive Removal of As(III) from Aqueous Solution by Zr(IV)-Loaded Collagen Fiber. *Industrial & Engineering Chemistry Research*, 47(15), 5623-5628.
- Huang, Y., Wu, J., & Hwang, K. C. (2006). Thickness of graphene and single-wall carbon nanotubes. *Physical Review B*, 74(24), 245413.
- Hurt, R. H., Monthieux, M., & Kane, A. (2006). Toxicology of carbon nanomaterials: Status, trends, and perspectives on the special issue. *Carbon*, 44(6), 1028-1033.
- Husain, T., & Ahmad, M. (2015). *Low cost adsorbent to reduce disinfection by-products from drinking water in small communities*. Paper presented at the Environmental Engineering and Computer Application: Proceedings of the 2014 International Conference on Environmental Engineering and Computer Application (ICEECA 2014), Hong Kong, 25-26 December 2014.
- Ilisz, I., Dombi, A., Mogyorosi, K., & Dekany, I. (2003). Photocatalytic water treatment with different TiO<sub>2</sub> nanoparticles and hydrophilic/hydrophobic layer silicate adsorbents. *Colloids and Surfaces a-Physicochemical and Engineering Aspects*, 230(1-3), 89-97.

- Ingebritsen, S. E., & Sanford, W. E. (1999). *Groundwater in geologic processes.*, Cambridge University Press, UK.
- Inglis, R. S., & Thomas, O. (1989). Microwave regeneration of adsorbent materials for reuse as drying agents: Google Patents.
- Ishaque, M., Khan, M. A., Ali, I., Khan, H. M., Iqbal, M. A., Islam, M. U., & Warsi, M. F. (2015). Impacts of yttrium substitution on FMR line-width and magnetic properties of nickel spinel ferrites. *Journal of Magnetism and Magnetic Materials*, 382, 98-103.
- Jeremias, F., Khutia, A., Henninger, S. K., & Janiak, C. (2012). MIL-100(Al, Fe) as water adsorbents for heat transformation purposes-a promising application. *Journal of Materials Chemistry*, 22(20), 10148-10151.
- Ji, W.-F., Chang, K.-C., Lai, M.-C., Li, C.-W., Hsu, S.-C., Chuang, T.-L., Liu, W.-R. (2014). Preparation and comparison of the physical properties of PMMA/thermally reduced graphene oxides composites with different carboxylic group content of thermally reduced graphene oxides. *Composites Part A: Applied Science and Manufacturing*, 65(0), 108-114.
- Jiang, Y. (2009). China's water scarcity. *Journal of Environmental Management*, 90(11), 3185-3196.
- Juang, R. S., & Shiau, R. C. (2000). Metal removal from aqueous solutions using chitosan-enhanced membrane filtration. *Journal of Membrane Science*, 165(2), 159-167.
- Kadirvelu, K., Thamaraiselvi, K., & Namasivayam, C. (2001). Adsorption of nickel(II) from aqueous solution onto activated carbon prepared from coirpith. *Separation and Purification Technology*, 24(3), 497-505.
- Kadirvelu, K., Thamaraiselvi, K., & Namasivayam, C. (2001). Removal of heavy metals from industrial wastewaters by adsorption onto activated carbon prepared from an agricultural solid waste. *Bioresource Technology*, 76(1), 63-65.
- Kamble, S. P., Jagtap, S., Labhsetwar, N. K., Thakare, D., Godfrey, S., Devotta, S., & Rayalu, S. S. (2007). Defluoridation of drinking water using chitin, chitosan and lanthanum-modified chitosan. *Chemical Engineering Journal*, 129(1-3), 173-180.
- Kang, J., Li, B., Song, J., Li, D., Yang, J., Zhan, W., & Liu, D. (2011). Defluoridation of water using calcined magnesia/pullulan composite. *Chemical Engineering Journal*, 166(2), 765-771.
- Karthe, D., Chalov, S., & Borchardt, D. (2015). Water resources and their management in central Asia in the early twenty first century: status, challenges and future prospects. *Environmental Earth Sciences*, 73(2), 487-499.
- Khandekar, M. S., Tarwal, N. L., Patil, J. Y., Shaikh, F. I., Mulla, I. S., & Suryavanshi, S. S. (2013). Liquefied petroleum gas sensing performance of cerium doped copper ferrite. *Ceramics International*, 39(5), 5901-5907.

- Kim, C. S., Chi, C., Miller, S. R., Rosales, R. A., Sugihara, E. S., Akau, J., Webb, S. M. (2013). (Micro)spectroscopic Analyses of Particle Size Dependence on Arsenic Distribution and Speciation in Mine Wastes. *Environmental Science & Technology*, 47, 8164-8171.
- Kim, K.-R., Lee, B.-T., & Kim, K.-W. (2012). Arsenic stabilization in mine tailings using nano-sized magnetite and zero valent iron with the enhancement of mobility by surface coating. *Journal of Geochemical Exploration*, 113(0), 124-129.
- Kobayashi, M., & Flytzani-Stephanopoulos, M. (2002). Reduction and Sulfidation Kinetics of Cerium Oxide and Cu-Modified Cerium Oxide. *Industrial & Engineering Chemistry Research*, 41(13), 3115-3123.
- Kondalkar, V., Mane, R., Sipra, C., & Khot, K. (2015). Hydrothermal Assisted Synthesis of Hierarchical Nanostructured Metal Oxide Thin Film. *Journal of Nanomedicine & Nanotechnology*, 2015.
- Konieczny, K., Bodzek, M., & Panek, D. (2008). Removal of volatile compounds from the wastewaters by use of pervaporation. *Desalination*, 223(1-3), 344-348.
- Kostopoulou, A., Brintakis, K., Vasilakaki, M., Trohidou, K. N., Douvalis, A. P., Lascialfari, A., . . . Lappas, A. (2014). Assembly-mediated interplay of dipolar interactions and surface spin disorder in colloidal maghemite nanoclusters. *Nanoscale*, 6(7), 3764-3776.
- Kröger, R., Moore, M. T., Locke, M. A., Cullum, R. F., Steinriede Jr, R. W., Testa Iii, S., . . . Cooper, C. M. (2009). Evaluating the influence of wetland vegetation on chemical residence time in Mississippi Delta drainage ditches. *Agricultural Water Management*, 96(7), 1175-1179.
- Kudin, K. N., Ozbas, B., Schniepp, H. C., Prud'Homme, R. K., Aksay, I. A., & Car, R. (2008). Raman spectra of graphite oxide and functionalized graphene sheets. *Nano Letters*, 8(1), 36-41.
- Kugler, T. A., Van Riper, D. C., Manson, S. M., Haynes II, D. A., Donato, J., & Stinebaugh, K. (2015). Terra Populus: Workflows for integrating and harmonizing geospatial population and environmental data. *Journal of Map & Geography Libraries*, 11(2), 180-206.
- Kundu, S., & Gupta, A. K. (2005). Analysis and modeling of fixed bed column operations on As(V) removal by adsorption onto iron oxide-coated cement (IOCC). *Journal of Colloid and Interface Science*, 290(1), 52-60.
- Kurniawan, T. A., Sillanpää, M. E. T., & Sillanpää, M. (2012). Nanoadsorbents for Remediation of Aquatic Environment: Local and Practical Solutions for Global Water Pollution Problems. *Critical Reviews in Environmental Science and Technology*, 42(12), 1233-1295.
- Kuzawa, K., Jung, Y.-J., Kiso, Y., Yamada, T., Nagai, M., & Lee, T.-G. (2006). Phosphate removal and recovery with a synthetic hydrotalcite as an adsorbent. *Chemosphere*, 62(1), 45-52.

- Kyle Onda, LoBuglio, J., & Jamie, B. (2013). Global Access to Safe Water: Accounting for Water Quality and the Resulting Impact on MDG Progress. *World Health & Population*, 14(3), 32-44.
- Kyzas, G. Z., & Matis, K. A. (2015). Nanoadsorbents for pollutants removal: A review. *Journal of Molecular Liquids*, 203, 159-168.
- Kyzas, G. Z., Siafaka, P. I., Pavlidou, E. G., Chrissafis, K. J., & Bikiaris, D. N. (2015). Synthesis and adsorption application of succinyl-grafted chitosan for the simultaneous removal of zinc and cationic dye from binary hazardous mixtures. *Chemical Engineering Journal*, 259, 438-448.
- Larbi, T., Haj Lakhdar, M., Amara, A., Ouni, B., Boukhachem, A., Mater, A., & Amlouk, M. (2015). Nickel content effect on the microstructural, optical and electrical properties of p-type Mn<sub>3</sub>O<sub>4</sub> sprayed thin films. *Journal of Alloys and Compounds*, 626(0), 93-101.
- Larbi, T., Ouni, B., Boukhachem, A., Boubaker, K., & Amlouk, M. (2014). Investigation of structural, optical, electrical and dielectric properties of catalytic sprayed hausmannite thin film. *Materials Research Bulletin*, 60(0), 457-466.
- Lazaridis, N. K., Bakoyannakis, D. N., & Deliyanni, E. A. (2005). Chromium(VI) sorptive removal from aqueous solutions by nanocrystalline akaganeite. *Chemosphere*, 58(1), 65-73.
- Leyva Ramos, R., Bernal Jacome, L. A., Mendoza Barron, J., Fuentes Rubio, L., & Guerrero Coronado, R. M. (2002). Adsorption of zinc(II) from an aqueous solution onto activated carbon. *Journal of Hazardous Materials*, 90(1), 27-38.
- Li, J., Lu, H., Guo, J., Xu, Z. M., & Zhou, Y. H. (2007). Recycle technology for recovering resources and products from waste printed circuit boards. *Environmental Science & Technology*, 41(6), 1995-2000.
- Li, Y. H., Ding, J., Luan, Z. K., Di, Z. C., Zhu, Y. F., Xu, C. L., Wei, B. Q. (2003). Competitive adsorption of Pb<sup>2+</sup>, Cu<sup>2+</sup> and Cd<sup>2+</sup> ions from aqueous solutions by multiwalled carbon nanotubes. *Carbon*, 41(14), 2787-2792.
- Li, Y. J., Zeng, X. P., Liu, Y. F., Yan, S. S., Hu, Z. H., & Ni, Y. M. (2003). Study on the treatment of copper-electroplating wastewater by chemical trapping and flocculation. *Separation and Purification Technology*, 31(1), 91-95.
- Lin, Y. H., Fiskum, S. K., Yantasee, W., Wu, H., Mattigod, S. V., Vorpagel, E., Xu, J. D. (2005). Incorporation of hydroxypyridinone ligands into self-assembled monolayers on mesoporous supports for selective actinide sequestration. *Environmental Science & Technology*, 39(5), 1332-1337.
- Liu, A. M., Hidajat, K., Kawi, S., & Zhao, D. Y. (2000). A new class of hybrid mesoporous materials with functionalized organic monolayers for selective adsorption of heavy metal ions. *Chemical Communications*(13), 1145-1146.
- Loganathan, P., Vigneswaran, S., Kandasamy, J., & Naidu, R. (2013). Defluoridation of drinking water using adsorption processes. *Journal of Hazardous Materials*, 248-249, 1-19.

- Longley, P. A., Goodchild, M. F., Maguire, D. J., & Rhind, D. W. (2015). *Geographic information science and systems*. USA: John Wiley & Sons.
- Lu, C., & Liu, C. (2006). Removal of nickel(II) from aqueous solution by carbon nanotubes. *Journal of Chemical Technology & Biotechnology*, 81(12), 1932-1940.
- Lu, C. Y., & Liu, C. T. (2006). Removal of nickel(II) from aqueous solution by carbon nanotubes. *Journal of Chemical Technology and Biotechnology*, 81(12), 1932-1940.
- Ma, W., Lv, T., Song, X., Cheng, Z., Duan, S., Xin, G., Pan, D. (2014). Characteristics of selective fluoride adsorption by biocarbon-Mg/Al layered double hydroxides composites from protein solutions: kinetics and equilibrium isotherms study. *J. Hazard. Mater.*, 268, 166-176.
- Ma, X., & Ouyang, F. (2013). VOCs adsorption by modified MCM-41 and a new way to recycle adsorbents. *Adsorption*, 19(5), 889-895.
- Mahmood, Q., Baig, S. A., Nawab, B., Shafqat, M. N., Pervez, A., & Zeb, B. S. (2011). Development of low cost household drinking water treatment system for the earthquake affected communities in Northern Pakistan. *Desalination*, 273(2-3), 316-320.
- Mandal, S., & Mayadevi, S. (2009). Defluoridation of water using as-synthesized Zn/Al/Cl anionic clay adsorbent: Equilibrium and regeneration studies. *Journal of Hazardous Materials*, 167(1-3), 873-878.
- Martinez, S. A., Rodriguez, M. G., Aguilar, R., & Soto, G. (2004). Removal of chromium hexavalent from rinsing chromating waters electrochemical reduction in a laboratory pilot plant. *Water Science and Technology*, 49(1), 115-122.
- Masters, A. F., & Maschmeyer, T. (2011). Zeolites – From curiosity to cornerstone. *Microporous and Mesoporous Materials*, 142(2-3), 423-438.
- Matis, K. A., Zouboulis, A. I., Gallios, G. P., Erwe, T., & Blocher, C. (2004). Application of flotation for the separation of metal-loaded zeolites. *Chemosphere*, 55(1), 65-72.
- McAllister, M. J., Li, J.-L., Adamson, D. H., Schniepp, H. C., Abdala, A. A., Liu, J., Aksay, I. A. (2007). Single Sheet Functionalized Graphene by Oxidation and Thermal Expansion of Graphite. *Chemistry of Materials*, 19(18), 4396-4404.
- McClements, D. J. (2012). Nanoemulsions versus microemulsions: terminology, differences, and similarities. *Soft matter*, 8(6), 1719-1729.
- Meidanchi, A., & Akhavan, O. (2014). Superparamagnetic zinc ferrite spinel-graphene nanostructures for fast wastewater purification. *Carbon*, 69, 230-238.
- Melero, J. A., Calleja, G., Martinez, F., Molina, R., & Pariente, M. I. (2007). Nanocomposite Fe<sub>2</sub>O<sub>3</sub>/SBA-15: An efficient and stable catalyst for the catalytic wet peroxidation of phenolic aqueous solutions. *Chemical Engineering Journal*, 131(1-3), 245-256.

- Mexmain. (1971). Contribution a l'etude du ferrite cuivreux et de ses solutions solides avec le ferrite cuivrique. *J., Annales de Chimie*, 297-308.
- Mirzaee, O., Mohamady, R., Ghasemi, A., & Farzin, Y. A. (2015). Study of the magnetic and structural properties of Al–Cr codoped Y-type hexaferrite prepared via sol–gel auto-combustion method. *International Journal of Modern Physics B*, 29(14), 1550090.
- Mondal, O., Mitra, S., Pal, M., Datta, A., Dhara, S., & Chakravorty, D. (2015). Reduced graphene oxide synthesis by high energy ball milling. *Materials Chemistry and Physics*, 161, 123-129.
- Mwabi, J. K., Adeyemo, F. E., Mahlangu, T. O., Mamba, B. B., Brouckaert, B. M., Swartz, C. D., . . . Momba, M. N. B. (2011). Household water treatment systems: A solution to the production of safe drinking water by the low-income communities of Southern Africa. *Physics and Chemistry of the Earth, Parts A/B/C*, 36(14–15), 1120-1128.
- Naseri, E., Reyhanitabar, A., Oustan, S., Heydari, A. A., & Alidokht, L. (2014). Optimization arsenic immobilization in a sandy loam soil using iron-based amendments by response surface methodology. *Geoderma*, 232-234, 547-555.
- Nguyen, A. T., Nguyen, L. T. M., Nguyen, C. K., Truong, T., & Phan, N. T. S. (2014). Superparamagnetic Copper Ferrite Nanoparticles as an Efficient Heterogeneous Catalyst for the alpha-Arylation of 1,3-Diketones with C-C Cleavage. *Chemcatchem*, 6(3), 815-823.
- Niaz Akhtar, M., Azhar Khan, M., Ahmad, M., Murtaza, G., Raza, R., Shaukat, S. F., Raza, M. R. (2014).  $Y_3Fe_5O_{12}$  nanoparticulate garnet ferrites: Comprehensive study on the synthesis and characterization fabricated by various routes. *Journal of Magnetism and Magnetic Materials*, 368(0), 393-400.
- Nieto-Delgado, C., & Rangel-Mendez, J. R. (2012). Anchorage of iron hydro(oxide) nanoparticles onto activated carbon to remove As(V) from water. *Water Res.*, 46(9), 2973-2982.
- Ojea-Jiménez, I., López, X., Arbiol, J., & Puentes, V. (2012). Citrate-Coated Gold Nanoparticles As Smart Scavengers for Mercury(II) Removal from Polluted Waters. *ACS nano*, 6(3), 2253-2260.
- Olsen, J. B., Beacham, T. D., Wetklo, M., Seeb, L. W., Smith, C. T., Flannery, B. G., & Wenburg, J. K. (2010). The influence of hydrology and waterway distance on population structure of Chinook salmon *Oncorhynchus tshawytscha* in a large river. *Journal of Fish Biology*, 76(5), 1128-1148.
- Onda, K., LoBuglio, J., & Bartram, J. (2012). Global Access to Safe Water: Accounting for Water Quality and the Resulting Impact on MDG Progress. *International Journal of Environmental Research and Public Health*, 9(3), 880-894.
- Onyango, M. S., Kojima, Y., Aoyi, O., Bernardo, E. C., & Matsuda, H. (2004). Adsorption equilibrium modeling and solution chemistry dependence of fluoride removal from water by trivalent-cation-exchanged zeolite F-9. *Journal of Colloid and Interface Science*, 279(2), 341-350.

- Orem, W., Gilmour, C., Axelrad, D., Krabbenhoft, D., Scheidt, D., Kalla, P., Aiken, G. (2011). Sulfur in the South Florida Ecosystem: Distribution, Sources, Biogeochemistry, Impacts, and Management for Restoration. *Critical Reviews in Environmental Science and Technology*, 41, 249-288.
- Ozaki, H., Sharma, K., & Saktaywin, W. (2002). Performance of an ultra-low-pressure reverse osmosis membrane (ULPROM) for separating heavy metal: effects of interference parameters. *Desalination*, 144(1-3), 287-294.
- Pacheco, S., Medina, M., Valencia, F., & Tapia, J. (2006). Removal of inorganic mercury from polluted water using structured nanoparticles. *Journal of Environmental Engineering-Asce*, 132(3), 342-349.
- Pacheco, S., Tapia, J., Medina, M., & Rodriguez, R. (2006). Cadmium ions adsorption in simulated wastewater using structured alumina-silica nanoparticles. *Journal of Non-Crystalline Solids*, 352(52-54), 5475-5481.
- Peng, X. J., Luan, Z. K., Ding, J., Di, Z. H., Li, Y. H., & Tian, B. H. (2005). Ceria nanoparticles supported on carbon nanotubes for the removal of arsenate from water. *Materials Letters*, 59(4), 399-403.
- Petrovic, C., Pagliuso, P., Hundley, M., Movshovich, R., Sarrao, J., Thompson, J., & Fisk, Z. (2001). Heavy-fermion superconductivity in CeCoIn<sub>5</sub> at 2.3 K. *arXiv preprint cond-mat/0103168*.
- Pillay, K., Cukrowska, E. M., & Coville, N. J. (2009). Multi-walled carbon nanotubes as adsorbents for the removal of parts per billion levels of hexavalent chromium from aqueous solution. *Journal of Hazardous Materials*, 166(2-3), 1067-1075.
- Pimentel, B. R., Parulkar, A., Zhou, E. k., Brunelli, N. A., & Lively, R. P. (2014). Zeolitic Imidazolate Frameworks: Next-Generation Materials for Energy-Efficient Gas Separations. *ChemSusChem*, 7(12), 3202-3240.
- Pitoniak, E., Wu, C. Y., Mazyck, D. W., Powers, K. W., & Sigmund, W. (2005). Adsorption enhancement mechanisms of silica-titania nanocomposites for elemental mercury vapor removal. *Environmental Science & Technology*, 39(5), 1269-1274.
- Pluta, I. (2001). Barium and radium discharged from coal mines in the Upper Silesia, Poland. *Environmental Geology*, 40(3), 345-348.
- Potts, J. R., Dreyer, D. R., Bielawski, C. W., & Ruoff, R. S. (2011). Graphene-based polymer nanocomposites. *Polymer*, 52(1), 5-25.
- Poursaberi, T., & Hassanisadi, M. (2013). Magnetic Removal of Reactive Black 5 from Wastewater Using Ionic Liquid Grafted-Magnetic Nanoparticles. *CLEAN – Soil, Air, Water*, n/a-n/a.
- Priyadarshana, G., Kottogoda, N., Senaratne, A., de Alwis, A., & Karunaratne, V. (2015). Synthesis of Magnetite Nanoparticles by Top-Down Approach from a High Purity Ore. *Journal of Nanomaterials*, 2(1), 1-8.

- Qu, X., Brame, J., Li, Q., & Alvarez, P. J. J. (2012). Nanotechnology for a Safe and Sustainable Water Supply: Enabling Integrated Water Treatment and Reuse. *Accounts of Chemical Research*, 46(3), 834-843.
- Raju, K., Venkataiah, G., & Yoon, D. H. (2014). Effect of Zn substitution on the structural and magnetic properties of Ni-Co ferrites. *Ceramics International*, 40(7), 9337-9344.
- Ranjith Kumar, E., Jayaprakash, R., & Kumar, S. (2014). The role of annealing temperature and bio template (egg white) on the structural, morphological and magnetic properties of manganese substituted  $MFe_2O_4$  ( $M=Zn, Cu, Ni, Co$ ) nanoparticles. *Journal of Magnetism and Magnetic Materials*, 351, 70-75.
- Rao, C. R. N., & Karthikeyan, J. (2012). Removal of Fluoride from Water by Adsorption onto Lanthanum Oxide. *Water, Air, & Soil Pollution*, 223(3), 1101-1114.
- Rao, P., Godbole, R. V., Phase, D. M., Chikate, R. C., & Bhagwat, S. (2015). Ferrite thin films: Synthesis, characterization and gas sensing properties towards LPG. *Materials Chemistry and Physics*, 149-150, 333-338.
- Rashad, M. M., Soltan, S., Ramadan, A. A., Bekheet, M. F., & Rayan, D. A. (2015). Investigation of the structural, optical and magnetic properties of  $CuO/CuFe_2O_4$  nanocomposites synthesized via simple microemulsion method. *Ceramics International*, 41(9), 12237-12245.
- Raymond, S. N., Quinn, T., & Lunine, J. I. (2004). Making other earths: dynamical simulations of terrestrial planet formation and water delivery. *Icarus*, 168(1), 1-17.
- Rehman, M., Yusoff, I., Ahmmad, R., & Alias, Y. (2015). Arsenic Adsorption Using Palm Oil Waste Clinker Sand Biotechnology: an Experimental and Optimization Approach. *Water, Air, & Soil Pollution*, 226(5), 1-13.
- Rehman, M. A., Yusoff, I., & Alias, Y. (2015). Fluoride adsorption by doped and undoped magnetic ferrites  $CuCe_xFe_{2-x}O_4$ : Preparation, characterization, optimization and modeling for effectual remediation technologies. *Journal of Hazardous Materials*, 299, 316-324.
- Rehman, M. A., Yusoff, I., & Alias, Y. (2015). Structural, morphological and magnetic investigations of  $CuCe_{0.2}Fe_{1.8}O_4$  graphene-supported nanocomposites. *Ceramics International*, 4(1), 1399-1407.
- Reidy, B., Haase, A., Luch, A., Dawson, K., & Lynch, I. (2013). Mechanisms of Silver Nanoparticle Release, Transformation and Toxicity: A Critical Review of Current Knowledge and Recommendations for Future Studies and Applications. *Materials*, 6(6), 2295-2350.
- Renault, F., Morin-Crini, N., Gimbert, F., Badot, P.-M., & Crini, G. (2008). Cationized starch-based material as a new ion-exchanger adsorbent for the removal of C.I. Acid Blue 25 from aqueous solutions. *Bioresource Technology*, 99(16), 7573-7586.

- Rezaei, F., Rownaghi, A. A., Monjezi, S., Lively, R. P., & Jones, C. W. (2015). SO<sub>x</sub>/NO<sub>x</sub> Removal from Flue Gas Streams by Solid Adsorbents: A Review of Current Challenges and Future Directions. *Energy & Fuels*, 29(9), 5467-5486.
- Rezlescu, E., Sachelarie, L., Popa, P. D., & Rezlescu, N. (2000). Effect of substitution of divalent ions on the electrical and magnetic properties of Ni-Zn-Me ferrites. *Magnetics, IEEE Transactions on*, 36(6), 3962-3967.
- Roberts, W. (2015). The Role of the Contract Hydrographic Surveyor. *The International Hydrographic Review*, 54(2).
- Roig, A., Cayuela, M. L., & Sanchez-Monedero, M. A. (2006). An overview on olive mill wastes and their valorisation methods. *Waste Management*, 26(9), 960-969.
- Rosen, M. J., & Kunjappu, J. T. (2012). *Surfactants and interfacial phenomena*. USA: John Wiley & Sons.
- Roy, P., Mondal, N. K., & Das, K. (2014). Modeling of the adsorptive removal of arsenic: A statistical approach. *Journal of Environmental Chemical Engineering*, 2(1), 585-597.
- Roy, P., Mondal, N. K., & Das, K. (2014). Modeling of the adsorptive removal of arsenic: A statistical approach. *J. Environ. Chem. Eng.*, 2(1), 585-597.
- Ruddell, B., & Wagener, T. (2015). Grand Challenges for Hydrology Education in the 21st Century. *Journal of Hydrologic Engineering*, 20(1), A4014001.
- Ryan, J. V., Lemieux, P. M., Pollard, K., Workman, R., Antley, B., & Yurk, J. (2000). Characterization of organic emissions from hazardous waste incineration processes under the new EPA draft Risk Burn Guidance: measurement issues. *Waste Management*, 20(5-6), 347-353.
- Sahoo, B. N., & Kandasubramanian, B. (2014). Recent progress in fabrication and characterisation of hierarchical biomimetic superhydrophobic structures. *RSC Advances*, 4(42), 22053-22093.
- Salameh, P. R., Baldi, I., Brochard, P., Raherison, C., Abi Saleh, B., & Salamon, R. (2003). Respiratory symptoms in children and exposure to pesticides. *European Respiratory Journal*, 22(3), 507-512.
- Salipira, K. L., Mamba, B. B., Krause, R. W., Malefetse, T. J., & Durbach, S. H. (2007). Carbon nanotubes and cyclodextrin polymers for removing organic pollutants from water. *Environmental Chemistry Letters*, 5(1), 13-17.
- Santhosh, C., Kollu, P., Doshi, S., Sharma, M., Bahadur, D., Vanchinathan, M. T., Grace, A. N. (2014). Adsorption, photodegradation and antibacterial study of graphene-Fe<sub>3</sub>O<sub>4</sub> nanocomposite for multipurpose water purification application. *RSC Advances*, 4(54), 28300.
- Savage, N., & Diallo, M. (2005). Nanomaterials and Water Purification: Opportunities and Challenges. *Journal of Nanoparticle Research*, 7(4-5), 331-342.

- Schueller, B. S., & Yang, R. T. (2001). Ultrasound Enhanced Adsorption and Desorption of Phenol on Activated Carbon and Polymeric Resin. *Industrial & Engineering Chemistry Research*, 40(22), 4912-4918.
- Schwarzenbach, R. P., Egli, T., Hofstetter, T. B., Von Gunten, U., & Wehrli, B. (2010). Global water pollution and human health. *Annual Review of Environment and Resources*, 35, 109-136.
- Sen Gupta, B., Chatterjee, S., Rott, U., Kauffman, H., Bandopadhyay, A., DeGroot, W., Mukherjee, S. (2009). A simple chemical free arsenic removal method for community water supply--a case study from West Bengal, India. *Environ Pollut*, 157(12), 3351-3353.
- Shahid, M. M., Pandikumar, A., Golsheikh, A. M., Huang, N. M., & Lim, H. N. (2014). Enhanced electrocatalytic performance of cobalt oxide nanocubes incorporating reduced graphene oxide as a modified platinum electrode for methanol oxidation. *RSC Advances*, 4(107), 62793-62801.
- Shahid, M. M., Rameshkumar, P., Pandikumar, A., Lim, H. N., Ng, Y. H., & Huang, N. M. (2015). An electrochemical sensing platform based on a reduced graphene oxide-cobalt oxide nanocube@ platinum nanocomposite for nitric oxide detection. *Journal of Materials Chemistry A*, 3(27), 14458-14468.
- Shanmugaprakash, M., & Sivakumar, V. (2013). Development of experimental design approach and ANN-based models for determination of Cr(VI) ions uptake rate from aqueous solution onto the solid biodiesel waste residue. *Bioresour. Technol.*, 148(0), 550-559.
- Shen, F., Chen, X., Gao, P., & Chen, G. (2003). Electrochemical removal of fluoride ions from industrial wastewater. *Chemical Engineering Science*, 58(3-6), 987-993.
- Sheppard, N. (2006). *The historical development of experimental techniques in vibrational spectroscopy*. India: Wiley Online Library.
- Shuang, C. D., Yang, F., Pan, F., Zhou, Q., Yang, W. B., & Li, A. M. (2011). Preparation of magnetic anion exchange resin and their adsorption kinetic behavior of reactive blue. *Chinese Chemical Letters*, 22(9), 1091-1094.
- Simsek, E. B., Özdemir, E., & Beker, U. (2013). Process Optimization for Arsenic Adsorption onto Natural Zeolite Incorporating Metal Oxides by Response Surface Methodology. *Water Air Soil Poll.*, 224(7), 1614.
- Singh, R., Singh, S., Parihar, P., Singh, V. P., & Prasad, S. M. (2015). Arsenic contamination, consequences and remediation techniques: A review. *Ecotoxicology and Environmental Safety*, 112, 247-270.
- Singh, S., Kumar, V., Vashisht, K., Singh, P., Banerjee, B. D., Rautela, R. S., . . . Rai, A. (2011). Role of genetic polymorphisms of CYP1A1, CYP3A5, CYP2C9, CYP2D6, and PON1 in the modulation of DNA damage in workers occupationally exposed to organophosphate pesticides. *Toxicology and Applied Pharmacology*, 257(1), 84-92.

- Skubal, L. R., & Meshkov, N. K. (2002). Reduction and removal of mercury from water using arginine-modified TiO<sub>2</sub>. *Journal of Photochemistry and Photobiology a-Chemistry*, 148(1-3), 211-214.
- Skubal, L. R., Meshkov, N. K., Rajh, T., & Thurnauer, M. (2002). Cadmium removal from water using thiolactic acid-modified titanium dioxide nanoparticles. *Journal of Photochemistry and Photobiology a-Chemistry*, 148(1-3), 393-397.
- Smith, A. H., Lingas, E. O., & Rahman, M. (2000). Contamination of drinking-water by arsenic in Bangladesh: a public health emergency. *Bulletin of the World Health Organization*, 78(9), 1093-1103.
- Smuleac, V., Varma, R., Sikdar, S., & Bhattacharyya, D. (2011). Green synthesis of Fe and Fe/Pd bimetallic nanoparticles in membranes for reductive degradation of chlorinated organics. *Journal of Membrane Science*, 379(1-2), 131-137.
- Stankovich, S., Dikin, D. A., Dommett, G. H., Kohlhaas, K. M., Zimney, E. J., Stach, E. A., . . . Ruoff, R. S. (2006). Graphene-based composite materials. *Nature*, 442(7100), 282-286.
- Stek, P. E. (2008). *Urban Groundwater Extraction in Kuala Lumpur, Malaysia*. International Islamic University Malaysia, International Islamic University Malaysia.
- Stevens, S. (1997). *Conservation through cultural survival: Indigenous peoples and protected areas*. California: Island Press.
- Stuart, B. (2005). *Infrared spectroscopy*. USA: Wiley Online Library.
- Su, Y., Peng, L., Guo, J., Huang, S., Lv, L., & Wang, X. (2014). Tunable Optical and Photocatalytic Performance Promoted by Nonstoichiometric Control and Site-Selective Codoping of Trivalent Ions in NaTaO<sub>3</sub>. *The Journal of Physical Chemistry C*, 118(20), 10728-10739.
- Sun, H., Cao, L., & Lu, L. (2011). Magnetite/reduced graphene oxide nanocomposites: One step solvothermal synthesis and use as a novel platform for removal of dye pollutants. *Nano Research*, 4(6), 550-562.
- Sun, J., Fu, Y., Xiong, P., Sun, X., Xu, B., & Wang, X. (2013). A magnetically separable P25/CoFe<sub>2</sub>O<sub>4</sub>/graphene catalyst with enhanced adsorption capacity and visible-light-driven photocatalytic activity. *RSC Advances*, 3(44), 22490.
- Suryanarayana, C., & Norton, M. G. (2013). *X-ray diffraction: a practical approach*. Washington, Springer Science.
- Sutter, R. D., Wainscott, S. B., Boetsch, J. R., Palmer, C. J., & Rugg, D. J. (2015). Practical guidance for integrating data management into long-term ecological monitoring projects. *Wildlife Society Bulletin*, 39(3), 451-463.
- Świetlik, J., Laskowski, T., & Kozyatnyk, I. (2015). Adsorption of Natural Organic Matter onto the Products of Water-Pipe Corrosion. *Water, Air, & Soil Pollution*, 226(7), 1-9.

- Tang, L., Zhang, S., Zeng, G.-M., Zhang, Y., Yang, G.-D., Chen, J., Deng, Y.-C. (2015). Rapid adsorption of 2,4-dichlorophenoxyacetic acid by iron oxide nanoparticles-doped carboxylic ordered mesoporous carbon. *Journal of Colloid and Interface Science*, 445(0), 1-8.
- Thakre, D., Dixit, P., Waghmare, S., Manwar, N., Labhsetwar, N., & Rayalu, S. S. (2015). Synthesis optimization and fluoride uptake properties of high capacity composite adsorbent for defluoridation of drinking water. *Environmental Progress & Sustainable Energy*, 34(6), 1576–1585.
- Thammawong, C., Opaprakasit, P., Tangboriboonrat, P., & Sreearunothai, P. (2013). Prussian blue-coated magnetic nanoparticles for removal of cesium from contaminated environment. *Journal of Nanoparticle Research*, 15(6), 1-10.
- Thota, S., & Kumar, J. (2007). Sol-gel synthesis and anomalous magnetic behaviour of NiO nanoparticles. *Journal of Physics and Chemistry of Solids*, 68(10), 1951-1964.
- Tian, H., Li, Y., Wang, W., Wu, P., & Ru, S. (2012). Exposure to monocrotophos pesticide during sexual development causes the feminization/demasculinization of the reproductive traits and a reduction in the reproductive success of male guppies (*Poecilia reticulata*). *Toxicology and Applied Pharmacology*, 263(2), 163-170.
- Trois, C., & Cibati, A. (2015). South African sands as a low cost alternative solution for arsenic removal from industrial effluents in permeable reactive barriers: Column tests. *Chemical Engineering Journal*, 259, 981-989.
- Tuna, A. Ö. A., Özdemir, E., Simsek, E. B., & Beker, U. (2013). Optimization of Process Parameters for Removal of Arsenic Using Activated Carbon-Based Iron-Containing Adsorbents by Response Surface Methodology. *Water Air Soil Poll.*, 224(9), 1685.
- Tung, V. C., Allen, M. J., Yang, Y., & Kaner, R. B. (2009). High-throughput solution processing of large-scale graphene. *Nature Nano*, 4(1), 25-29.
- Tuzen, M., Saygi, K. O., Usta, C., & Soylak, M. (2008). *Pseudomonas aeruginosa* immobilized multiwalled carbon nanotubes as biosorbent for heavy metal ions. *Bioresource Technology*, 99(6), 1563-1570.
- Uheida, A., Salazar-Alvarez, G., Bjorkman, E., Yu, Z., & Muhammed, M. (2006). Fe<sub>3</sub>O<sub>4</sub> and gamma-Fe<sub>2</sub>O<sub>3</sub> nanoparticles for the adsorption of Co<sup>2+</sup> from aqueous solution. *Journal of Colloid and Interface Science*, 298(2), 501-507.
- Urano, K., & Tachikawa, H. (1992). Process development for removal and recovery of phosphorus from wastewater by a new adsorbent. 3. Desorption of phosphate and regeneration of adsorbent. *Industrial & Engineering Chemistry Research*, 31(6), 1510-1513.
- Uzum, C., Shahwan, T., Eroglu, A. E., Hallam, K. R., Scott, T. B., & Lieberwirth, I. (2009). Synthesis and characterization of kaolinite-supported zero-valent iron nanoparticles and their application for the removal of aqueous Cu<sup>2+</sup> and Co<sup>2+</sup> ions. *Applied Clay Science*, 43(2), 172-181.

- Uzum, C., Shahwan, T., Eroglu, A. E., Lieberwirth, I., Scott, T. B., & Hallam, K. R. (2008). Application of zero-valent iron nanoparticles for the removal of aqueous  $\text{Co}^{2+}$  ions under various experimental conditions. *Chemical Engineering Journal*, 144(2), 213-220.
- Vamvasakis, I., Subrahmanyam, K. S., Kanatzidis, M. G., & Armatas, G. S. (2015). Template-Directed Assembly of Metal–Chalcogenide Nanocrystals into Ordered Mesoporous Networks. *ACS nano*, 9(4), 4419-4426.
- Velazquez-Jimenez, L. H., Hurt, R. H., Matos, J., & Rangel-Mendez, J. R. (2013). Zirconium–Carbon Hybrid Sorbent for Removal of Fluoride from Water: Oxalic Acid Mediated Zr(IV) Assembly and Adsorption Mechanism. *Environmental Science & Technology*, 48(2), 1166-1174.
- Wahba, A. M., & Bakr Mohamed, M. (2015). Structural and magnetic characterization and cation distribution of nanocrystalline  $\text{Co}_x\text{Fe}_{3-x}\text{O}_4$  ferrites. *Journal of Magnetism and Magnetic Materials*, 378, 246-252.
- Wang, H., Shen, Q., Tang, B.-s., Lu, C., Peng, Y., & Tang, L. (2014). A framework of decision-making factors and supporting information for facilitating sustainable site planning in urban renewal projects. *Cities*, 40, 44-55.
- Wang, H. J., Zhou, A. L., Peng, F., Yu, H., & Yang, J. (2007). Mechanism study on adsorption of acidified multiwalled carbon nanotubes to Pb(II). *Journal of Colloid and Interface Science*, 316(2), 277-283.
- Wang, Q., Luo, J., Zhong, Z., & Borgna, A. (2011).  $\text{CO}_2$  capture by solid adsorbents and their applications: current status and new trends. *Energy & Environmental Science*, 4(1), 42-55.
- Wang, S.-y., Tang, Y.-k., Chen, C., Wu, J.-t., Huang, Z., Mo, Y.-y., Chen, J.-b. (2015). Regeneration of magnetic biochar derived from eucalyptus leaf residue for lead(II) removal. *Bioresource Technology*, 186, 360-364.
- Wang, S., Wang, R., & Li, X. (2005). Research and development of consolidated adsorbent for adsorption systems. *Renewable Energy*, 30(9), 1425-1441.
- Wang, S. G., Gong, W. X., Liu, X. W., Yao, Y. W., Gao, B. Y., & Yue, Q. Y. (2007). Removal of lead(II) from aqueous solution by adsorption onto manganese oxide-coated carbon nanotubes. *Separation and Purification Technology*, 58(1), 17-23.
- Wang, X., Zhao, C. M., Zhao, P., Dou, P. P., Ding, Y., & Xu, P. (2009). Gellan gel beads containing magnetic nanoparticles: An effective biosorbent for the removal of heavy metals from aqueous system. *Bioresource Technology*, 100(7), 2301-2304.
- Wang, Y., Chen, H., Tang, J., Ye, G., Ge, H., & Hu, X. (2015). Preparation of magnetic metal organic frameworks adsorbent modified with mercapto groups for the extraction and analysis of lead in food samples by flame atomic absorption spectrometry. *Food Chem*, 181, 191-197.
- Warren, B. E. (1969). *X-ray Diffraction.*, Courier Corporation, USA.

- Waterman, K. C. (2004). Pharmaceutical kit for oxygen-sensitive drugs: Google Patents.
- Wei, X. C., & Viadero, R. C. (2007). Synthesis of magnetite nanoparticles with ferric iron recovered from acid mine drainage: Implications for environmental engineering. *Colloids and Surfaces a-Physicochemical and Engineering Aspects*, 294(1-3), 280-286.
- Witek-Krowiak, A., Chojnacka, K., Podstawczyk, D., Dawiec, A., & Pokomeda, K. (2014). Application of response surface methodology and artificial neural network methods in modelling and optimization of biosorption process. *Bioresour. Technol.*, 160, 150-160.
- Wong, E. T., Chan, K. H., & Idris, A. (2015). Kinetic and equilibrium investigation of Cu(II) removal by Co(II)-doped iron oxide nanoparticle-immobilized in PVA–alginate recyclable adsorbent under dark and photo condition. *Chemical Engineering Journal*, 268, 311-324.
- Wu, X., Yu, H., Dong, H., & Geng, L. (2014). Enhanced infrared radiation properties of CoFe<sub>2</sub>O<sub>4</sub> by single Ce<sup>3+</sup>-doping with energy-efficient preparation. *Ceramics International*, 40(4), 5905-5911.
- Wu, Z.-S., Ren, W., Gao, L., Zhao, J., Chen, Z., Liu, B., Cheng, H.-M. (2009). Synthesis of Graphene Sheets with High Electrical Conductivity and Good Thermal Stability by Hydrogen Arc Discharge Exfoliation. *ACS nano*, 3(2), 411-417.
- Wyckoff, R. W. G. (1963). *Crystal structures*. New York: Interscience Publishers.
- Xiao, G., Huang, X., Liao, X., & Shi, B. (2013). One-Pot Facile Synthesis of Cerium-Doped TiO<sub>2</sub> Mesoporous Nanofibers Using Collagen Fiber As the Biotemplate and Its Application in Visible Light Photocatalysis. *The Journal of Physical Chemistry C*, 117(19), 9739-9746.
- Xing, Q., Tosi, L., Braga, F., Gao, X., & Gao, M. (2015). Interpreting the progressive eutrophication behind the world's largest macroalgal blooms with water quality and ocean color data. *Natural Hazards*, 1-15.
- Xu, W.-H., Wang, L., Wang, J., Sheng, G.-P., Liu, J.-H., Yu, H.-Q., & Huang, X.-J. (2013). Superparamagnetic mesoporous ferrite nanocrystal clusters for efficient removal of arsenite from water. *CrystEngComm*, 15(39), 7895.
- Xu, X., Song, C., Andresen, J. M., Miller, B. G., & Scaroni, A. W. (2002). Novel Polyethylenimine-Modified Mesoporous Molecular Sieve of MCM-41 Type as High-Capacity Adsorbent for CO<sub>2</sub> Capture. *Energy & Fuels*, 16(6), 1463-1469.
- Yadav, A. K., Kaushik, C. P., Haritash, A. K., Singh, B., Raghuvanshi, S. P., & Kansal, A. (2007). Determination of exposure and probable ingestion of fluoride through tea, toothpaste, tobacco and pan masala. *J. Hazard. Mater.*, 142(1-2), 77-80.
- Young, O., & Steffen, W. (2009). The Earth System: Sustaining Planetary Life-Support Systems. In C. Folke, G. P. Kofinas & F. S. Chapin (Eds.), *Principles of Ecosystem Stewardship* (pp. 295-315): Springer New York.

- Younger, M., Morrow-Almeida, H. R., Vindigni, S. M., & Dannenberg, A. L. (2008). The built environment, climate change, and health: opportunities for co-benefits. *American journal of preventive medicine*, 35(5), 517-526.
- Younger, P. L., & Wolkersdorfer, C. (2004). Mining impacts on the fresh water environment: technical and managerial guidelines for catchment scale management. *Mine water and the environment*, 23, s2-s80.
- Yu, C., Dong, X., Guo, L., Li, J., Qin, F., Zhang, L., Yan, D. (2008). Template-free preparation of mesoporous Fe<sub>2</sub>O<sub>3</sub> and its application as absorbents. *The Journal of Physical Chemistry C*, 112(35), 13378-13382.
- Yu, L., Yang, X., He, J., He, Y., & Wang, D. (2015). Synthesis of magnetically separable N, La-doped TiO<sub>2</sub> with enhanced photocatalytic activity. *Separation and Purification Technology*, 144, 107-113.
- Yu, Y., Yu, L., & Paul Chen, J. (2015). Adsorption of fluoride by Fe–Mg–La triple-metal composite: Adsorbent preparation, illustration of performance and study of mechanisms. *Chemical Engineering Journal*, 262, 839-846.
- Yu, Y., Zhang, X.-M., Ma, J.-P., Liu, Q.-K., Wang, P., & Dong, Y.-B. (2014). Cu(i)-MOF: naked-eye colorimetric sensor for humidity and formaldehyde in single-crystal-to-single-crystal fashion. *Chemical Communications*, 50(12), 1444-1446.
- Zaman, A. U., & Lehmann, S. (2013). The zero waste index: a performance measurement tool for waste management systems in a 'zero waste city'. *Journal of Cleaner Production*, 50, 123-132.
- Zeng, W. M., Gao, L., & Guo, J. K. (1998). A new sol-gel route using inorganic salt for synthesizing Al<sub>2</sub>O<sub>3</sub> nanopowders. *Nanostructured Materials*, 10(4), 543-550.
- Zeng, Z., Liu, J., & Savenije, H. H. G. (2013). A simple approach to assess water scarcity integrating water quantity and quality. *Ecological Indicators*, 34(0), 441-449.
- Zhang, H., Gao, S., Shang, N., Wang, C., & Wang, Z. (2014). Copper ferrite-graphene hybrid: a highly efficient magnetic catalyst for chemoselective reduction of nitroarenes. *RSC Advances*, 4(59), 31328-31332.
- Zhang, H., Gao, S., Shang, N., Wang, C., & Wang, Z. (2014). Copper ferrite-graphene hybrid: a highly efficient magnetic catalyst for chemoselective reduction of nitroarenes. *RSC Advances*, 4(59), 31328.
- Zhang, H., Wang, J., Gao, X., Wang, Z., & Wang, S. (2014). The electrochemical activity of polyaniline: An important issue on its use in electrochemical energy storage devices. *Synthetic Metals*, 187(0), 46-51.
- Zhang, H., Zhao, Y., Liu, W., Gao, S., Shang, N., Wang, C., & Wang, Z. (2015). Preparation of magnetically separable Cu<sub>6/7</sub>Co<sub>1/7</sub>Fe<sub>2</sub>O<sub>4</sub>-graphene catalyst and its application in selective reduction of nitroarenes. *Catalysis Communications*, 59, 161-165.

- Zhang, J., & Seeger, S. (2011). Polyester Materials with Superwetting Silicone Nanofilaments for Oil/Water Separation and Selective Oil Absorption. *Advanced Functional Materials*, 21(24), 4699-4704.
- Zhang, M., Bai, X. J., Liu, D., Wang, J., & Zhu, Y. F. (2015). Enhanced catalytic activity of potassium-doped graphitic carbon nitride induced by lower valence position. *Applied Catalysis B-Environmental*, 164, 77-81.
- Zhang, X., Li, K., Li, H., Lu, J., Fu, Q., & Chu, Y. (2014). Graphene nanosheets synthesis via chemical reduction of graphene oxide using sodium acetate trihydrate solution. *Synthetic Metals*, 193, 132-138.
- Zhang, Y., Yuan, S., Zhao, Y., Wang, H., & He, C. (2014). Synthesis of novel yttrium-doped graphene oxide nanocomposite for dye removal. *Journal of Materials Chemistry A*, 2(21), 7897.
- Zhang, Y., Zhou, E., Li, Y., & He, X. (2015). A novel nonenzymatic glucose sensor based on magnetic copper ferrite immobilized on multiwalled carbon nanotubes. *Anal. Methods*, 7(6), 2360-2366.
- Zhao, H., Zhang, D., Wang, F., Wu, T., & Gao, J. (2008). Modification of ferrite-manganese oxide sorbent by doping with cerium oxide. *Process Safety and Environmental Protection*, 86(6), 448-454.
- Zhao, Y., He, G., Dai, W., & Chen, H. (2014). High Catalytic Activity in the Phenol Hydroxylation of Magnetically Separable  $\text{CuFe}_2\text{O}_4$ -Reduced Graphene Oxide. *Industrial & Engineering Chemistry Research*, 53(32), 12566-12574.
- Zheng, W., Maurin, M., & Tarr, M. A. (2005). Enhancement of sonochemical degradation of phenol using hydrogen atom scavengers. *Ultrasonics Sonochemistry*, 12(4), 313-317.
- Zhou, Y. T., Nie, H. L., Branford-White, C., He, Z. Y., & Zhu, L. M. (2009). Removal of  $\text{Cu}^{2+}$  from aqueous solution by chitosan-coated magnetic nanoparticles modified with alpha-ketoglutaric acid. *Journal of Colloid and Interface Science*, 330(1), 29-37.
- Zhu, B., Wu, D., Yang, Y., Chen, Y., Li, W., Guo, J., & Wang, Q. (2011). Selective Removal of La(III) Ions Using Super-Paramagnetic Nanosorbent Coated by Saponified sec-Octylphenoxy Acetic Acid. *Journal of Chemical & Engineering Data*, 57(2), 553-560.
- Zhu, C., & Anderson, G. (2002). *Environmental applications of geochemical modeling.*, Cambridge University Press, UK.
- Zouboulis, A. I., Matis, K. A., Lazaridis, N. K., & Golyshin, P. N. (2003). The use of biosurfactants in flotation: application for the removal of metal ions. *Minerals Engineering*, 16(11), 1231-1236.

## LIST OF PUBLICATIONS AND PAPERS PRESENTED

1. Rehman, M.A, Yusoff, I., Ahmmad, R., & Alias, Y. (2015). Arsenic Adsorption Using Palm Oil Waste Clinker Sand Biotechnology: an Experimental and Optimization Approach. *Water, Air, & Soil Pollution*, 226(5), 1-13.
2. Rehman, M. A., Yusoff, I., & Alias, Y. (2015). Fluoride adsorption by doped and un-doped magnetic ferrites  $\text{CuCe}_x\text{Fe}_{2-x}\text{O}_4$ : Preparation, characterization, optimization and modeling for effectual remediation technologies. *Journal of Hazardous Materials*, 299, 316-324.
3. Rehman, M. A., Yusoff, I., & Alias, Y. (2015). Structural, morphological and magnetic investigations of  $\text{CuCe}_{0.2}\text{Fe}_{1.8}\text{O}_4$  graphene-supported nanocomposites. *Ceramics International*, 4(1), 1399–1407.
4. Rehman, M. A., Yusoff, I., Ahmad, P., & Alias, Y. (2015).  $\text{CuYb}_{0.5}\text{Fe}_{1.5}\text{O}_4$  nanoferrite adsorbent structural, morphological and functionalization characteristics for multiple pollutant removal by response surface methodology. *Journal of Molecular Liquids*, 224, 1256–1265.

## LIST OF PRESENTATIONS

1. "Ultrasonic Accelerated Removal and Determination of Acephate on POC Using HPLC Method" National postgraduate conference on Engineering 2014, 18 October 2014.
2. A facile one pot hydrothermal modification of amino silica by cerium nanoparticles for adsorption of phenosephranine: kinetics, isotherms and mechanism study, 1<sup>st</sup> ICRIL-International Conference on Innovation in Science & Technology, UTM, Kula Lumpur, 20<sup>th</sup> April 2015.
3. One day course on advanced nanomaterial: Synthesis and characterization, Nanotechnology & catalysis research center (NANOCAT), IPS Building, University of Malaya, 26<sup>th</sup> May 2015.
4. The Magnetic Garnet Ferrites: Preparation, Characterization, Applications and Response Surface Modeling for Hydrological remediation, the International Conference for Young Chemists (ICYC) 2015, City Bayview Hotel, Georgetown, Penang, Malaysia on 5 - 7 August 2015.
5. A field sampling and testing strategy for the assessment of drinking water contaminants levels in hydrological samples from Kula Lumpur water supply system. The 2<sup>nd</sup> International Conference on Waste Management & Environment (ICMWE) 20<sup>th</sup> – 22<sup>nd</sup> August 2015 at Kuala Lumpur, Malaysia.
6. Adsorption of nitrates on factory rejected palm oil waste clinker sand: a response surface method (RSM) optimization strategy. The 2<sup>nd</sup> International Conference on Waste Management & Environment (ICMWE) 20<sup>th</sup> – 22<sup>nd</sup> August 2015 at Kuala Lumpur, Malaysia.